Nonlinear Modeling and Identification of Unsteady Aerodynamics at Stall

Mallesh Vithappa Bommanahal

A thesis submitted in partial fulfilment of
the requirements for the degree of

Doctor of Philosophy
at

Faculty of Technology, De Montfort University
Leicester, United Kingdom
with research support from
CSIR National Aerospace Laboratories, India

June 2015

Abstract

For an aircraft with delta wing shape, aerodynamics in stall angles-of-attack at both low and high-subsonic Mach conditions is known to be unsteady and nonlinear in nature. In these conditions, the longitudinal aerodynamic loads depend on the history of angle-of-attack and side-slip. The classical method of using damping or acceleration aerodynamic derivatives for modeling the unsteady variation of coefficients is unsuitable. Hence, two novel approaches for modeling aerodynamic loads in these conditions are proposed in this thesis.

The unsteady effect in stall conditions at low Mach number is reflected in forced oscillation wind tunnel tests as dependence of longitudinal loads on amplitude and frequency of sinusoidal angle-of-attack input. The variations in longitudinal loads are nonlinear as their power spectrum contains super-harmonics of input frequency. The approaches presented in literature are equivalent when these are reduced to equivalent linear transfer function formulation, while their nonlinear adaptations are semi-empirical or adhoc. Hence, Volterra Variational Modeling (VVM) is proposed as a systematic approach to capture the nonlinear nature of unsteady variations.

The VVM is derived from Volterra series as a set of parametric differential equations of the so-called kernel states. The kernel-states have special harmonic input response properties which are leveraged to develop a systematic methodology to capture the nonlinear unsteady variations in pitching moment coefficient. VVM is shown to inherently reproduce the nonlinear features of unsteady aerodynamic loads like amplitude dependence of nonlinear variations, different effective time-scale for pitch-up and pitch-down motions and same number of super-harmonics as seen in the experimental data. Hence, it offers several advantages compared to all the modeling approaches in literature.

The VVM is a powerful approach due to following features: (i) Mathematically rigorous structure, (ii) Physical interpretations of parameters, (iii) it facilitates linear analysis of the flight modes (iv) simple identification methodology using forced oscillation wind tunnel test data (v) open to innovations in model structure and estimation technique. These concepts are demonstrated for the Generic Tailless Aircraft and F16XL aircraft using comprehensive sets of wind tunnel test data .

The unsteady phenomena at high sub-sonic Mach number is called Abrupt Wing Stall, and novel model called ”Bifurcational Model of Aerodynamic Asymmetry” is proposed for modeling it. It shown to be a topologically rich structure which can model the static hysteresis and unsteady variations in rolling moment coefficient versus the side-slip angle, in order to reproduce the effects of Abrupt Wing Stall on flight dynamics.

Acknowledgements

Firstly, I thank Mr.Shyam Chetty Director, CSIR-NAL, for providing me the wonderful opportunity to work with Prof.Mikhail Goman on High-angle-of-attack Flight Mechanics. My heartfelt thanks to the Aeronautical Development Agency for sponsoring the research and development activities at NAL, and supporting my research. I take this opportunity to also thank IIT Bombay, India for providing me generous scholarships for my undergraduate studies.

I am deeply obliged to Prof.Mikhail Goman, my supervisor for this PhD, for inspiring me and giving directions to my research work. This PhD has fructified "standing on the shoulders of giants", and Prof.Goman is the tallest one of those giants for me.

I would like to thank my colleagues at National Aerospace Laboratories, Aeronautical Development Agency and De Montfort University, for their encouragement and support. In particular, I would like to thank Mr.M. Devprakash, Dr.Abhay Pashilkar, Mr.PVS Murthy and Dr.Amitabh Saraf, for many fruitful collaborations and discussions during the course of this research. Special thanks are due to Dr.Nikolay Abramov for always being available to help me with the software tools used in this research. I thank Dr.Patrick Murphy of NASA-LaRC for providing F16XL wind tunnel test data and other discussions.

I would like to dedicate this thesis to my Awesome daughter Aashita, and my lovely wife Smriti. They define joy in every part of my life. I thank my parents, for always saying "Yes" to whatever I wanted to do. My heartfelt thanks to my parent-in-laws for being immensely cooperative, and entertaining my silly requests. I thank my sisters Vajreshwari, Sujata, Suma; brother-in-laws, nephews and nieces, for all the caring and sharing. I thank my friends Bhaiya, Laxman, Shanky, Prasun, Shraddha, Nivedita, Madhuri, Nidhi, Richa, Aditya, Anup, Vinit, Chaitanya, Vishal, Venky and many others, for all the good-times, essential for positive and creative thinking.

The perpetual motion machine that I invented eighteen years ago does not look like a wasteful exercise today.

Mallesh Vithappa Bommanahal
14th February 2015

Contents

List of Figures

List of Tables

List of Terms and Symbols

C^{att} : Coefficient of force or moment assuming attached flow.

C^{pt} : Coefficient of force or moment assuming potential flow.

C_{L_q} : Derivative of lift force coefficient with q.

C_X : Axial force coefficient.

C_Y : Side force coefficient.

$C_{Z_{\alpha,\omega_0}}$: In-phase derivative of C_Z.

$C_{Z_{\dot{\alpha},\omega_0}}$: Out-of-phase derivative of C_Z.

$C_{Z_{raw}}$: Raw wind tunnel test data for normal force coefficient.

C_Z : Normal force coefficient.

C_a : Any aerodynamic force or moment coefficient.

C_{dyn} : Unsteady component of force or moment coefficient.

C_{exp} : Experimental data for force or moment coefficient.

C_{l_0} : Asymmetric component of Rolling moment coefficient.

C_{l_p} : Roll damping derivative.

$C_{l_{dyn}}$: Unsteady component of rolling moment coefficient.

$C_{l_{st}}$: Steady state value of rolling moment coefficient.

C_l : Rolling moment coefficient.

C_{mod} : Model output for force or moment coefficient.

C_m : Pitching moment coefficient.

C_n : Yawing moment coefficient.

C_{st} : Steady state force or moment coefficient.

C_{vb} : Coefficient of force or moment due to vortical flow.

$F(d/dt)$: Higher order differential operator.

G_n : n-dimensional fourier transform of n-th Volterra Kernel.

K_i : Parameters of Volterra variational model.

M : Mach number.

$U(f)$: Fourier transform of input $u(t)$.

V_∞ : Free wind speed (m/s).

$X_n(f)$: Fourier transform of n-th kernel state.

α_c : Angle of attack of critical state crossing.

α_{cr} : Critical Angle of attack of AWS.

α : Angle of attack (deg).

$\bar{c}$: Mean aerodynamic chord length (m).

β : Angle of sideslip.

ω : Frequency of harmonic input (rad/s).

ϕ : Roll (Euler) angle in body axes.

π : Ratio of circumference of circle to its diameter.

ρ^* : Convergence radius of Volterra variational model.

τ_2 : Time-constant of convective-lag, boundary layer effects etc..

τ_i : Local time-variable in Volterra kernel.

τ : Time-scale of unsteady variation.

θ : Pitch (Euler) angle in body axes.

φ_e : Inclination of ellipse in BMAA.

φ_l : Inclination of line in BMAA.

a_i : Coefficient of x^i in PoDE model.

b_i : Coefficient of $x^{i-1}u$ in PoDE model.

b : Wing-span length of aircraft (m).

f : Frequency of harmonic input (Hz).

h_n : n-th order Volterra Kernel.

j : Complex number exponent.

k : Non-dimensional or reduced frequency.

p : Roll rate (deg/s).

q : Pitch rate (deg/s).

r : Yaw rate (deg/s).

u : Input to a system.

x_0 : Location of Vortex breakdown point (normalized).

x_n : n-th kernel state of Volterra variational model.

AWS : Abrupt Wing Stall.

BMAA : Bifurcational Model of Aerodynamic Asymmetry.

BMSH : Bifurcational Model of Static Hysteresis.

CFD : Computational Fluid Dynamics.

Delta-60 : Delta-wing model with 65^o leading edge sweep angle.

DOF : Degrees-of-Freedom of Aircraft.

F16XL : a NASA version of Lockheed Martin F16.

FOM : Figure-of-Merit.

FTR : Free-to-Roll.

GTA : Generic Tailless Aircraft.

LAFO : Large Amplitude Forced Oscillation test.

NASA : National Aeronautics and Space Administration, USA.

PoDE : Polynomial Differential Equation.

PSD : Power Spectrum Density.

SAFO : Small Amplitude Forced Oscillation test.

VVEs : Volterra Variational Equations.

VVM : Volterra Variational Model.

Chapter 1

Introduction

1.1 Introduction to Unsteady Aerodynamics

1.1.1 Unsteady Aerodynamic Phenomena

Unsteady aerodynamics arises due to various flow phenomena which cause time-dependent change in pressure distribution on the surface of a wing or airfoil. This can be in response to change in boundary conditions affected by change in flow incidence angles, control surface deflection etc. or due to flow instability. A high-performance delta-wing aircraft, whose typical geometry is as given in Fig.(1.1,a), encounters significant effects of unsteady aerodynamics in three regions of its flight envelope [1]. The blue region in Fig.(1.2) is the normal operating flight envelope of an aircraft. In this region, the flow on wings is attached. The effects of unsteady aerodynamics are well understood and the modeling of loads can be done using any one of the numerical simulation methods, wind tunnel test data and flight test data . The unsteady aerodynamic phenomena called Stall and Abrupt Wing Stall (AWS) are observed on the flight envelope boundaries of a high performance aircraft as indicated in Fig.(1.2). Identification of these two phenomena using experimental data is the main objective of this thesis.

The occurrence of these unsteady aerodynamic phenomena restricts the two flight envelope boundaries of a high-performance aircraft as these are difficult to model and then utilized in the design process. However, these envelope boundaries are critical for the aircraft's operational effectiveness. The first boundary at high angle-of-attack and low-Mach number flight conditions is restricted by unusual flight dynamics due to occurrence of Stall. In a tactically advantageous position, a delta-wing high-performance aircraft is required to perform a nose pointing maneuver even at the cost of low-speed (low-energy state). This requires the aircraft to venture into high angle-of-attack flight regimes near stall at low Mach number [2].

At stall angle-of-attack, flow separates from the upper surface of an airfoil. The

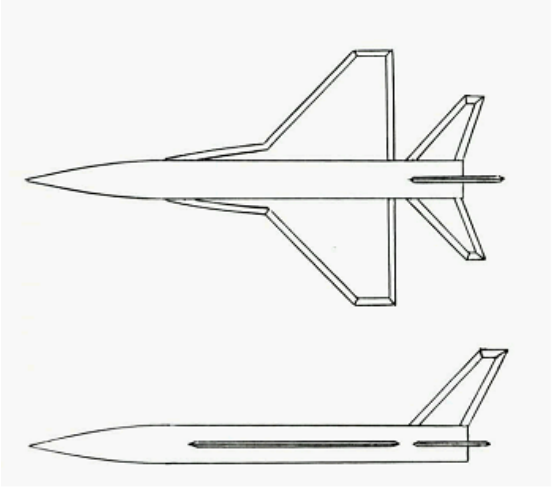

(a) WG16B Delta-wing research model [3].

(b) Vortices on the F18-HARV in flight [4].

Fig. 1.1. Geometry and Wing leading-edge Vortices of a delta-wing high-performance aircraft.

normal force acting on the airfoil remains approximately same, and then decreases with increase in angle-of-attack. The location of flow separation point on the airfoil shifts towards leading edge in a quasi-steady pitch-up motion. In case of low aspect-ratio delta-wing configurations, there are vortices formed from the leading edges of wings, as seen in the smoke flow visualization on the F18-HARV aircraft in flight in Fig.(1.1,b). These vortices cause a suction effect on the upper surface and hence an additional lift component. Similar to airfoil stall, these vortices breakdown on the surface of a wing at stall angle-of-attack. The chordwise vortex breakdown location on the wing also shifts upstream with increase in angle-of-attack.

The unsteady aerodynamics in stall conditions is fundamentally different from that in attached flow conditions. The location of the point of flow separation on an airfoil or vortex breakdown location on a delta wing, have a dominating effect on the surface pressure distribution and hence on the aerodynamic loads. These points move on the surface with a finite time-lag in response to pitching or plunging motions. Therefore, the aerodynamic loads are dependent on the history of aircraft motion, and not just it's instantaneous kinematic states. The resulting incremental change in unsteady variation of loads is significant. Therefore, the mathematical model of an aerodynamic load in stall conditions should be able to reproduce the effect of different aircraft motion time-histories on the aerodynamic load. Moreover, this dependence needs to be identified using a finite amount of dynamic wind tunnel test data.

In the stall angle-of-attack region, the reduced frequency of motion k of vortex breakdown location is of the order of $k \in [0.1\, 0.2]$. The reduced frequency of operation of a rapidly maneuvering aircraft is of comparable magnitude. Hence, the unsteady variation of aerodynamic loads and flight mechanics of the aircraft in the stall region significantly

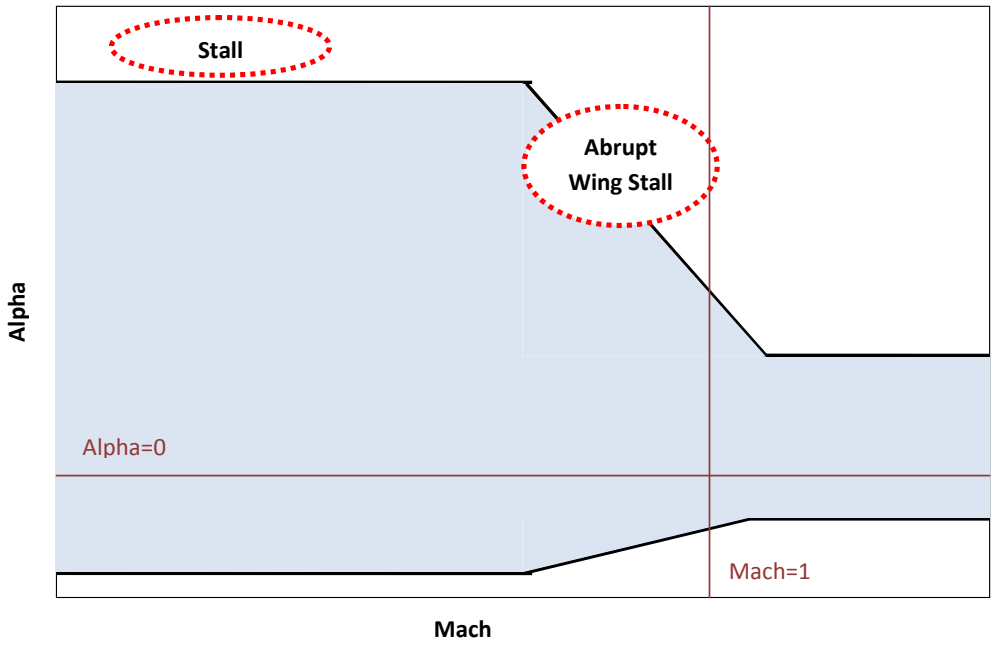

Fig. 1.2. Flight envelope boundaries that have significant nonlinear and unsteady aerodynamics.

affect each other. Therefore, it is important to develop a high fidelity model of unsteady aerodynamic loads, and to characterize its effects on flight mechanics.

The second flight envelope boundary is restricted by occurrence of AWS phenomena at high sub-sonic Mach number and high angle-of-attack. An aircraft in a dog-fight produces best performance by executing rapid rolling, turn-around maneuvers in a high energy state. Such flights happen on this part of the flight envelope. However, this fight envelope boundary of a delta-wing aircraft is conservatively curtailed for many aircraft due to problems in its lateral stability [5].

At high subsonic Mach numbers, there are shock pockets formed on the surface of a delta-wing. The shock-pockets have multiple equilibrium locations for the same kinematic state of the aircraft. When the equilibrium flow dynamics on the two sides of the wing are different, the aircraft exhibits a lateral instability. This is due to rolling moment caused by the asymmetrical flow even when the side-slip angle is zero. Hence, the aircraft rolls about its body axis and can exhibit a variety of trajectories like abrupt roll-of motion, wing-rock motion etc. This can be critical to the controlled flight and safety of the aircraft.

While this unsteady aerodynamic phenomena has been known to cause problems in flight for three to four decades, it has been studied comprehensively only recently [5]. Therefore, there is limited information on flow dynamics in AWS conditions. The

two most prominent features of variation in rolling moment in AWS conditions are the presence of static hysteresis and mild unsteady variations with respect to side-slip.

1.1.2 Challenges in Unsteady Aerodynamic Modeling

In the normal flight envelope regime, classical methods developed almost a century ago are used for modeling the unsteady component of aerodynamic loads. However, these methods are not suitable for modeling the unsteady aerodynamic loads at higher angles-of-attack, and both low and high sub-sonic Mach number regions of the flight envelope indicated in Fig.(1.2). This is due to various reasons highlighted in this section.

The unsteady variation of aerodynamic loads can be considered in time-domain or frequency domain. The dependence of longitudinal aerodynamic loads on the time-history of angle-of-attack $\alpha(t)$ can be considered in different ways. In the classical formulations, it is considered using a Taylor series expansion about a certain mean value α_0. In this case, the unsteady variation of loads becomes a function of time derivatives, i.e $\alpha(t), \dot{\alpha}(t), \ddot{\alpha}(t)...$ and $\beta(t), \dot{\beta}(t), \ddot{\beta}(t)....$ The aerodynamic coefficient is linearized with respect to these variables, and the resulting derivatives, $C_{Z_{\dot{\alpha}}}$ and $C_{m_{\dot{\alpha}}}$ are used in the aerodynamic model. An alternative time-domain approach called the Functional expansion approach has not been explored much in literature, and it is discussed in Section 1.3.

In frequency domain, the unsteady variation of loads is interpreted in terms of change in phase angle and amplitude in comparison to input flow incidence angles. The change in phase angle shows the effect of lag in response of a force or moment to change in incidence angle. In wind tunnel experiments using harmonic inputs in $\alpha(t)$, it is found that the unsteady variation of loads can be approximated by a simple first order transfer function for low α or attached flow conditions. This does not hold good in stall region as the response load contains higher order harmonics of input frequency and it depends on the amplitude of input. In AWS conditions, the variation of aerodynamic loads is bifurcational in nature. In frequency domain, such a response produces sub-harmonics of the input frequency.

In the low angle-of-attack region or attached flow conditions, the effect of unsteady variation of loads is not significant. Hence, using just the first two terms of the Taylor series expansion of angle-of-attack time history suffice. These two terms are called the stability derivative and acceleration (or damping) derivative. These derivatives are included in the aircraft's aero-database in the form of look-up tables as a function of angle-of-attack and sometimes side-slip. This approach is widely used in the industry to model the unsteady aerodynamic effects for both high-performance and transport aircraft configurations. The derivatives are estimated from wind tunnel experiments or numerical

methods. However, this mathematical structure cannot represent the unsteady variation of aerodynamic loads in the stall region [6].

Assuming incompressible and attached flow conditions, simple numerical models of unsteady aerodynamics can be derived from first principles. Theodorsen developed an analytical closed-form model of unsteady aerodynamics due to pitching or plunging motion of thin airfoils [7]. This solution is a function of kinematic states and Theodorsen functions (in frequency domain). Since the model was derived for aeroelastic flutter applications, a disturbance in the form of small amplitude harmonic pitching motion was considered in its derivation. He further established that the significance of unsteadiness of flow is completely indicated by the dimensionless or reduced frequency $k = \frac{\omega \bar{c}}{2V_\infty}$, and that it can be neglected for motions with $k < 0.2$. In the stall region, although the reduced frequency of pitching motion is less than 0.2, the unsteady component of load is significant.

The classical concepts proposed by Theodorsen and the follow-on works of Wagner and Küssner, have inspired the methods for modeling unsteady aerodynamic loads in other parts of the flight envelope. Wagner developed a model considering the time-lag in lift on a wing starting from rest. Such a motion of the wing corresponds to step input in angle-of-attack (and resulting change in aerodynamic load is called indicial response) [8]. The model structure was in the form of a convolution integral in time domain, which was later simplified to be in the form of ordinary differential equations. Küssner investigated the unsteady effect of gust on an airfoil (impulse input in angle-of-attack) [9]. All these formulations are valid only at low speeds and attached flow conditions.

The time-history dependence of an aerodynamic load in the stall region is reflected in a forced oscillation wind tunnel test as its dependence on frequency and amplitude of sinusoidal pitching motion input. In other words, the stability and acceleration derivatives become functions of the frequency of sinusoidal pitching inputs. Moreover, these derivatives are not well-defined for variation in aerodynamic loads in response to large amplitude sinusoidal inputs. Therefore, a special mathematical model structure with an inherent correlation with the fundamental features of flow dynamics is essential for modeling the unsteady variation of aerodynamic loads in stall. This problem is the primary focus of this thesis.

In the AWS region, the flow dynamics is complicated and the numerical methods of modeling have met with limited success. In addition to unsteady effects, the quasi-steady variation of rolling and yawing moments also exhibits hysteresis with respect to side-slip. This is a strong nonlinear phenomena which cannot be modeled using the unsteady modeling approaches proposed for stall region. The research on this topic has been limited due to lack of availability of experimental data. Free-to-roll tests are used for prediction of

occurrence of this phenomena, and this data can only be used qualitatively for modeling the variations in rolling and yawing moments.

Some of the methods for modeling the generic hysteresis phenomena proposed in literature are discussed in Chapter 6. These methods are found to be unsuitable for representing AWS. Hence, there is a need for special mathematical structure for modeling this phenomena. The identification approaches for this phenomena proposed in literature are semi-empirical and not generic. Hence, a novel approach for modeling AWS is presented in this thesis.

The rest of this chapter is focused on modeling the unsteady aerodynamic loads at low Mach number regimes. The literature on modeling of unsteady loads in AWS conditions is severely limited. Hence, it is presented along with the research on modeling AWS in chapter 6.

The nonlinear and unsteady aerodynamics at Stall and AWS boundaries are difficult to model, and thereby impede the design of a safe and reliable control system. Hence, the current thesis is directed towards development of reduced order mathematical models of aerodynamic loads in these regions of the flight envelope. This thesis presents a comprehensive theory for identification of unsteady aerodynamic loads using a novel approach called the Volterra variational modeling approach for delta-wing aircraft configurations. The theory is demonstrated by application of this approach to modeling the longitudinal coefficients of Generic Tailless Aircraft (GTA) and a NASA version of Lockheed Martin F16 (F16XL) aircraft using forced oscillation wind tunnel data. A novel mathematical model of the rolling moment coefficient at AWS conditions is presented in this thesis.

Before discussing the approaches for modeling the unsteady aerodynamic loads proposed in literature, the applications in which the research presented in this thesis is important are discussed briefly in the next section.

1.1.3 Unsteady Aerodynamics in Various Applications

A modern high performance aircraft is expected to undertake high angle-of-attack maneuvers to exhibit superior combat capabilities [2]. In such flight conditions, the aerodynamic loads acting on the aircraft are normally investigated in dynamic wind tunnel tests with inputs like sinusoidal oscillation, ramp pitching, wind-axis rolling etc. [1]. A high fidelity model of unsteady aerodynamic loads acting on the aircraft is essential for flight dynamic analysis, flight system identification, 6DOF simulation for pilot training and analysis of the flight envelope protection features of the Flight Control System [10]. Hence, it has been studied extensively in dynamic wind tunnel tests [3], and a variety of mathematical modeling approaches have been proposed in literature [11, 12, 6].

Fig. 1.3. Nanohummingbird, a flapping wing Miniature-aerial-vehicle developed by Aerovironment Inc.

Accurate prediction of aerodynamic loads acting on the rotor blades of a wind turbine is essential for optimizing their structural strength and performance. At higher wind speed conditions, the rotor blade aerodynamics is affected by flow separation and dynamic stall. A major challenge in predicting the aerodynamic loads on wind turbine blades is the mathematical modeling of the variation of unsteady aerodynamic loads acting on it [13]. There are fundamental limitations in some models proposed in literature, and in some cases their implementation is ambiguous or complicated. A review of the application of all the currently available approaches to this problem has highlighted their shortcomings [13]. It concluded the need for a more sophisticated nonlinear modeling approach for unsteady aerodynamic loads acting on the rotor blades.

The problem of aero-elastic modeling of the buffeting of helicopter blades requires a reliable model of unsteady aerodynamics [14]. The helicopter blades undergo a sinusoidal motion in pitching in each rotation during forward motion of the helicopter. This pitching motion is typically at high-rates and results in unsteady variation of loads acting on it. An unsteady aerodynamic model is also required to determine the performance limitation of the aircraft due to fatigue of the unsteady aerodynamic loads.

Recently, miniature flapping wing aircraft of span less than $30cm$ have been developed; for example Nano-Hummingbird developed by Aerovironment.Inc is shown in Fig.(1.3). These aircraft use a bird-like flapping motion to generate much higher unsteady lift due to vortices. Although, the associated aerodynamics is known to be complicated for mathematical modeling; for advancement in technologies for flapping wing aircraft, a simple and nonlinear unsteady aerodynamic modeling method is important [15].

1.2 Unsteady Aerodynamic Modeling Approaches in Literature

For all the applications stated in the previous section, researchers have developed reduced order mathematical models representing the nonlinear and unsteady variation of aerodynamic loads acting on the aircraft. Most of the research has been focused on use of appropriate model structures and its parameter estimation methods using dynamic wind tunnel test data. The traditional method of using stability and acceleration derivatives is known to have several mathematical and practical problems to model this unsteady variation of aerodynamic loads [16]. Hence, a variety of advanced mathematical model structures have been proposed in literature, which are briefly discussed in this section.

The dependence of aerodynamic loads on the aircraft's motion pre-history in stall region can be expressed mathematically in two fundamental forms; the exterior differential representation by Van der Schaft [17], and the functional expansion of nonlinear system response by Vito Volterra [18]. Goman-Khrabrov presented a State-Space model based on the former theory [11], while Tobak-Schiff extended the later concept to pioneer a new formulation called the Indicial Theory [12]. Most of the model structures proposed in literature are based on either of these mathematical theories, and have been consistently applied to many aircraft case studies. There are some other semi-empirical modeling approaches which have fewer advantages than shortcomings. All these approaches are briefly presented in this section. Some of these model structures will be shown to be directly connected to and consistent with the approach presented in this thesis.

1.2.1 State-Space Approach based Models

State-space approach for modeling unsteady variation of aerodynamic coefficients uses differential equations to represent the effect of input history on the output state. The identification of aerodynamic load using experimental data simple reduces to parameter estimation using any experimental data. The mathematical properties of the structure and interpretation of its parameters can be correlated to the phenomenological features of unsteady aerodynamics, to establish a link between them. This also implies that the estimated model is not just data-true but a systematic representation of system dynamics. It is because of these advantages, that the State-space approach for modeling unsteady aerodynamics proposed by Goman and Khrabrov has been widely used in the research

related to the topic [11].

$$F_k(C, \frac{dC}{dt} ... \frac{d^kC}{dt^k}) = N(h, \frac{dI}{dt} ... \frac{d^kI}{dt^k}) \tag{1.1}$$

Goman and co-workers have presented several model formulations in the state-space form, based on the structure in Eq.(1.1), and the phenomenological features of aerodynamics in the stall angle-of-attack regime. In this equation, the unsteady aerodynamic system can be defined by the outputs $C = (C_X, C_Y, C_Z, C_l, C_m, C_n)$ and inputs $I = (\alpha, \beta, p, q, r)$. This nonlinear differential structure can account for the effect of the history of inputs $I(t)$ on the output of the system $C(t)$ as proved in [17].

$$\begin{aligned} C_L = C_L^{nl}(\alpha, x) + C_{L_q}^{att} \frac{qc}{2V} + C_{L_{\dot\alpha}}^{att} \frac{\dot\alpha c}{2V} \\ \tau_1 \frac{dx}{dt} + x = x_0(\alpha - \tau_2 \dot\alpha) \end{aligned} \tag{1.2}$$

The first seminal work that appeared in English in 1994, is based on their hypothesis of characteristic time scales of vortex breakdown location governing the unsteady variation of aerodynamic loads. In this structure, the lift coefficient consists of three components. The components $C_{L_q}^{att}$ and $C_{L_{\dot\alpha}}^{att}$ represent the unsteady effect of change in q and $\dot\alpha$ respectively, assuming attached flow conditions. The component $C_L^{nl}(\alpha, x)$ represents the quasi-steady and nonlinear variation of lift determined by the combined effect of angle-of-attack and vortex breakdown location. Thus, it captures the strong unsteady lift variation in stall region.

The vortex breakdown location or flow separation point is represented by an internal state variable x. The first order differential equation in x in Eq.(1.2) models the lag in change in vortex breakdown location due to pitching motion, and the time-constant τ_1 represents its characteristic time-scale. In low angle-of-attack region or attached flow conditions, this characteristic time-scale is one order of magnitude smaller than that in the stall region. The second time-constant τ_2 is assumed to be the characteristic time-scale of other effects like convective lag, boundary layer effects etc.

This model has been shown to produce accurate results for unsteady variations in C_Z, C_m and C_l coefficients estimated using extensive forced oscillation wind tunnel data for both airfoils and delta-wing aircraft [11]. The model structure was also validated by system identification using appropriate flight test data at Central Aero-hydrodynamic Research Institute (TsAGI), Russia [11] and the German Aerospace Research center (DLR) [19]. The model has been used in a variety of applications like modeling aerodynamic flutter at stall.

This model is accurate but insufficient on two grounds. The basic hypothesis of

the internal state representing the vortex breakdown location on a delta-wing or flow separation point on an airfoil, holds good. But it was later found that the value of time-constant τ_1 and the time-scale measured in experimental flow visualization studies in wind tunnel and water tunnel tests, are different by an order of magnitude [11]. Therefore, the interpretation of τ_1 and estimation based on it, is erroneous.

The second problem is the incapability of the structure to model nonlinear variations in time, typically significant for the pitching moment coefficient of delta-wing aircraft. The nonlinear variations in pitching moment coefficient are manifested as higher order harmonics in the harmonic input experimental data, discussed in detail in the later sections. Although the variation of coefficient due to change in angle-of-attack is nonlinear due to the second time-constant τ_2, it cannot be used to capture the nonlinear variations reliably. This issue was first discussed in [20], and is revisited in this thesis.

$$\begin{aligned} C_L &= C_L^{pt}(\alpha) + C_{L_q}^{pt}\frac{qc}{2V} + C_{vb}(t) \\ \tau_1\frac{dC_{vb}}{dt} &= \sum_{i=1}^{i=m} k_i(C_{vb_0}(\alpha) - C_{vb})^m \end{aligned} \tag{1.3}$$

These problems are done away with by the second model structure, as given in Eq.(1.3), called the Abramov-Goman model. In this structure, there is no term for the vortex breakdown location, and the unsteady variation is modeled for an incremental component of load. It is based on the hypothesis of partitioning of loads according to their source as potential flow C^{pt} (excludes the lift created by vortices), and Vortical flow C_{vb} [21, 22]. The unsteady component of load due to vortex breakdown dynamics is modeled using a nonlinear differential equation of C_{vb}. In this equation, $C_{vb_0}(\alpha) = C_{L_{st}} - C_L^{pt}$, which represents the incremental lift force due to vortices when the wind tunnel model is held static. The polynomial terms in the differential equation model the nonlinear nature of unsteady variation of loads observed for large amplitude inputs in angle-of-attack. A maximum of cubic polynomial nonlinearity has been found to be sufficient for various aircraft.

$$\begin{aligned} C(t) &= C^{att}(\alpha) + C_q^{att}\frac{qc}{2V} + C_{dyn}(t) \\ \Delta C(\alpha) &= C_{st}(\alpha) - C^{att}(\alpha) \\ \tau\frac{dC_{dyn}}{dt} + C_{dyn} &= k_1\Delta C(\alpha)\dot{\alpha} + \sum_{i=2}^{i=m} k_i(\Delta C(\alpha) - C_{dyn})^m \end{aligned} \tag{1.4}$$

In a revised form of the Abramov-Goman model presented in [23], an aerodynamic load (C_Z, C_m, C_l) is partitioned into the components of attached flow C^{att}(obtained using Polhamus suction analogy) and a hypothetical dynamical component $C_{dyn}(t)$, as given

in Eq.(1.4). This structure is not restricted by the classification of components based on its origin. The parameters (τ, k_1) characterise the linear variations in time, while $(k_2, k_3, ...)$ tune the model to capture nonlinear nature of unsteady variations. The model parameters are also estimated separately using data which exhibit linear or nonlinear unsteady variation of coefficients.

A unique advantage of the revised Abramov-Goman model is that it can reproduce the strong nonlinear variations arising from bifurcational aerodynamics phenomena like the so-called static hysteresis [20]. Some of the airfoils have a distinct static hysteresis in variation of C_Z and C_m versus α. The same model structure, but with a different parameter estimation procedure was also shown to be useful for modeling the static hysteresis in C_Z and C_m coefficients in [20]. To model unsteady variations in presence of static hysteresis, Lutze.et.al considered the Goman-Khrabrov model with two steady-state functions depending on whether aircraft is pitching up or down [24]. This model produces clearly unreliable results for the case when aircraft does not cross the critical states or the aerodynamic bifurcation points of the static hysteresis curves.

Fan and co-workers presented several adaptations of the Goman-Khrabrov model. They included an additional time-constant τ_3 to correct the effective angle-of-attack, although the physical interpretation of this term is ambiguous [25, 24]. The steady-state value of the aerodynamic coefficient was modeled using an inverse exponential function with two additional parameters. They also introduced more complications to the Goman-Khrabrov model, like considering two internal states, static lift dependence as a quadratic polynomial of internal state. It seems that these nonlinear correction terms were introduced to obtain better accuracy at the cost of loss in simplicity and interpretations of the model structure.

$$x_0(\alpha) = \frac{1}{2}\{1 - \tanh[A_1(\alpha - \alpha^*)]\} \tag{1.5}$$

For estimation of aerodynamic load coefficients in the stall region using flight test data, Singh and Jategaonkar used Goman-Khrabrov model successfully [19, 26]. The only difference from the standard structure in Eq.(1.2) being that the static variation of internal state $x_0(\alpha)$ was approximated by an hyperbolic tangent function of angle-of-attack as given in Eq.(1.5). In this equation, α^* is the angle-of-attack at which vortex breakdown reaches half of the root-chord length of the wing $x_0(\alpha^*) = 0.5$, and A_1 is a parameter defining static stall characteristics of the airfoil. It can be determined from the wind tunnel test data or identified from flight test data.

This model is shown to produce satisfactory results for longitudinal coefficients [19]. To model the rolling moment coefficient, separate models of vortex breakdown location or the internal state were considered for the left and right wings. Although some minor

unexplained discrepancies were observed in the time-histories of (p, q, r) rates, the results were overall satisfactory [26]. These studies also showed the fundamental nature of the Goman-Khrabrov model.

Pashilkar presented an adaptation of Goman-Khrabrov model, in which weighting function of the contributions from attached flow and separated flow was modeled considering multivariate orthogonal polynomial functions of internal state [27].

1.2.2 Nonlinear Indicial Theory based Models

The Indicial theory is the second most widely stated modeling approach presented in literature. The system is assumed to be linear time invariant and causal. The linear indicial formulation is based on use of a convolution integral of the transients of a system response to step change in boundary (input) conditions. A generic formulation of the system response $f(t)$ to input $u(t)$, assuming that $f(t)$ is a smooth function of $u(t)$ and can be locally linearized at $u = u_0$, is as given in Eq.(1.6). In this equation, τ is the running time variable, and t is time.

$$f(t) = \frac{\partial f}{\partial u} \mid_{u=u_0} u(0) + \int_0^t \frac{\partial f}{\partial u}(t-\tau)\frac{du}{d\tau}d\tau \tag{1.6}$$

In this formulation, $\frac{\partial f}{\partial u} \mid_{u=u_0}$ is called "indicial function" and it is the basic unit characterizing the system dynamics. This local approximation becomes accurate at $\Delta u \to 0$, and is an exact solution if $f(t)$ is a linear function of $u(t)$.

$$C_a(t) = C_a(0) + \int_0^t \frac{\partial C_a}{\partial \xi}(t-\tau)\frac{d\xi}{d\tau}d\tau \tag{1.7}$$

Based on this theory, the linear indicial mode of an unsteady aerodynamic coefficient can be stated as in Eq.(1.7). In this equation, C_a is an aerodynamic force or moment coefficient, ξ is vector of aircraft states affecting the coefficient like (α, β, p, q), and $\frac{\partial C_a}{\partial \xi}$ is the indicial function. The indicial function can be interpreted as a transient load due to step change in ξ at a particular instant. Variety of methods for identification of indicial functions of aerodynamic coefficients have been proposed in literature.

The linear indicial functions presented an approach to model a dynamic system using just a few indicial responses over the relevant range of operational conditions. This formulation was extended using the Duhamel's superposition integrals to introduce a nonlinear formulation by Tobak and Schiff [12]. The indicial functions are considered as nonlinear functionals of angle-of-attack and pitch-rate [28, 29], based on Volterra's original conception of the "Functional expansion representation of dynamic systems" [18]. A generic Nonlinear Indicial theoretical formulation was shown to encompass the

Volterra series in [29].

Tobak.et.al. provided a detailed interpretation and simplification of their nonlinear indicial formulation for modeling unsteady aerodynamics in [12]. Since the mathematically rigorous formulation cannot be used for identification of a reduced order model of unsteady aerodynamics using wind tunnel data, they introduced a series of simplifications based on a number of assumptions. The most important assumptions are that, (i) functionals are considered to be dependent on elapsed time assuming that the system has limited memory, and (ii) the aerodynamic coefficient is linear analytic (can be expressed as a polynomial in α) over the angle-of-attack range under consideration.

$$C_a(t) = C_a(0) + \int_0^\infty C_{a_\alpha}(t-\tau;\alpha(\tau),q(\tau))\dot{\alpha}(\tau)d\tau + \int_0^\infty C_{a_q}(t-\tau;\alpha(\tau),q(\tau))\dot{q}(\tau)d\tau \tag{1.8}$$

The resulting simplified form of the model is given by Eq.(1.8). In this equation, C_{a_α} is the indicial response at an instant τ due to input $\dot{\alpha}(\tau)$, and C_{a_q} is similarly defined. This is further simplified as,

$$C_a(t) = C_a(0) + \frac{l}{V}C_{a_q}(\alpha)q(t) + \int_0^\infty F_{a_\alpha}(t-\tau;\alpha(\tau),q(\tau))\dot{\alpha}(\tau)d\tau \tag{1.9}$$

The deficiency functional $F_{a_\alpha}(\cdot)$, when considered as a decaying exponential function, reduces the model to a simple linear differential form as [30],

$$\begin{aligned} C_a(t) &= C_a(0) + \frac{\bar{c}}{2V}C_{a_q}(\alpha)q(t) - \eta(t) \\ \dot{\eta}(t) + a\eta(t) &= b_1\dot{\alpha}(t) \end{aligned} \tag{1.10}$$

where, $\eta(t)$ represents incremental unsteady effect. Thus, the unsteady effect is captured by a linear differential equation with $\frac{1}{a} = \tau$ as the relaxation time-constant, and b_1 as the dynamic gain parameter. This simplified model structure is widely referred to in literature as the linear indicial model of unsteady aerodynamic loads. In this form, indicial model is equivalent to many other unsteady modeling approaches presented in literature as discussed in Section 1.2.4.

This model is insufficient to model the nonlinear dynamical variations especially witnessed in the pitching moment coefficient of delta-wing aircraft. To introduce this capability, the model parameters were assumed as continuous functions of angle-of-attack $a(\alpha)$, $b_1(\alpha)$. In [30], these parameter functions were assigned a definite dimension by considering them in the form of polynomial functions of angle-of-attack. This model was shown to be sufficiently accurate for identification of the aerodynamic coefficients

of F16XL using forced oscillation wind tunnel data [30, 31]. Similar model was used to model the rolling moment coefficient of a transport aircraft in the stall region [32].

$$C_L(t) = C_L(t;\alpha_0) + \int_0^{\tau_c-\epsilon} C_{L_\alpha}(t,\tau;\alpha(\xi))\dot{\alpha}(\tau)d\tau + \int_0^{\tau_c+\epsilon} C_{L_\alpha}(t,\tau;\alpha(\xi))\dot{\alpha}(\tau)d\tau + \Delta C_L(t;\alpha_c) \tag{1.11}$$

The linear Indicial model of Eq.(1.8) is not capable of modeling the bifurcation points or critical states in static variation of coefficients (like C_L vs. α, C_n vs. β). The discontinuities in the static variation, termed mathematically as lack of Frechet differentiability, are called as the critical states. Hence, a critical state functional $\Delta C_L(t;\alpha_c)$ for modeling the transients during crossing of critical angle-of-attack α_c was introduced, as given in Eq.(1.11) [28]. The unsteady variation of coefficient on either side of the critical state is modeled separately.

The only application of this formulation was for modeling the variation of rolling moment coefficient with roll angle, by Myatt in [33]. The transient response for critical state crossing is identified from special WT tests with ramp-hold motions across the identified critical states. The transient functionals are complicated combinations of sinusoidal and exponential functions. Whether these are generic, both mathematically and for the physical flow process, can be debated. Later, Myatt.et.al. presented a nonlinear model obtained by scheduling the parameters of linear models between each critical state crossing; and they also proved the connection of this model to the Nonlinear indicial response model with critical states crossing [34].

1.2.3 Other Unsteady Aerodynamic Modeling Approaches

Although the modeling approaches based on State-pace and Linear indicial theory have been most widely used for high performance aircraft, some modeling approaches have been proposed for other applications involving unsteady aerodynamic loads. Some of these approaches have been applied to high performance aircraft with limited success. The most important one of these are ONERA dynamic stall model and Neural Network model. The modeling approaches based on the Functional expansion formulation like Volterra series are discussed in a separate section.

ONERA dynamic stall model is primarily used to model the unsteady aerodynamic loads on helicopter blades near stall. In this case, there are higher frequency oscillations in the variation of aerodynamic loads in response to sinusoidal pitching motion input of high non-dimensional frequency [35, 36]. This model continues to be considered till date for modeling the unsteady aerodynamics of Helicopter blades [14].

The ONERA dynamic stall model is given by equations,

$$\begin{aligned} C_L(t) &= F_1 + F_2 \\ \dot{F}_1 + \lambda F_1 &= \lambda F_l + (\lambda s + \sigma)\dot{\alpha} + s\ddot{\alpha} \\ \ddot{F}_2 + a\dot{F}_2 + rF_2 &= -(r\Delta + e\dot{\Delta}) \end{aligned} \tag{1.12}$$

where, $F_1(t)$ indicates variation in the linear aerodynamics angle-of-attack regimes, and $F_2(t)$ gives variations in the stall angle-of-attack regime. The parameters λ, s, σ, a, r are function of angle-of-attack, to be estimated from experimental data. The function $F_l(\alpha)$ is extrapolation of the linear static curve to high angle-of-attack beyond stall. The function $\Delta(\alpha)$ is the difference between $F_l(\alpha)$ and actual nonlinear static curve from WT data. The first order differential equation in $F_1(t)$ in effect reproduces the effect of stability and acceleration derivatives, while the second order differential equation in $F_2(t)$ produces unsteady load in stall regime considering the difference in load between attached flow and vortex-breakdown flow as an input.

This model makes use of two important concepts in the model structure formulation, (i) use of second order differential to introduce the effect of two time-scales into the model, and (ii) capability of the model to capture higher frequency oscillations in variation of loads. These concepts are pertinent to the Volterra Variational Model (VVM) proposed in this thesis as well, as discussed in Section $5.4.4$.

ONERA dynamic stall model was applied to modeling the unsteady variation of longitudinal coefficients using a comprehensive set of experimental data in [35]. The results are not satisfactory for C_Z and there is a gross mismatch in case of C_m. This happens because parameters are not considered as function of α, while the characteristics of unsteady flow are dependent on it. The second issue in this model is that there is no clear distinction or demarcation between linear and nonlinear nature of unsteady variations as in the case of other unsteady modeling approaches.

Neural Network approach is often considered to be a can-do-all technique for modeling various systems. It was applied to modeling unsteady aerodynamics in [37]. In this approach, a network of functions is "trained" using the given experimental data until it fits consistently across the entire set. Hence, the approach can produce the best fit to the given data. Moreover, it is so generic that it is applicable to any aircraft configuration and any experimental data type.

However, the Neural network approach suffers from several practical shortcomings. It can be termed as a data-true only model, as the model often fails to interpolate or extrapolate for other inputs. For example, if a sinusoidal input test data is used in training, the results may not be satisfactory for simulations using step inputs. It is also

a "Black-box" model, as it does not provide any physical interpretations. Hence, there is no guarantee about its consistency with the aerodynamic features observed in various experiments. Also, there is no knowledge about the limits of operational conditions under which it can be used in simulations and analysis. Therefore, the Neural network approach is not suitable for modeling unsteady aerodynamic loads of aircraft.

A Neural-network approach using a Nonlinear auto-regressive model with exogenous variables structure is applied to model unsteady variation of loads in [38, 39]. In this model structure, the current state of the system is considered as a weighted sum of the inputs and system states at nine previous time-steps. The weighting functions are inverse exponential functions, and their parameters are estimated using wind tunnel test data. It is shown to produce better accuracy than the Abramov-Goman State-space model. However, it suffers from the usual shortcomings of a neural network model.

In the latest publication on the topic, a novel method called "Nonlinear Dependency on Angular Rate" for modeling the nonlinear unsteady variation of C_m is proposed in [38]. It simply uses spline curve fitting of $C_{m_{\dot{\alpha}}}$ versus non-dimensional pitching rate $(\dot{\alpha})$ at each angle-of-attack. This is based on the hypothesis that the wind tunnel model pitching rate $\dot{\alpha} = \Delta\alpha\omega sin(\omega t)$ in a forced oscillation test, includes the effect of both amplitude and frequency in a sinusoidal motion. Hence, the term $C_{m_{\dot{\alpha}}}(\alpha, \dot{\alpha})\frac{\dot{\alpha}\bar{c}}{2V}$ is expected to capture the effect of input amplitude and frequency on the unsteady component of aerodynamic load. Even though this argument is validated using harmonic input wind tunnel test data, it does not hold true for generic inputs like step and ramp pitching motions. This is because the modeling approach inherently assumes that the aerodynamic load can be completely determined by instantaneous values of $(\alpha, \dot{\alpha})$ and may be independent of their trajectory in phase diagram. This is contrary to the basic phenomena of dependence of aerodynamic loads on the aircraft motion-history which causes unsteady variation. The authors have failed to mention the assumption and its repercussion.

Reisenthel.et.al. presented a Volterra Series based approach for modeling nonlinear unsteady variation of aerodynamic coefficients [40]. Since the Volterra kernels cannot be identified using typical harmonic input wind tunnel test data, they are parameterized using orthogonal exponential functions. While identification of the first kernel requires nine parameters, the second kernel requires a 10×10 matrix of parameters.Therefore, the estimation problem becomes unwieldy even for estimation of mild nonlinearity using two kernels. There is no physical interpretation of the model parameters. Hence, this method can be termed to be partially successful at best. This method is revisited and compared with the proposed VVM in detail in Chapter 5.

Flow-Incidence-Rate-Model is another approach presented in literature [41]. It makes use of a recurrence relation to model the internal state representing the vortex breakdown

Sr. No.	Model/Author	Dynamic Gain	Time-scale
1	State-space/Goman-Khrabrov	$-\frac{K(\alpha)}{\tau_1}, (1+\frac{\tau_2}{\tau_1})\frac{\partial C_L}{\partial x}\frac{\partial x_0}{\partial \alpha}$	$\frac{1}{\tau_1}$
2	PoDE/Abramov-Goman	$\frac{\partial(C_{N_{st}}-C_{N_{pt}})}{\partial \alpha}$	$\frac{1}{\tau}=k_1$
3	Linear differential/Greenwell	$C_{l_{\beta,sep}}$	$\frac{1}{\tau_{sep}}$
4	Linear Indicial/Klien-Murphy	$\frac{T_1+T_a}{T_1}\frac{d\eta_0}{d\alpha}C_{N\eta}$	$\frac{1}{T_1}$
5	ONERA/Tristrant	$\frac{G}{T}$	$\frac{1}{T}$
6	FIRM/Pashikar	$-\frac{C_{Z_{st}}k_1^{\pm}+k_2^{\pm}}{\tau}$	$\frac{1}{\tau}$

Table 1.1. Equivalent parameters of the linearized form of unsteady aerodynamic models available in literature, as presented in [42].

location, while lag in vortex breakdown location is modeled using a first order differential equation of $\dot{\alpha}$. The recurrence relation is mathematically equivalent to a differential equation, but the interpretation of parameters is difficult. The lag in vortex breakdown location changes effective α and not $\dot{\alpha}$. Hence, this model is phenomenologically inconsistent.

1.2.4 Discussion of the Modeling Approaches

A comparative analysis of these modeling approaches in terms of their mathematical structure, physical interpretations and quantitative accuracy for modeling an aerodynamic coefficient, was presented by Greenwell.et.al. in [42, 6]. They drew two conclusions,

1. Most of the successful model structures are equivalent in their linearized form, as per the definition of the model parameters given in Table.(1.1).

2. There is no consensus on the nonlinear model of unsteady aerodynamics, although the revised Abramov-Goman model produces best match for identification using forced oscillation wind tunnel data

All the models listed in Table (1.1) can be reduced to a simple first order transfer function or a linear differential equation with the time-scale and dynamic gain parameters defined as presented in the table. While time-scale parameter is simple in interpretation, the definition of dynamic gain parameter is complicated. This is due to introduction of an extension term to accommodate nonlinear nature of unsteady variations for some aerodynamic coefficients like C_m. Often, this nonlinear term is mathematically empirical or adhoc. Hence, it is difficult to bridge the nonlinear forms of these model structures to allow any coherent interconnection between them.

These models are unsatisfactory on various grounds; the most important ones of which are summarized in Table.(1.2).

Sr. No.	Model	Explanation
1	State-space	No term for nonlinear unsteady variations
2	PoDE	Tuning nonlinear terms is difficult
3	Volterra series	Difficult to estimate, analyse and interpret
4	Linear Indicial	Cannot model nonlinearity in pitching moment
5	ONERA	Unsatisfactory results for delta-wing data
6	PoDE-Static hysteresis	Poor accuracy in some cases
7	Indicial-Static Hysteresis	Special experimental data required

Table 1.2. Shortcomings of the model structures in literature for nonlinear modeling of unsteady aerodynamic loads

The State-space model by Goman and Khrabrov does not include any term to include the nonlinear nature of unsteady variations. The differential equation governing vortex breakdown location is nonlinear due to the time-constant τ_2, which actually is used to model convective time-lag. Also, if the accuracy of the estimated model is unsatisfactory, there is no scope provided to adapt the model structure. This is also a reason for a number of minor changes to this model structure proposed in literature by different researchers.

The PoDE model stucture (Abramov-Goman model) is a simple and practical technique. But, the nonlinearity in the structure cannot be extended to sufficiently model the complex unsteady variations in pitching moment coefficients of some aircraft and high-frequency pitching airfoils. This model is bifurcational in nature which makes its estimation difficult. Onset of bifurcation should be avoided during parameter estimation using a constraint equation. This further hampers the flexibility in model topology to capture the nonlinearity in unsteady variations.

Although the nonlinear indicial theory is a rigorous mathematical framework, its simplified form used in most applications is a locally linear first-order ordinary differential equation. The nonlinear extensions presented in literature are insufficient for modeling nonlinear unsteady variations in pitching moment coefficient. Therefore, the mathematical background of the formulation bears hardly any significance considering the simplified structure that is used in practical applications.

For modeling the coefficients which exhibit hysteresis in their steady variation with flow incidence angles α or β, there are only two model structures proposed in literature. The PoDE model with static hysteresis, also called as the Bifurcational Model of Static Hysteresis (BMSH) presented by Abramov in [20], is a simple and practical model. It can be estimated from commonly available static and dynamic wind tunnel test data. The nonlinear indicial model with critical state crossing requires data from ramp-and-hold input wind tunnel tests. Hence, it is not generic.

Since there is no static hysteresis in variation of longitudinal coefficients with α for delta-wing configurations, these models are not required for modeling unsteady aerodynamics in stall. However, modeling the AWS phenomenon requires such models. However, these models were not suitable for modeling the static hysteresis in rolling moment coefficient versus side-slip seen in AWS conditions. Hence, a novel model is proposed in this thesis. This issue is discussed in Chapter 6, along with a more detailed literature survey.

1.2.5 Parameter Estimation Methodologies

The most commonly used methods for parameter estimation presented in literature are Output-error method [43] and two-step regression technique [22]. The parameters of State-space models are estimated by two-step regression method proposed in [22]. In the first step, the model is linearized considering a small amplitude sinusoidal disturbance. The resulting equations presented a linear relationship between in-phase and out-of-phase derivatives estimated from the small amplitude forced oscillation test data. Therefore, the in-phase and out-of-phase derivatives from at least three different frequencies, are used to estimate the model parameters (τ, k_1) by linear regression method [43]. The remaining parameters introduce nonlinear corrections. These are estimated by output-error method using the entire set of large amplitude forced oscillation data.

Murphy.et.al. have presented two new techniques for parameter estimation. The first one is a frequency domain estimation of parameters using equivalent transfer function of differential models [44], and the second is using Genetic Algorithms [45]. A comparison of the estimated values of parameters using the same WT data, from frequency-domain maximum-likelihood estimation and two-step regression methods, showed that the two methods produce equivalent results subject to tolerance bounds. However, this study was done only for the normal force coefficient and small amplitude forced oscillation inputs of $5\,\mathrm{deg}$ amplitude. The measurements of pitching moment are known to be more sensitive to noise and it is also nonlinear in nature. Hence, the equivalence of results from different estimation methods needs to be probed further.

The identification of coefficients using wind tunnel test data is complicated by the issues of noise in the measured data and nonlinear nature of the dynamic variations.The experimental data is marred by interfering physical effects, measurement noise etc. Some of these issues affecting the experimental data and their effect on the estimated model parameters are presented in [46]. These challenges have been presented in details by comparison of various wind tunnel test data in the AGARD report [3]. In case of F16XL it was noticed that the pitching moment measurements from the experiments with $5\,\mathrm{deg}$ amplitude of input were so corrupted by noise that it could not be used for model

parameter estimation [31]. Therefore, resolving the issues in experimental measurements and nonlinear unsteady variations is important for parameter estimation, and hence the fidelity of the model.

The issues in data processing need to be investigated before using them for parameter estimation. For example, Harmonic analysis and Coefficient-of-determination are used for data-analysis in [32]. The Coefficient-of-determination is used to analyze the effect of filtering on noisy data. This helps to arrive at an engineering judgement of the bandwidth to be used for filtering measured data. However, aggressive filtering of the forced oscillation test data affects the estimated values of in-phase and out-of-phase derivatives. Harmonic analysis indicates the presence of significant components of higher order harmonics in the response data, and hence its nonlinear nature.

The wind tunnel data from forced oscillation tests with large and small amplitudes for various frequencies are commonly used in literature for parameter estimation. Some new testing methods have been developed in the recent past. Application of wide-band inputs implemented as Schroeder sweep was proposed in order to avoid repetitive testing with one frequency input at a time [44]. This is one of the most promising methods for identification of a dynamical system over its operational bandwidth [43].

1.3 Functional Expansion Approaches for Nonlinear System Identification

Three methods are prevalent in literature based on the functional expansion representation of the response of a nonlinear dynamical system as proposed by Vito Volterra in [18]. The nonlinear Indicial theory was developed primarily for modeling unsteady variation of aerodynamic loads, and the related literature is briefly discussed in the last section. Volterra Series and Nonlinear Auto-Regressive Modeling with Exogenous inputs (NARMAX) models are two other widely used modeling approaches presented in literature [47].

Volterra series consists of convolution integrals in higher dimensions and it is determined by its multi-dimensional integrands called Volterra kernels. Although Volterra series is widely used for modeling electrical and physiological systems, it is not much used for identification of nonlinear mechanical systems using experimental data [48]. This is due to two reasons, (i) Volterra kernel estimation requires data obtained using Gaussian random input or multi-tone inputs with very high harmonics [49, 50]; (ii) it is a non-parametric model and offers no physical interpretations which can be correlated with the experimental observations [51].

Application of Volterra Series for modeling has been presented for some aerospace

applications. It was applied for modeling the nonlinear longitudinal dynamics of an aircraft by identification of discretised kernels using neural-network architecture [52]. An approach to model the local nonlinear dynamics of aircraft has also been presented in [53]. Volterra kernel approximation method for modeling aeroelasticity problems is presented in [54]. W. Silva presented a review of its application to aeroelasticity problems for computational and numerical studies [55]. He also presented a method for identification of Volterra kernels using aerodynamic impulse responses from numerical experiments [56].

Reisenthel.et.al. presented several papers on modeling unsteady aerodynamics by identification of approximate kernels in parametric form, and demonstrated its application to X31 aircraft data [40, 57, 58, 59]. This method is discussed again in Chapter 5.

NARMAX is a discrete time recursive model that considers a weighted effect of the past states and inputs on the current state, as well as coupled effect of noise [60]. Although parametric, it does not provide physical interpretation and estimation of noise model is complicated as it may cause the optimization to diverge [61]. However, NARMAX model can be used for estimation of Fourier transform of Volterra kernels called Generalized Frequency Response Functions (GFRFs) [62].

VVM proposed in this thesis is derived from Volterra series, and hence belongs to this category of models. This thesis is the first application of the Volterra variational structure to model any aerospace system, and even any mechanical system, to the best of our knowledge.

1.4 Motivation

There is a tremendous interest in the industry on modeling of the aircraft aerodynamics at high angle-of-attack. Recently, the American aviation regulator Federal Aviation Administrator has mandated that the commercial airline pilots be exposed to flight dynamics outside the normal flight envelope on Flight Simulators. There were two major international research programs with a particular focus on modeling the stall conditions of a transport aircraft. National Aeronautics and Space Administration, USA (NASA)-Langley Research Center pioneered a major project under the "Aviation Safety Program" in the US [63], and a similar program called "Simulation of Upset Recovery in Aviation" (SUPRA) was undertaken in Europe through the Framework Program-7 research support [64, 65]. Some of the methods previously developed for delta-wing configurations were applied to transport aircraft aerodynamic modeling in these projects. These efforts have highlighted the need for a generic and nonlinear approach to modeling unsteady aerodynamic loads, as discussed in [32].

There is still no commonly acceptable nonlinear model structure for modeling unsteady aerodynamic loads in the stall conditions. The unsteady aerodynamic modeling approaches discussed in the previous section can successfully reproduce the unsteady variation of normal force coefficient, which is mildly nonlinear. However, variations in pitching moment coefficient are significantly nonlinear for Delta-wing, Double-delta and Transport aircraft configurations. Therefore, there is a need for a model structure which can capture the nonlinearity in unsteady variation of aerodynamic loads using variety of wind tunnel test data reliably.

A high-fidelity unsteady aerodynamic modeling approach is essential for improving the design or performance of the systems discussed in the Section 1.2, that is wind-turbine blades, flapping wing aerodynamics, aero-elastic flutter etc.

The problem of unsteady aerodynamics at high angle-of-attack and high subsonic Mach numbers has been known for many years. But it has been a investigated systematically only recently as a part of the NASA-Langley Research Center lead AWS Program. The state-of-the-art of this technology in terms for wind tunnel experiments, analysis methods, modeling methods, is still in preliminary stages. There is a need to improve the modeling techniques of AWS phenomenon so that it can be further used in control law design and flight dynamic analysis processes to improve the aircraft maneuverability.

1.5 Objectives of the Thesis

The objectives of this thesis are as follows:

1. Formulate a modeling approach with the following features which are desired for its adoption by the industry : (i) a generic model structure applicable to a variety of situations in the design process, (ii) a simple parameter estimation procedure which can produce a model of sufficient accuracy, (iii) it can be integrated with the aircraft equations of motion for simulation and flight dynamic analysis, (iv) clear correlation of its mathematical interpretations to features of unsteady aerodynamics.

2. Demonstrate the capabilities of the proposed approach by identification of unsteady aerodynamic loads using industrial-grade data from the wind tunnel tests of the type prevalent in the research community and the industry. Compare the accuracy of results obtained from the proposed approach to that using the PoDE model (as it is the most promising method available in literature).

3. Perform a comparative analysis to show the advantages and disadvantages of using the proposed modeling approach relative to those frequently cited in literature. Prove its consistency or justify a lack of it, to these approaches.

4. Perform flight dynamic analysis using the proposed model to show the effect of unsteady aerodynamics on aircraft dynamics.

5. Present adaptations of the modeling approach which may be useful for modeling other applications involving the unsteady aerodynamic phenomena.

6. Develop a generic model structure for modeling the static hysteresis and unsteady variation in the rolling moment coefficient versus sideslip due to AWS phenomena. Demonstrate its application to the GTA aircraft data obtained from static and Free-to-roll wind tunnel tests.

1.6 Thesis Overview

In chapter 2, the theory of Volterra variational modeling approach using harmonic input response data is presented. Volterra variational equations are derived in the frequency domain, as the Volterra series representation of a generic nonlinear differential system of the type commonly used in systems theory. The proof of a generic method for computation of input bounds for convergence of Volterra series called the Helie-Laroche algorithm [66] is presented in the frequency domain. This proof is simpler and intuitive than the time-domain proof given in [66]. Then, the harmonic input response properties of VVM are presented to develop concepts for the identification procedure. Finally, a comparison of the model structures of PoDE and VVM modeling approaches is presented. These concepts are demonstrated by two examples.

In chapter 3, VVM structure and parameter estimation approach are formulated for identification of the unsteady aerodynamic loads of delta-wing aircraft configurations using forced oscillation wind tunnel data. The implications of different types of nonlinear aerodynamic phenomena, use of dynamic wind tunnel test data, parameter estimation procedure, on the proposed system identification approach are presented in details in this chapter. Mathematical approximations or interpretations of VVM are presented to show its inherent capability to model the features of unsteady aerodynamics, irrespective of the experimental data available.

In chapter 4, three important case studies on identification of aerodynamic coefficients using comprehensive sets of forced oscillation wind tunnel test data, are presented in details. These case studies are for two industrial-grade delta wing aircraft configurations, F16XL and GTA. These case studies demonstrate the proposed identification algorithm

in details; like selection of model structure, processing raw wind tunnel test data, estimation of model parameters using linear and nonlinear VVM structures, selection of appropriate pitching input bandwidth in experiments etc. A quantitative comparison of the performance of VVM and PoDE for modeling the C_m coefficient of GTA is presented to show the superior accuracy of VVM.

In chapter 5, flight dynamic analysis using the VVM and a comparative analysis of the important modeling approaches in literature with VVM, are presented. The impact of unsteady aerodynamic loads on the Short-period mode of an aircraft is demonstrated using classical tools from linear systems theory. Comparative analysis and possible adaptations of VVM structure to produce the features of other model structures presented in literature, are discussed here. Unique advantages in identification of VVM using other experimental inputs like Schroeder-sweep and Ramp inputs are presented. It is shown that the VVM encompasses the mathematical features of all the major modeling approaches presented in literature.

In chapters 6, modeling and analysis of the effects of the AWS phenomena using Free-to-Roll (FTR) and static wind tunnel test data is presented. A literature review is presented to summarize the aerodynamics of AWS and the modeling approaches presented in literature. A novel mathematical structure to model the rolling moment coefficient is proposed. This model is shown to reproduce the static hysteresis in rolling moment coefficient versus sideslip and the features of unsteady variation in rolling moment coefficient as seen in FTR wind tunnel test data. Results from 1Degrees-of-Freedom of Aircraft (DOF), 5DOF and 6DOF simulation studies show that the model is qualitatively satisfactory.

1.7 List of Publications

1. **Bommanahal, M.** and Goman, M., "Nonlinear Unsteady Aerodynamic Modeling by Volterra Variational Approach", *AIAA Atmosperic Flight Mechanics Conference and Exhibit*, AIAA 2012-4654, Minnesota, Minneapolis, USA, August 2012.

2. Devprakash, M., **Bommanahal, M.**, and Saraf, A., "Mathematical Modeling of Abrupt Wing Stall of a Generic Tailless delta wing Aircraft for Flight simulation", *Symposium on Applied Aerodynamics and Design of Aerospace Vehicles 2013*, Hyderabad, India, December 2013.

3. Abramov, N., **Bommanahal, M.**, Chetty, S., Murthy, PVS., and Goman, M., "Flight Envelope Expansion VIA Active Control Solution for a Generic Tailless Aircraft", *29th Congress of the International Council of Aeronautical Science*, St.Petersburg,

Russia, September 2014.

4. Chetty, S., **Bommanahal, M.**, Murthy, PVS., and Goman, M., ”Recent Initiatives in Computational Flight Dynamics and Control at CSIR-NAL”, *AeroIndia International Seminar 2015*, Bangalore, India, February 2015.

A copy of these publications is attached at the end of the thesis.

Chapter 2

Properties of Volterra Variational Equations

2.1 Introduction

Volterra series is a functional expansion of a nonlinear system response to any arbitrary input. It was proposed by Vito Volterra in 1880s as a generalization of the Taylor series to represent nonlinear dynamical systems for which output depends on history of input [18]. It was later applied to modeling nonlinear electrical phenomena like inter-modulation distortion in power amplifiers by Norbert Weiner in 1950s. Since then it has been widely used for system identification of electrical and physiological systems which are known to be significantly nonlinear.

Volterra series consists of a linear sum of the convolution integral of higher power inputs with a set of multi-dimensional integrands called Kernels. A finite set of kernels can completely characterize a nonlinear dynamic system. However, a parametric model is always preferred over a non-parametric one because it can be estimated using simpler experimental techniques from System Identification Theory [43], and can provide physical interpretations. So, Volterra Variational Equations (VVEs) are derived as a parametric form of the Volterra series. This is done by considering a class of systems which are analytic in state and affine in input [51]. The mathematical structure of this system consists of an ordinary differential equation with polynomial terms in state. This structure is commonly used for modeling the nonlinearity of a mechanical system, and in this thesis it is called Polynomial Differential Equation (PoDE). VVEs are obtained as the Volterra series representation of PoDE model in Section 2.2.

PoDE model is in fact a generic mathematical form of the Abramov-Goman model which has been reported to be the best approach for modeling of nonlinear unsteady aerodynamic loads in literature [42]. As VVEs are derived from the PoDE model, it is expected that the two methods have some commonalities. Hence, the methodologies of

identification using the two model structures and their harmonic input response properties are compared in this chapter. From the perspective of System identification, these are two independent model structures. Hence, in practical application there is no need to consider the correlation between them. If the dynamics of a system is given in the form of PoDE, one can analytically derive its equivalent representation as VVEs. This equivalence if true for the two models estimated separately subject to certain bounds on input.

VVEs consist of differential equations of the kernel states which are response of each kernel to any input. Infinite number of kernel states are essential for the output of VVEs to match that of PoDE asymptotically; but practically first few states suffice in many cases. The steady state response of truncated Volterra series or a reduced set of VVEs (called the Volterra variational model) converges to that of PoDE for certain bounds on input as proved in [67]. The magnitude of input defining the bounds for equivalence of the two models can be computed using a recently proposed algorithm by Helie and Laroche [66]. Helie-Laroche algorithm provides a guaranteed estimate of input bounds for convergence of the truncated Volterra series of an analytic and input-affine class of nonlinear system. An alternative proof of this algorithm is presented in frequency domain in Section 2.3. This proof is simpler than the original time-domain one given in literature [66].

However, the estimated input bound is a conservative estimate and it can be considered to be an approximate value in identification of physical systems. If the identified model is found to be stable for the system's operational input magnitudes, the estimation of input bound can be ignored. As discussed in Chapter 1, VVM cannot model system with multiple equilibrium in its operational conditions but PoDE can. Estimation of input bounds becomes important for such nonlinear systems. In this case, it is important to know the comparison of the input bounds defining the region of attraction of the equilibrium of interest, to the estimated input bound for convergence of VVM. If the value of the former is greater than the later, the estimated value of input bound defines the limits of applicability of the identified VVM.

Application of PoDE and VVM for System Identification using experimental data are different from each other. Typically, nonlinear systems excite harmonics in response to sinusoidal inputs. Hence, it is important to correlate them with the harmonic input response properties of the model structure. The harmonic input response properties of the kernel states are presented in Section 2.4. The number of kernel states sufficient for modeling a given nonlinear system is determined by super-harmonics in the harmonic input response. A comparison of PoDE and VVM in the context of system identification, is presented in detail in Section 2.5. The theoretical concepts presented in this chapter are illustrated using numerical experimental data generated from a Duffings-type oscillator system, in Section 2.6.

2.2 Volterra Variational Equations

An analytical form of the Volterra series can be derived from the differential equations governing the dynamics of a given system using the methods stated in [62]. In this section, a special class of nonlinear differential equations with polynomial nonlinear terms, called PoDE, is considered. Its Volterra series representation is derived in frequency domain, and the resulting infinite series of differential equations are called the Volterra variational equations. The time-domain derivation is available in [51].

Volterra series for a Single-input-single-output system is given by,

$$\begin{aligned} x(t) &= h_0(t) + \int_0^\infty h_1(\tau_1)u(t-\tau_1)d\tau_1 \\ &\quad + \sum_{n=2}^{\infty} \int_0^\infty \cdots \int_0^\infty h_n(\tau_1, \cdots, \tau_n) \prod_1^n u(t-\tau_n)d\tau_n \end{aligned} \tag{2.1}$$

where $h_n(\tau_1, ..., \tau_n)$ is called n-th symmetric kernel of the Volterra series, and τ_i is the local time-variable. Kernels are unique functionals characterizing the system dynamics. For a linear system, only the first kernel $h_1(\tau_1)$ is significant, and all higher order kernels are zero. It is simply the impulse response of the system. In this sense, higher order kernels are a special kind of impulse responses of the system in higher dimensions. Volterra series is a direct superposition of the responses of kernels to any input. Higher order Volterra kernels produce relatively more significant contribution to response for larger magnitude of inputs. Hence, they reflect the dependence of nonlinear nature of system dynamics on magnitude of input.

Following PoDE model is commonly used for identification of physical systems with memory,

$$F(\frac{d}{dt})x(t) + \sum_{i=2}^{n} a_i x(t)^i = \sum_{i=1}^{n} b_i x(t)^{i-1} u(t);\ t \geq 0 \tag{2.2}$$

$$y(t) = Cx(t) + y_0(t);\ x(0) = 0 \tag{2.3}$$

$$F(\frac{d}{dt}) = \sum_{i=1}^{m} p_j \frac{d^j}{dt^j} + a_1 \tag{2.4}$$

where, $x(t)$ and $u(t)$ are the system state and input respectively, while $\{(a_i, b_i) \forall\, i \in [1\, n]\}$ are constant scalars. $F(d/dt)$ is a m-th order polynomial differential operator in d/dt as given in Eq.(2.4). Its coefficients $p_j \forall\, j \in [1\, m]$ are independent of $x(t)$, $u(t)$ and t, as the system is Linear-time-invariant and Causal, as defined in systems theory. $y_0(t)$ is the zero-input response and initial condition of state is $x(0) = 0$. Since the output $y(t)$ is simply a scalar multiple of state, we consider only the input-state dynamics in further

derivations.

PoDE can have multiple stable or unstable equilibriums. However, in derivation of Volterra series it is assumed that the system has a single stable equilibrium for given input conditions. Hence, the system dynamics can be modeled in the form of Volterra series only in the region of attraction of a single stable equilibrium. Hence, the Volterra series presentation of PoDE is derived assuming that the system operates in the region of attraction of equilibrium at $x = 0$. This can be translated to any other equilibrium by addition of that constant value to the output equation. Limit cycle oscillations are excluded from this consideration. Also, the equilibrium at $x = 0$ is required to be locally stable which implies that $a_1 < 0$.

Volterra series expressed in frequency domain offers interpretation of the effect of input amplitude and frequency (Bode plot style) on the nonlinear system output. Hence, a n-fold Fourier transform of the Volterra kernels called the Generalized Frequency Response Functions (GFRFs) is commonly used in literature to present various results. A recurrence relation for GFRFs of the nonlinear system in Eq.(2.2), is derived in this section by extension of the results given in [62]; and it is used to derive VVEs. This also gives the analytical relationship between Volterra series, PoDE, GFRFs and VVM.

If the response of kernel $h_n(\cdot)$ is defined as the kernel-state $x_n(t)$ for all $n \in \mathbb{N}$, then Eq.(2.1) becomes,

$$x(t) = x_1(t) + x_2(t) + x_3(t) + ... + x_n(t) + ... \tag{2.5}$$

Now, all the above equations are considered in frequency domain for a simpler algebraic representation of the derivations presented in this chapter. GFRF or the n-fold Fourier transform of the n-th kernel $h_n(\cdot)$ is defined as,

$$G_n(f_1, .., f_n) = \int_{-\infty}^{\infty} d\tau_1 .. \int_{-\infty}^{\infty} h_n(\tau_1, .., \tau_n) \cdot \exp^{-2\pi j(f_1\tau_1 + ... + f_n\tau_n)} \, d\tau_n \tag{2.6}$$

Let $U(f)$ and $X(f)$ be the Fourier transform of $u(t)$ and $x(t)$ respectively. Then, the Volterra series in frequency domain is given by [62],

$$X(f) = \frac{1}{1!}G_1(f)U(f) + \frac{1}{2!}\int_{-\infty}^{\infty} G_2(f_1, f - f_1)U(f_1)U(f - f_1)df_1 + ... \tag{2.7}$$

Let $X_n(f)$ be the Fourier transform of $x_n(t)$, then,

$$X(f) = X_1(f) + X_2(f) + X_3(f) + ... + X_n(f) + ... \tag{2.8}$$

where,

$$\begin{aligned} X_1(f) = &\quad \frac{1}{1!}G_1(f)U(f) \\ X_2(f) = &\quad \frac{1}{2!}\int_{-\infty}^{\infty} df_1 G_2(f_1, f-f_1)U(f_1)U(f-f_1) \end{aligned} \tag{2.9}$$

....

This infinite series is the frequency domain representation of the Volterra series. The GFRFs of the PoDE system are substituted in this expression to obtain the differential equations of kernel states governing the system dynamics. The GFRFs of the PoDE system are derived as follows.

As shown in ([62], $section\ 5.A$), n-th order GFRF of the polynomial term $[x(t)]^l$ is obtained as,

$$G_n^{(l)}(f_1, ..., f_n) = \quad l! \sum_{(\nu;l,n)} {\sum_{N}}' G_{\nu_1}^l(f_1, ..., f_{\nu_1}) \cdots G_{\nu_n}^l(f_\mu, .., f_n) \tag{2.10}$$

where l is a positive integer such that ($1 \leq l \leq n$), and $G_n^{(l)} = 0$ for $l > n$. ${\sum_N}'$ indicates N permutations of frequencies and $\mu = \nu_1 + .. + \nu_{l-1} + 1$. $(\nu; l, n)$ denotes summation over integers ν_i such that,

$$\begin{aligned} &\nu_1 + \nu_2 + ... + \nu_l = n; \\ &1 \leq \nu_1 \leq \nu_2 \leq .... \leq \nu_l; \\ &N = n!/\nu_1!\nu_2!...\nu_1!r_1!r_2!...r_k! \end{aligned} \tag{2.11}$$

where $r_i, i \in [1\, k]$ is the number of ν_i terms with the same value. For Volterra series, harmonic input gives harmonic output. So for input,

$$u(t) = e^{j2\pi f_1 t} + e^{2\pi j f_2 t} + ... + e^{2\pi j f_n t} \tag{2.12}$$

where f_i are incommensurate frequencies and j is the complex number exponent; Volterra series output is given by,

$$x(t) = \sum_{m_1=0}^{\infty} ... \sum_{m_n=0}^{\infty} C_{m_1 m_2 ... m_n} e^{(m_1 f_1 + ... m_n f_n)2\pi j t} \tag{2.13}$$

It is known that $G_n(f_1, f_2, ..., f_n) = C_{111..n-times}$ = [coefficient of $e^{(f_1+...+f_n)2\pi j t}$ in $x(t)$]. Hence, substituting equations (2.12) and (2.13) in to system dynamics Eq.(2.2), and equating the coefficient of $e^{(f_1+...+f_n)2\pi j t}$ on both the sides, gives the general recurrence

relation defining n-th GFRF as,

$$F(2\pi jf_1 + ... + 2\pi jf_n)G_n(f_1, ..., f_n) + \sum_{l=1}^{n} a_l G_n^{(l)} = \sum_{l=2}^{n}\sum_{k=1}^{n} G_{n-1}^{(l-1)}(f_1, ..., f_{k-1}, f_{k+1}, ..., f_n) \tag{2.14}$$

From expansion of this expression, the first three GFRFs of the system are,

$$\begin{aligned} G_1(f_1) &= \frac{b_1}{F(2\pi jf_1)}; \\ G_2(f_1, f_2) &= \frac{b_2[G_1(f_1) + G_1(f_2)] - 2a_2 G_1(f_1)G_1(f_2)}{F(2\pi jf_1 + 2\pi jf_2)}; \\ G_3(f_1, f_2, f_3) &= \frac{2!b_2 \sum_3^{'} G_2(f_1, f_2) - 2a_2 \sum_3^{'} G_1(f_1)G_2(f_1, f_2)}{F(2\pi jf_1 + 2\pi jf_2 + 2\pi jf_3)} \\ &\quad + \frac{3!b_3 \sum_3^{'} G_1(f_1)G_1(f_2) + 6a_3 G_1(f_1)G_1(f_2)G_1(f_3)}{F(2\pi jf_1 + 2\pi jf_2 + 2\pi jf_3)} \end{aligned} \tag{2.15}$$

where, $\sum_3^{'}$ indicates sum of 3 terms with permutation of frequencies (f_1, f_2, f_3).

The equations governing the kernel-states are obtained by substituting the GFRFs in Eq.(2.15), in to the frequency domain Volterra series in Eq.(2.9). Solving for $X_1(f)$ gives,

$$\begin{aligned} X_1(f) &= \frac{1}{1!}G_1(f)U(f) \\ F(2\pi jf)X_1(f) &= b_1 U(f) \end{aligned} \tag{2.16}$$

Applying inverse Fourier transform to this equation gives Eq.(2.19). Following a similar simplification for $X_2(f)$ gives,

$$F(2\pi jf)X_2(f) = \int_{-\infty}^{\infty}[-a_2\frac{U(f_1)U(f-f_1)}{F(2\pi jf_1)F(j(2\pi f - 2\pi f_1)} + b_2\frac{U(f_1) + U(f-f_1)}{F(2\pi jf_1)F(j(2\pi f - 2\pi f_1)}]df_1 \tag{2.17}$$

Substituting the expression of $X_1(f)$ in this equation gives,

$$\begin{aligned} F(2\pi jf)X_2(f) &= \int_{-\infty}^{\infty}[-a_2 X_1(f_1)X_1(f-f_1) + b_2 U(f_1)X_1(f-f_1) + \\ &\quad b_2 X_1(f_1)U(f-f_1)]df_1 \end{aligned} \tag{2.18}$$

Applying inverse Fourier transform to Eq.(2.18) gives Eq.(2.20). Similarly, the

expressions for higher kernel-states can be obtained.

$$F(\frac{d}{dt})x_1(t) = b_1u(t) \tag{2.19}$$

$$F(\frac{d}{dt})x_2(t) + a_2x_1^2(t) = b_2x_1(t)u(t) \tag{2.20}$$

$$F(\frac{d}{dt})x_3(t) + 2a_2x_1(t)x_2(t) + a_3x_1(t)^3 = b_2x_2(t)u(t) + b_3x_1(t)^2u(t) \tag{2.21}$$

$$...\infty$$

where, $x_1(0) = 0$, $x_2(0) = 0$, $x_3(0) = 0$. This series is called Volterra variational equations.

In this section, the GFRFs in Eq.(2.14) and Volterra variational equations were derived for the systems of type in Eq.(2.2). However, these results can also be extended to the systems which have non-polynomial nonlinearities. Considering the Weirstrass's theorem for approximation of a nonlinearity in the form of polynomial, the condition on linear-analyticity of the system can be relaxed.

2.3 Input Bounds for Convergence

Polynomial nonlinearity of degree n contributes to all the kernels of order $l \geq n$. Therefore, infinite number of kernel-states are required in the Volterra variational representation to obtain an exactly equivalent of the system Eq.(2.2). However, physical systems usually have fading memory, i.e the current output depends on certain finite history of inputs. For such systems, Volterra series can be truncated to first few kernels [67, 68].

Helie and Laroche proposed an algorithm that determines a minimum of the input bound for guaranteed convergence of truncated Volterra series of system Eq.(2.2). To prove this algorithm the Volterra kernels are assumed in a special (complicated) format called the "Kernel-recursive construction" given in ([66], Prop.1). In this section, we present a frequency domain derivation of the input bounds for convergence of VVM following the similar approach, but without assuming kernels in any special format.

2.3.1 Proof of Helie-Laroche Algorithm in Frequency domain

The proof of Helie-Laroche algorithm is presented in this section in three steps. First, a gain bound function is obtained as sum of the supremum of the response of each kernel of Volterra series. In the second step, a majorising sequence of the gain bound function is defined and proved using induction. Finally, the guaranteed estimate of convergence

bound for any input type is obtained a minimum value of this majorising series.

2.3.1.1 Gain Bound Function

For system Eq.(2.2) with stable equilibrium at $x = 0$, GFRFs are defined by Eq.(2.6) and VVM is given by Eq.(2.19). $G_n(f_1, .., f_n)$ is defined on vector space of functions $\nu^n_{\mathbb{C}} : \mathbb{R}^n \to \mathbb{C}$, and the norm in this space defined by,

$$\|G_n(f_1, .., f_n)\| = \sup_{f\epsilon\mathbb{R}} |\int_{-\infty}^{\infty} ... \int_{-\infty}^{\infty} G_n(f_1, .., f_n)\delta_n(f - f_1 .. - f_n)d\widetilde{f}_{n-1}| \quad (2.22)$$

for all $n \geq 2$. Here, $d\widetilde{f}_{n-1} = df_1 df_2 .. df_{n-1}$ and the delta function gives $f_n = f - f_1 - f_2 - ... - f_{n-1}$. For $n = 1$, the norm on $\nu^1_{\mathbb{C}} : \mathbb{R}^1 \to \mathbb{C}$ for $G_1(f_1)$ is obtained at $f_1 = 0$ as,

$$\|G_1(f_1)\| = \sup_{f\epsilon\mathbb{R}} |\frac{b_1}{(2\pi j f_1 + a_1)}| = |\frac{b_1}{a_1}| \quad (2.23)$$

Consider a function $\varphi(X) = \sum_{m\epsilon N^*} \|G_m(.)\|_{\nu^m_C} X^m$ and assume that it has radius of convergence $\rho > 0$. Then the gain bound function $\varphi(z)$ of the frequency domain Volterra series of $\|G_m(.)\|_{m\epsilon N^*}$ is defined for all $z\epsilon C$ such that $|z| < \rho$. If $\rho > 0$ for $\varphi(z)$, then the Volterra series is convergent for inputs $\|U\| < \rho$; and it satisfies $\|X\| \leq \varphi(\|U\|) < \infty$. This can be proved as follows.

Let $\|U\| < \rho$, then by definition of $\varphi(\|U\|)$, we get $\varphi(\|U\|) < \infty$. Now taking the norm of n-th kernel state gives,

$$\begin{aligned} \|X_n\| &= \sup_{f\epsilon R}(|\int_{-\infty}^{\infty} .. \int_{-\infty}^{\infty} G_n(f_1, ..f_n)U(f_1)..U(f_n)\delta_n(f - f_1 .. - f_n)d\widetilde{f}_{n-1}|) \quad (2.24) \\ &\leq \sup_{f\epsilon R}(|\int_{-\infty}^{\infty} ... \int_{-\infty}^{\infty} G_n(f_1, f_2, ..., f_n)\delta_n(f - f_1 - .. - f_n)d\widetilde{f}_{n-1}|)(\|U(f)\|)^n \\ &\leq \|G_n\|_{\nu^N_C}(\|U\|)^n \end{aligned}$$

Therefore, norm of the Volterra variational equations output is bounded as follows:

$$\begin{aligned} \|X\| &= \|X_1 + X_2 + X_3 + ... + X_n\| \quad (2.25) \\ &\leq \|X_1\| + \|X_2\| + \|X_3\| + ... + \|X_n\| \\ &\leq \sum_{n\epsilon N^*} \|G_n\|_{\nu^N_C}(\|U\|)^n \\ &\leq \varphi(\|U\|) \end{aligned}$$

In the next part, a majorising series of this gain bound function is obtained.

2.3.1.2 Majorising Sequence of Gain Bound Function

The supremum of GFRFs is obtained in terms of model parameters, and it is used to deduce a series that is maximum of the Volterra variational response. For this, the objective is to prove by induction that,

$$\|G_m\|_{\nu_C^N} \leq \psi_m \tag{2.26}$$

where ψ_m is a general supremum function of the m-th GFRF defined by,

$$\psi_m = \sum_{l=2}^{m} \frac{|a_l|\psi_m^{(l)} + \sum_{k=1}^{m} |b_l|\psi_{(m-1)}^{(l-1)}(f_1..f_{k-1}, f_{k+1}.., f_m)}{|a_1|} \tag{2.27}$$

for $m \geq 2$, and for $m = 1$, $\psi_1 = \|G_1(f)\| = |\frac{b_1}{a_1}|$. This is proved as follows.

It is evident that Eq.(2.26) holds good for $m = 1$. For $m = 2$ we have,

$$\begin{aligned}
&\|G_2(f_1, f_2)\|_{\nu_C^2} = \sup_{f \epsilon R} |\int_{-\infty}^{\infty}\int_{-\infty}^{\infty} G_2(f_1, f_2)\delta_2(f - f_1 - f_2)df_1 df_2| \qquad (2.28)\\
&= \sup_{f \epsilon R} |\int_{-\infty}^{\infty}\int_{-\infty}^{\infty} \frac{-2a_2 G_1(f_1)G_1(f - f_1) + b_2[G_1(f_1) + G_1(f - f_1)]}{F(2\pi j f_1 + j(2\pi f - 2\pi f_1))} df_1 df_2|\\
&\leq \frac{1}{|a_1|} \sup_{f \epsilon R} |\int_{-\infty}^{\infty}\int_{-\infty}^{\infty} -2a_2 G_1(f_1)G_1(f - f_1)df_1 df_2\\
&+ \sup_{f \epsilon R} |\int_{-\infty}^{\infty}\int_{-\infty}^{\infty} b_2[G_1(f_1) + G_1(f - f_1)]df_1 df_2|\\
&\leq \frac{|a_2|2!\psi_1\psi_1 + |b_2|(\psi_1 + \psi_1)}{|a_1|}\\
&\leq \psi_2
\end{aligned}$$

Now, assume that Eq.(2.26) is true for $m \in [1,\ (n-1)]$, and prove that it holds true for $m = n$. Consider the norm of $G_n^{(l)}$,

$$\begin{aligned}
\|G_n^{(l)}(f_1, ..., f_n)\| &= \|l! \sum_{(\nu;l,n)} {\sum_{N}}' G_{\nu_1}(f_1, ..., f_{\nu_1})...G_{\nu_n}(f_\mu, ..., f_n)\| \qquad (2.29)\\
&\leq l! \sum_{(\nu;l,n)} {\sum_{N}}' \|G_{\nu_1}(f_1, ..., f_{\nu_1})\|...\|G_{\nu_n}(f_\mu, ..., f_n)\|\\
&\leq l! \sum_{(\nu;l,n)} \psi_{\nu_1}\psi_{\nu_2}...\psi_{\nu_l}\\
&\leq \psi_n^l
\end{aligned}$$

Therefore, norm of n-th GFRF becomes,

$$\begin{aligned}\|G_n(f_1,...,f_n)\| &= \sup_{f\epsilon R}|\int_{-\infty}^{\infty}...\int_{-\infty}^{\infty}\sum_{l=2}^{n}\frac{-a_l G_n^{(l)}}{F(2\pi j f_1+...+2\pi j f_n)}+ \\ &\quad \frac{\sum_{k=1}^{n}G_{n-1}^{(l-1)}(f_1,..f_{k-1},f_{k+1},..f_n)}{F(2\pi j f_1+..+2\pi j f_n)}\delta(f-f_1..f_n)d\widetilde{f}_{n-1}| \\ &\leq \sum_{l=2}^{n}\frac{|a_l|\psi_n^{(l)}+\sum_{k=1}^{n}|b_l|\psi_{(n-1)}^{(l-1)}(f_1..,f_{k-1},f_{k+1}..f_m)}{|a_1|} \\ &\leq \psi_n\end{aligned} \tag{2.30}$$

Thus, Eq.(2.26) is true for any $n\epsilon N^*$. Therefore, the maximum of Volterra series response is given by the maximum of Gain bound function as,

$$\|X\|\leq\varphi(\|U\|)\leq\sum_{n\epsilon N^*}\psi_n U^n \tag{2.31}$$

2.3.1.3 Lower Bound of Convergence Radius

The minimum or the most conservative estimate of of the convergence radius is obtained by majorising the series $\Psi(X)$. Assume that, $P(X)=\sum_2^\infty\frac{|a_m|}{|a_1|}X^m$ and $Q(X)=\sum_2^\infty\frac{|b_m|}{|a_1|}X^{m-1}$. Define a function $R(X)$ using them as,

$$\begin{aligned}R(X) &= P(\Psi(X))+XQ(\Psi(X)) \\ &= \sum_{k=2}^{\infty}(\frac{|a_k|}{|a_1|}[\Psi(X)]^k+\frac{|b_k|}{|a_1|}[\Psi(X)]^{k-1}X) \\ &= \sum_{k=2}^{\infty}(\frac{|a_k|}{|a_1|}[\sum_{n\epsilon N^*}\psi_n X^n]^k+\frac{|b_k|}{|a_1|}[\sum_{n\epsilon N^*}\psi_n X^n]^{k-1}X) \\ &= \sum_{k=2}^{\infty}(\frac{|a_k|}{|a_1|}\psi_n^{(k)}+\frac{|b_k|}{|a_1|}\psi_{n-1}^{(k-1)})X^n \\ &= \psi_n X^n \\ &= \Psi(X)-\psi_1 X\end{aligned} \tag{2.32}$$

Therefore,

$$\Psi(X)-P(\Psi(X))=(\psi_1+Q(\Psi(X)))X \tag{2.33}$$

Define a function $\mathcal{F}(X)$ as,

$$\mathcal{F}(X)=\frac{(\psi_1+Q(X))X}{X-P(X)} \tag{2.34}$$

This gives,

$$\begin{aligned} \mathcal{F}(\Psi(X)) &= \frac{(\psi_1 + Q(\Psi(X)))\Psi(X)}{\Psi(X) - P(\Psi(X))} \\ X\mathcal{F}(\Psi(X)) &= \frac{(\psi_1 + Q(\Psi(X)))X}{\Psi(X) - P(\Psi(X))}\Psi(X) \\ &= \Psi(X) \end{aligned} \tag{2.35}$$

This function $\Psi(X)$ is analytic at $X = 0$, and has a convergence radius ρ^* given by the following algorithm. It is proved as $Lemma\ A$ in the Helie-Laroche's paper [66]. Since, $\Psi(X)$ is the majorising sequence of the gain bound function, its convergence radius is also the input bound for convergence of the Volterra series. Helie-Laroche provide an algorithm to compute the convergence radius for a Multi-dimensional system. This and its application to the PoDE system are presented in the next section.

2.3.2 Algorithm for Input Bound

2.3.2.1 Helie-Laroche Algorithm

Let r be the radius of convergence of $\mathcal{F}(X)$ at $X = 0$. Then, the equation $X\mathcal{F}'(X) - \mathcal{F}(X)$ has either one solution σ ($case\,1$) or zero solution ($case\,2$) in $]0, r[$, and the radius of convergence of $\Psi(X) = X\mathcal{F}(\Psi(X))$ is given by,

$$(case\,1) \qquad \rho^* = \frac{\sigma}{\mathcal{F}(\sigma)} \tag{2.36}$$

$$(case\,2) \qquad \rho^* = \lim_{x \to r^-} \frac{x}{\mathcal{F}(x)} \tag{2.37}$$

2.3.2.2 Input Bound Computation

Evaluation using the system parameters in accordance with the above definitions gives the function $\mathcal{F}(X)$ is defined as,

$$\mathcal{F}(X) = \frac{|\frac{b_1}{a_1}| + \sum_{k=2}^{\infty} |\frac{b_k}{a_1}| X^{k-1}}{1 - \sum_{k=2}^{\infty} |\frac{a_k}{a_1}| X^{k-1}} \tag{2.38}$$

The radius of convergence of $\mathcal{F}(X)$ at $X = 0$ is $r = |b_1/a_1|$, and that a_1 is positive for a stable system.

Next, if a unique positive solution σ of $X\mathcal{F}'(X) - \mathcal{F}(X) = 0$ in $]0, r[$ is found, by numerical computations, then the radius of convergence is given by $\rho^* = \frac{\sigma}{\mathcal{F}(\sigma)}$. If no such

σ is found, then it is given by,

$$\rho^* = \lim_{\sigma \to r^-} \frac{\sigma}{\mathcal{F}(\sigma)} = \frac{1 - \sum_{k=2}^{\infty} \frac{|a_k|}{(a_1)} |\frac{b_1}{a_1}|^{k-1}}{1 + \sum_{k=2}^{\infty} \frac{|b_k|}{a_1} |\frac{b_1}{a_1}|^{k-2}} \tag{2.39}$$

Illustrative examples using this formula are given in Section 2.6.

2.4 Model Order Determination using Harmonic Input Response

The kernel states of VVM inherit harmonic input response properties of the Volterra kernels. Hence, VVM parameters can be estimated using Volterra kernel estimation techniques proposed in literature. These methods of kernel estimation require system response data obtained using special inputs like Gaussian random signal, and estimation is done by spectral correlation techniques [60]. Especially in case of mechanical systems, due to difficulties in developing sophisticated experimental setup to implement wide-band inputs, and relatively low signal-to-noise ratio, it difficult to use these methods. If the output noise is Gaussian white noise, both VVM and PoDE model parameters can be estimated by regression methods, otherwise Output-Error method can be used [43]. However, VVM being a set of parametric differential equations, much simpler methods can be utilized. In this section, we present interpretations of harmonic input responses of VVM and PoDE models, which are later utilized in the parameter estimation process.

Volterra series response to harmonic input $u(t) = Acos(2\pi f_p t)$ is given by,

$$x_\omega(t) = \sum_{n=1}^{\infty} \sum_{k=0}^{n} (\frac{A}{2})^n \frac{\exp[j(2k-n)\omega_p t]}{k!(n-k)!} G_{k,n-k}(f_p) \tag{2.40}$$

where, $\omega_p = 2\pi f_p$ and $G_{k,n-k}(f_p)$ stands for $G_n(f_1, ..., f_n)$ with the first k of f_i equal to f_p and remaining $n-k$ equal to $-f_p$ [62]. Substituting definitions of GFRFs in Eq.(2.10) gives VVM response to harmonic input.

In Eq.(2.40), the system response contains only the integral multiples of input frequency. This implies that the Volterra series and VVM can produce only the super-harmonics of input frequency in response. Power Spectrum Density (PSD) diagrams of harmonic input responses of a system provide information about the harmonics excited due to nonlinear nature of system dynamics. If sub-harmonics are present in PSD diagrams then the system dynamics has bifurcations, and it cannot be modeled by VVM structure [69]. Thus, one should verify the presence of only super-harmonics in the response PSD diagrams.

n-th GFRF (and hence kernel-state) produces sinusoidal components of n-th harmonic frequency and lower order harmonics of same parity. For example, G_5 produces harmonic components of frequencies $(5\omega, 3\omega, 1\omega)$ in the response. If PSD plot contains a peak at frequency $n \times \omega$, then at least one of the GFRFs $G_n, G_{n+2}, ..$ is nonzero. However, if there is no peak at frequency $(n+2)\omega$ then all $G_{n+2}, G_{n+4}, ...$ are zero. Thus, if the PSD plot shows a peak at a maximum frequency of $\omega_{max} = l\omega$, then $G_l \neq 0$, and hence x_l is the highest order kernel-state to be included in the model, and VVM equations should be truncated to $\dot{x_l}$.

From Eq.(2.6), if $G_n \neq 0$, then at least one of the parameters $(a_i \forall i \in [2, n])$ is non-zero. Therefore, we must include all the kernel states x_i to x_l in the model structure. For example, if there is a peak at 2ω, then at-least one of $G_2, G_4, G_{2n}..$ is/are non-zero. Additionally, if there is no peak at $4 \times \omega$, then $G_4 = 0, G_{2n} = 0$, and hence x_2 must be considered in the model structure. This implies that $a_2 \neq 0$. For VVM, a_2 excites all higher order kernel states, and hence odd order $x_i \forall i \in [2,\ l]$ should also be included in the model structure. Thus, the kernel states to be included in VVM can be determined from the PSD of the harmonic input response data of the system.

2.5 Comparison of VVM and PoDE Models for System Identification

The Abramov-Goman model of unsteady aerodynamic loads (which is based on PoDE), was applied to model the longitudinal and lateral directional coefficients of GTA, F16XL, Delta-60 wing and X31, with satisfactory results [20, 22, 23]. This model is the most intuitive extension to the Goman-Khrabrov model in [11], to account for nonlinearity in the unsteady variation of aerodynamic coefficients. As shown in previous sections, VVM is mathematically equivalent to PoDE with two conditions, that the PoDE model has single stable steady state and it is subject to certain input bounds. However, there are differences between the two in their consideration for system identification. Hence, a comparative study of the two structures is presented in this section.

The topology of the PoDE model can exhibit nonlinear phenomena like critical states crossing, hysteresis and limit cycles oscillations, period doubling leading to chaos etc. This is because PoDE model can have multiple equilibrium and it can move from the region of attraction of one to another in response to inputs. Such dynamics cannot be represented by Volterra series or VVM, as these models always converge to a particular equilibrium state when the input is within certain bounds, as proved in [68]. In this sense, the topology of VVM is similar to linear dynamical systems but stretched to higher number of parameters to account for nonlinearity of the response in time. Therefore,

although the two models are equivalent when their dynamics is restricted to the region of attraction of a particular stable equilibrium, their global dynamics for a wide range of inputs can be significantly different. There is currently no mathematical solution to either bridge this gap or an alternative structure which exhibits the properties of both the models.

This difference in topology of the two model structures offers some advantages and disadvantages. The capability of PoDE model to capture unsteady aerodynamic loads in presence of static hysteresis in $C_{Z_{st}}(\alpha)$ and $C_{m_{st}}(\alpha)$, as well as critical state crossing in $C_{n_st}(\beta)$ and $C_{l_{st}}(\phi)$ is an important advantage. The identification using such a model can be performed using "Bifurcational Model of Static Hysteresis" presented by Abramov in his Thesis [20]. These phenomena and application of BMSH are discussed in detail in Chapter 5. Such aerodynamic phenomena cannot be modeled using VVM. The complementary nature of PoDE model properties to VVM can be useful for modeling many aerodynamic systems.

However, the number of parameters in PoDE for tuning the static hysteresis and unsteady variation of an aerodynamic coefficient is sometimes insufficient. In Chapter 6, the nonlinear and unsteady modeling of rolling moment due to the Abrupt Wing Stall phenomena is presented. In this case, a cubic PoDE model with just four parameters is not good enough to capture the unsteady variations and static hysteresis in C_l versus β. Hence, a novel model called "Bifurcational Model of Aerodynamic Asymmetry" is proposed and is demonstrated to produce satisfactory results.

A practical problem in using PoDE model for system identification is that the topology of the identified model can be significantly different from that of the physical system in some cases. For a particular set of values of estimated parameters of PoDE, the identified model may exhibit bifurcation dynamics which do not exist for the physical system under consideration. Hence, during parameter estimation of a PoDE model, it is important to include additional constraints on parameters in order to have a single real equilibrium. This problem does not arise for VVM as the response always converges to zero, which in turn can be translated to the stable steady-state value of the system.

Nonlinearity of many physical systems are typically excited for high energy inputs, while for low energy inputs dynamics is approximately linear. Amplitude dependence of nonlinearity is an inherent feature of VVM. If the input amplitude to VVM is scaled by a factor of γ, then $x_n(t)$ gets scaled by a factor of γ^n. Therefore, for a sinusoidal input of particular frequency, if amplitude is decreased, relative contribution of higher order kernels to total response decreases in magnitude. For sufficiently small amplitude input the system response is approximately linear. This is true for any input shape in general. Thus, VVM is the most intuitive model to represent physical systems that show approximately linear behavior for small amplitude and nonlinear for larger amplitude

inputs. In case of PoDE model, the correlation between the responses to small or large amplitude inputs is not so distinct. The linear or nonlinear nature of the response is case specific. The model fit obtained by parameter estimation is good if the system characteristics actually correspond to the order of polynomial nonlinearity used in the model structure.

For the PoDE model, parameters can be estimated by least-squares technique and validated using the criteria like goodness-of-fit or parameter co-variances from System identification theory. However, the order of polynomial nonlinearities to be included in the model structure cannot be determined apriori. In case of VVM, the kernel states to be included in the model structure can be determined directly using harmonic input response data over systems operational conditions as presented in the previous section.

A higher degree polynomial term in PoDE can produce any number of harmonics in response to sinusoidal input, which may not be the case as seen in the experimental data of the system. On the other hand, the kernel states of a VVM model produce a definite set of harmonics in response to sinusoidal input. Thus, the VVM model structure can have exact correlation with the harmonics of available system response, while PoDE model may not.

As nonlinearity of the output of PoDE model increases, higher order kernel states are essential to produce an accurate match between the responses of the two models. This is illustrated in the next section, and more examples are available in [66]. However, the estimated model response using same experimental data is significantly different. In case of PoDE model, the relative magnitudes of parameters get tuned automatically to match nonlinearity in the experimental response data. In case of VVM, higher order kernel states need to be included in the model structure explicitly.

A truncated VVM is convergent for certain bounds on input, and we presented a criteria for convergence as a lower bound on the maximum magnitude of input. Although Helie-Laroche algorithm gives a conservative estimate, it specifies the likely order of magnitude of the input bound. Currently there are no algorithms in literature to get an accurate estimate of the input bounds for convergence.

In case of VVM it is straight forward to consider a second order differential operator in the model, to get a model similar to the "ONERA Dynamic Stall model". This is presented in detail in chapter (5). In case of PoDE, it becomes a Duffings oscillator and gives rise to all the complex nonlinear dynamics exhibited by it. Thus, VVM structure provides flexibility to included higher order differential formulation while a PoDE model does not.

To conclude, VVM structure is suitable for modeling systems which have only super-harmonics in PSD of response, and an approximately linear response for small amplitude

input; while PoDE structure is better suited for those systems which have sub-harmonics or large number of super-harmonics in PSD of the response, and exhibit bifurcations for certain input conditions.

2.6 Illustrative examples

The theory and system identification concepts presented in this chapter are illustrated for two contexts. Firstly, the similarities and differences in the two model structures VVM and PoDE for system identification are demonstrated using data generated from Duffings oscillator system. In the second example, equivalence of the two model responses subject to input bounds, and difference in their response power spectrum, are presented. For this, responses of both the models with same values of parameters are compared for different types of input.

2.6.1 Identification of Duffings Oscillator System

Duffings oscillator is commonly used to model systems with nonlinear stiffness, especially the structural systems subject to high input excitation levels like the ones with beams, panels etc. In this example, PoDE and VVM model parameters are estimated using the data generated from Duffings oscillator system Eq.(2.41). Their results are compared to show their relative effectiveness in identification of this type of system. Note that, we can obtain an equivalent VVM of the Duffings oscillator equations analytically, but in this exercise it is simply used to generate input-output data, without assuming any knowledge of the actual system.

$$m\ddot{y} + c\dot{y} + k_1 y + k_3 y^3 = u \tag{2.41}$$

An approximate solution of the Duffings oscillator system is obtained by the perturbation analysis. This shows that the Duffings oscillator system exhibits primary and secondary resonance [70]. The characteristics of the primary resonance are identical to the corresponding linear system, while secondary resonances arise due to significance of nonlinearity. The super-harmonic resonance occurs when the excitation input frequency is close to one-third of the natural frequency of the system. This produces a third harmonic component of significant magnitude in the response. We consider Duffings oscillator with the harmonic inputs around super-harmonic resonance. Since this frequency range is away from the primary resonance, other nonlinear phenomena of Duffings oscillator such as jump, symmetry-breaking, period-doubling leading to chaos etc. do not occur.

Consider the Duffings oscillator system operating over a very wide range of input

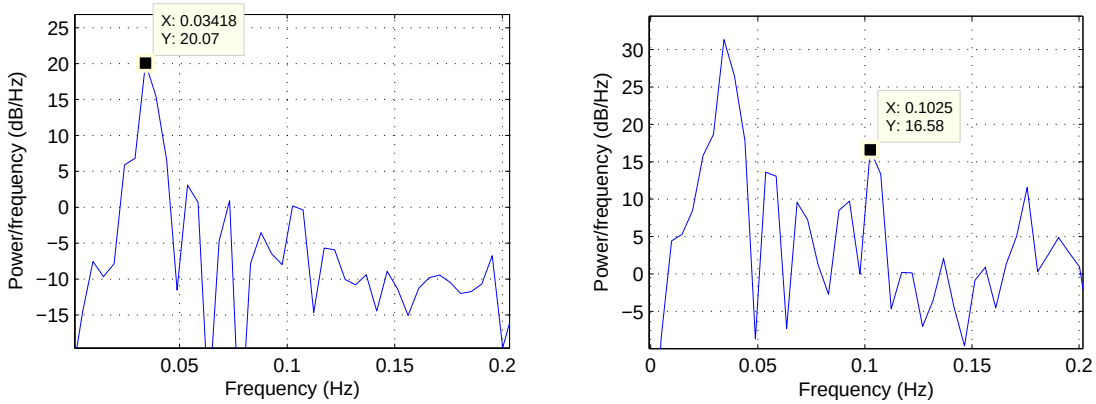

(a) Input $A = 1$, $f = 0.035Hz$ (b) Input $A = 20$, $f = 0.035Hz$

Fig. 2.1. PSD maps of the responses of Duffings oscillator to harmonic inputs of different amplitudes and same frequency.

amplitudes. For system Eq.(2.41) with $m = 1, c = 1.1, k_1 = 0.5, k_3 = 0.3$, the undamped natural frequency is $f_n = 0.112Hz$ and that for super-harmonic resonance is $f_s = 0.0375Hz$. So, the harmonic input response data is generated for amplitude $A = 1$ and frequencies of $f_{exp} = [0.025,\ 0.03,\ 0.035,\ 0.04,\ 0.045]Hz$. To make the data realistic, a gaussian white noise of $SNR = 5$ is added to the response. For this data, the first harmonic dominates the responses, as shown in the PSD plot in Fig.(2.1,a). Next, nonlinear responses of the system are generated using inputs with amplitude and frequency combinations $(A, f) = [(10, 0.035), (15, 0.035), (20, 0.035), (15, 0.025), (10, 0.045)]$. The PSD plot in Fig.(2.1,b) shows a significant peak at third harmonic also.

Since the system response contains a maximum of third harmonic in the response, we can include x_1, x_2, x_3 in the model structure. However, there is no second harmonic in the response. Hence, one can remove x_2 from the model structure. Even if x_2 is included, the parameter estimation yields a_2, b_2 values so small that $x_2(t) = 0$. The estimation of model parameters is preformed using Output-Error method and it converges to the values given in Table.(2.1).

Table 2.1. Estimated parameter values of VVM and PoDE models (not related).

Parameters	a_1	b_1	a_3	b_3	RMS
VVM estimate	1.2921	0.5047	0.0173	-0.012	1.095
PoDE estimate	0.3391	0.6936	-0.1681	-0.0096	0.9845

Next, the parameters of PoDE model with cubic nonlinearity are estimated using the same data set. The estimated values of both the models are listed in Table (2.1). Even in this case the values of a_2, b_2 are found to be approximately equal to zero. The values of parameters of the two models cannot be compared as the PoDE and VVM are identified separately. The root-mean-square of the modeling error of both the models are compared

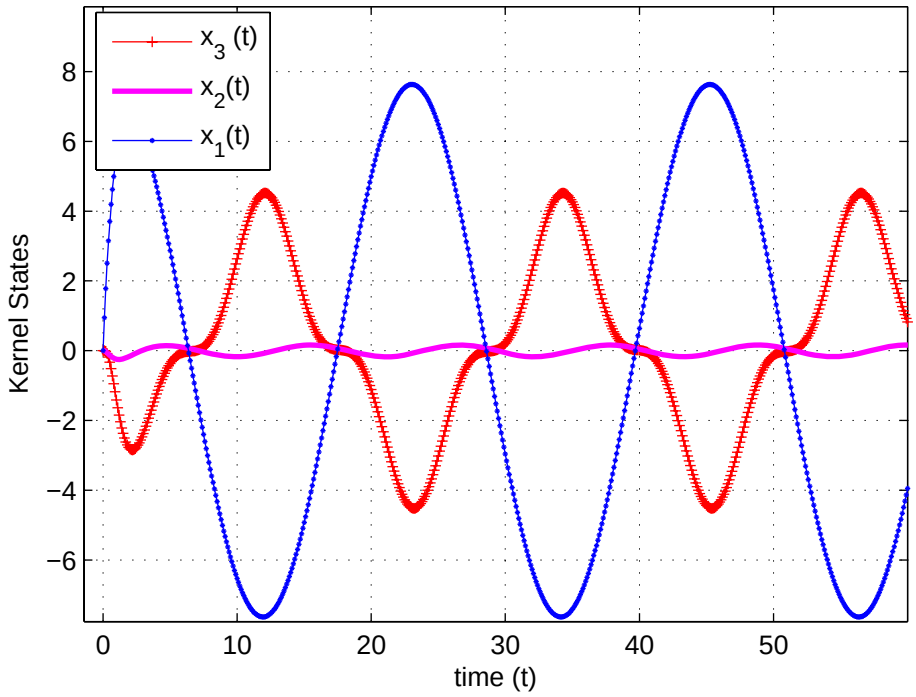

Fig. 2.2. Kernel states of VVM response to sinusoidal input of $A = 20$, $f = 0.045Hz$.

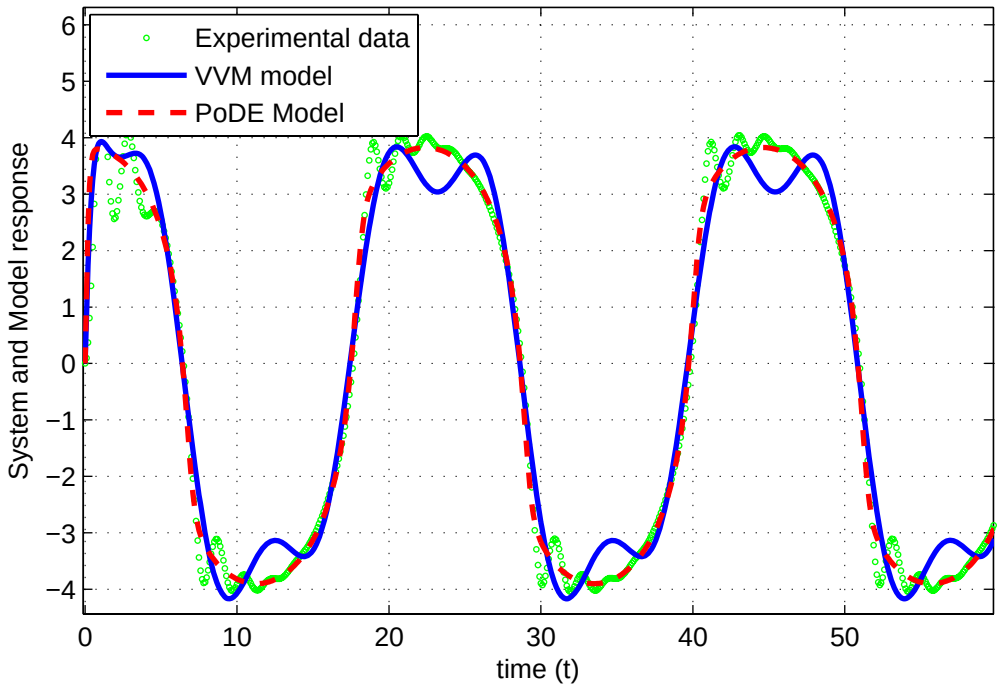

Fig. 2.3. Comparison of responses of VVM and PoDE to experimental data, for sinusoidal input of $A = 20$, $f = 0.045Hz$.

in Table (2.1). The root-mean-square error using VVM is approximately 10% higher than that for PoDE model. Hence, PoDE model produced a better accuracy of prediction. This is because the cubic polynomial term can excite higher order kernel states to closely match the Duffings oscillator behaviour reflected into the data set.

In Fig.(2.2), as expected the kernel state $x_2(t) = 0$ for any input amplitude. The magnitude of $x_3(t)$ is approximately 50% of that of $x_1(t)$ at some instants. This shows that the system response is highly nonlinear. Comparison of the responses of VVM and PoDE models to system response for an input which was not used in identification process is presented in Fig. (2.3). One can see that both the models produce reasonably good match to system response in terms of amplitude and frequency of response.

It is important to note that the system in this case is Duffings oscillator, which is also a type of PoDE model. Therefore, the results in this example show a cunningly good match between them. However, this may not always be the case. Nevertheless, this example shows that VVM model can be as accurate as PoDE model to represent a systems nonlinear dynamics with higher order harmonics.

2.6.2 Comparison of Responses of VVM and PoDE

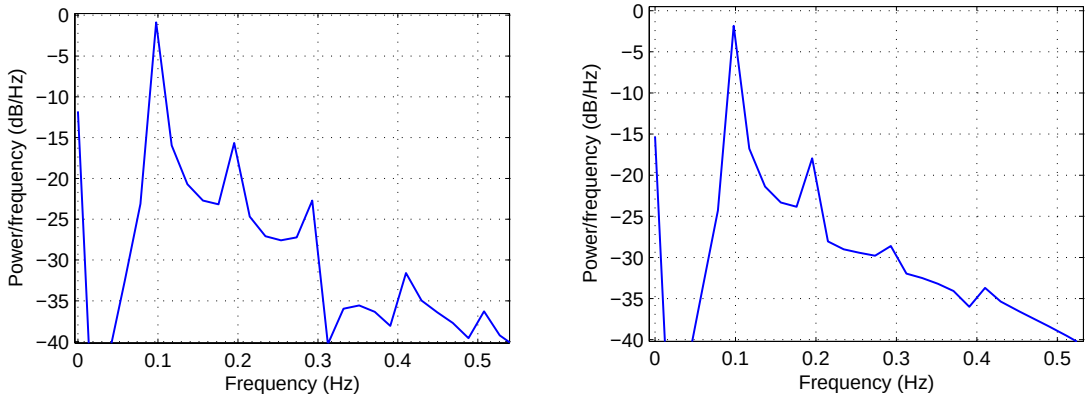

(a) PoDE model (b) Volterra variational model

Fig. 2.4. Comparison of PSD maps of the responses of VVM and PoDE models to sinusoidal input of $A = 0.32$, $f = 0.1Hz$.

Consider a first-order nonlinear system with cubic nonlinearity as in Eq.(2.42). This is actually the PoDE model without input-state coupling terms. For parameter values of $(k_1, k_2, k_3) = (-2, -3, 5)$, the system has two unstable roots at $y_r = (1, -0.4)$, and a stable root at $y_r = 0$. So, the region of attraction for the stable root is between $(1, -0.4)$.

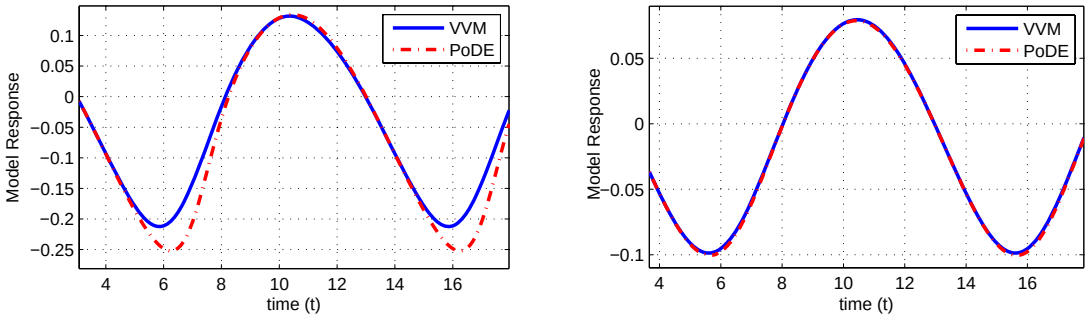

(a) For $A > \rho^*$ (b) For $A < \rho^*$

Fig. 2.5. Comparison of the responses of VVM and PoDE to sinusoidal inputs of $f = 0.1Hz$ for (1) $A = 0.32$ and (2) $A = 0.2$.

Next, the output of VVM in the region of attraction of $y_r = 0$ is investigated.

$$\dot{y} = k_1 y + k_2 y^2 + k_3 y^3 + u \tag{2.42}$$

Computation of input bounds using Helie-Laroche algorithm gives $\rho^* = 0.2163$. Comparison of the responses of 3-state VVM and PoDE model, for sinusoidal input of amplitude $(0.32 > \rho^*)$ and frequency $(0.1Hz)$ is given in Fig.(2.5,a). It can be seen that the responses do not match accurately. This can be explained from their power spectrum. In Fig.(2.4), the PSD of the response of model Eq.(2.42) contains up to fourth order harmonics, while that of VVM has only up to second order harmonics with a significant peak. This happens even when four states are used in VVM. For the case of amplitude $(0.2 < \rho^*)$, the responses of the two models, as shown in Fig.(2.5,b) produce a perfect match. This shows that the two model structures produce approximately equivalent response subject to input bounds.

2.7 Summary

Volterra variational equations are derived as Volterra series representation of an analytic, input-affine polynomial nonlinear differential system. An alternative proof of Helie-Laroche algorithm which is used for computation of input bounds for convergence of VVM, is derived in frequency-domain. This is more intuitive and elegant that the time-domain proof available in literature. Harmonic input response properties of VVM are probed to show that the number of kernel-states required in it can be determined from PSD of harmonic input experimental data. A comparative study of the VVM and PoDE structure from the perspective of system identification of nonlinear physical systems is presented, as Abramov-Goman model of unsteady aerodynamic loads based on PoDE is

a well established technique in literature. In the end, numerical examples illustrated the concepts presented in this chapter, using the data generated from a Duffings oscillator system.

Chapter 3

Volterra Variational Modeling of Unsteady Aerodynamics

3.1 Introduction

3.1.1 Overview of the Approach

Volterra variational equations are derived from Volterra series for a system operating in the region around a stable equilibrium state, as presented in Chapter 2. Although it has been stated in the literature for four decades [51, 67], it is not as widely used as Volterra series for modeling physical systems [48, 61]. Hence, many of its properties useful for system identification of nonlinear dynamical systems remain unexplored. In this chapter, a formulation of nonlinear unsteady variation of aerodynamic coefficients in the form of VVM and its parameter estimation procedure using forced oscillation wind tunnel data are presented. The formulation is generic, and can easily be adapted for other unsteady aerodynamics applications stated in Chapter 1. The presentation here is focused on the Delta-wing high-performance aircraft configurations.

The model structure is in the form of parametric differential equations. VVEs consist of differential equations of the kernel states corresponding to contribution of each kernel to the Volterra series output. The first state represents linear component of response of the system, typically observed for low energy inputs. So, its time-constant is obtained from the experimental data with small amplitude oscillation inputs. Higher order states introduce corrections due to nonlinear variations which are normally witnessed for large amplitude oscillation inputs. These nonlinear terms change the effective time-scale of variation of aerodynamic loads in response to large-amplitude input. As shown in the case studies of modeling unsteady aerodynamic loads in the Chapter 4, only one to three states in VVM are sufficient for the purpose.

System identification is an iterative process involving the steps of; (i) Model

structure determination, (ii) Experimental data gathering using certain input types, (iii) Consistency and accuracy check for sufficiency of the identified model, and (iv) Validation using independent data [43, 71]. It may be required to reiterate the process with a different option in any of these steps, if the accuracy of the model obtained is not satisfactory. The VVM approach proposed in this chapter offers several options in each step of the system identification process. In this approach, the model structure and parameter estimation method to be used are determined from the available wind tunnel test data.

The proposed model for unsteady aerodynamics based on Volterra variational equations offers some unique practical advantages. The number of kernel states required in the model of an aerodynamic coefficient is determined by the number of super-harmonics in the forced oscillation response. Therefore, the model structure is contingent on the data-based evidence, unlike all the other nonlinear modeling approaches presented in the literature. The model structure is formulated as an incremental effect of unsteady aerodynamics, and hence it can be easily augmented to a classical aero-database type of model. This also makes it useful for validation using flight test data. The model is linear in parameters, and hence it can be estimated from variety of experimental data.

It is important to note that the modeling approaches in literature can usually represent a certain type of nonlinearity in unsteady variation of aerodynamic loads. Although, most of the models in literature can model the mildly nonlinear or practically linear variations in the normal force coefficient, the variations in pitching moment coefficient are significantly nonlinear [42]. The variations in pitching moment coefficient are usually nonlinear for large amplitude or high pitch-rate change in angle-of-attack [1]. The nonlinear extensions of the models proposed in literature are empirical or ad-hoc. For example, Fan and Lutze's state-space model includes three time-constants to tune the model better to the available data, but there is little physical or mathematical basis for it [25]. Hence, there is a need for systematic modeling of the nonlinearity in dynamical variations specific to an application. Therefore, the unsteady modeling approaches are classified based on the nonlinear unsteady aerodynamic phenomena they can model, as given in the next section.

The model structure is expected to be consistent with the physics of flow affecting the unsteady variation of loads. Hence, features of unsteady aerodynamics in the stall angle-of-attack regimes as observed in experimental studies, are summarized in Section 3.2. An overview of dynamic wind tunnel test techniques which are used for identification of unsteady aerodynamic loads is provided in Section 3.3. For delta wing configurations, data generated from small and large amplitude forced oscillation wind tunnel tests are commonly used for modeling. Also, only this type of data is available for modeling the longitudinal aerodynamic coefficients in this research. Hence, based on the features of unsteady aerodynamics and forced oscillation wind tunnel test method, VVM structure

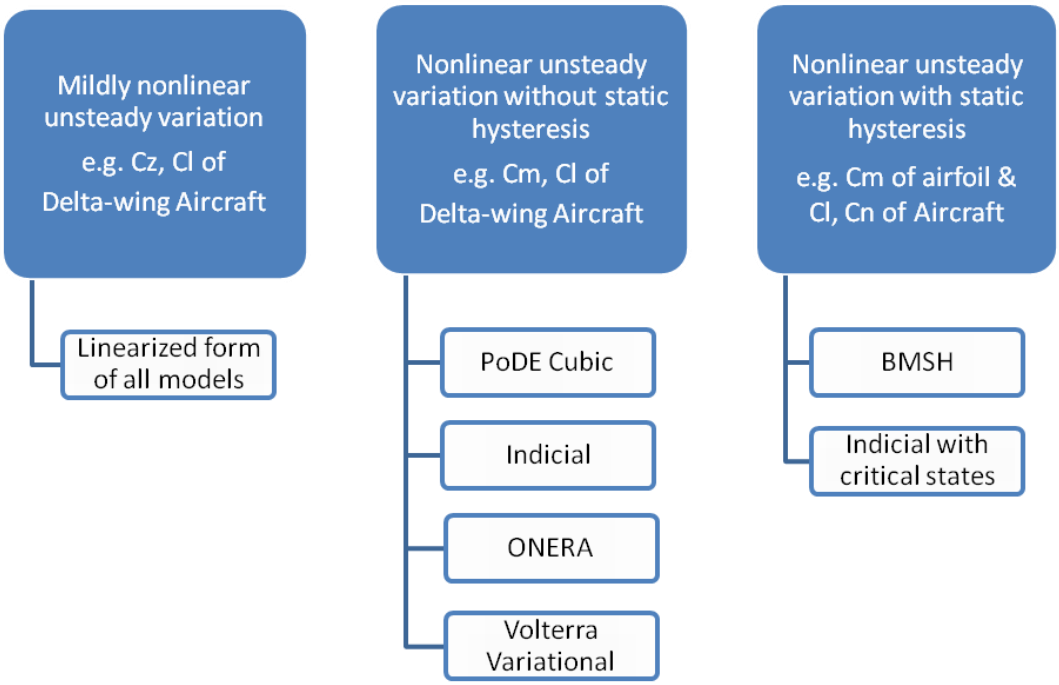

Fig. 3.1. Classification of models based on nonlinear nature of unsteady aerodynamic phenomena.

for modeling unsteady aerodynamic longitudinal loads is formulated in Section 3.4. The model parameter estimation methods using forced oscillation wind tunnel test data are presented in Section 3.5. The implications and interpretations of VVM are shown to be consistent with the experimental observations presented in Section 3.2, in Section 3.6. Alternative formulations with potential applications to other unsteady aerodynamic systems are discussed in chapter (5).

3.1.2 Classification of Modeling Approaches

For the purpose of unsteady aerodynamic modeling using forced oscillation wind tunnel data, we can classify the model structures into three groups based on the nonlinear nature of underlying aerodynamics that they can model, as shown in Fig.(3.1), and discussed here.

1. Mildly nonlinear or practically linear unsteady variation (typical of variation in normal force coefficient)

2. Nonlinear unsteady variation for large amplitude pitching (typical of pitching moment coefficient of Delta-wing configurations) or high-rate pitching motions

(typical of helicopter blades)

3. Strong nonlinearity at aerodynamic critical states crossing, like static hysteresis in longitudinal coefficients in the stall regime and static hysteresis in rolling moment versus roll angle. (typical of airfoil and aircraft wing)

Most of the modeling approaches presented in literature are equivalent in their linearized form or when they are reduced to a linear transfer function form, as discussed in the Chapter 1 and in [6, 42]. These are categorized here as Case (1). It has been observed in many wind tunnel tests that the spectrum of variation of loads in response to small amplitude sinusoidal inputs contains only the first harmonic [72, 73]. Therefore, a first order differential model or a linear transfer function is sufficient to model the unsteady variation of loads with mild nonlinearities. In this chapter, it is shown that VVM can model the mild nonlinearity in unsteady variations which is typically observed for normal force coefficient.

The unsteady variation of aerodynamic coefficients can be significantly nonlinear, and such problems are categorized as Case (2). The mathematical model structures of interest are (i) Linear Indicial model [30](ii) PoDE model [23](iii) ONERA Dynamic Stall model [35] and (iv) Volterra Series model [40]. These models include some nonlinear feature or a term to tune the model to nonlinearity in unsteady variations. These modeling approaches have one of the features of; mathematical rigor, simple estimation approach, and consistent with the qualitative features of aerodynamic flow. The VVM approach presented in this chapter is particularly useful for solving problems belonging to this category. It is shown in Chapter 5 that the VVM can be adapted to or bears connection to all these partially successful nonlinear modeling approaches.

Case (3) usually occurs for the longitudinal coefficients of airfoil; rolling moment coefficient versus roll-angle and yawing moment coefficient versus sideslip angle, for some delta-wing configurations. Myatt presented an application of nonlinear indicial model to the case of rolling moment variation with critical state crossing [33]. Two critical state crossings are considered to model static hysteresis in variation of a coefficient. However, this method requires special experimental data to model the transients during critical state crossing which severely limits its scope of applications. Abramov presented an alternative estimation procedure for the Abramov-Goman model which can simultaneously include the static hysteresis and unsteady variation in the coefficient [20]. This approach is called the Bifurcational Model of Static Hysteresis, and is denoted in Fig.(3.1) as BMSH. It is the only model in literature which can be applied using forced oscillation wind tunnel data. It is found to produce satisfactory results in most of the cases.

VVM cannot be used to model the problems belonging to Case (3) as it is applicable only when the system has a single stable equilibrium. In other words, the systems which encounter bifurcational dynamics in the operational conditions of interest cannot be modeled using VVM. In this sense, the topology of VVM is similar to linear systems which is stretched to incorporate nonlinear variations in time only. Bifurcational model of static hysteresis or the PoDE structure can exhibit variety of bifurcational phenomena. Although the equivalence of VVM and PoDE for system dynamics in the region of attraction of a single stable equilibrium was shown in chapter 2, an intermediate mathematical form which can exhibit spectral properties of VVM and bifurcational dynamics properties of PoDE, remains an open mathematical challenge.

Due to this deficiency, VVM cannot be used for modeling the static hysteresis in $C_l \, vs. \, \beta$ in AWS region. Hence, a new model structure called the Bifurcational model of Aerodynamic Asymmetry (BMAA) is proposed in this thesis. It serves as an alternative to BMSH, when greater number of parameters are required. The BMAA mathematical properties and its application to modeling the static hysteresis and unsteady variation in $C_l \, vs. \, \beta$ in AWS region is presented in Chapter 6.

The rest of the chapter deals with formulation of VVM and investigation of its properties which are particularly useful for modeling nonlinear unsteady aerodynamic loads in the stall regime.

3.2 Characteristics of Vortex Breakdown Effecting Aerodynamic Loads

The unsteady variation of aerodynamic forces and moments in response to change in a flow incidence angle happens due to lag in vortical flow readjustment on the wings. Hence, many of the features of vortical flow are reflected in to variations of aerodynamic forces and moments acting on a maneuvering aircraft. Therefore, understanding the nature of vortical flow is an essential starting point in the formulation of model structure. It is also important because the proposed model structure is expected to be generic enough to reproduce the variations in loads due to input-types not considered in the process of identification. Hence, many of the models for unsteady aerodynamics in literature are formulated using the features of vortical flow phenomenon.

The aerodynamics of delta-wing configurations at stall angles-of-attack and low Mach number is dominated by leading edge vortices on the wing [4]. This is also true for double-delta and strake-delta configurations. All the modern high-maneuverability, high-performance aircraft have one of these three wing-shapes. Hence, extensive experimental studies of vortical flow on delta wings are available in literature. These studies have been

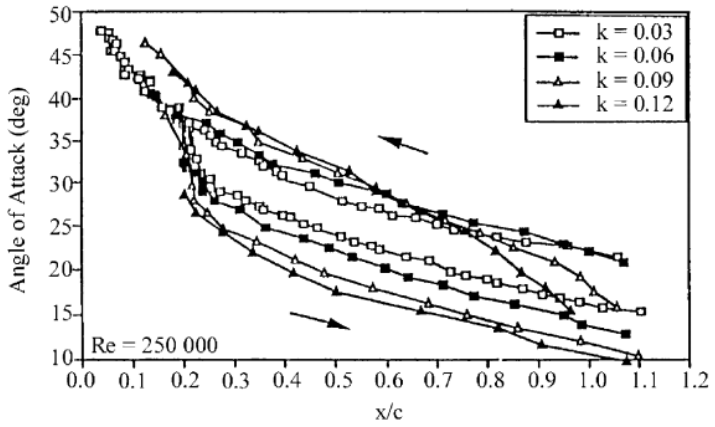

(a) Vortex breakdown location on a wing in response to pitch-up and pitch-down motion at various non-dimensional rates

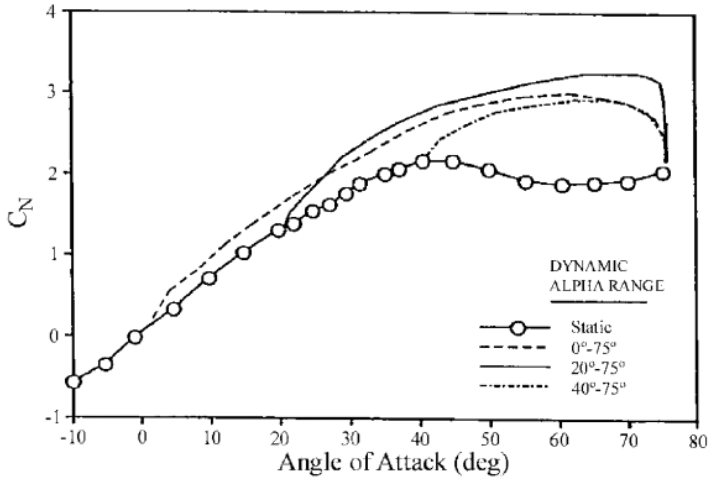

(b) Lift overshoot due to pitch-up motion of a wing starting from different initial α

Fig. 3.2. Features of variation in lift coefficient due to unsteady aerodynamics in the stall region [4].

appropriately reviewed from modeling perspective in [4, 6] and aerodynamics perspective in [74].

For a delta wing with leading edge sweep-angle in 45 to 75 degree range, the flow on the wing leading edge separates to form a flow structure called vortices at a certain moderate angle-of-attack α_v. The vortex core has an axial flow component of very high velocity and low pressure. This creates a suction peak on the wings. It produces an aerodynamic normal force component in addition to that created by the potential flow. Variation of the normal force and pitching moment acting on the wings beyond α_v, depends on these leading-edge vortices.

The strength of the vortices or the airspeed in vortex core increases with increase in angle-of-attack. At a certain angle-of-attack α_b, the vortex structure breaks down

on the wings. This drastically changes the pressure distribution on the wings. As the angle-of-attack is increased beyond α_b, the normal force does not change much and eventually starts decreasing. This nonlinear variation of normal force and pitching moment coefficients is commonly called Stall. Unlike airfoils, the variation in C_Z and C_m for delta-wing aircraft is smooth in this region. There is no static hysteresis versus angle-of-attack either.

The vortex breakdown location on the wings is a function of angle-of-attack and direction of pitching, as shown in Fig.(3.2,a). One can notice that the vortex breakdown location is different in pitch-up and pitch-down motion at a particular angle-of-attack. This is because it shifts towards wing leading edge or away from it with a certain finite time-lag in response to sudden change in angle-of-attack. The variation in load in response to pitch-up input also depends on initial angle-of-attack, as evident from Fig.(3.2,b). These features imply that the pressure on the wing has a memory, that is, the instantaneous pressure on the wing depends on the aircraft motion history [4]. As seen in Fig.(3.2,a), the vortex breakdown location follows a different trajectory in pitch-up and pitch-down motions depending on the non-dimensional pitching rate. It is therefore necessary to perform dynamic experiments in a wind tunnel to capture the transient responses in variation of forces and moments due to change in flow-incidence angles.

Change in angle-of-attack (α) at zero sideslip (β) primarily effects the longitudinal loads acting on the aircraft. Change in sideslip effects both longitudinal and lateral-directional loads. α and β are fundamental flow angles. Hence, the response of aerodynamic loads to variation in α and β is sufficient to model unsteadiness of aerodynamic loads acting on the aircraft [75]. Alternatively, the effect of unsteady aerodynamics on all the aerodynamic coefficients can be simultaneously excited by considering pitching with non-zero sideslip as done in [76]; or by considering body-axis rolling motion as done in [77]. In a forced oscillation wind tunnel test, the model is subject to sinusoidal variation of one of the flow incidence angles $\{\alpha, \beta, \phi\}$. These data are considered to be sufficient for modeling the unsteady variation of longitudinal and lateral-directional aerodynamic loads.

For modeling longitudinal loads experimental data is generated for inputs in (α, β), while for lateral-directional loads inputs in (ϕ, β) are used. This is based on an implicit assumption that the aerodynamic loads can be modeled separately. Although there is some coupling between longitudinal and lateral-directional loads due to change in any flow incidence angle, currently there are no methods for generating suitable data for modeling the loads in an integrated fashion. In this thesis, we focus only on the effect of change in angle-of-attack on the normal force and pitching moment.

Forced oscillation wind tunnel tests characterize the unsteady aerodynamic effects

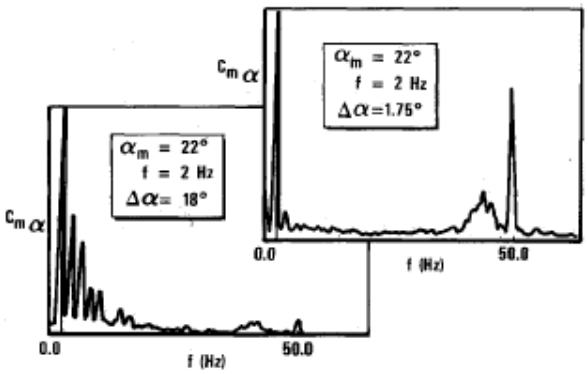

Fig. 3.3. Power spectrum plots showing harmonics in the pitching moment coefficient responses due to harmonic inputs of different amplitudes [73].

in terms of amplitude and frequency of sinusoidal inputs. A forced oscillation test in pitching motion, shows that the aerodynamic loads also vary periodically. A plot of the normal force or pitching moment coefficient shows dynamic hysteresis with respect to their steady state values. Cunningham and Boer observed that for sinusoidal input of small amplitude of the order of $3^o - 5^o$ variation of loads is also sinusoidal, while for larger amplitude inputs higher harmonic components are also generated [72, 73]. This is evident from the power spectrum plots in Fig.(3.2), of the pitching moment coefficient of a double-delta wing configuration. For sinusoidal input of amplitude $\Delta\alpha = 18^o$ there are three harmonics of input frequency excited, while for $\Delta\alpha = 1.75^o$ there is only the first harmonic. In the same experiments, the pressure measurement data also showed the existence of second and third harmonics of the input frequency for large amplitude inputs. The presence of these harmonics implies that the variation of aerodynamic loads is nonlinear in nature.

The linear nature of unsteady variations is also evident from the linear relationship between the in-phase and out-of-phase derivatives estimated from small amplitude forced oscillation test data. Assuming the unsteady variation of aerodynamic loads to be linear for small amplitude inputs in angle-of-attack, it has been shown that the in-phase versus out-of-phase derivatives estimated for an aerodynamic coefficient have a linear relationship between them [22]. As seen in the plot of in-phase versus out-of-phase derivatives in Fig.(3.4), the solid-curve connecting the points for different frequencies is approximately linear for normal force and pitching moment coefficients. Thus, the linear nature of unsteady aerodynamics can be verified from this type of a plot. Such plots or the linear relation, have been reported to be true for many delta-wing configurations like X31 [78], F16XL [31], GTA , Delta-wing model with 65^o leading edge sweep angle (Delta-60)

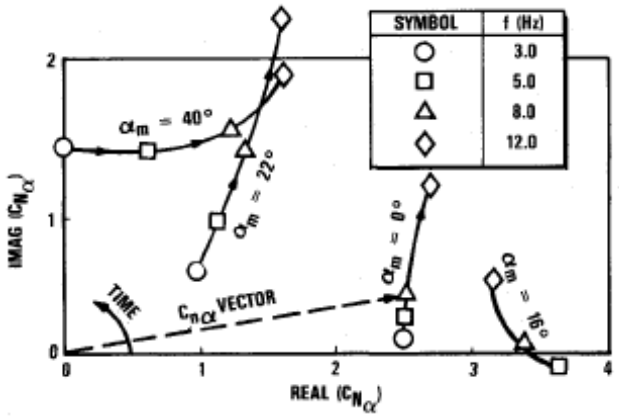

(a) For Normal force coefficient

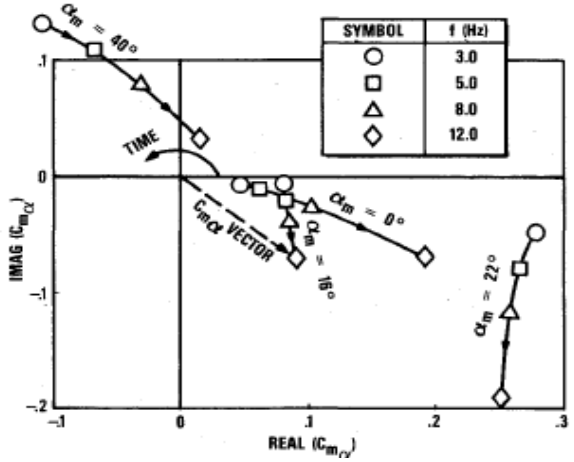

(b) For Pitching moment coefficient

Fig. 3.4. In-phase versus Out-of-phase derivatives estimated from SAFO data for C_Z and C_m of a double-delta wing [73].

wing [22] etc. Therefore, the approximately linear nature of unsteady aerodynamic loads due to small amplitude inputs for delta-wing configurations is a fundamental feature of the aircraft unsteady aerodynamics.

The measurement of time-lag in readjustment of vortex breakdown location also provides evidence of the nonlinear nature of pressure and load variations. Resienthel.et.al. studied the effect of change in pressure gradient on vortex breakdown location by oscillation of the vertical fins of an aircraft model in wind tunnel tests [79]. It was found that the transient response of the vortex-breakdown location in response to change in external pressure gradient (which can be due to any one of angle-of-attack, rolling motion, Elevators, Fins etc.) follows a trajectory similar to that of the response of a linear first-order differential equation to step input. Also, the time-constant for movement of vortex break-down location upstream is higher than the time-constant of its motion down-stream

[79]. These features have been observed for variation of loads in many other experiments presented in literature [74, 3]. The difference in time-constant depending on direction of motion causes the dynamic hysteresis in vortex breakdown location to be nonlinear.

All these experimental evidences imply that that a nonlinear model structure is essential to represent the nonlinear nature of unsteady aerodynamic loads.

3.3 Wind Tunnel Test Techniques

Unsteady aerodynamic models are estimated for a given aircraft using dynamic wind tunnel test data. Small and large amplitude forced oscillation wind tunnel test data are primarily used for modeling the aerodynamic loads at stall. The rotary balance wind tunnel tests provide steady aerodynamic loads for conical motion, which is primarily of interest in the angle-of-attack range covering steep or flat spins [3]. Wind tunnel facilities for capturing such data are available in many organizations across the world, and have been in use for more than four decades. Hence, most of the experimental studies and estimation of the model parameters is done using this type of data for delta-wing configurations and some airfoils. A detailed description of all the important dynamic wind tunnel test methods and their comparative analysis for consistency of the data, are available in [3].

Other methods of obtaining data for estimation and validation of the unsteady aerodynamic model are flight tests and Computational Fluid Dynamics (CFD). There are two attempts presented in literature where the flight test data was used for estimation or validation of unsteady variation in normal force coefficient. Data from the flight tests done at TsAGI, Russia were used to validate the Goman-Khrabrov State-space model, which was estimated using wind tunnel data [11]. The second flight tests done at DLR, Germany on a C-160 aircraft were used for estimation of the parameters for a similar model structure [19, 26]. These results were good and so important to the research community that it forms the cover page of the popular textbook by Jategaonkar [71].

There are continuing efforts towards unsteady aerodynamics numerical simulations using CFD techniques. A significant progress has been made recently, for example the work in [80]. A comparative study of the CFD results with the flight test data was presented in [81]. However, these methods have not been shown to be effective for modeling any aircraft unsteady aerodynamic loads.

3.3.1 Forced Oscillation Wind Tunnel Test

Forced oscillation wind tunnel tests have been performed on many delta-wing configurations in order to model the unsteady variation of coefficients in the stall angle-of-attack

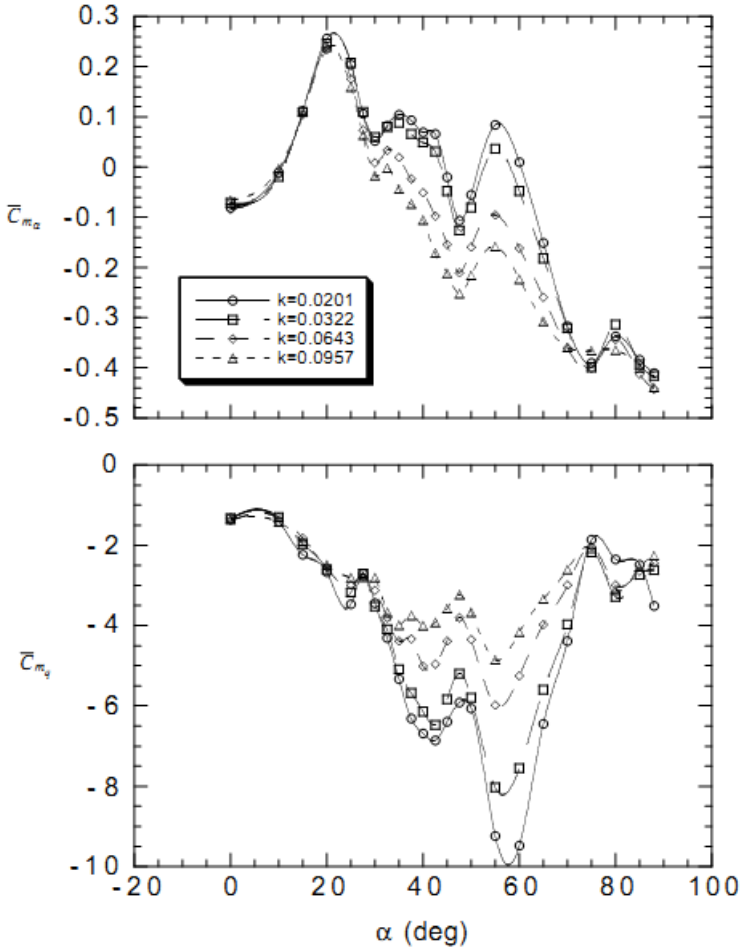

Fig. 3.5. Small amplitude forced oscillation wind tunnel test data for X31 aircraft [78].

regime. The rigs for performing this test are available in Central Aero-hydrodynamic Institute (Russia), ONERA (France), NASA-Langley Research Center (USA), Indian Institute of Science (India) etc. These rigs are designed to provide inputs to the model by changing α or β or ϕ. In this test, the models pitch-angle is varied in a sinusoidal manner at a particular amplitude and frequency. The tests are performed with different amplitude and frequency combinations to obtain responses in a variety of conditions. These tests are performed in two sets classified by the amplitude of input as, (i) Small Amplitude Forced Oscillation test (SAFO), and (ii) Large Amplitude Forced Oscillation test (LAFO).

Classically, small amplitude forced oscillation test data is reduced to in-phase and out-of-phase derivatives by numerical computation of the first two terms of the Fourier series expansion. This is possible because the aerodynamic coefficient variation is also found to be sinusoidal. The out-of-phase derivative which is commonly referred to as damping derivative, is incorporated as a table in an aero-database. However, in the stall angle-of-attack regime, it is found to be a strong function of frequency as shown in Fig.(3.5) for

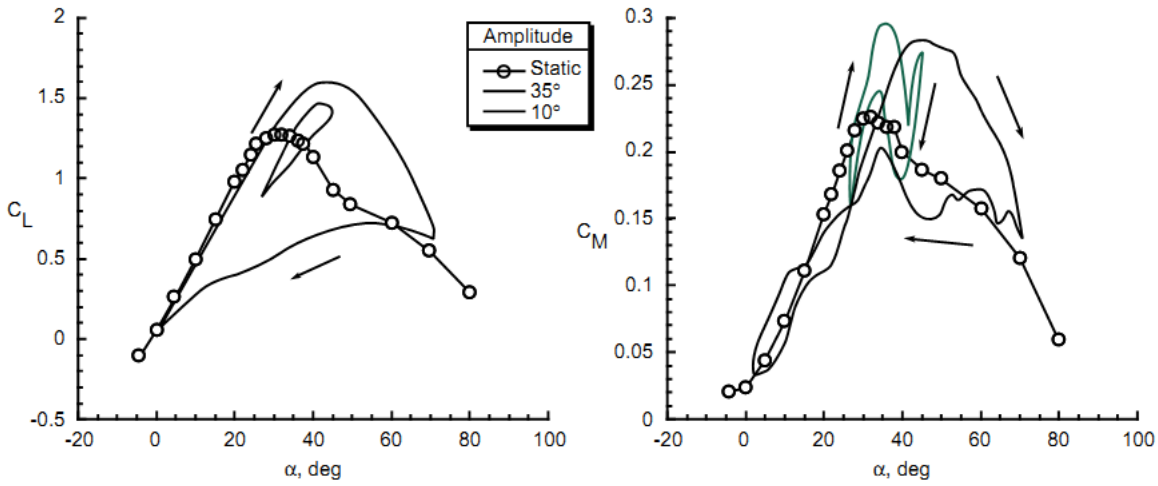

Fig. 3.6. Large amplitude forced oscillation wind tunnel test data for F16XL, with sinusoidal inputs of amplitudes $\Delta\alpha = 10^o, 35^o$, maximum pitch-rate $k_{max} = 0.02$, and $\alpha_0 = 36^o$ [82].

pitching moment coefficient of X31 aircraft.

The variations in the normal force and pitching moment coefficients of F16XL in response to large amplitude sinusoidal inputs is shown in Fig.(3.6). In case of C_L, the values for two input amplitudes differ by up to 0.5 in pitch down motion. In case of C_m, the oscillation cycle is twisted indicating aerodynamic damping and anti-damping. These figures show that the aerodynamic loads are also a strong function of input amplitudes. The power-spectrum-density maps of these coefficients showed that there are super-harmonics, which implies that the variations are also nonlinear in nature.

Similar observations have been made from the small and large amplitude forced oscillation tests for many delta-wing aircraft [4]. Therefore, the amplitude and frequency dependence of aerodynamic loads is a fundamental aerodynamic feature of any delta-wing configuration in the stall region.

3.3.2 Rotary Balance Rig

Rotary balance test is one of the oldest dynamic wind tunnel tests. In this test, the aircraft model is rotated about the wind axis at a steady rotation rate. The model is rotated over a range of non-dimensional rates corresponding to the likely coning rate in spin for the given aircraft configuration. The wind tunnel model motion is similar to steady stable spin of an aircraft, except that the radius of rotation is equal to zero. The test was conceived to characterize the aerodynamic loads on an aircraft in steady spin conditions. Hence, this data is primarily used to model aerodynamic loads in the spin angle-of-attack regime which is usually at much higher angle-of-attack than the stall conditions.

The stability derivatives for the lateral-direction coefficients can also be estimated

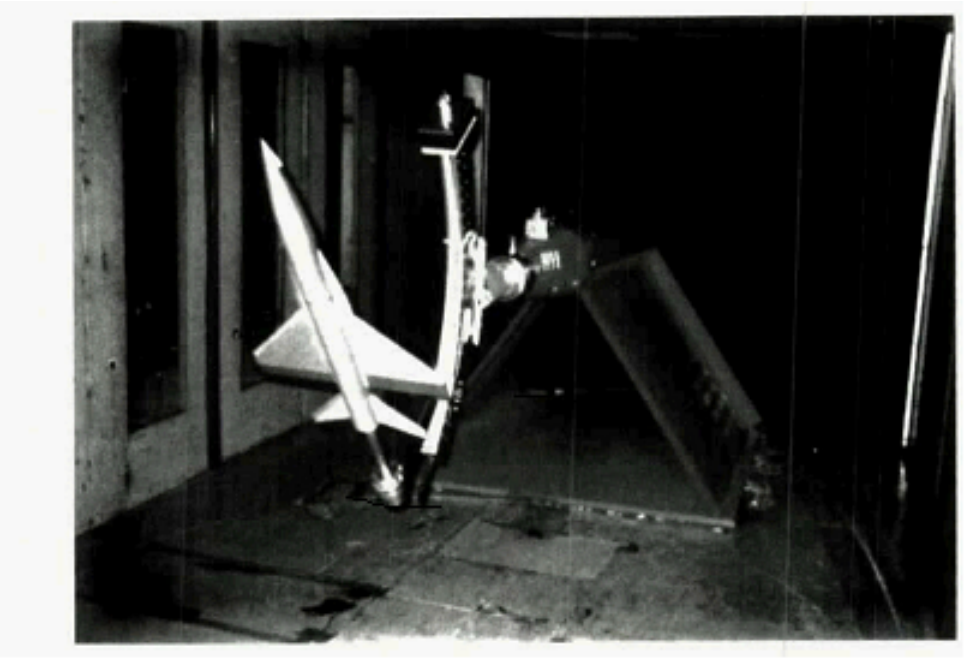

Fig. 3.7. NASA/Editics Rotary Balance Rig with WG16B research model installed [3].

from this data. Details of various rotary balance test rigs in different organizations across the world and their comparative analysis is presented in [3]. This data is not directly useful for unsteady modeling of longitudinal coefficients, but it is complementarily used in development of an aerodynamic model for the full angle-of-attack range of $(-90^o\ 90^o]$.

3.3.3 Some Novel Rigs

Recently, novel rigs for performing wind tunnel tests in which model can be moved about multiple-axis and multiple degree-of-freedom have been developed at University of Bristol [83] and Indian Institude of Technology Kanpur [84]. The rig developed at Bristol is shown in Fig.(3.8). The rig can provide all degrees-of-freedom except the axial motion of the aircraft model. Hence, it can closely simulate the aircraft's initial response and steady state response to external flow conditions. The rig has mechanism to restrict some of the degrees-of-freedom and to asses the aircraft's dynamic response in specific axis. Thus, it is possible to undertake a variety of novel dynamic wind tunnel tests for high-fidelity unsteady modeling and its validation.

A wide-band input in the form of a Schroder-sweep was used for performing dynamic tests at NASA-Langley using Eidetics corporation water tunnel [44]. Such a method can save the need for repetitive tests with multiple frequencies, and save time and cost. It is also expected to show better correlation with load variations obtained from other tests as the data is representative of the system response over a bandwidth instead of some

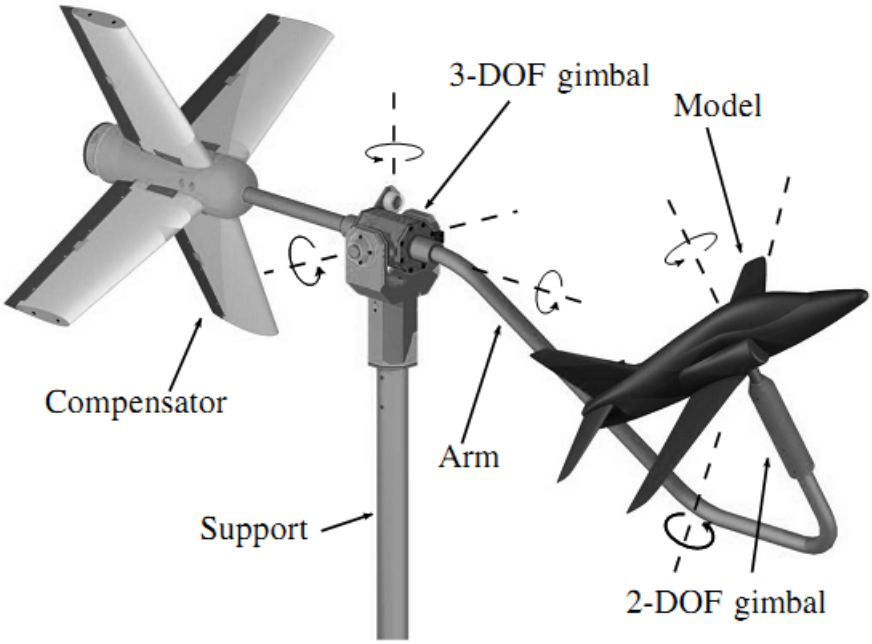

Fig. 3.8. Five Degrees-of-freedom rig developed at the University of Bristol for dynamic wind tunnel tests [83].

discrete frequencies. This concept is discussed in Chapter 5.

A novel rig called the Dynamic-pitch-plunge-rig was developed in Virginia-Tech University, USA and used for modeling the unsteady variation of rolling moment coefficient of delta-wing configurations [33]. This method is a promising approach for obtaining coupled variation of different moment coefficients from wind tunnel experiments for the purpose of modeling.

3.4 Model Structure for Longitudinal Coefficients

3.4.1 Requirements for Validity of the Model Structure

The features of unsteady aerodynamics are summarized in Section (3.2), while VVEs were derived in Chapter 2. For application of VVEs to model variations in $C_Z(t)$ and $C_m(t)$ in the stall angle-of-attack regimes, these coefficients should meet the assumptions made in derivation of VVEs.

The Volterra series is used to model the systems with memory effect, i.e the systems for which instantaneous output depends on the history of inputs. As presented in the previous sections, the variation in longitudinal loads depends on initial angle-of-attack α_0 and trajectory of $\alpha(t)$ input. Thus, the longitudinal force or moment coefficient is determined by history of input $\alpha(t)$.

When the aircraft comes to rest at a particular angle-of-attack, $C_Z(t)$ and $C_m(t)$ always converge to a steady state value, which is known from static wind tunnel tests. Thus, they meet the essential system requirement that the system must have a single stable steady state for given inputs.

The VVEs are equivalent to Volterra series for a system which is analytic in state and input-affine, in addition to the conditions stated above. From static wind tunnel tests data, it is known that the $C_Z(\alpha)$ and $C_m(\alpha)$ of the delta wing aircraft are smooth enough to be approximated by a polynomial in α. There is no static hysteresis or any other bifurcation. Therefore, longitudinal coefficients are analytic. In the model structure formulation presented in the next section, the system of aerodynamic coefficients is assumed to be input-affine with $\dot{\alpha}$ as input.

Physical systems should have fading-memory in order to model it using Volterra series truncated to a finite number of kernels. This is evident if the system produces a periodic response to a periodic input [68]. In forced oscillation tests the normal force and pitching moment coefficients settle to a periodic variation in response to sinusoidal inputs. This shows that the coefficients have fading memory and depend only on a finite history of motion $\alpha(t)$. Thus, longitudinal coefficients exhibit fading memory effect.

Thus, $C_Z(t)$ and $C_m(t)$ for an aircraft maneuvering in the stall regime satisfy all the conditions essential to model them in the form VVM.

3.4.2 Proposed Model Structure

A classical aero-model, commonly referred to as aero-derivative model or an aero-database, is built using data from static wind tunnel tests. It is in the form of data-tables which consist of incremental change in coefficient as a function of flow-angles and control surface deflections. The effect of unsteady aerodynamics is incorporated in the form of so called damping derivatives. At the angles-of-attack before stall, damping derivatives are included in a look-up table with angle-of-attack as the look-up parameter.

An aero-database is used for performing both flight dynamic analysis and for real-time flight simulation studies. If the aero-database has been validated from flight test data, it is expected that the model is kept intact for any further modeling or analytical studies. Therefore, the proposed model structure for C_Z and C_m to account for unsteady aerodynamic effects, is formulated as an add-on over the aero-database.

$$C_Z(t) = C_{Z_{st}}(\alpha(t)) + C_{Z_q}(\alpha(t))\frac{q\bar{c}}{2V} + C_{dyn}(\alpha(t), \dot{\alpha}(t)) \tag{3.1}$$

Consider the splitting of $C_Z(t)$ into the components of corresponding steady state value and incremental unsteady variations as given in Eq.(3.1). $C_{Z_{st}}(\alpha)$ is the steady state

value of C_Z at each angle-of-attack, and it is known from static wind tunnel tests. C_{Z_q} represents the incremental effect of steady pitching motion on C_Z. $C_{dyn}(t)$ represents the unsteady variation due to rate of change in flow incidence angles. In this thesis, we consider the unsteady effect of change in angle-of-attack only. This component is required to be identified from dynamic wind tunnel test data.

C_{Z_q} is the pitch-rate derivative that represents the damping effect due to pure pitching motion of the aircraft. This corresponds to vertical rotational motion of a particular radius, in which angle-of-attack remains constant ($\dot{\alpha} = 0$). In an aero-derivative model, it is estimated using empirical methods. It can also be estimated from flight test data by system identification techniques [71]. But this is valid only for low angles-of-attack or the regions of linear aerodynamics. It cannot be estimated directly from the small amplitude forced oscillation test data, as in this test the pitching motion of the wind tunnel model simultaneously produces pitch-rate and change in angle-of-attack, such that $\dot{\alpha} = q$. The contribution of C_{Z_q} to C_Z is usually found to be of small magnitude, while C_{m_q} can produce significant contribution to C_m.

A recent study, by Khrabrov and Greenwell, presented two methods for computing the effect of steady pitch rate on the normal force and pitching moment coefficients of a 2D airfoil [85]. In these models the derivatives C_{N_q} and C_{m_q} are accurately modeled as a function of flow separation point x_s and the non-dimensional pitching frequency, in stall angle-of-attack region. This model was not considered in the proposed model formulation as the flow separation point (or vortex break-down location) is not included in it. In the proposed VVM formulation, the pitch-rate derivatives are estimated simultaneously with parameters of the model of $C_{dyn}(t)$ using SAFO data.

The component $C_{dyn}(t)$ represents the incremental component of force due to unsteady aerodynamics. This is modeled based on VVM. Any change in angle-of-attack produces a non-zero value of $C_{dyn}(t)$. Hence, consider $\dot{\alpha}(t)$ to be the input and $C_{dyn}(t)$ to be the output of the system. This system has a stable equilibrium $[C_{dyn}(t), \dot{\alpha}(t)) = (0, 0)]$ over the domain $\alpha \in [-90^o, 90^o)$. The input $\dot{\alpha}$ has an upper-bound which depends on operational conditions of the given aircraft type. From Eq.(3.1), it is evident that $C_Z(t)$ converges to $C_{Z_{st}}(t)$ with a finite time delay when $(\dot{\alpha} = 0)$, and its time-scale is the same as that governing $C_{dyn}(t)$. Thus, $C_{dyn}(t)$ sufficiently represents the unsteady component of load for modeling using VVM.

The VVEs are given as equations (2.19-2.21), in Chapter 2. The response of vortex breakdown location to change in angle-of-attack is known to be similar to first-order linear differential system [74], and all the models except the ONERA Dynamic Stall model can be reduced to an equivalent first-order differential equation [42]. Hence, the differential operator in VVEs is taken to be of first-order only, i.e. $F(d/dt) = d/dt + a$. The

differential equations of only first three kernel states are used in this formulation because three states were found to be sufficient in the case studies in Chapter 4 and the equations of higher order kernel states are much more complicated. In order to avoid confusion between the equivalence of PoDE model parameters and VVEs as extensively dealt with in Chapter 2, different notations for the parameters of VVM are used in the formulations presented here onwards. Input gain parameter $b_1 = K_1$ and the time-scale parameter $a_1/p_1 = -a = 1/\tau$. Other parameters have been redefined in terms of K_i as, $a_2 = K_{21}$, $b_2 = K_{22}$, $a_3 = K_{31}$, $b_3 = K_{32}$. Taking into account all these aspects, the Volterra variational model of $C_{dyn}(t)$ is given by,

$$\begin{aligned}
C_{dyn}(t) &= x_1(t) + x_2(t) + x_3(t) \\
\dot{x}_1(t) &= a(t)x_1(t) + K_1(t)u(t),\ x_1(0) = 0 \\
\dot{x}_2(t) &= a(t)x_2(t) + K_{21}(t)x_1^2(t) + K_{22}(t)x_1(t)u(t),\ x_2(0) = 0 \\
\dot{x}_3(t) &= a(t)x_3(t) + K_{21}(t)x_1^3(t) + K_{31}(t)x_1(t)x_2(t) + \\
&\quad K_{32}(t)x_2(t)u(t) + K_{22}(t)x_1^2(t)u(t),\ x_3(0) = 0
\end{aligned} \tag{3.2}$$

For a time-invariant system, all the parameters of the model can be considered to be constants. In case of unsteady aerodynamics, the variations in loads depend on initial angle-of-attack, and its characteristic time-scale is a function of angle-of-attack. This angle-of-attack dependence is accounted for by considering the model parameters as function of angle-of-attack. As presented in the previous chapter, any constant value of the parameters can reproduce amplitude and frequency dependence. Therefore, we consider all the parameters to be functions of instantaneous angle-of-attack α. Thus, the model for $C_{dyn}(t)$ becomes as in Eq.(3.3).

$$\begin{aligned}
C_{dyn}(t) &= x_1(t) + x_2(t) + x_3(t) \\
\dot{x}_1(t) &= a(\alpha)x_1(t) + K_1(\alpha)\dot{\alpha}(t),\ x_1(0) = 0 \\
\dot{x}_2(t) &= a(\alpha)x_2(t) + K_{21}(\alpha)x_1^2(t) + K_{22}(\alpha)x_1(t)\dot{\alpha}(t),\ x_2(0) = 0 \\
\dot{x}_3(t) &= a(\alpha)x_3(t) + K_{21}(\alpha)x_1^3 + K_{31}(\alpha)x_1(t)x_2(t) + \\
&\quad K_{32}(\alpha)x_2(t)\dot{\alpha}(t) + K_{22}(\alpha)x_1^2(t)\dot{\alpha}(t),\ x_3(0) = 0
\end{aligned} \tag{3.3}$$

The VVM gives differential equations for second and third kernels containing nonlinear terms in x_1, x_2, x_3. The parameter values in these equations give a certain definite kernel shape, and this has been obtained computationally in [86]. Further, an interpretation of each of these terms as the effect on time-constant of a step response is also provided. Using these interpretations it is possible to choose or reject a certain term in the model structure beforehand. This is especially useful when the parameter of

a term is found to be insignificant and hence can be removed from the model structure. Excluding a certain nonlinear term implies that the kernel shape is constrained. However, reducing the parameters to be estimated in a three state model can improve the accuracy of the model.

It is important to note that, in this formulation there is no assumption of the type of data implicitly or explicitly, as done in other model structures proposed in literature. Therefore, this model structure is generic and can be further extended to any application, and estimated from any data using an appropriate approach.

In the next step, the parameter functions are required to be estimated from small and large amplitude forced oscillation wind tunnel test data, as discussed in the next section.

3.5 Identification using Forced Oscillation Wind Tunnel Data

3.5.1 Model Order Determination

As shown in chapter 2, the sinusoidal input response of VVE has some special properties. The response contains only super-harmonics. The n-th kernel state produces n-th harmonic and lower order harmonics of same parity. Therefore, for a model with n kernel states, n-th harmonic is the highest order harmonic in the response. In the response to relatively small amplitude input, only $x_1(t)$ is significant. Hence, the response of VVM is approximately linear. These properties are in direct correlation with the forced oscillation wind tunnel data.

The number of kernel states to be considered in the model can be determined using Power Spectrum Density (PSD) of the harmonic input response data. As discussed in Section 3.2, the variation in aerodynamic forces and moments on the wing in response to large amplitude sinusoidal change in angle-of-attack contains only super-harmonics. For small amplitudes of input, the force and moment variations contain only first harmonic. Hence, the entire LAFO test data is scanned to determine the highest harmonic n_{max} present in any of the responses. Then, model structure for the aerodynamic load consisting of n_{max} kernel states is sufficient.

The experimental data can be marred by low-frequency noise, and hence the highest frequency peak in the PSD may not have sufficient power relative to noise. In such cases, it is left to the judgement of the modeler to consider a low order VVM. Such a model may not be the best-fit but is essentially devoid of the effects of noise.

3.5.2 Estimation of Time-scale using SAFO Data

The linear response model parameters, time-constant $a(\alpha_0)$ and dynamic-gain $K_1(\alpha_0)$ are estimated in two steps at each angle-of-attack α_0. The first step is identification of time-scale by linear regression. This is due to linear relation between in-phase versus out-of-phase derivatives. This is proved for VVM by linearizing the single-state model in Eq.(3.3) at α_0, and then deriving an analytical representation of in-phase and out-phase derivatives of its response to sinusoidal input.

In a small amplitude forced oscillation test, the wind tunnel model is oscillated in pitch in a sinusoidal motion as $\alpha(t) = \alpha_0 + \Delta\alpha sin(\omega t)$. The measured normal force coefficient $C_Z(t)$ is converted to in-phase derivative $C_{Z_{\alpha,\omega_0}}(\alpha_0)$ and out-of-phase derivative $C_{Z_{\dot{\alpha},\omega_0}}(\alpha_0)$ by harmonic analysis of the time-series data. The pitching frequency is non-dimensionalised as $\bar{\omega} = \frac{\omega\bar{c}}{2V}$, where, $\bar{c}$ is mean aerodynamic chord and V is the air speed. Therefore, the steady-state response of the normal force coefficient measured in a wind tunnel test is given by,

$$C_Z(t) = C_{Z_0}(\alpha_0) + C_{Z_{\alpha,\omega_0}}(\alpha_0)\Delta\alpha\sin(\omega t) + C_{Z_{\dot{\alpha},\omega_0}}(\alpha_0)\bar{\omega}\Delta\alpha\cos(\omega t) \tag{3.4}$$

Now consider the response of VVM given by Eq.(3.3). For small amplitude input, only first kernel state is significant and the model response is linear. So for small amplitude pitching motion $C_{dyn}(t) = x_1(t)$. Therefore, the output $C_{dyn}(t)$ to the input $\dot{\alpha} = \Delta\alpha\bar{\omega}\cos(\omega t)$ is given by,

$$\begin{aligned} \dot{C}_{dyn}(t) &= \dot{x}_1(t) \\ &= a(\alpha_0)x_1 + K_1(\alpha_0)\dot{\alpha}(t) \\ &= a(\alpha_0)x_1 + K_1(\alpha_0)\bar{\omega}\Delta\alpha\cos(\omega t) \end{aligned} \tag{3.5}$$

Solving this differential equation, the steady-state solution $C_{dyn}(t)_{ss}$ is obtained as,

$$C_{dyn}(t)_{ss} = \frac{K_1\Delta\alpha\bar{\omega}^2}{a^2+\bar{\omega}^2}sin(\omega t) - \frac{K_1\Delta\alpha\bar{\omega}a}{a^2+\bar{\omega}^2}\cos(\omega t) \tag{3.6}$$

Then the Eq.(3.1) is linearized at α_0 and the above equation is substituted in it to get the total normal force coefficient as,

$$\begin{aligned} C_Z(t)_{ss} &= C_{Z_0}(\alpha_0) + C_{Z_{\alpha,st}}(\alpha_0)\Delta\alpha sin(\omega t) + C_{Z_q}(\alpha_0)\bar{\omega}\Delta\alpha\cos(\omega t) \\ &+ \frac{K_1\bar{\omega}^2}{a^2+\bar{\omega}^2}\Delta\alpha sin(\omega t) - \frac{K_1 a}{a^2+\bar{\omega}^2}\Delta\alpha\cos(\omega t) \end{aligned} \tag{3.7}$$

Equations (3.4) and (3.7) represent steady state variation of the aerodynamic

coefficient from the wind tunnel test and VVM response respectively. Hence, comparing them gives the relation between model parameters and experimental derivatives as,

$$\begin{aligned} C_{Z_{\alpha,\omega_0}}(\alpha_0) &= C_{Z_{\alpha,st}}(\alpha_0) + \frac{K_1\bar{\omega}^2}{a^2+\bar{\omega}^2} \\ C_{Z_{\dot{\alpha},\omega_0}}(\alpha_0) &= C_{Z_q}(\alpha_0) - \frac{K_1 a}{a^2+\bar{\omega}^2} \end{aligned} \tag{3.8}$$

Rearranging the terms in Eq.(3.8), a linear relation between $C_{Z_{\alpha,\omega_0}}(\alpha_0)$ and $C_{Z_{\dot{\alpha},\omega_0}}(\alpha_0)$ is evident as given in Eq.(3.9). $C_{Z_{\alpha,\omega_0}}(\alpha_0)$ and $C_{Z_{\dot{\alpha},\omega_0}}(\alpha_0)$ are known from SAFO test data at various α_0 for at least three frequencies.

$$C_{Z_{\alpha,\omega_0}}(\alpha_0) = aC_{Z_{\dot{\alpha},\omega_0}}(\alpha_0) + [C_{Z_{\alpha,st}}(\alpha_0) + K_1 - C_{Z_q}(\alpha_0)] \tag{3.9}$$

The linear relation between in-phase versus out-of-phase derivative must be validated before estimation of the first kernel state parameters using SAFO data. In the parameter estimation process, in-phase and out-of-phase derivatives are estimated from the SAFO data. The effects of measurement noise and mild nonlinearities are removed. However, it is important to check the harmonics in small amplitude response and nonlinearity in static variation on the range of angle-of-attack corresponding to the amplitude used in the test.

Then, $a(\alpha_0), K_1(\alpha_0)$ at each α_0 in the stall region can be estimated by the two-step regression method presented in [22]. This method is given in APPENDIX 1 and the estimation procedure is illustrated in the the next chapter.

3.5.3 Estimation of Nonlinear Model Parameters using LAFO Data

The parameters of the first kernel state represent linear-dynamical variations, and are identified from SAFO data at certain mean angle-of-attack intervals. However, the time-constant of vortex dynamics changes with angle-of-attack. Hence, the parameters of VVM are considered as functions of angle-of-attack. This in turn makes the unsteady aerodynamic model nonlinear for large-amplitude changes in angle-of-attack. It is important that the resulting nonlinear response of the model be identified to be consistent with the nonlinear variations captured in the LAFO data. Hence, defining a parameter function by simply using the linear interpolation of the values from the first step is inadequate. Therefore, the LAFO data should be first used to tune the parameter functions $(a(\alpha), K_1(\alpha))$.

For large amplitude sinusoidal inputs, the nonlinear nature of variations is indicated by the presence of higher order harmonics. Hence, the higher order kernel states become important. So, the estimated parameter functions $(a(\alpha), K_1(\alpha))$ are frozen, and then the

parameters of higher order kernel states are estimated by the output-error method. since VVM is linear in parameters, the estimates obtained from output-error method are also the maximum likelihood estimates [43].

Estimation of parameter functions becomes tricky due to the issues of, number of node-points and optimization algorithm to be used. As known from the system identification theory, a larger number of node-points than essential will cause the variance of the estimated values to be larger. This implies that the bounds on values of parameters at node-points will be bigger. Although larger number of node-points improve the accuracy of results, it reduces the fidelity of the model for simulation using random inputs.

A proper choice of optimization algorithms is important because the parameters need to be estimated using a large data-set. A combination of both gradient and steepest-descent based methods are used in the current study. These issues are illustrated in the case studies presented in the Chapter 4.

3.5.4 Estimation of Input bounds for Convergence

Helie-Laroche algorithm for estimation of input bounds for convergence of Volterra series or Volterra variational equations was presented in Chapter 2. This method has been demonstrated to be effective using the example of Duffings oscillator system in Section 2.6. In case of VVM, the parameters are not constants but a function of angle-of-attack. Hence, the input bounds can also be computed as function of angle-of-attack. Its validity though is questionable as the parameters vary continuously with change in angle-of-attack. This is a mathematically complex problem which was not probed further in this work.

It was realized during its application to the unsteady aerodynamic models estimated for coefficients of GTA and F16XL that the estimated value is too small. This is because the Helie-Laroche algorithm gives a conservative estimate of bounds by considering the minima for any input type. The estimated bound corresponds to the case of constant input, i.e. zero frequency. Therefore, there is a need to extend the result to the case of input trajectories like step, ramp and harmonic input. An approach to compute input bound for the case of Duffings oscillator system considering harmonic input is due to Pang and Lang given in [87]. Several attempts to follow a combination of the two approaches to obtain an appropriate estimate considering harmonic inputs did not succeed.

Estimation of convergence bounds for the estimated unsteady models is apparently not necessary. With the estimated unsteady models for GTA and F16XL presented in the next chapter, the convergence was never found to be an issue. These models have been used in a variety of flight simulation studies, and the estimated VVMs have never been found to diverge to infinity or produce any unreasonable response. Therefore, for

the problem of modeling unsteady aerodynamic loads using VVM, convergence is not an important issue. This may also be a reason why it has been ignored in the applications to physiological systems presented in the book [48].

3.6 Phenomenological Interpretations of VVM

In this section, the VVM is shown to be consistent with the aerodynamic features observed in the experimental studies for delta-wing aircraft, as summarized in Section 3.2.

The time-scale of unsteady variation can be determined from the response to low-energy input while the effective time-scale for high-energy input is different due to excitation of higher-order states. This can be explained considering a mildly nonlinear coefficient which is adequately modeled by the two-state VVM in Eq.(3.10). Even for a large amplitude input, the kernel state $x_1(t)$ produces the most dominant contribution, that is $\|x_1\| > \|x_2\|$, and hence we can assume that $C_{dyn} = x_1$ in Eq.(3.11). In this case, the differential equation for $C_{dyn}(t)$ can be approximated as,

$$\begin{aligned} \dot{C}_{dyn}(t) &= \dot{x_1}(t) + \dot{x_2}(t) && (3.10) \\ &= a(\alpha)x_1(t) + K_1(\alpha)\dot{\alpha}(t) + a(\alpha)x_2(t) + K_{21}(\alpha)x_1(t)\dot{\alpha}(t) + K_{22}(\alpha)x_1(t)^2 \\ &\simeq [a(\alpha) + K_{21}(\alpha)\dot{\alpha}(t)]C_{dyn}(t) + K_{22}(\alpha)C_{dyn}(t)^2 + K_1(\alpha)\dot{\alpha}(t) && (3.11) \end{aligned}$$

where $\alpha(t)$ is replaced by α. In this formulation, the effective time-constant for unsteady variation of $C_{dyn}(t)$ is the effective time-constant of nonlinear unsteady variation of the aerodynamic coefficient, which is due to large amplitude pitching motion input.

The Eq.(3.11) is nonlinear in $C_{dyn}(t)$, and excluding the input term the remaining expression has two solutions, $C_{dyn,1} = 0$ and $C_{dyn,2} = \frac{-a(\alpha)}{K_{22}}$. The solution $C_{dyn,2}$ is unrealistic for typical values of $a(\alpha), K_{22}(\alpha)$ presented in the next chapter. So $C_{dyn,1} = 0$ is the only realistic solution. The effective time-constant for equilibrium at $C_{dyn,1} = 0$ is given by $[a(\alpha) + K_{21}(\alpha)\dot{\alpha}]$. In this expression, the effective time-constant depends on $\dot{\alpha}$, which implies that it is determined by the direction of pitching motion. For a stable VVM $a(\alpha) < 0$, and the estimated values of $K_{21}(\alpha) \leq 0$ as seen in the case studies in Chapter 4. Therefore, in pitch-up motion $\dot{\alpha} > 0$, and $[a(\alpha) + K_{21}(\alpha)\dot{\alpha}]$ has a larger magnitude than in pitch-down motion. This has been observed to be true for unsteady variation of normal force or pressure variation in at least two experimental studies discussed in the following paragraphs.

Reisenthel.et.al observed in their experiments on the effect of oscillating fin on vortex breakdown location that the time-constant for upstream motion of vortex breakdown location is larger than that for downstream motion [79]. Upstream motion of vortex

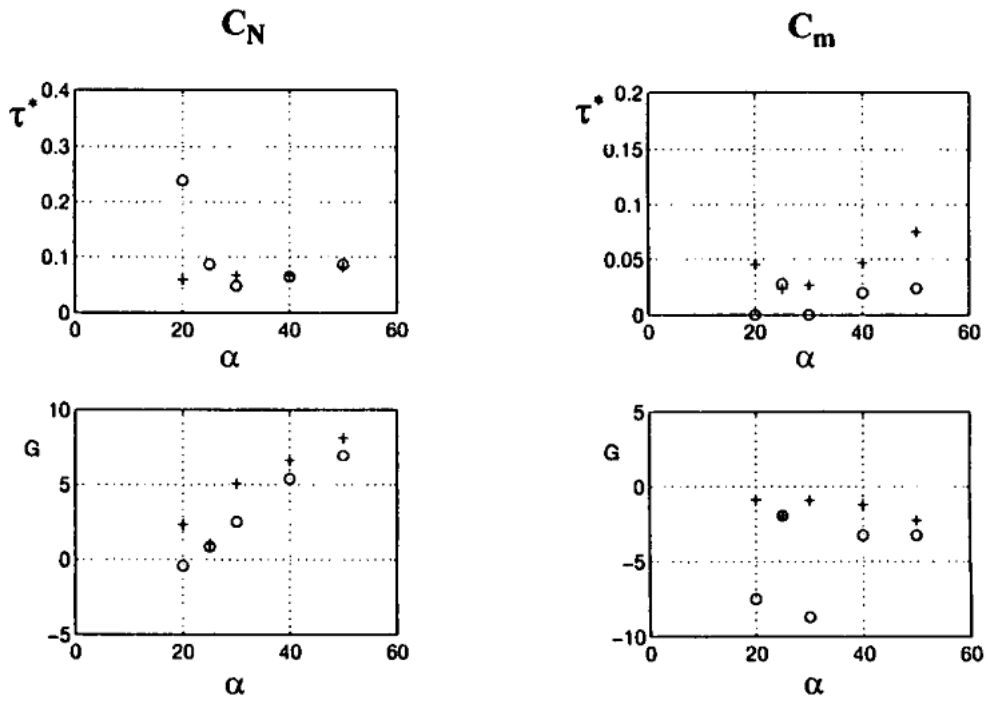

Fig. 3.9. Time-scale τ^* and dynamic gain G of a linear transfer function model identified from experimental data by Tristrant; for pitch-up motion ($+$) and pitch-down motion (o) [3].

breakdown location corresponds to pitch-up and downstream motion to pitch-down. Therefore, the time-constant for pitch-up is larger than that in pitch-down motion.

This phenomena was also observed in the wind tunnel test data based studies reported in [3]. A linear transfer function type of unsteady model was used for identification using the wind tunnel test data from pitch-up and pitch-down motions separately. The estimated value of gain and time-constant parameters are as presented in Fig.(3.9). This clearly shows that the time-constant in pitch-up motion is greater than in pitch-down motion, for large amplitude inputs in the stall region. This phenomena has also been observed consistently for some other experimental studies report in the review paper [74]. Thus, VVM inherently incorporates the effect of different effective time-constants for small amplitude, large amplitude pitch-up and large amplitude pitch-down motion inputs.

The higher-order kernel states of VVM produce higher harmonics of the sinusoidal input frequency in response to high energy input [48]. A high energy input, which in case of unsteady model is large value of $\dot{\alpha}$ or large amplitude change in α, excites higher-order states. Higher-order kernel states produce nonlinear corrections as demonstrated in modeling of pitching moment coefficient of GTA in the next chapter. Thus, the time-constant of the response of normal force coefficient is dependent on the amplitude of pitching input.

The linearized equations of VVM in Eq.(3.9) are similar to that obtained by

Abramov.et.al [23]. A comparison of the two models gives $K_1(\alpha) = \Delta C_Z(\alpha) = C_{Z_{att}}(\alpha) - C_{Z_{st}}(\alpha)$. Here, $C_{Z_{att}}(\alpha)$ is the normal force with no flow separation or vortex breakdown on the wings, that can be obtained from the Polhamus Suction-analogy method. Therefore, the dynamic gain parameter function $K_1(\alpha)$ in the VVM actually represents the loss in normal force due to vortex breakdown on the wings.

The effect of the nonlinear terms in the differential equation $\dot{x_2}(t)$ in VVM on the model response has been recently presented in [86]. In response to harmonic inputs, the nonlinear terms in this differential equation effect the steady state and initial response characteristics. It is noted that the bilinear term $K_{22}(\alpha)x_1u$ does not modify the effective time-constant and therefore the transient response, but it changes the steady state oscillation cycle. The quadratic term $K_{21}x_1^2$ changes the settling time or the effective time-constant of the response. This shows that inclusion of just the second kernel state can reproduce the nonlinear phenomena in unsteady variation of coefficients. Thus, the parameters of these terms tune the effective time-constant of VVM to be dependent on the amplitude and rate of pitching motion input.

3.7 Summary

A class of nonlinear modeling approaches for unsteady aerodynamic loads was clearly defined, in order to place the VVM approach among the right set of competing approaches presented in literature. VVM model structure and a parameter estimation approach were formulated based on the qualitative features of unsteady aerodynamics and commonly available forced oscillation wind tunnel test data. It is shown that, in this formulation the model structure is directly correlated to the level of nonlinearity in unsteady variation of loads recorded in forced oscillation tests. Phenomenological features like a linear response for small amplitude inputs and different time-constants depending on direction of pitching motion for large amplitude inputs, were shown to be the mathematical properties of the VVM structure.

Chapter 4

Identification of Longitudinal Aerodynamic Coefficients of GTA and F16XL

The Volterra variational model structure and concepts for identification of the longitudinal aerodynamic coefficients were presented in the previous chapter. The parameter estimation procedure is based on the assumption that sufficient amount of good quality data from small and large amplitude forced oscillation tests is available. However, the identification procedure to be used is usually case specific, as different aerodynamic coefficients exhibit different level of nonlinearity and signal-to-noise ratio of the data may be low. Also, it may not be feasible to reiterate the expensive wind tunnel tests if the available data is found to be insufficient.

In such cases, there is a need to adapt the identification procedure to suit the available data, and the limitations of the estimated model, if any, should be specified. The VVM modeling process can be adapted in terms of (i) number of kernel-states used in VVM, (ii) processing of the wind tunnel test data and (iii) steps in estimation of parameter functions. These adaptations in VVM are useful to obtain a model which is consistent with the available data set, such that its accuracy is sufficient for use in flight simulation and analysis. An algorithm for estimation of VVM parameter functions for delta-wing aircraft configurations is proposed in this chapter based on the concepts presented in the last chapter. The principles of identification are demonstrated by modeling the aerodynamic coefficients of two delta-wing aircraft, GTA and F16XL. These principles can be applied to identification of aerodynamic coefficients of other delta-wing configurations.

The forced oscillation test data sets for GTA and F16XL research aircraft were provided by CSIR-NAL, India and NASA-Langley Research Center, USA respectively. These tests were performed in industrial-grade wind tunnels considering a wide range of inputs. The available data set represents the best-in-class data from forced oscillation tests. There are three case studies presented in this chapter to demonstrate identification process in three completely different situations which are summarized as follows,

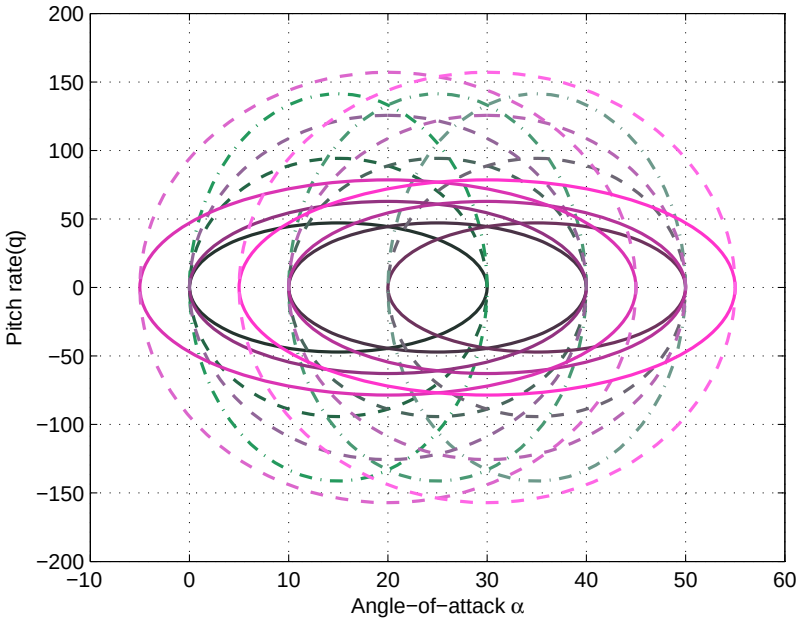

Fig. 4.1. Range of inputs used in LAFO tests of GTA; solid-line $f = 0.5Hz$, dash-line $f = 1Hz$, dash-dot-line $f = 1.5Hz$.

1. C_Z of GTA : Parameter estimation using small and large amplitude forced oscillation test data, when variation in load is mildly nonlinear

2. C_m of GTA : Parameter estimation using small and large amplitude forced oscillation test data when variation in load is complex due to multiple damping and anti-damping dynamic hysteresis loops. The LA data covers three mean angles-of-attack, three amplitudes and three frequencies.

3. C_m of F16XL : Parameter estimation using small amplitude data with low Signal-to-Noise ratio, and large amplitude data set that covers one mean angle-of-attack, three amplitudes and three frequencies

The estimation results for C_Z of F16XL are also presented for the sake of completeness. In the end of the chapter, the issue of using inputs of appropriate maximum pitch-rate to obtain a data set suitable for unsteady aerodynamic modeling is discussed.

4.1 Wind Tunnel Test Data Available

4.1.1 Data for GTA

GTA is a delta-wing configuration research aircraft with leading-edge sweep angle of 60^o. It has a typical geometry of high-performance, high-maneuverability aircraft. The wind

tunnel tests were conducted on a $1:15$ scale model of GTA in an industrial grade wind tunnel. Static and forced oscillation wind tunnel test data are partially available for the current research.

Forced oscillation tests were conducted with sinusoidal pitching motion inputs of 3^o amplitude at three frequencies $(0.5, 1, 1.5)Hz$. These tests were performed at angle-of-attack intervals of 5^o in $[0^o\ 90^o]$ range. The sensors recorded variations in normal force and pitching moment coefficients at a frequency of $100Hz$. These response data are reduced to in-phase and out-of-phase derivatives by numerical computation of Fourier coefficients at respective input frequencies. Only these derivatives are available for modeling. The 2σ confidence bounds of the estimated values of these derivatives are not available.

Large amplitude forced oscillation data set is very comprehensive. Sinusoidal inputs of amplitudes of $15, 20$ and 25 degrees, over mean angles-of-attack of $[15, 25, 30, 35, 45]$ deg and frequencies of $[0.5, 1, 1.5]Hz$ were used in these tests. This data-set covers wide range of pitch-rate, frequency and amplitude combinations as visualized in Fig.(4.1). The corresponding non-dimensional frequencies of pitch oscillation are $[0.0024\, 0.0047\, 0.0071]$. It is comprehensive enough to capture the effects of nonlinear unsteady aerodynamics relevant to aircraft's operational bandwidth.

A limited set of raw wind tunnel data from large amplitude forced oscillation tests is also available, but only for C_Z. Static wind tunnel test data from the same rig and using the same model are also available. These data are available for all the force and moment coefficients recorded at angle-of-attack intervals of 5 degrees. The overall quality of the data can be considered to be on par with the best available in literature.

4.1.2 Data for F16XL

F16XL is a cranked-arrow delta-wing configuration of a high-performance aircraft with high sweep angle, and its geometry is given in Fig.(4.2) [31]. It is a research purpose aircraft extensively tested in wind tunnels by the NASA-LaRC to study its high-angle-of-attack aerodynamic and flight dynamic characteristics. Following our presentation of initial results in [88], and on request by Prof.Mikhail Goman, the forced oscillation and static wind tunnel test data for F16XL were made available to us by Dr.Patrick Murphy, Scientist at NASA-LaRC, for the current research. The publications based on this data available in open literature are [31, 30, 89, 90].

The forced oscillation and static wind tunnel tests were conducted using a 1:10 scale model. Small amplitude forced oscillation tests were conducted using input amplitude of $5\,\mathrm{deg}$, for five frequencies $[0.6,\ 1,\ 1.41,\ 1.75,\ 2.94]Hz$. The data covers angle-of-attack range of $[0\, 90]\,\mathrm{deg}$, at intervals of $5\,\mathrm{deg}$. Reduced data in the form of in-phase and out-of-phase derivatives, as well as raw wind tunnel test data are available for C_Z and C_m

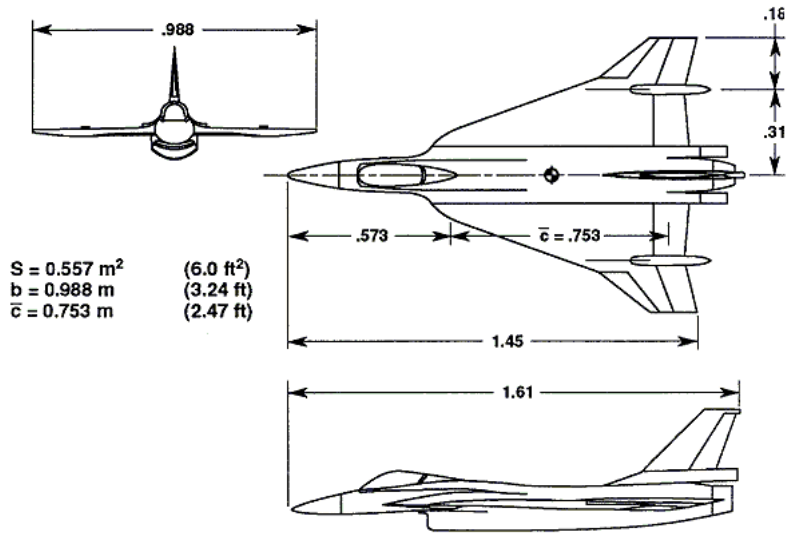

Fig. 4.2. 1:10 scale model of F16XL used in wind tunnel tests [31].

coefficients.

Large amplitude forced oscillation tests were conducted about a fixed mean angle-of-attack $\alpha = 35^o$. Sinusoidal inputs of three amplitudes $(10^o, 20^o, 35^o)$ and thirteen frequencies in the range $f = [0.08\, 1.47]Hz$ were used in these tests. The inputs used in the experiments are visualized in Fig.(4.3), where each ellipse indicated the pitch-rate and angle-of-attack combinations covered by it. The ratio of minor axis to major axis of the ellipse gives the frequency of input. Both raw and filtered measurements of aerodynamic coefficients from LAFO tests are available.

The forced oscillation test data is for a different type of combination of mean-angle-of-attack, amplitude and frequency of inputs than that for GTA. As seen in Fig.(4.3), this data is intended to capture the aerodynamics effects at a range of input-frequencies, while that for GTA is focused on obtaining data at comprehensive range of amplitude and pitch-rate combinations.

Static wind tunnel test data for C_Z and C_m are sampled at angle-of-attack interval of one degree. Dynamic wind tunnel tests were also performed for ramp pitch-up and pitch-down inputs at various rates in the range $18\,\mathrm{deg}/s$ to $220\,\mathrm{deg}/s$. These data are not used in the process of identification, and hence are used for validation of the identified model.

A proper selection of amplitudes and frequencies for performing the wind tunnel tests is important to obtain a model of reasonable correlation with the operational conditions of the aircraft. Some of the LAFO and ramp input tests were conducted at very high pitch-rates where the basic aerodynamic phenomena responsible for unsteady aerodynamics changes. This is explained in detail in the last section. The high-rate pitching input test data for which the reduced frequency $k > 0.034$ were unsuitable for the modeling

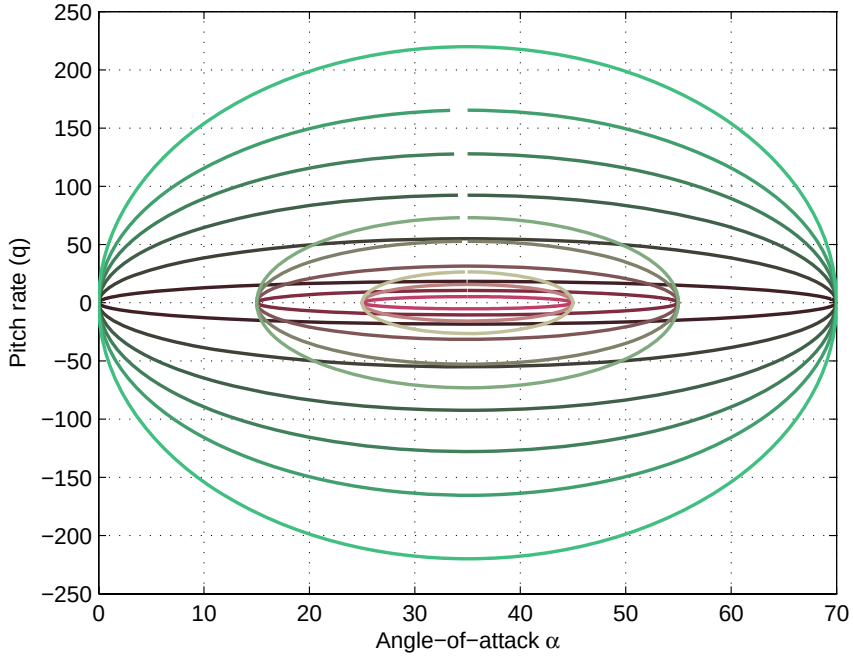

Fig. 4.3. Range of inputs used in LAFO tests of F16XL.

exercise, and were not used in parameter estimation.

4.2 Parameter Estimation Methodology

The methodology adopted for estimation of parameters of VVM using forced oscillation wind tunnel test data is presented in Fig.(4.4). Note that this methodology incorporates flexibility in the identification procedure in terms of both the available data and number of kernel states in the model structure. The small amplitude forced oscillation test data can also be interpreted as the data in which only the first harmonic is significant in the response aerodynamic coefficient.

A simple estimation procedure following this algorithm is found to work well for identification of C_Z of GTA and F16XL using small and large amplitude forced oscillation wind tunnel test data. A single-state VVM was found to produce satisfactory results. In case of C_m of GTA iterations were performed by increasing the number of kernel-states in VVM, and accurate results were obtained for a three state VVM. In case of C_m of F16XL, the model had to be estimated using only LAFO data as the data from SAFO was found to have unacceptable level of noise. The details of these estimation case studies are presented in the following sections.

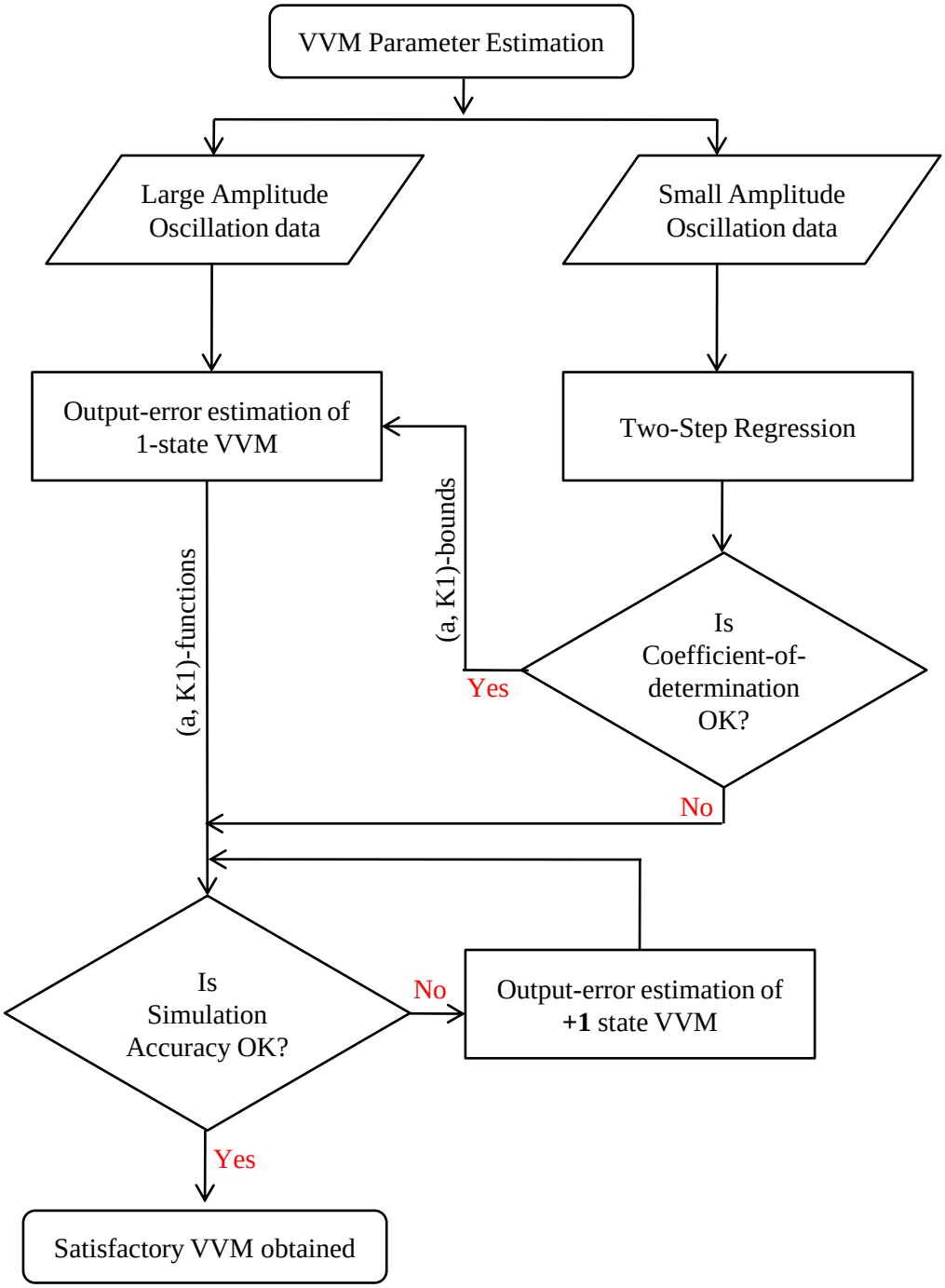

Fig. 4.4. Parameter Estimation procedure for VVM using forced oscillation Wind tunnel test data.

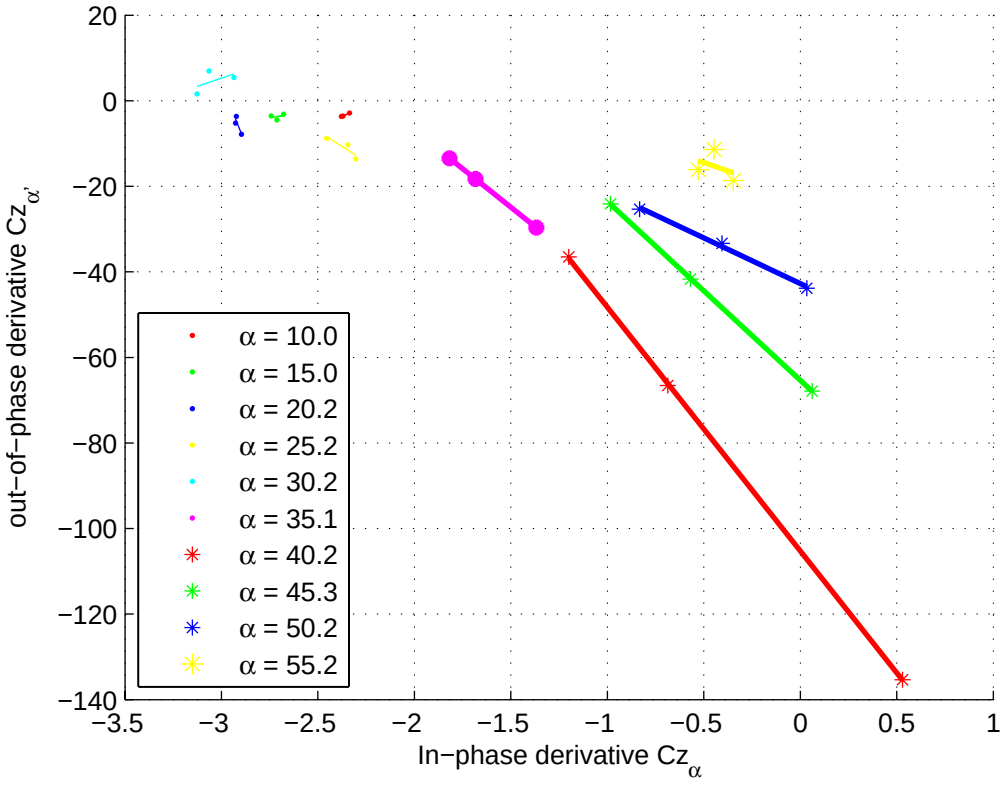

Fig. 4.5. Linear relation between In-phase vs. Out-of-phase derivatives for C_Z of GTA, from SAFO data.

4.3 Identification of Normal force coefficient of GTA

Unsteady model of C_Z is estimated in two steps. Firstly, the parameters $(a(\alpha_0), K_1(\alpha_0))$ of the first-kernel state are estimated using SAFO data. Then, the LAFO data is used to tune the model's nonlinearity properties using the parameter functions $(a(\alpha), K_1(\alpha))$.

4.3.1 Estimation using SAFO data

The validity of the linearized form of VVM in Eq.(3.9), for the given SAFO data is checked using the power spectrum density (PSD) maps of $C_Z(t)$. This is important as variation of force and moment coefficients becomes nonlinear beyond a certain input amplitude. However, raw wind tunnel test data is not available for this purpose, while this conclusion cannot be drawn reliably from averaged and filtered response data. The processed $C_Z(t)$ oscillation cycle shows a significant power only upto first harmonic frequency. This also an indicator of the primarily linear nature of variation of $C_Z(t)$.

As shown in chapter 3, linearized form of VVM implied a linear relation between in-phase and out-of-phase derivatives extracted from SAFO data. This linear relationship is found to be true for C_Z of GTA, as shown in Fig.(4.5). The separation between

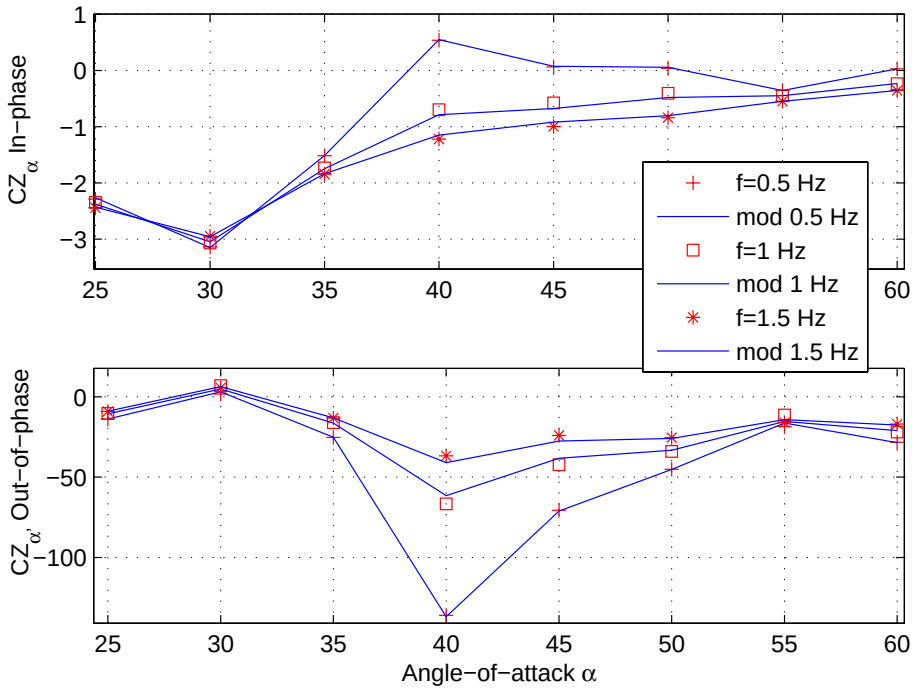

Fig. 4.6. Comparison of in-phase and out-of-phase derivatives from the estimated model and experimental data for C_Z of GTA.

the points for different frequencies is distinct only in the angle-of-attack range where unsteady aerodynamic loads are significant, that is $\alpha \in (30^o\, 55^o)$. Hence, $a(\alpha_0), K_1(\alpha_0)$ are estimated in this angle-of-attack range by the two-step regression method proposed in [16, 22], and given in APPENDIX A. Accordingly, $a(\alpha_0)$ is estimated by linear regression considering Eq.(3.9), and then these values are used in the second step to estimate $K_1(\alpha_0)$ and $C_{Z_q}(\alpha_0)$ considering Eq.(3.8).

Static wind tunnel test data defines the steady state solutions of the model. The derivative of $C_Z\, vs.\, \alpha$ curve, denoted as $C_{Z_\alpha,st}(\alpha_0)$ is estimated from static wind tunnel data and it is used as a constraint in the second step of regression. Since the static data for C_Z of GTA is available at only $5\,\mathrm{deg}$ intervals of angle-of-attack, its derivative has a high uncertainty. This is especially an important issue in the stall angle-of-attack region where $C_{Z,st}(\alpha)$ changes rapidly. Hence, $C_{Z,st}(\alpha)$ is curve-fitted with a 7-th degree polynomial function and then differentiated to get $C_{Z_\alpha,st}(\alpha_0)$. In small amplitude forced oscillation tests, pitching motion causes a filtering effect on $C_{Z,st}\, vs.\, \alpha$. Also, the oscillation in angle-of-attack is over a small range of $\alpha = 6^o$. Hence, the approximation of the value of slope by curve-fitting is likely to be close to the actual value.

Since the co-variances of in-phase and out-of-phase derivatives are not given, the linear regression is performed by Weighted-Least-Squares method in several iterations. In this process, the estimation error covariance matrix is computed in each iteration, and

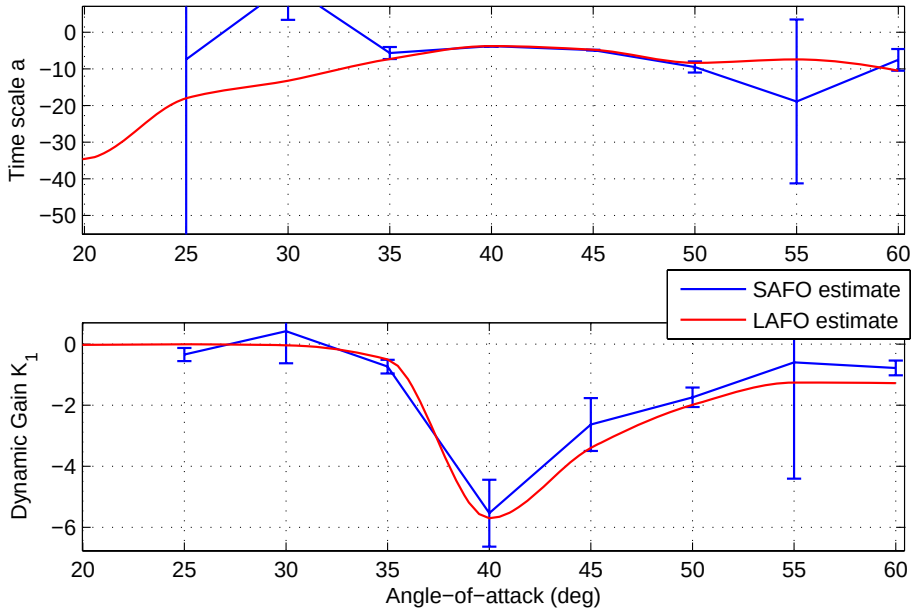

Fig. 4.7. Estimated bounds on the first kernel-state parameters and parameter functions for C_Z of GTA.

its inverse is the weighting matrix for the next iteration. This procedure converges to a best-fit in few iterations. The final value of error-covariance matrix is used to calculate the confidence bounds on estimated values of parameters $(a(\alpha_0), K_1(\alpha_0))$, as given in APPENDIX A.

The experimental data and model prediction using the estimated values of parameters are found to match accurately as seen in Fig.(4.6). The goodness-of-fit for the estimated values is given by parameter variance or 95% confidence bounds on estimated values of parameters, and coefficient of determination R, at each angle-of-attack α_0. The confidence bounds account for measurement noise and coefficient of determination shows the variations in the measured output that are captured by the estimated model. The parameter bounds are indicated by vertical bars in Fig.(4.7). These values are acceptable for $\alpha\epsilon[35^o\ 50^o]$.

The coefficient of determination is relatively low at $\alpha = (30^o, 55^o)$, as seen in Fig.(4.8). Unsteady aerodynamics is not sufficiently excited by the small amplitude inputs at these angles-of-attack. Hence, signal-to-noise ratio is poor, and linear relation between in-phase and out-phase derivatives is unclear, as seen in Fig.(4.5). Thus, from SAFO data, $\alpha \in [30^o\, 55^o]$ seems to be the region of significant unsteady normal force. However, the LAFO data shows that the unsteady component of normal force coefficient is significant for $\alpha \in [25^o\, 60^o]$. Therefore, (a, K_1) are estimated at $\alpha = (25^o, 60^o)$ using LAFO data in the next step.

Outside the stall angle-of-attack region, i.e. $\alpha \in \{[0\, 25^o], [60^o\, 90^o]\}$, $C_{dyn}(t)$ is

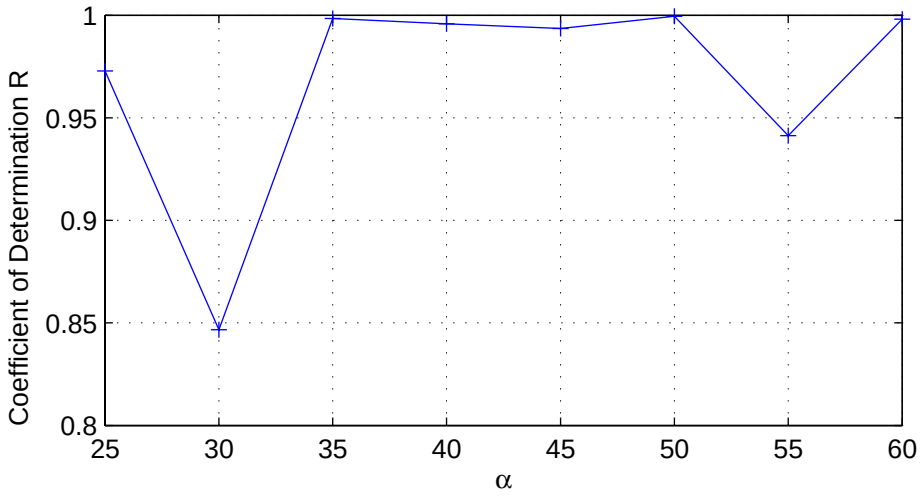

Fig. 4.8. Coefficient of determination for the estimated model parameters for C_Z of GTA.

expected to be zero. This is affected by considering the magnitude of time-scale parameter to be relatively very large of about $a < -20$; while K_1 is simply zero, as seen in Fig.(4.5). The linear unsteady effects in this region are captured by the damping derivative (out-of-phase derivative) term included in the aero-database.

The linear component of the model or the single-state VVM has successfully captured the frequency dependence of unsteady normal force variation due to small amplitude inputs. The identified model incorporates the dependence of in-phase and out-of-phase derivatives on the frequency of input in time-domain. Thus, it is useful for simulation of loads due to small amplitude change in angle-of-attack. For large amplitude change in angle-of-attack, variation of $C_Z(t)$ is nonlinear in nature.

In the region of unsteady aerodynamics, $i.e. \alpha \in [25^o\, 60^o]\,\mathrm{deg}$, the time-constant of flow dynamics on the wings change continuously with angle-of-attack. This is also reflected in the estimated values of (a, K_1) in Fig.(4.7). But, these parameters are estimated at 5^o intervals. This resolution is insufficient to realize the actual continuous model parameter functions. Hence, the parameter functions $(a(\alpha), K_1(\alpha))$ are defined by the estimated values of parameter bounds at the node-points. This is refined in the next step using LAFO data.

4.3.2 Estimation using LAFO Data

The estimated one-state VVM reproduces a qualitatively satisfactory output $C_Z(t)$ due to large amplitude change in angle-of-attack, but the accuracy is insufficient. The entire LAFO data available for C_Z of GTA contains only a steady state oscillation cycle. Each $C_Z(t)$ is obtained by filtering the raw data over an appropriate bandwidth, and averaging

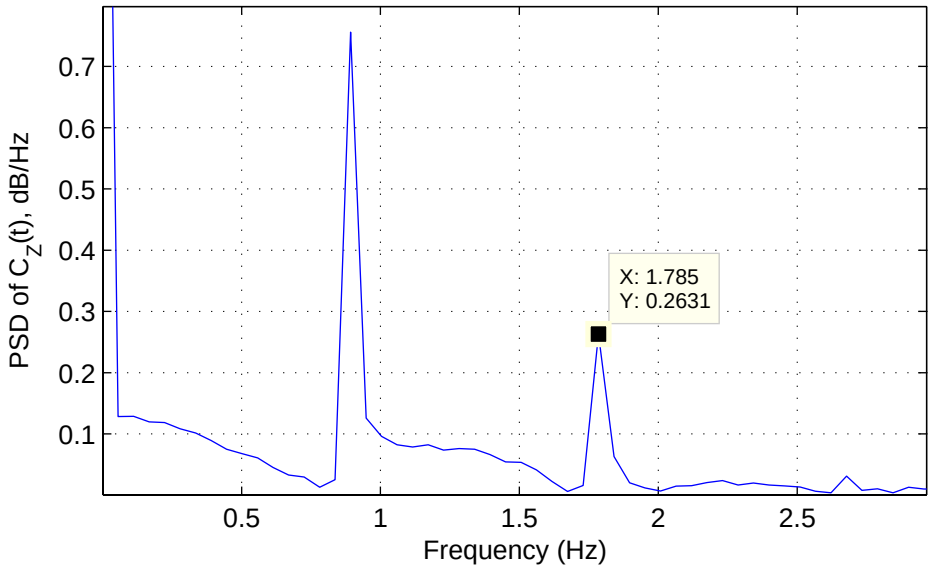

Fig. 4.9. Power Spectrum Density map of $C_Z(t)$ of GTA in LAFO test with input $\alpha_0 = 30^o$, $\Delta\alpha = 25^o$ and $f = 1Hz$.

the multiple oscillation cycles.

The estimation of model parameters from LAFO data was performed using a specialized software called "Package for Interactive Identification" (PII), developed for this purpose by Goman and co-workers. The user manual of the software is in [91, 92], and case studies on identification of nonlinear unsteady aerodynamic model using this software are given in [93, 94]. A combination of the gradient and steepest-descent algorithms is used in the optimization process. The software provides a Graphical-User-Interface to check the quality of fit-obtained and alter the options of the optimization process.

Few samples of raw wind tunnel data from LAFO tests are available. As seen in PSD of $C_Z(t)$ presented in Fig.(4.9), there are significant peaks at first and second harmonics of input frequencies. This implies that the C_Z variation for large amplitude inputs is nonlinear in nature. PSD of the steady state oscillation cycle for C_Z shows a significant power only up to second harmonic frequency, for all the data. Hence, a two-state VVM is sufficient for modeling C_Z.

Before estimation of the higher order kernel state equation parameters, the parameter functions $(a(\alpha), K_1(\alpha))$ need to be defined. A simplistic approach is to define these parameter functions by using linear interpolation of the values of $(a(\alpha_0), K_1(\alpha_0))$ for $\alpha \in [35 : 5 : 55]$. This definition is clearly insufficient for large amplitude simulations. So, the model is updated with second kernel-state and used to estimate the parameters $(K_2(\alpha), K_3(\alpha))$ using LAFO data, to get an accurate model. However, it is observed that the contribution of $x_2(t)$ is small in comparison to $x_1(t)$, that is $|x_2(t)| < |x_1(t)|$. Hence,

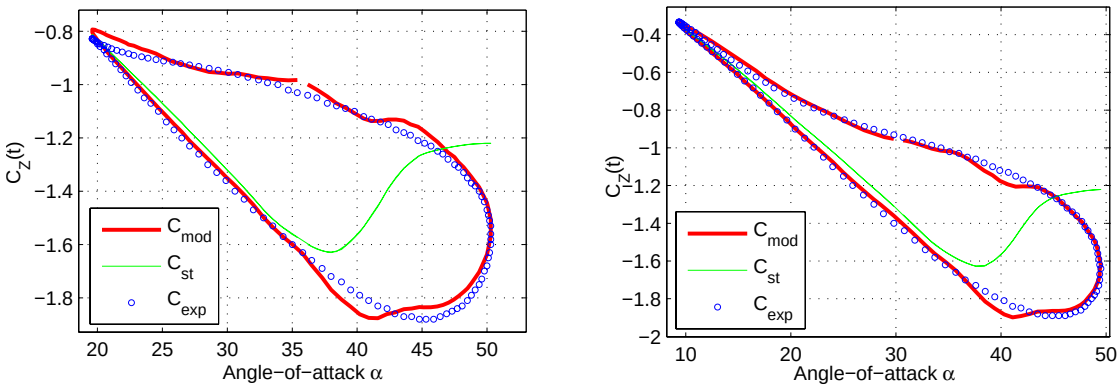

(a) $\alpha_0 = 35^o, \Delta\alpha = 15^o, f = 1Hz$ (b) $\alpha_0 = 30^o, \Delta\alpha = 20^o, f = 0.5Hz$

Fig. 4.10. Comparison of the output of VVM and wind tunnel test data, due to large amplitude oscillation input, for C_Z of GTA.

the role of second kernel state in this model is questionable.

It was observed that the mild nonlinearities in the variation of C_Z can be captured by tuning of the nonlinear parameter functions $(a(\alpha), K_1(\alpha))$ using LAFO data. In fact, the parameter functions are not defined completely as the values of $(a(\alpha_0), K_1(\alpha_0))$ were estimated only for $\alpha \in [35^o\ 55^o]$. The modeling and measurement noises in SAFO data are quantified by the error co-variance matrix. This co-variance matrix in turn gives the bounds on $(a(\alpha_0), K_1(\alpha_0)$. As shown in Fig.(4.7), the parameter bounds are a quiet significant percentage of the mean value. Hence, it is essential to tune $(a(\alpha), K_1(\alpha))$ using the parameter bounds to account for the effects of noise as well as to estimate them over the extended range of $\alpha \in [25^o\ 60^o]$.

So, the functions $(a(\alpha), K_1(\alpha))$ are estimated considering these bounds as constraints and to produce a best fit with the LAFO data. The single-state VVM and Output-Error method are used in estimation of the parameter functions. An optimization is setup with root-mean-square-error between model output and experimental data as the cost function. Entire LAFO data is used simultaneously in the estimation process. It is found that the solution always converges to an approximately equivalent values of the parameter functions $a(\alpha)$ and $K_1(\alpha)$. These are indicated by red solid lines, overlaid on the estimated parameter bounds from SAFO data, in Fig.(4.7). These estimated parameter functions are consistent with both SAFO and LAFO data.

The simulation results of the model thus obtained produce a good match with the LAFO data consistently. A sample of results of simulations is given in Fig.(4.10). Only the steady state oscillation cycle generated by the model is plotted in the figures. In these figures, C_{exp} indicates LAFO test data, C_{st} indicated the curve-fit of static test data, and C_{mod} indicates the model output. Same convention is followed throughout this chapter. The parameter function $K_1(\alpha)$ is especially nonlinear near $\alpha = 40^o$. Also, the variations

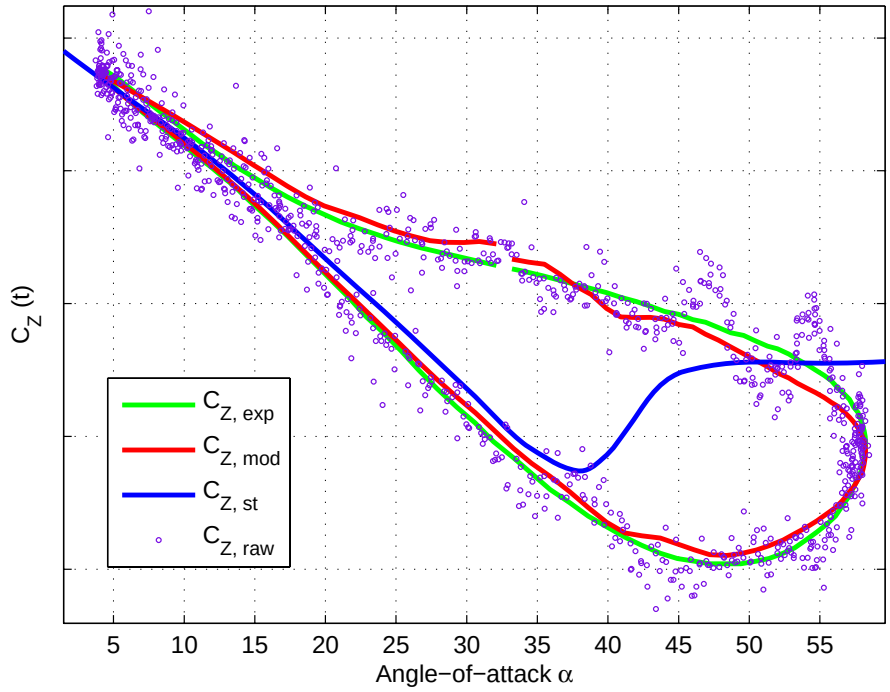

Fig. 4.11. Comparison of VVM output with raw wind tunnel test data for C_Z of GTA, due to sinusoidal input of $\alpha_0 = 30^o, \Delta\alpha = 25^o, f = 1Hz$.

at this angle-of-attack are very sensitive to external conditions. Hence, there is a minor inaccuracy in the model response at $\alpha = 40^o$. The break in oscillation cycle in Fig.(4.10,a) is seen when the angle-of-attack at last data point is not the same as first one. The rest of the results for LAFO data set are given in the APPENDIX C.

This model still produces minor inaccuracies at some angles-of-attack, with respect to the processed LAFO data. Consider Fig.(4.11), in which the model output is plotted with the raw wind tunnel data indicated by $C_{Z_{raw}}$. It is evident that the single-state VVM response is within the uncertainty bounds of the raw wind tunnel data, and hence the results are of acceptable accuracy. This also shows that, if the second kernel state is also included, it's value is in the error tolerance limits, and hence it may not be realistic.

There are some higher frequency variations in $C_{Z_{raw}}(t)$ in Fig.(4.11) in the region of sharp change in normal force coefficient. This can be observed in both pitch-up and pitch-down motion, but restricted to $[40^o\ 55^o]$ range. The source of such higher frequency local variations is unclear. Since the raw wind tunnel test data is severely limited, the consistency of this phenomenon cannot be confirmed either. It can be aerodynamic, or even due to external vibrations of the sting of test-rig. A better understanding of the test technique or flow dynamics is essential to resolve this matter. However, force and moment data are often filtered and processed using special techniques by the aerodynamicists. So,

these vibrations are not reflected in the processed LAFO data which are used in parameter estimation. Hence, the model output does not exhibit this phenomenon either.

4.4 Identification of Pitching moment coefficient of GTA

Variations in the pitching moment coefficient in the region of unsteady aerodynamics is much more complex than that for the normal force coefficient. Pitching moment $C_m(t)$ response to large amplitude sinusoidal input has three dynamic hysteresis loops. These loops are typically associated with damping and anti-damping aerodynamic effects. Moreover, the mean value of these loops appears to be shifted from the steady state values obtained from static wind tunnel tests. An unsteady model is expected to reproduce these nonlinear variations seen in the experimental data.

The data for GTA is more comprehensive than the data for F16XL [31], X31 [78], Delta-65^o [20], Delta-70^o wings [4] and many other airfoils presented in literature [36]. Unlike the forced oscillation data for these cases, the data for C_m of GTA is gathered for combinations of three different mean angles-of-attack and amplitudes. This makes the estimation problem more challenging.

Since raw wind tunnel data was not available for the pitching moment coefficient, the model order or the number of kernel states required in the model cannot be determined using PSD map of the data. However, PSD of the data for steady-state oscillation cycle showed significant power only up to third-harmonic of input frequency for the largest input amplitude. Hence, it was postulated that a three state VVM is required to model C_m of GTA. It can be further assumed that even two state model can be satisfactory, as parameter functions are nonlinear function of angle-of-attack.

4.4.1 Estimation using SAFO Data

Parameter function $(a(\alpha), K_1(\alpha))$ were estimated by a procedure similar to that for C_Z. The plot of in-phase versus out-of-phase derivatives is linear, and hence the linearized form of VVM is valid for given SAFO data. In the first step $(a(\alpha_0), K_1(\alpha_0))$ are estimated by two-step regression. The estimated parameters produced fairly accurate match with the in-phase and out-of-phase derivatives from SAFO data as shown in Fig.(4.12). The parameter bounds and coefficient of determination for parameter estimates at $\alpha = (35^o, 40^o, 45^o, 50^o)$ are good.

As expected, at $\alpha = (30^o, 55^o)$ in-phase and out-of-phase derivatives for the three input oscillation frequencies are approximately equivalent. The unsteady aerodynamic effects for small amplitude oscillation inputs are not significant at these points. Hence,

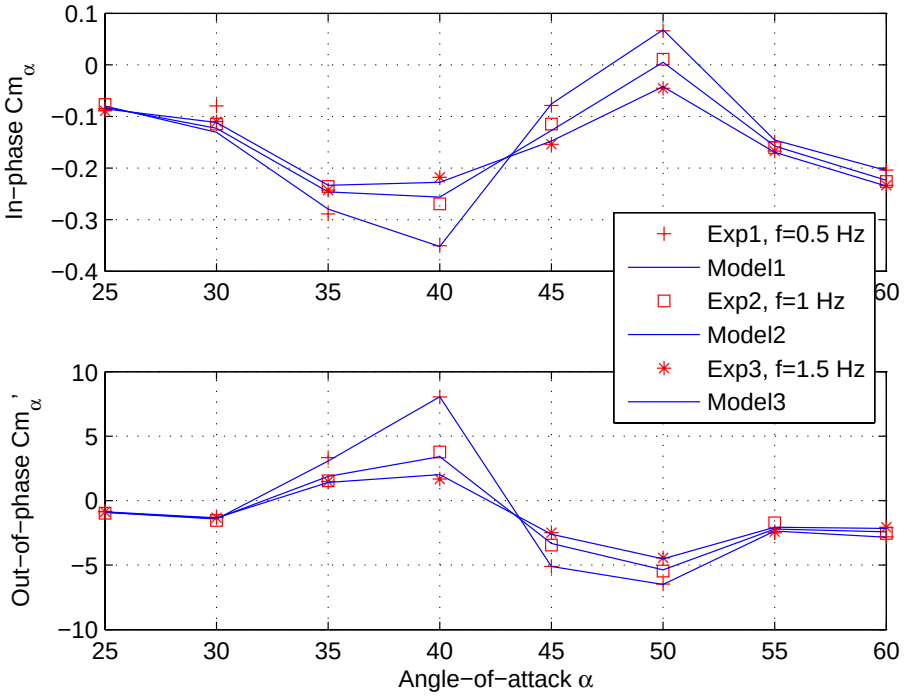

Fig. 4.12. Comparison of in-phase and out-of-phase derivatives from the estimated model and experimental data for C_m of GTA.

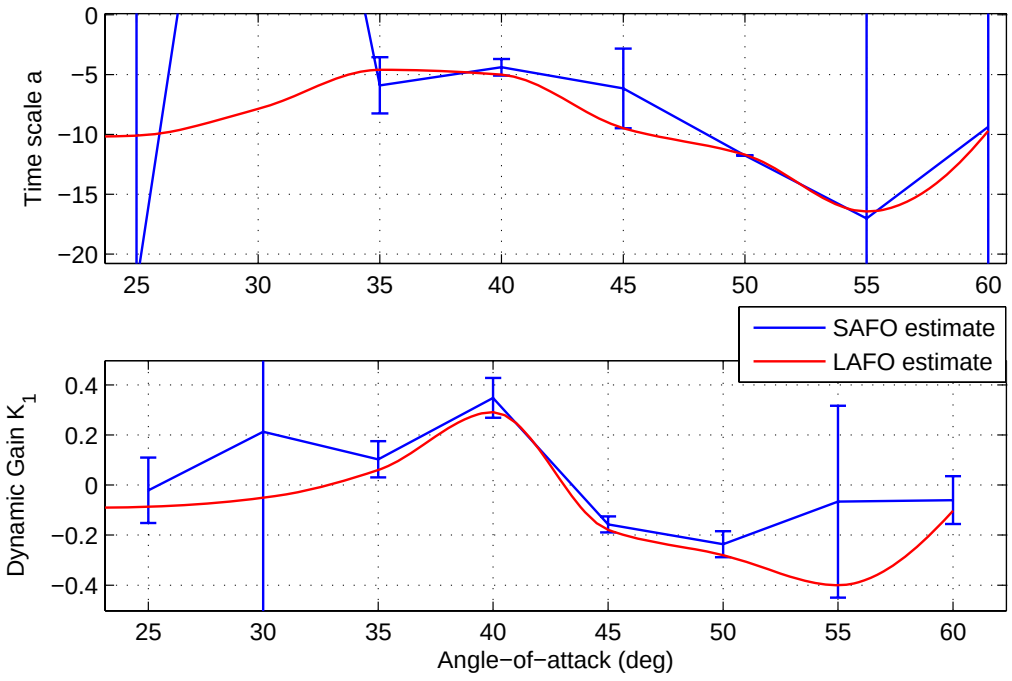

Fig. 4.13. Estimated parameters of one-state VVM, for C_m of GTA.

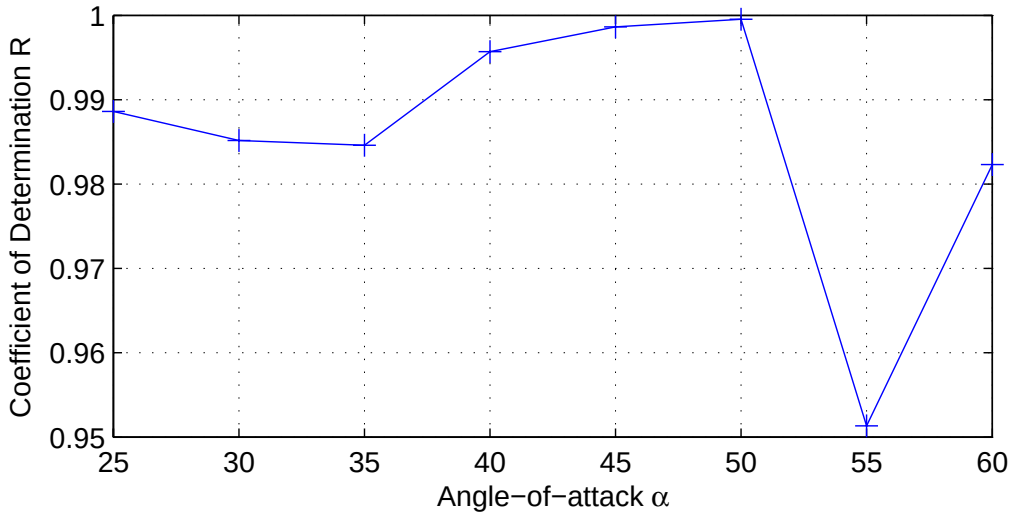

Fig. 4.14. Coefficient of determination for the estimated model parameters of VVM, for C_m of GTA.

the model parameters are found to have very large bounds. Hence, the estimated values of parameters at these angle-of-attack are rejected.

4.4.2 Estimation using LAFO Data

Then, the parameter functions $(a(\alpha), K_1(\alpha))$ are estimated using the estimated parameter bounds on $(a(\alpha_0), K_1(\alpha_0))$, and by output-error method using LAFO data. This single-state VVM is found to be not sufficiently accurate.

Then, a two-state VVM is considered for estimation. In this step the parameter functions $(a(\alpha), K_1(\alpha))$ are subject to the constraints given by estimated bounds from SAFO data. This is implemented simultaneously with no constraints on parameter functions $K_{21}(\alpha)$ and $K_{22}(\alpha)$. The results from this estimated model produced a good qualitative match with the experimental data, in terms of multiple damping and anti-damping loops.

However, the model output is significantly inaccurate for some LAFO tests. A cross plot of the entire LAFO data revealed that the mean of $C_m(t)$ variations for these test cases are shifted downwards or upwards from $C_{m,st}(\alpha)$. A few are them are shown in Fig.(4.15), for example. This is unusual from other delta wing aircraft unsteady aerodynamic load. These cases cause the results from the two-state VVM to be inaccurate.

The experimental data is expected to be dispersed around the steady oscillation cycle, as seen in the case of C_Z. It is known that wind tunnel measurements of aerodynamic moments are very sensitive and hence contain much more noise than the force measurements. This is also observed in case of F16XL data, although it is from a different wind tunnel. However, the raw wind tunnel data for $C_m(t)$ is not available,

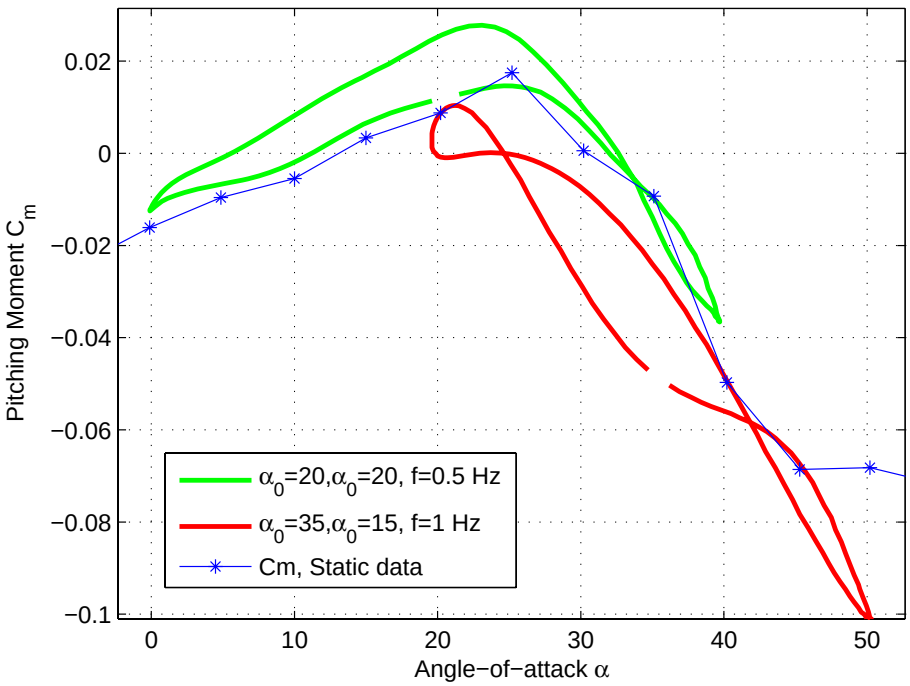

Fig. 4.15. LAFO test cases with shift in steady oscillation cycles from static curve.

and hence the variance of the measurements about the steady oscillation cycle cannot be confirmed. This shift in the mean of dynamic hysteresis loops is quiet significant to be an effect of disturbance, and hence seems to be realistic.

The accuracy of the model is improved by using a three-state VVM. Once again, the estimation is performed considering bounds on $(a(\alpha_0), K_1(\alpha_0))$ as constraints, and estimating all the model parameter functions simultaneously. The estimated values of $a(\alpha), K_1(\alpha)$ are consistent with the bounds estimated from SAFO data, as indicated by the red solid lines in the Fig.(4.13). The estimated model is found to produce consistently satisfactory results for all the LAFO test cases, figures given in APPENDIX C. As seen in the example in Fig.(4.16,a), the three-state VVM output matches the wind tunnel data accurately.

Higher order kernel states $x_2(t)$ and $x_3(t)$ introduce significant nonlinear corrections. The relative magnitudes for $x_2(t)$ and $x_3(t)$ are significant, as seen in Fig.(4.16,b). The nonlinear corrections are particularly important in $\alpha = [40^o\, 45^o]$ range, which is also the region of sharp stall. In [62], it is shown that the second kernel state produces a bias term in the harmonic input response of Volterra series. This is precisely the nonlinear correction produced by $x_2(t)$. It produces a correction of the shift of mean oscillation cycle in $\alpha = [40^o\, 45^o]$ range. It is also stated that the third Volterra kernel produces significant correction in effective time-constant among other effects. In the

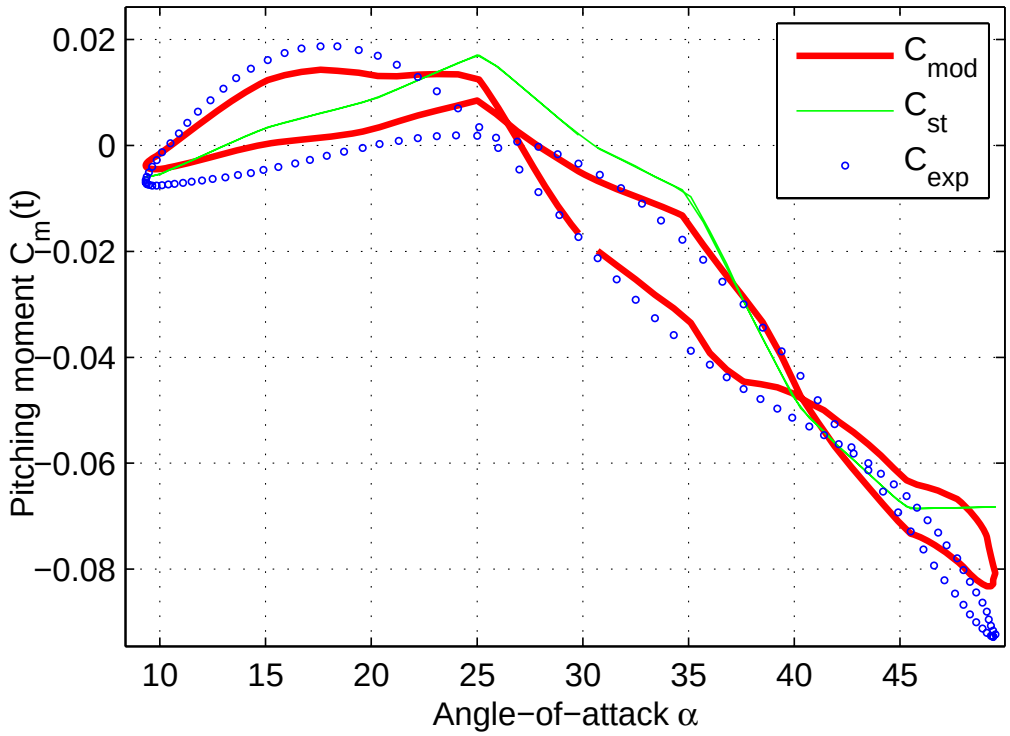

(a) C_m from VVM output and wind tunnel data.

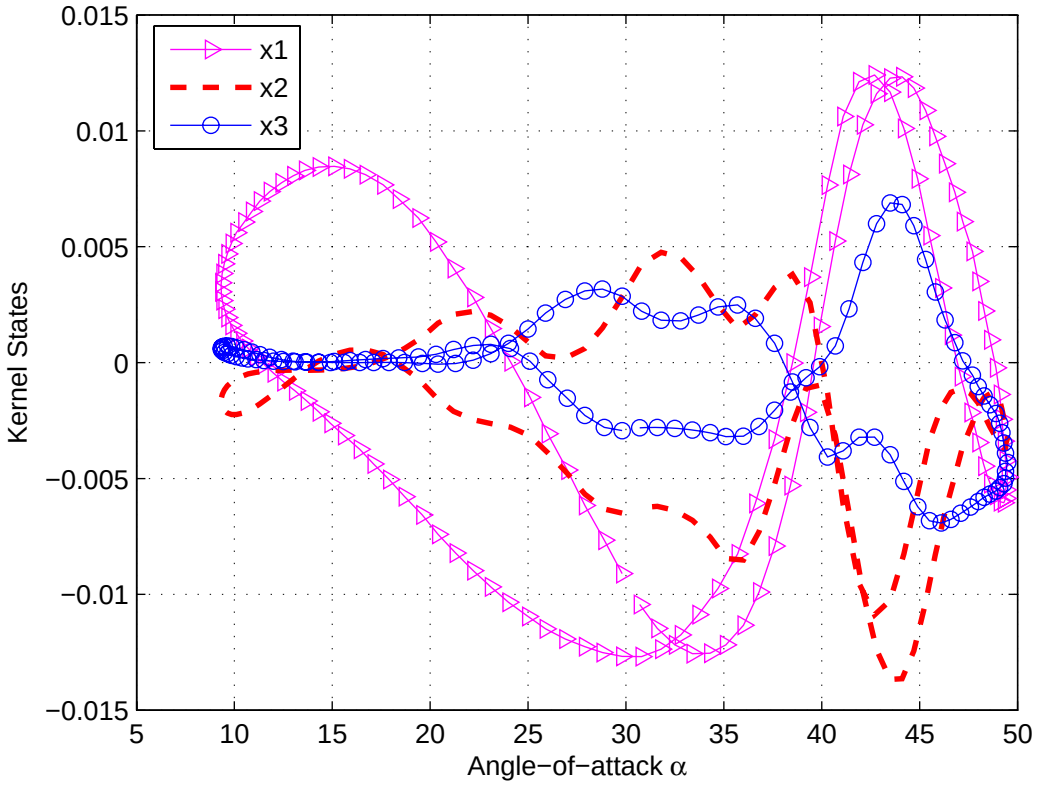

(b) Kernel states of VVM.

Fig. 4.16. Comparison of VVM output and experimental data for sinusoidal oscillation input $\alpha_0 = 30^o, \Delta\alpha = 20^o, f = 1Hz$, for C_m of GTA.

current case study, $x_3(t)$ corrects damping and anti-damping oscillations in the angle-of-attack ranges $[30^o\, 35^o]$ and $[40^o\, 45^o]$ respectively. This is also consistent with the analytical interpretations of Volterra kernel presented in [86],and some of the applications to physiological system presented in [48]. Therefore, kernel states $x_2(t)$ and $x_3(t)$ significant and systematic nonlinear corrections to the model response.

Definition of node-points for estimation of $(K_{21}(\alpha), K_{22}(\alpha))$ is complicated. This is due to a very large data set used in estimation and there is no method to define the co-variance for parameter functions. Fewer number of node-points give lower accuracy of the model fit, as expected from system identification theory. Larger number of node-points result in a non-smooth parameter functions of α. The node-points placed at 5^o intervals were found to be sufficient in the current estimation exercise. The parameter function estimation procedure requires several iterations to get the best-fit, and is an art at some level.

This case study has amply illustrated the capability of a three state VVM to model complex dynamical nonlinearities in variation of unsteady aerodynamic loads, including shift of the cycle with respect to steady state value and multiple damping and anti-damping loops. Typical variations in pitching moment coefficients of Delta-wing configurations are expected to be complex.

4.5 Identification of Pitching moment coefficient of F16XL

Identification of unsteady model of C_m of F16XL required a different approach than that for GTA, as the data available and nature of unsteady variations are quiet different. As reported in the NASA-LaRC report [30] the signal-to-noise ratio of the small amplitude forced oscillation test data is too poor to be used in identification. In this report the linear indicial model and a different parameter estimation method were applied to the same data. The investigations presented in this section draw similar conclusion.

In the first part of this section, some approaches and challenges in processing SAFO data are presented. Various data-processing methods and estimation approaches which were applied to the given raw and processed wind tunnel data in order to estimate (a, K_1). These exercises lead to a conclusion that indeed the signal-to-noise ratio is not good enough for use with any method. Hence, parameter estimation of VVM of C_m was performed using the LAFO test data only. The results from this approach are presented in the second subsection.

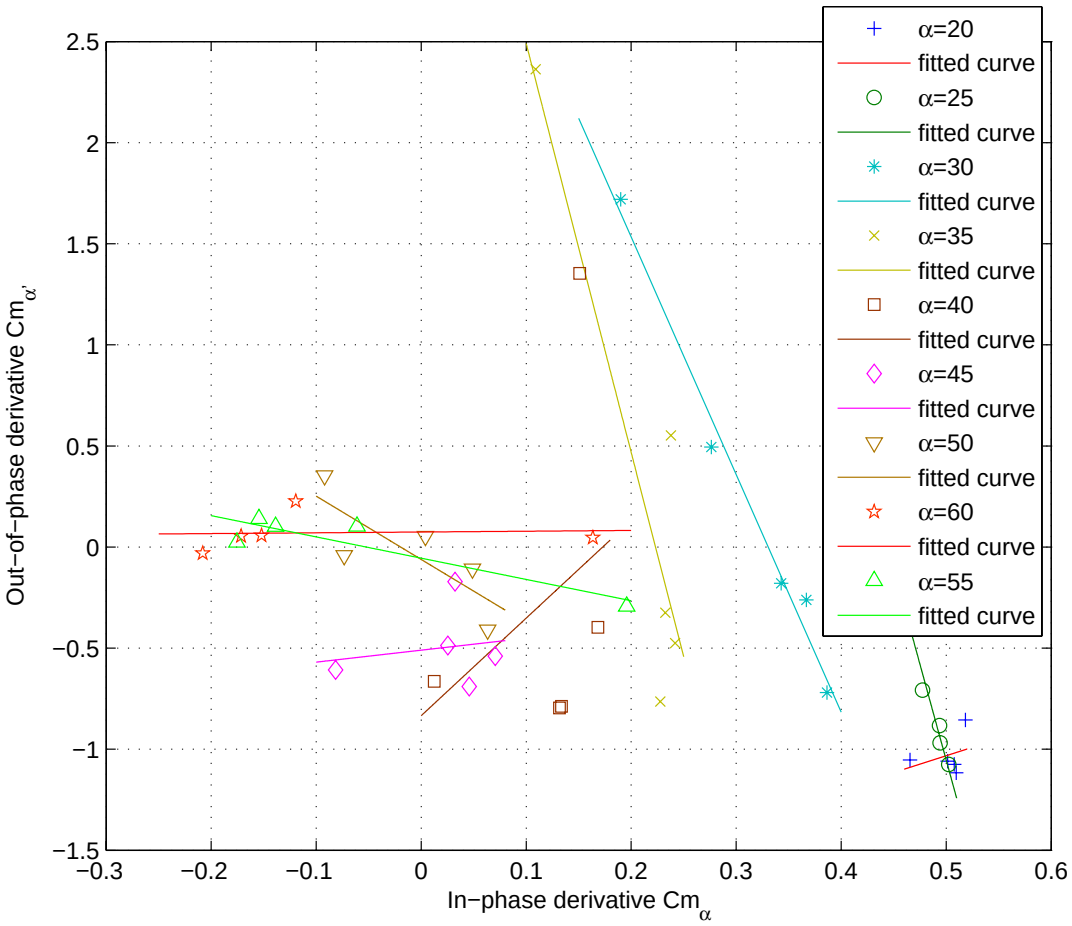

Fig. 4.17. In-phase vs. Out-of-phase derivatives for C_m of F16XL.

4.5.1 Estimation using SAFO Data

It is important to note that, although this data has been called Small amplitude forced oscillation test data, it is not really so. In the tests conducted on F16XL, 5^o amplitude was used at five different frequencies of inputs. However, the system response over 10^o angle-of-attack range covers different flow process in the near-stall and post-stall angle-of-attack regions. Moreover, these flow processes are sensitive to external flow disturbances. Hence, the pitching moment variation from these tests are is likely to be nonlinear. However, using a very small amplitude may not excite the unsteady effects sufficiently to produce a reasonable signal-to-noise ratio. Perhaps, it is due to this reason that 5^o amplitude was chosen in these experiments. The choice of amplitude is therefore a sensitive decision to be made before the tests. In case of F16XL, as discussed in this section, both these factors are at play.

The available data for F16XL contains both raw wind tunnel test data and filtered data

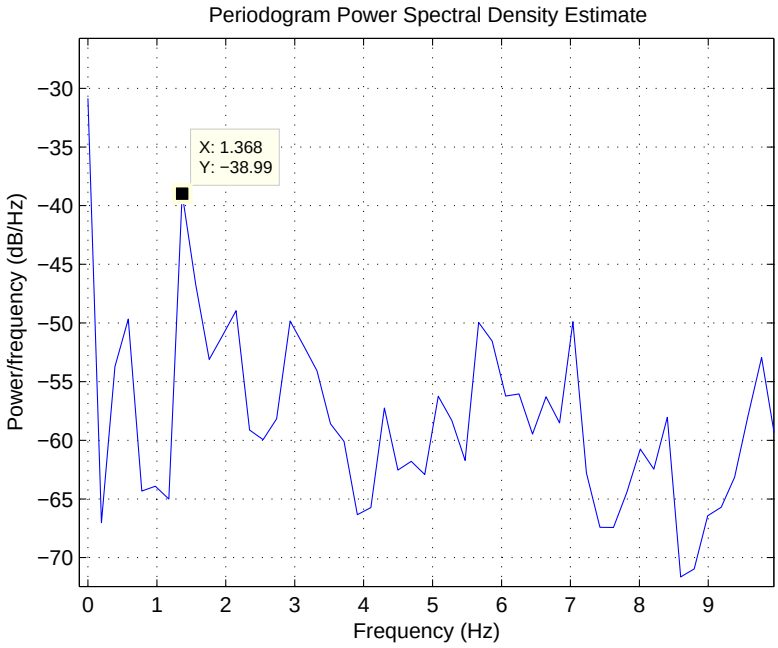

Fig. 4.18. PSD of raw data C_m of F16XL, with input of frequency $f = 1.4Hz$.

from SAFO tests. Firstly the PSD maps of the raw data and the plot of in-phase versus out-of-phase derivatives were investigated to check the linear nature of the pitching moment response to sinusoidal inputs. As seen in Fig.(4.17), there is no linear relation between the derivatives. This is atypical as the linear relation was found to hold good for various other delta-wing configurations like GTA presented here, and for Delta-65^o wing [23], X31 [78], etc. However, the PSD maps showed fair enough spike at first harmonic frequency relative to noise. Therefore, the raw data further investigated following two approaches.

In the stall angle-of-attack region, variations in $C_m(t)$ in the raw wind tunnel data showed periodic and distinguishable oscillations for only two to three cycles out of ten oscillations recorded. These were chosen and averaged for use in estimation. The signal-to-noise ratio is poor in some cases as seen in the PSD map of one of the test cases in Fig.(4.18). Such cases were rejected and only the best three cases at each angle-of-attack were selected for further investigations.

Three standard filtering techniques from literature, namely the Chebychev filter, Elliptic filter and Butterworth filter, were used to process the given raw-data to reduce the effect of noise. The effect of filtering on data was found to be more sensitive than earlier anticipated. A low-bandwidth filter of the order of three times the input frequency caused significant phase-distortion, and hence may have affected the values of in-phase and out-of-phase derivatives. A higher bandwidth filter did not remove the measurement noise effectively. These conclusions are evident from Fig.(4.19), where raw wind tunnel data and processed signals are plotted. The data filtering was also done by running the

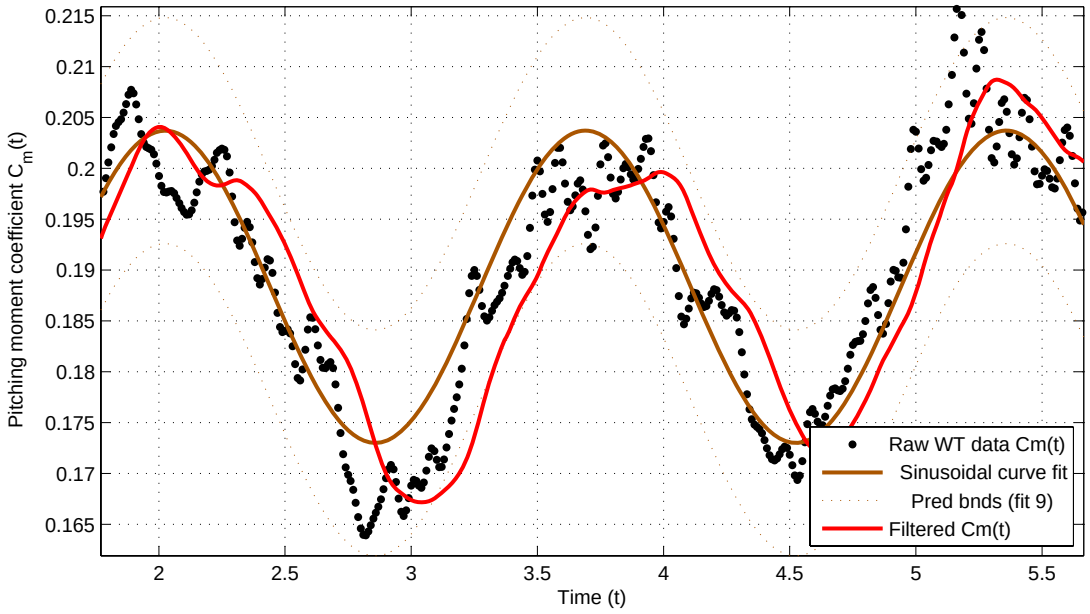

Fig. 4.19. Processing of $C_m(t)$ for F16XL SAFO data by filtering and sinusoidal curve-fitting to estimate in-phase and out-of-phase derivatives.

filters forward and backward to remove the effect of phase-distortion.

When the filtered data was used to obtain the in-phase and out-of-phase derivatives by numerical computations, the coefficient of determination improved but remained low for $\alpha = [45^o,\ 50^o,\ 55^o]$. The newly estimated values of in-phase and out-of-phase derivatives, although different from the original ones, did not show any linear relation between them for $\alpha > 40^o$. Therefore, the parameters (a, K_1) cannot be estimated by two step regression method.

An alternative hypothesis about the cause of these problems is the use of amplitude of 5^o in SAFO tests. Over 10 degrees angle-of-attack range, $C_{m_{st}}$ varies significantly, especially in the near stall and post-stall regimes. Therefore, the value of linearization of this term at a particular α_0 is an incorrect approximation over 10^o angle-of-attack range. Hence, the postulated linear relation between in-phase and out-of-phase derivatives for VVM and other important model structures in literature may not hold true for 5^o amplitude. Hence, functional dependence of the parameters on angle-of-attack needs to be considered for estimation using the so-called SAFO data with 5^o amplitude.

In the second attempt, the parameter functions $(a(\alpha), K_1(\alpha))$ were defined by node-points at $3\,\mathrm{deg}$ intervals for estimation of single-state VVM parameters by output-error method. This makes the single-state VVM capable of capturing mild nonlinearities in the data due to variations in parameter functions over the angle-of-attack range. The method also failed to converge to any promising solution.

In further discussions with Dr. Patrick Murphy of NASA-LaRC, who was involved in the F16XL wind tunnel tests and modeling, it was suggested that there are significant vibrations of the model in the wind tunnel tests [95]. These vibrations can also happen at lower frequencies and hence affect the wind tunnel data obtained. Therefore, the assumption that the available wind tunnel data is exclusively due to unsteady aerodynamics may not be true. It was also suggested that the application of a low-pass filter with a smaller bandwidth to the raw wind-tunnel test data needs to be done cautiously. Further research efforts on the wind tunnel testing aspect of the unsteady aerodynamic modeling are essential.

4.5.2 Estimation using LAFO Data

Since, the single-state VVM can also capture mild nonlinearity in the variation, it is first tuned using parameter functions $(a(\alpha), K_1(\alpha))$ to produce best match to the LAFO data set, by output-error method. The fit obtained is not sufficiently accurate.

So, a two-state VVM was considered to estimate all the parameter functions $(a(\alpha), K_1(\alpha), K_{21}(\alpha), K_{22}(\alpha))$ simultaneously. For all the estimated parameters node-points were set at 5^o intervals. The results of this model are satisfactory, as seen in the example in Fig.(4.20). The maximum correction introduced by the state x_2 is approximately 25% of the value of x_1 at that angle-of-attack, as seen in Fig.(4.21). Thus, it improves the accuracy of the model in some angle-of-attack ranges. In the current case, the first state parameters have been identified using large amplitude forced oscillation data itself, rather than the small amplitude forced oscillation test data. This case study demonstrates the capability of VVM approach to adapt to available data.

4.5.3 Validation using Ramp-pitching Test Data

For F16XL, the wind tunnel test data using ramp pitching inputs at different rates is also available. The pitch rates used in this test correspond to the maximum value of pitch-rate in the sinusoidal inputs in the LAFO data. This data is not used for estimation of model parameters, and it is used here for the purpose of model validation. Note that, ramp pitch-up and pitch-down is one of the ways that an aircraft executes pitching motion in operational conditions. Validation of the estimated model using this data also implies its applicability to generic input types.

The ramp-pitching response data showed some peculiarities. It was found that the nature of aerodynamic load responses for inputs beyond a certain threshold pitching rate are not consistent with that at lower-rates. These evidences are discussed in detail in the next section. Hence, only the data for lower rates in pitch-up and pitch-down motions are

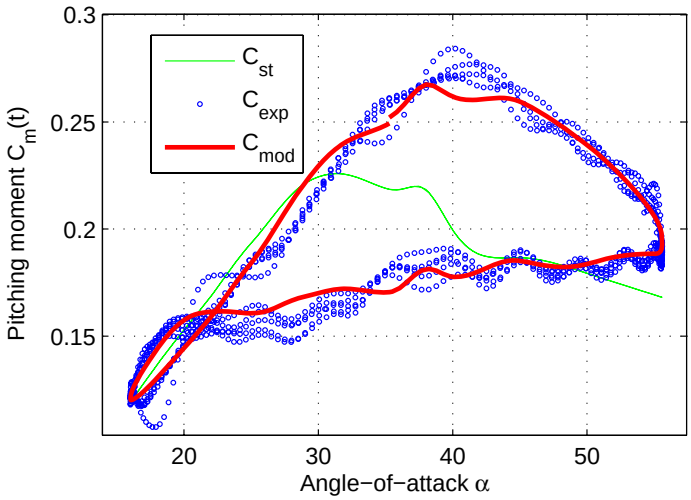

(a) Input $\alpha_0 = 35^o, \Delta\alpha = 20^o, f = 0.44Hz$

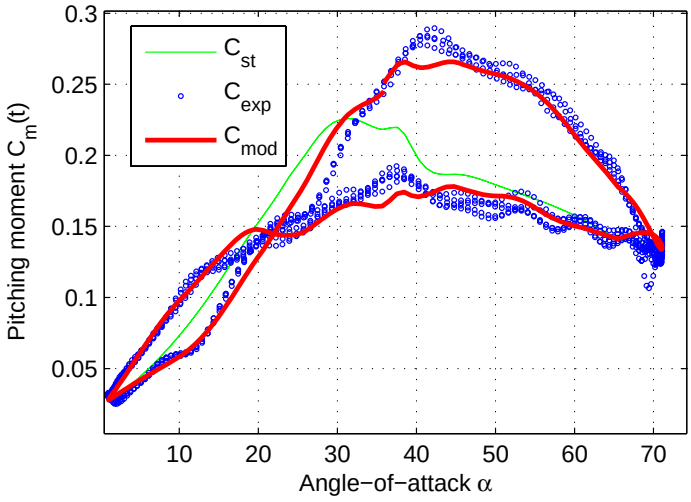

(b) Input $\alpha_0 = 35^o, \Delta\alpha = 35^o, f = 0.25Hz$

Fig. 4.20. Comparison of the output of VVM and experimental data due to large amplitude oscillation input for C_m of F16XL.

used for validation.

Some examples of the results from this case study are presented in Fig.(4.22), and the remaining are available in APPENDIX B. The response of one state VVM or the linear component of the model indicated as $C_{m_{lin}} = x_1(t)$ in the figure is observed to produce a fairly accurate match with the experimental data. However, the two state VVM response indicated by $C_{m_{mod}} = x_1(t) + x_2(t)$ is found to match well with the experimental data consistently for all the pitching inputs of different rates considered. While the magnitude of correction from $x_2(t)$ is not relative large, it shows important changes due to nonlinear nature of variations in the $[30^o\ 35^o]$ and $[60^o\ 65^o]$ angle-of-attack region.

This study shows that the identified VVM model is good for simulation using input

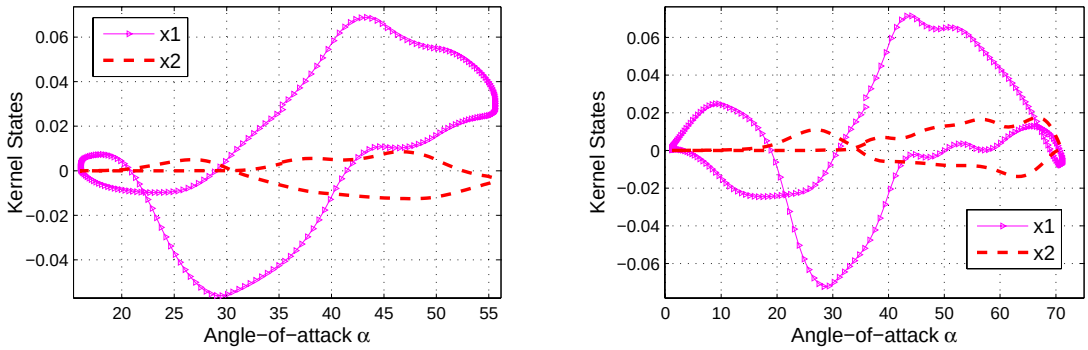

(a) Input $A = 20^o,\ f = 0.44Hz$ (b) Input $A = 35^o,\ f = 0.25Hz$

Fig. 4.21. Relative contribution of x_1 and x_2 to VVM output due to large amplitude oscillation input, for C_m of F16XL.

types not used in parameter estimation.

4.6 Identification of the Normal force coefficient of F16XL

Identification of C_Z model of F16XL is done following an approach similar to that for C_Z of GTA. The parameters of x_1 for C_Z are estimated by two step regression, and results are given in Fig.(4.23). The estimated parameters and coefficient of determination, using SAFO data are given in Fig.(4.25). The parameter functions are then tuned using large amplitude forced oscillation test data and the resulting single-state VVM was found to produce satisfactory match with the experimental data as seen in Fig.(4.24) for two test cases. This example shows that the wind tunnel data for C_Z and C_m coefficients for the same aircraft can be significantly different, and hence there is a remarkable difference in the identification method required for the two.

Based on observations for the normal force coefficients for GTA and F16XL, it can be concluded that for Delta-wing configurations a single-state VVM is usually sufficient to model the unsteady normal-force variations. For accurate estimation of parameter functions $(a(\alpha), K_1(\alpha))$, large amplitude forced oscillation test data is essential.

4.7 Comparison of VVM and PoDE Modeling Results for GTA

In this section, a quantitative comparison of the unsteady modeling results obtained from VVM and PoDE models for GTA are presented. A comparison of identification methodology between VVM and PoDE modeling approaches is presented in Section 2.5, where advantages of using VVM over PoDE model structure are highlighted. The

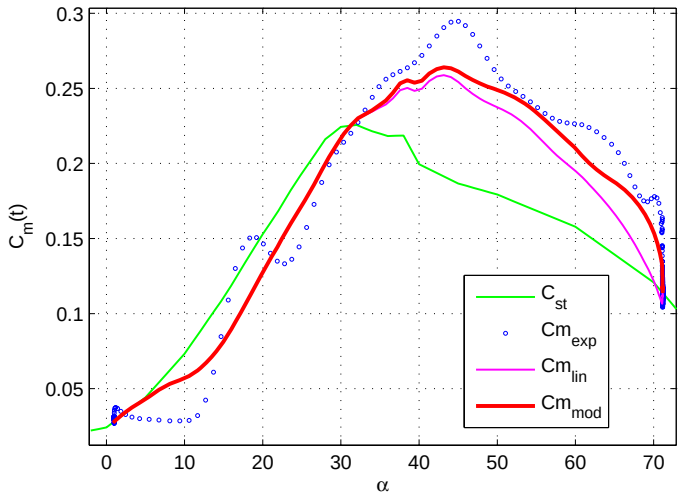

(a) Ramp-pitch up $92\,\mathrm{deg}/s$

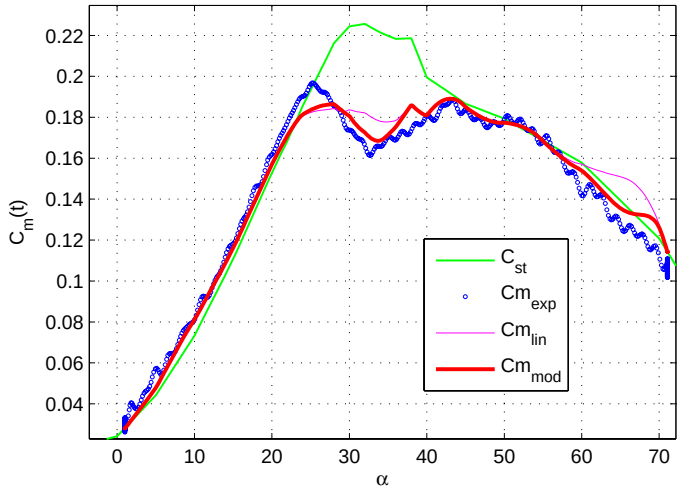

(b) Ramp-pitch down $18\,\mathrm{deg}/s$

Fig. 4.22. Comparison of the response of VVM and experimental data, due to ramp-pitching inputs for C_m of F16XL

quantitative comparison presented in this section is focused on accuracy of the model output.

There is not much difference in the accuracy of results for modeling C_Z of GTA using VVM and PoDE models. This is because both the models are equivalent in their linearised forms. The variation in $C_m(t)$ for large amplitude of inputs is significantly nonlinear, and hence it is a benchmark for comparison of the nonlinear unsteady modeling approaches. Only the results for C_m of GTA are discussed here.

As shown in Section 4.4 for GTA, the two state VVM reproduces all the qualitative features of variation in $C_m(t)$ due to sinusoidal input, while a three-state VVM is essential for higher accuracy results. In case of PoDE model, satisfactory results were obtained

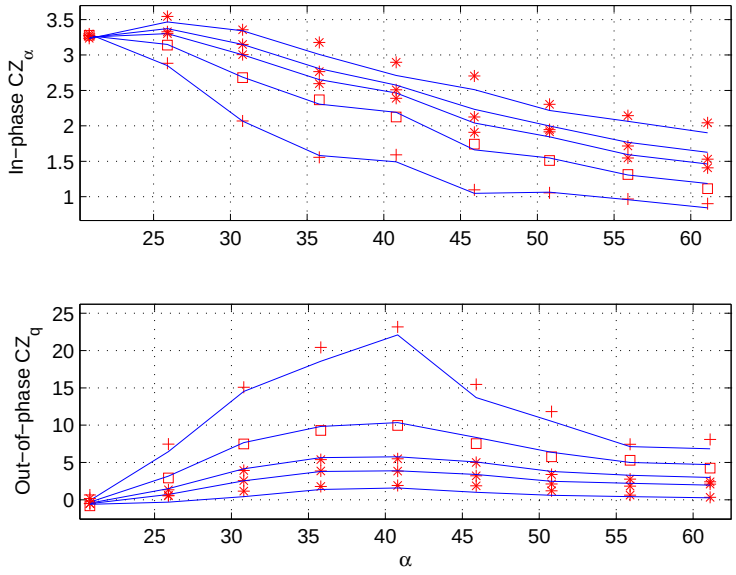

Fig. 4.23. Comparison of in-phase and out-of-phase derivatives from VVM and experimental data, for C_Z of F16XL.

with quadratic and cubic polynomial terms included in the model structure.

Simulations using VVM produced a better fit than that using PoDE model, as seen in Fig.(4.26). This is also true for the other wind tunnel test cases not shown here. The accuracy of the model fit is commonly quantified in terms of Root-mean-square error with respect to experimental data. A comparison of the Root-mean-square errors of the outputs of the two models is given in Table.(4.1) for all the wind tunnel test cases of GTA. Except for two cases highlighted in bold in this table, the RMS error is lower for VVM than the PoDE model. This shows that VVM produces higher accuracy results than the PoDE

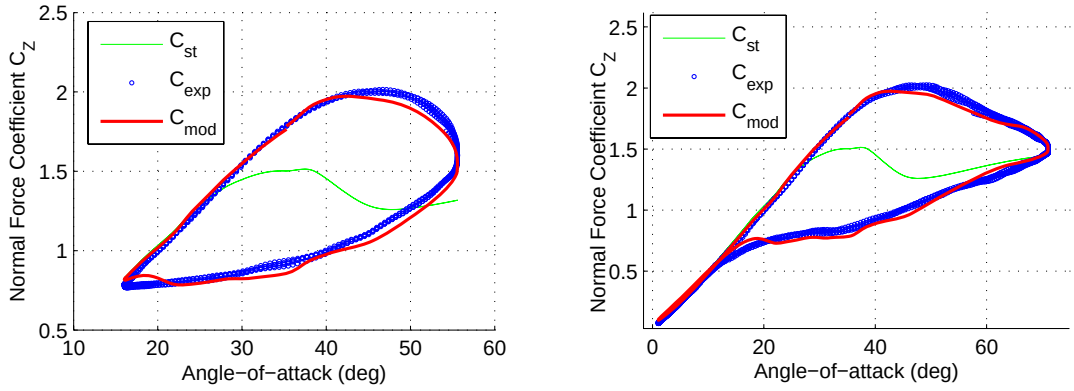

(a) Input $A = 20^o$, $f = 0.44Hz$ (b) Input $A = 35^o$, $f = 0.25Hz$

Fig. 4.24. Comparison of the simulation output of VVM and wind tunnel test data for C_Z of F16XL due to large amplitude oscillation inputs.

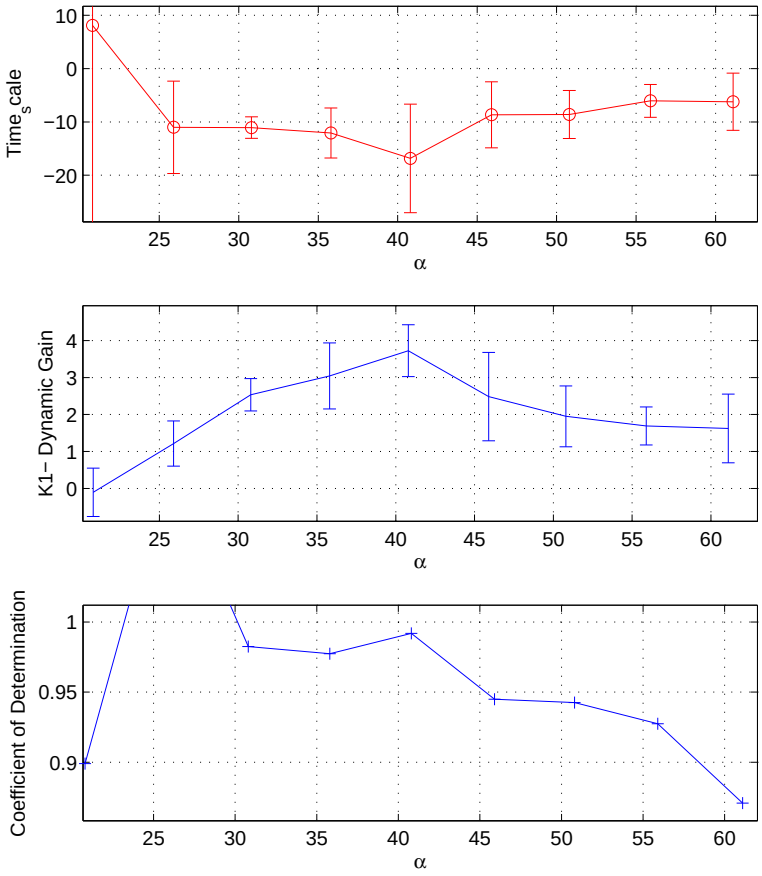

Fig. 4.25. Estimated parameter values and bounds, and coefficient-of-determination, for C_Z of F16XL.

model.

The difference in accuracy of results can be attributed to different number of parameter functions and harmonic input response properties. The difference in harmonic input response properties is discussed in Section 2.5. While PoDE model contains four parameter functions, VVM involved estimation of six parameter functions. Hence, the VVM identification offers a greater flexibility. But, as known from system identification theory, the covariance of the parameter functions of VVM is likely to be much higher than that for PoDE. This computation is not possible using the available methods in literature. It is important to note that the PoDE model, as proposed by Abramov-Goman, does not include input-state coupling terms in the differential equation.

An important side-note on a common feature of VVM and PoDE model results is discussed here. Both the models VVM and PoDE, showed a common feature, that the time-scales of C_Z and C_m are approximately equivalent, as seen in the case of GTA in Fig.(4.27). This was also found to be true for X31, Delta-65^o wings as shown in Fig.(4.28)

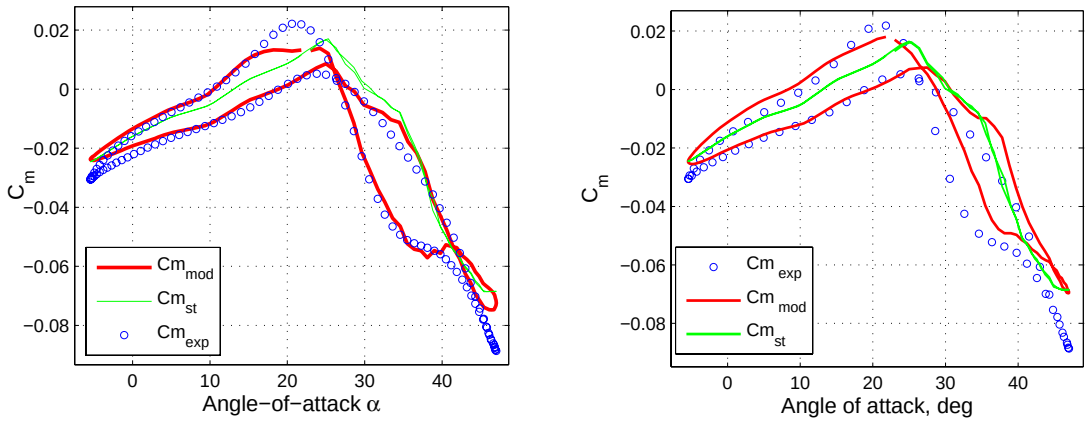

(a) For Volterra variational model

(b) For PoDE model

Fig. 4.26. Simulation of VVM and PoDE model response to large amplitude pitch oscillation input with $\Delta\alpha = 25^o$,$\alpha_m = 20^o$, $f = 0.5Hz$ for C_m of GTA

Sr. No.	α_0 deg	$\Delta\alpha$ deg	fHz	**PoDE**	**VVM**
1	15	15	0.5	0.0041	0.0031
2	15	15	1	0.0035	0.0028
3	15	15	1.5	**0.0022**	**0.0039**
4	25	15	0.5	0.0081	0.0061
5	25	15	1	0.0081	0.0059
6	25	15	1.5	**0.0079**	**0.0102**
7	35	15	0.5	0.014	0.0106
8	35	15	1	0.0164	0.0108
9	35	15	1.5	0.0103	0.0054
10	30	20	0.5	0.0108	0.0077
11	30	20	1	0.01	0.0056
12	20	25	0.5	0.0102	0.0062
13	20	25	1	0.0091	0.0057
14	30	25	0.5	0.0085	0.0053

Table 4.1. Comparison of RMS errors for VVM model and nonlinear PoDE models, relative to experimental data, for large amplitude oscillation input.

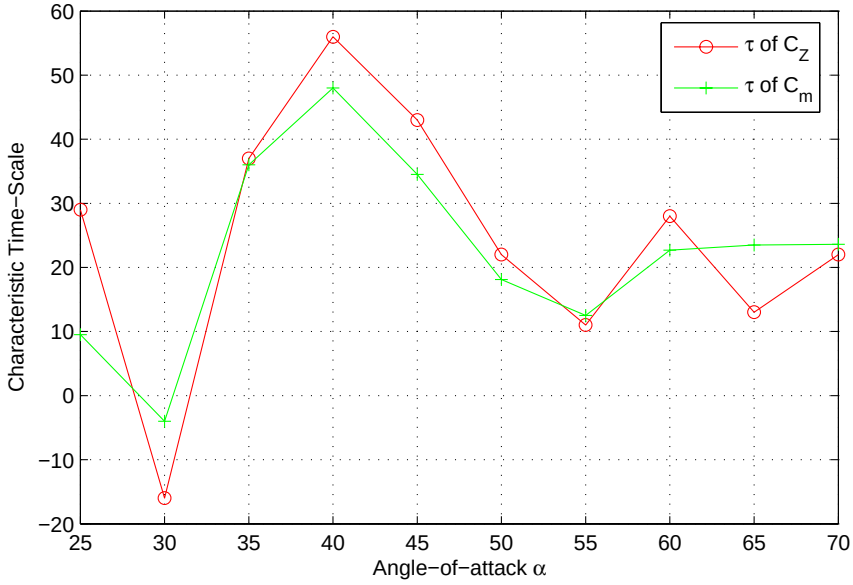

Fig. 4.27. Comparison of time-scale parameter $-1/a(\alpha_0)$ of C_Z and C_m of GTA.

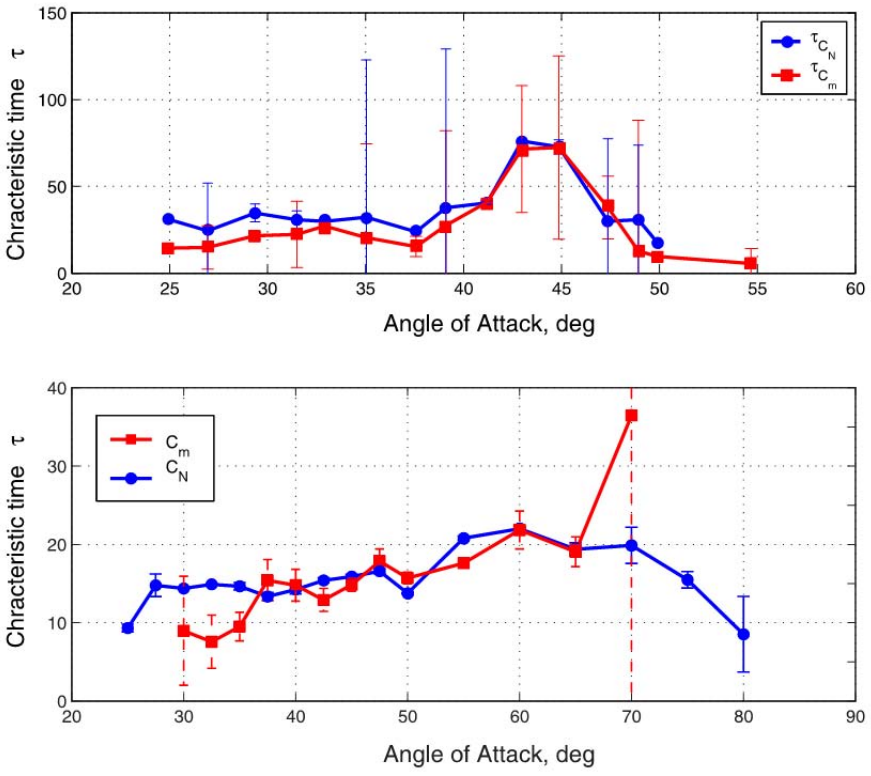

Fig. 4.28. Comparison of time-scales $a(\alpha)$ of C_Z and C_m for Delta-70 wing (top) and X31 aircraft (bottom) [20].

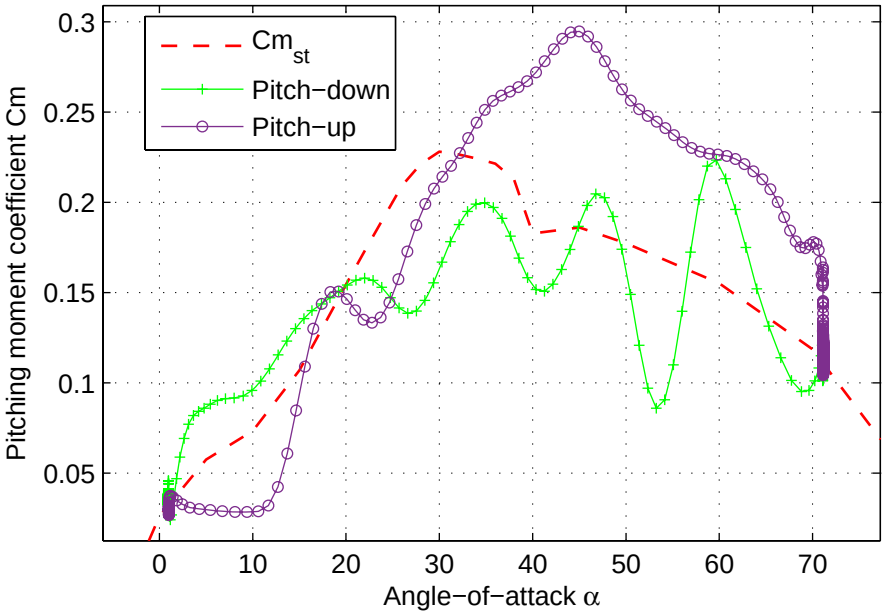

Fig. 4.29. Variation in C_m of F16XL in response to ramp pitching motion inputs at $92\,\mathrm{deg}/s$ in wind tunnel tests.

from [20]. This shows that there is an inherent relation between unsteady variation of C_Z and C_m, as is the case with real aerodynamics of a wing. This observation highlights two things, that VVM and PoDE are intuitively linked to the physics of flow and that both the model interpretations are also similar.

4.8 Anomalous Behaviour at High Pitch-rates

At high pitch-rate inputs, we observe an unusual variation in $C_m(t)$ in the available wind tunnel data for F16XL. This is found to occur consistently in response to ramp pitch-up, pitch-down and sinusoidal inputs. This and similar data from literature are analyzed in this section to discuss the issues into its use for identification of an unsteady model.

In ramp pitch-up and pitch-down motions of the F16XL model with non-dimensional rates $k = 0.034$, as presented in Fig.(4.29), variation of $C_m(t)$is quite arbitrary. It seems to have higher frequency oscillations whose mean value is shifted from the steady-state values. This happens even at low angles-of-attack region with attached flow. For lower non-dimensional pitch-rate, the dynamic hysteresis in the stall region of angle-of-attack is significant, and without these anomalies. This shows a different nature of unsteady aerodynamics in such cases.

In large amplitude forced oscillation tests, at the point of maximum acceleration at high-angle-of-attack, there are distinct oscillations in the $C_m(t)$, as seen in Fig.(4.30,a).

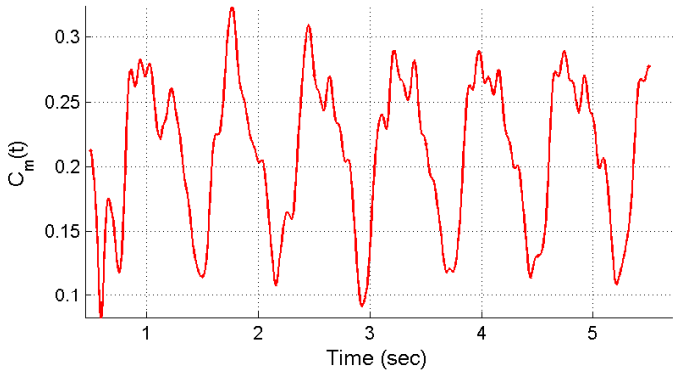

(a) Maximum pitch-rate of $92^o/s$

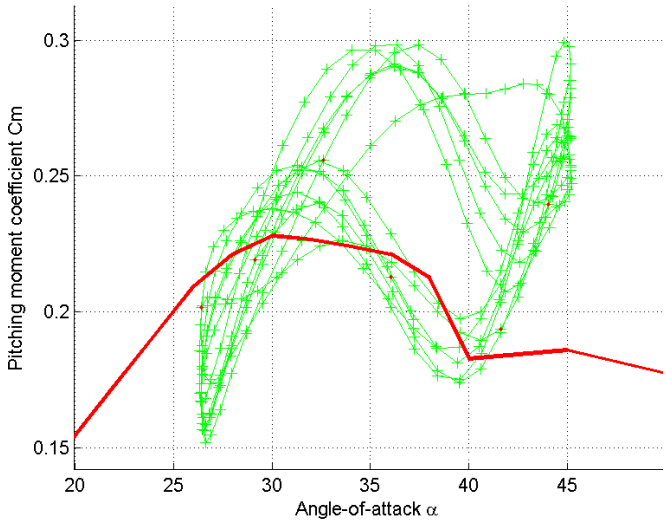

(b) Maximum pitch-rate of $220^o/s$

Fig. 4.30. Variation in C_m of F16XL in LAFO wind tunnel tests due to high maximum-pitch-rate inputs.

These oscillations produce very unusual trends, although they occur in each cycle. The resulting dynamic hysteresis in $C_m \, vs. \, \alpha$ also does not follow the normal trend with respect to static variation, as seen in Fig.(4.30,b). These anomalies occur only for the cases where maximum pitch-rate of the oscillation input is above a certain threshold $\dot{\theta}_{thr} = 92^o/s$ approximately. This is also the threshold value beyond which the anomalous variations were observed from ramp-pitching input test data. Thus, these higher frequency oscillations show-up consistently in different types of data.

Fixed wing aircraft usually do not encounter such high pitch rate in operational conditions, even in the event of departure due to loss of stability. Hence, they are not normally tested for such high pitch-rates, and such a wind tunnel data can be ignored during identification. However, the blades of a rotary wing aircraft encounter such high pitch-rates in a forward motion flight. Hence, helicopter blade airfoils have been

investigated for unsteady aerodynamics across a wide range of pitch rates.

A comprehensive data set of forced oscillation tests done on a variety of airfoils is available in [36, 96]. An airfoil of Boeing Vertol VR7 was tested for non-dimensional pitch-rates from 0.025 to 0.25. As seen in Fig.(4.31), there are high frequency oscillations in the lift force variation for the case of $k = 0.1$. This happens for all the cases with $k > 0.1$. However, for lower pitch rates, like in case of $k = 0.025$ in Fig.(4.31,b), the dynamic hysteresis has a single steady-state oscillation cycle. The small amplitude very high frequency oscillations in this figure are due to sting vibrations.

At lower pitch rates flow dynamics is dominated by vortex breakdown moving on the wing surface from trailing edge towards leading edge with increase in angle-of-attack. However, for higher pitch-rate inputs there is leading edge separation and vortex shedding. This can be observed from the progression of chordwise pressure distribution on the wing shown in Fig.(4.32). Consider the pressure variation over a phase cycle for the two oscillation frequencies $k = 0.025, 0.1$. In Fig.(4.32,b), consider the leading edge of the pressure line at different angle of attack. There is sudden loss in pressure between angle-of-attack of 14.9^o to 18^o. This indicates the presence of leading edge flow separation for $k = 0.1$. Now in Fig.(4.32,a) consider the trailing edge of pressure line, and there is gradual flattening of the pressure line between angle-of-attack of 11.2^o to 17.9^o. The pressure at the trailing edge recovers in similar angle-of-attack range. This indicates trailing edge flow separation for $k = 0.025$. Therefore, an airfoil or a wing can experience two different aerodynamic phenomena depending on the maximum reduced pitching frequency. It is also known that the leading and trailing edge flow separation phenomena have totally different time-scales [74].

Although the effect of different flow phenomena depending of reduced frequency of input angle of attack is also seen in variation of C_Z and C_L, it is more prominent for C_m. In NASA report [35], the forced oscillation test data for Boeing Vertol VR7 data is used for the estimation of the "ONERA Dynamic Stall model". As seen in Fig.(4.31), there are higher frequency oscillations in the variation of $C_L(t)$ at $k = 0.1$ and there is a simpler dynamic hysteresis for $k = 0.025$. The data used in parameter estimation spanned a wide range of reduced frequencies from 0.025 to 0.1. The identified models of C_Z and C_m produced poor accuracy with respect to the wind tunnel data used in estimation. This example shows that identification of a common model across a range of frequencies or pitch-rates stretching to two different physical phenomena may fail with one model structure or yield poor results. Hence, considering the reduced frequency of pitching motion input is important before using the data for identification.

The other concern in forced oscillation data is that the aircraft model experiences the test rig structural vibrations in the wind tunnel. This effect is especially strong at

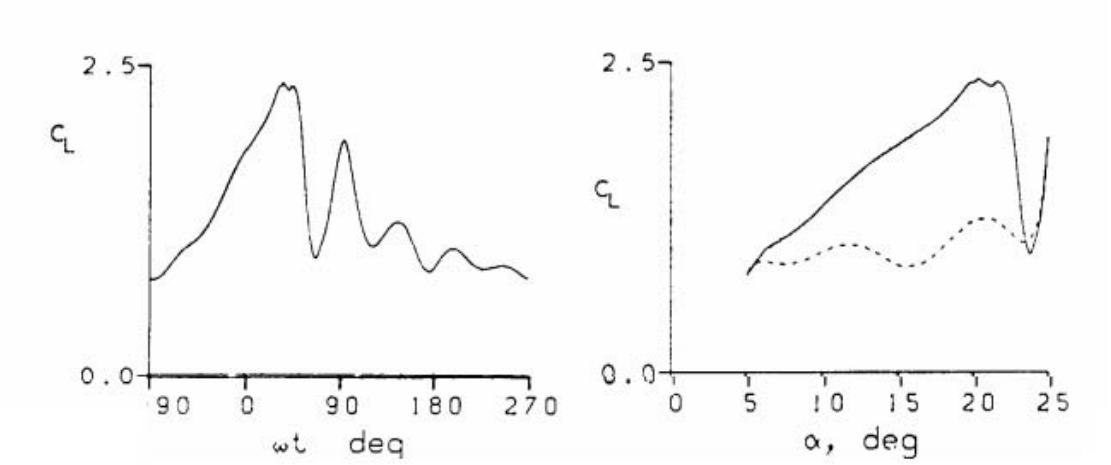

(a) For $k = 0.1$

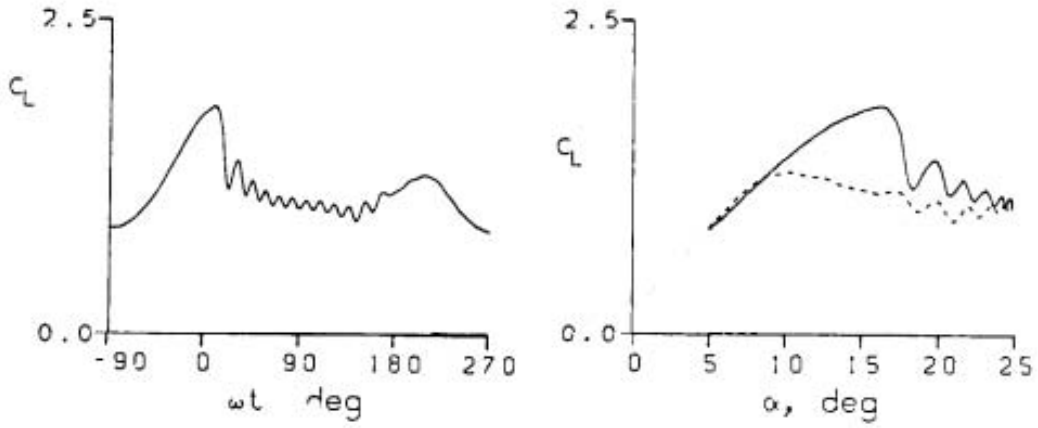

(b) For $k = 0.025$

Fig. 4.31. Variation of C_L for Boeing Vertol VR7 airfoil in a forced oscillation test with sinusoidal input of $\alpha_m = 15^o$ and $\Delta\alpha = 10^o$ at $M = 0.3$ [96].

the points of high impulse acceleration input. The random oscillations in C_m are found to occur at such points in the ramp input response data of F16XL. The sting vibration affects the vortex flow which is very sensitive to angle-of-attack input, and depends on the history of it. In effect, variation over the entire cycle is affected and the data obtained is not realistic. Note that, for the point of maximum acceleration at low-angle-of-attack, the vortical flow has lower strength and is more robust to vibration inputs. In case of ramp pitch-up, there is impulse acceleration at the beginning and end of the ramp. So this impulse in the beginning or end, causes vibrations which sustain for some time. So, the structural vibrations may also be responsible for corrupting the data corresponding to high pitch-rate ramp inputs.

For delta-wing configurations of fixed wing with low aspect-ratio, only lower

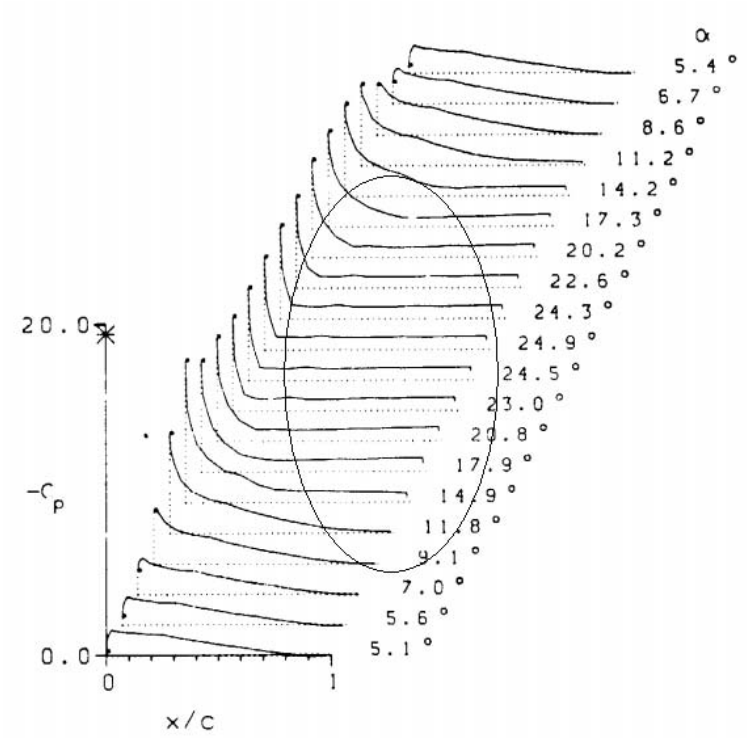

(a) For $k = 0.025$

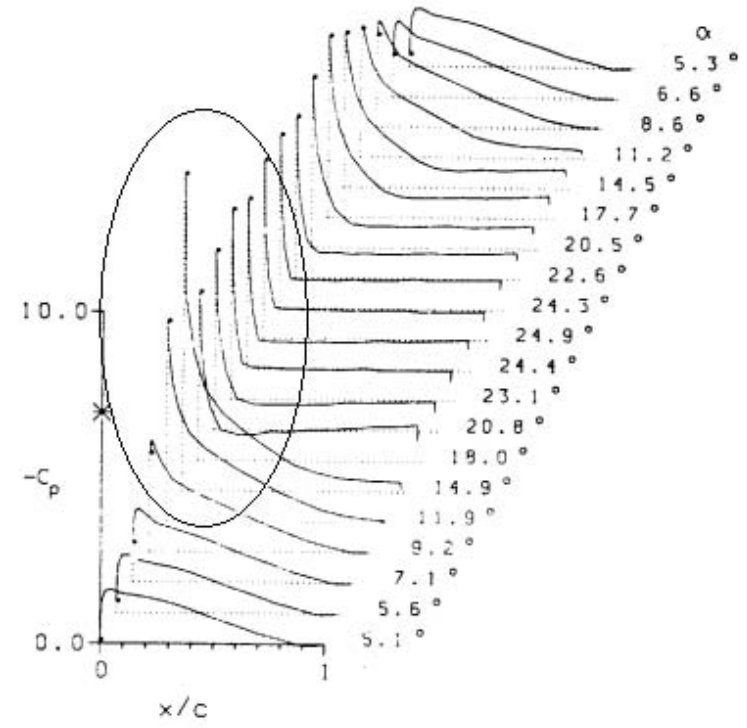

(b) For $k = 0.1$

Fig. 4.32. Variation of chord-wise pressure on Boeing Vertol VR7 airfoil in a forced oscillation test with $\alpha_0 = 15^o$, $\Delta\alpha = 10^o$ at $M = 0.3$ [96].

magnitude of pitch-rate, typically less than $70^o/s$ is relevant. Hence, some of the LAFO data for F16XL for which $\dot{\theta}_{max} > 92^o/s$ were excluded from the parameter estimation process. This in turn implies that the unsteady aerodynamic model for C_m of $F16XL$ is valid for pitch-rate lower than $92^o/s$.

4.9 Summary

The case studies for identification of the longitudinal coefficients of GTA and F16XL aircraft using the comprehensive forced oscillation test data, have amply proved the various capabilities of VVM. These include flexibility of the model structure, correlation of the level of nonlinearity to the model structure, simple parameter estimation approach, adaptation of the estimation approach to suit the available data. Identification of C_Z of both GTA and F16XL was straightforward, as these had mildly nonlinear unsteady variations. Fairly complex variations in C_m of GTA due to three damping/antidamping oscillation cycles in LAFO data, are reproduced accurately using a three state VVM. In case of C_m of F16XL, SAFO data was found to be corrupted by noise or vibrations in the experimental setup. Hence the linear model parameters cannot be estimated from it either by two-step regression or output-error methods. A two state VVM model was estimated using LAFO data and was shown to produce satisfactory results. A quantitative comparison between the identification results for C_m of GTA using VVM and PoDE models, showed that the accuracy of VVM is better. In the end, significance of the use of appropriate non-dimensional pitching rates or frequency in the experiments, and their use in parameter estimation was highlighted using different data from literaure.

Chapter 5

Flight dynamic Analysis and Alternative Formulations using VVM

5.1 Introduction

The Volterra variational model was shown to produce a high-fidelity representation of nonlinear unsteady variation of longitudinal aerodynamic loads. An aerodynamic model or aero-database is integrated with aircraft rigid body equations of motions and used in flight dynamic analysis. This involves flight simulation studies; trim and stability analysis of linearized equations of motion; control law design, and such other design and analysis tasks. More often, linear analysis tools from systems theory are used for the purpose. The classical aero-derivative formulation presented by Bryan in 1919 is straightforward for use in such analysis. In this chapter, it shown that the methods from classical flight dynamic analysis can be applied also when VVM is used to model unsteady aerodynamic loads in the stall angle-of-attack region.

VVM reproduces the nonlinear and unsteady variation of aerodynamic coefficients in time-domain in state-space form. This facilitates the use of classical methods from linear systems theory. The effect of the unsteady variation of longitudinal coefficients of GTA on its Short-period mode, and failure of a classical aero-database model to capture this effect, are presented in Section 5.3.

Due to the legacy of the modeling approaches discussed in Chapter 1, it is essential to present their comparative analysis with the VVM approach presented in this thesis. The similarities in model structure and interpretations of these approaches with VVM, further highlight its consistency for modeling unsteady aerodynamic loads. It is also shown that the VVM structure can be adapted to match the mathematical or aerodynamic features of these approaches. Note that this comparative analysis is not a quantitative comparison of the accuracy of the outputs of different model structures. This topic is covered in detail in Section 5.4.

Recently, novel unsteady aerodynamic data from wind tunnel tests or CFD computations obtained using Schroeder-sweep input [44], step input [53], ramp input, and impulse inputs [56] etc. have been presented in literature. VVM approach offers some natural advantages in identification using these input types. Hence, the use of these data types in identification using VVM is also discussed in section 5.4.

5.2 Application of VVM to 6DOF Flight Simulation

A classical aero-derivative model or the aero-database is formulated as,

$$C_i(t) = C_{i,st}(\alpha, \beta) + C_i(\delta C) + C_{i_{(q+\dot{\alpha})}}(\alpha)\frac{(q+\dot{\alpha})\bar{c}}{2V} \;\; \forall \; i = Z, m \tag{5.1}$$

where δC indicates control surfaces deflections, and $C_{i,st}$ indicates steady state value of the coefficient. The unsteady component of aerodynamic loads is simply modeled by the $C_{Z_{(q+\dot{\alpha})}}$ and $C_{m_{(q+\dot{\alpha})}}$ derivatives obtained by empirical methods or from small amplitude forced oscillation test data.

However, as also discussed in the previous chapters, these derivatives are not unique in the stall angles-of-attack region. In frequency domain, these are function of frequency and amplitude of input. Therefore, in order to use these derivatives in time-domain simulations, a data-table of their values at a particular frequency and small amplitude of input is added to the aero-database. However, the change in angle-of-attack in a maneuvering aircraft comprises of a range of frequencies, and it is infeasible to map the component frequencies to any particular data-table. Hence, using the aero-derivatives in simulations produces incorrect unsteady loads. Therefore, the classical aero-database is not a true representative of aerodynamic loads acting on an aircraft in the stall region.

$$\begin{aligned} \frac{dC_{Z_d}}{dt} &= f_{vvm}(C_{Z_d}, \dot{\alpha}, a_{1m}(\alpha), K_{1Z}(\alpha)) \\ \frac{dC_{m_d}}{dt} &= g_{vvm}(C_{m_d}, \dot{\alpha}, a_{1m}(\alpha), K_{1m}(\alpha), K_{21m}(\alpha), K_{22m}(\alpha)) \end{aligned} \tag{5.2}$$

The VVM can be easily integrated with the available aero-database of that aircraft, because it is formulated as an incremental contribution of unsteady aerodynamic loads, as presented in Chapter 3. This feature is important in industrial-grade applications where an aero-database comprises of a large number of data tables. The functional form of VVM are represented by C_{Z_d} and C_{m_d} as given in Eq.(5.2). In this equation, functionals f_{vvm} and g_{vvm} are VVM of C_Z and C_m of GTA respectively.

For the purpose of simulation, these differential equations are augmented to

the 6DOF rigid-body equations of motion of the aircraft, and integrated along with them at each time-step. In the pre-stall and post-stall regions the values of parameters are such that $C_{Z_d} = 0$ and $C_{m_d} = 0$, as explained in Chapter 4. Therefore, these equations are integrated even in these angle-of-attack ranges, but do not produce any additional component of loads. The parameter functions $\{a_{1m}(\alpha), K_{1Z}(\alpha), a_{1m}(\alpha), K_{1m}(\alpha), K_{21m}(\alpha), K_{22m}(\alpha)\}$ are included as lookup-tables in the aero-database. Such a model can then be used in any flight simulation studies.

The aircraft flight dynamics can be considered to have two additional states due to unsteady variation of aerodynamic loads. Its use for flight dynamic analysis and control law design is explained in the next section. Note that, there is no need to make any changes to the original aero-database of the aircraft available in the simulation setup. Thus, VVM can be seamlessly and simply used in 6DOF simulation studies of a given aircraft.

5.3 Influence of Unsteady Aerodynamic Effects on Flight Mechanics

In this section, it is shown that the classical aero-database which has been used in the industry for long, can cause significant errors in flight dynamic analysis. The unsteady aerodynamic models of GTA which are integrated with the aero-database as explained in the previous section, are used in the following analysis.

The fast flight dynamic modes are of primary interest in this analysis. This is because the dynamics of slower modes is affected by unsteady aerodynamics to a much lesser extent and it can be corrected by the pilot or the autopilot control laws. For the purpose of flight dynamic analysis, using a 5^{th} order set of equations of motions is sufficient as presented in details in [97, 98]. The states included in this set are (α, β, p, q, r). The linearization of this set of equations results in the flight dynamic modes of Short-period, Roll-subsidence and Dutch-roll. It is known that the time-scales of these modes are one order of magnitude smaller than the slower modes like Phugoid and Spiral. Hence, the results from this reduced set of equations of motion are not affected significantly by the slower modes.

The 5^{th}-order setup is subject to trim, linearization and stability analysis. An altitude of $H = 6000m$ and Mach number $M = 0.4$ are used in this analysis. At trim points, $\dot{\alpha} = 0$, and hence the steady-state solutions of Eq.(5.2) are $[C_{Z_d}, C_{m_d}] = [0, 0]$. So, the trim solutions are obtained at the same aircraft kinematic states (α, β, p, q, r) as that from an aero-database without unsteady model. Therefore, the unsteady model does not affect the trim solutions directly, but causes difference in the transient dynamics between two steady states. The longitudinal trim solutions were investigated in the range $\alpha \in [28^o\ 40^o]$,

and there were no trim solutions beyond this angle-of-attack.

The unsteady model is found to influence the stability properties of the trim solutions significantly. The aircraft dynamics equations are linearized at trim points, and their eigen spectrum is analyzed to understand the stability characteristics. Since the linear stability analysis is valid for only small range of angle-of-attack around the trim-point, only the first kernel state of the estimated VVM is used in this analysis. Since the equations of motion consist of two additional states $C_{Z_d}(t), C_{m_d}(t)$, there are two additional poles (eigenvalues) corresponding to them.

A locus of the two real eigenvalues produced by the unsteady model states for $\alpha \in [28^o\, 40^o]$ is presented in Fig.(5.1,a). The real-part of the poles are found to approach zero with increasing angle-of-attack. This shows that the time-scales of the unsteady modes decrease as the aircraft enters stall angle-of-attack region; and their effect on flight dynamics becomes more prominent. As these poles come close to imaginary axis, they repel the eigenvalues of other modes away from them. Thus, the unsteady modes effect other flight modes significantly.

Only the effects on short-period mode are predominant here as only the longitudinal unsteady aerodynamic effects are included in the aerodynamic model. We consider the root-locus of the positive frequency of the short-period complex conjugate pair of eigenvalues. The first root-locus is obtained using the aero-database with the values of aero-derivative for frequency $f = 1Hz$ from SAFO data. The second root-locus is for VVM, which accommodates the frequency dependence of damping derivatives in the form of unsteady model poles.

A comparison of these two root-locii is presented in Fig.(5.1,b). While the first root-locus shows that the Short-period pole crosses imaginary axis and becomes unstable at $\alpha > 36^o$; the second root-locus shows that this happens at $\alpha > 32^o$. Thus, the aero-database gives an optimistic estimate of the angle-of-attack for onset of pitching mode instability. This can cause significant error in the designed control law and hence aircraft stability and performance.

This observation cannot be generalized as the stability trend is reversed at higher angle-of-attack. Here, the unsteady model shows recovery in stability of the mode, while the aero-database shows higher level of instability. There is also significant difference in the Short-period mode frequency over the entire angle-of-attack range. Thus, even the trends predicted by the aero-database model are unreliable.

In the control-law design, the effect of unmodeled dynamics is expected to be accommodated by the robustness of estimated feedback control loop-gains. However, even in this case the handling qualities of the closed-loop aircraft dynamics are likely to be severely effected as shown in [22]. Thus, it is important to develop a high fidelity unsteady

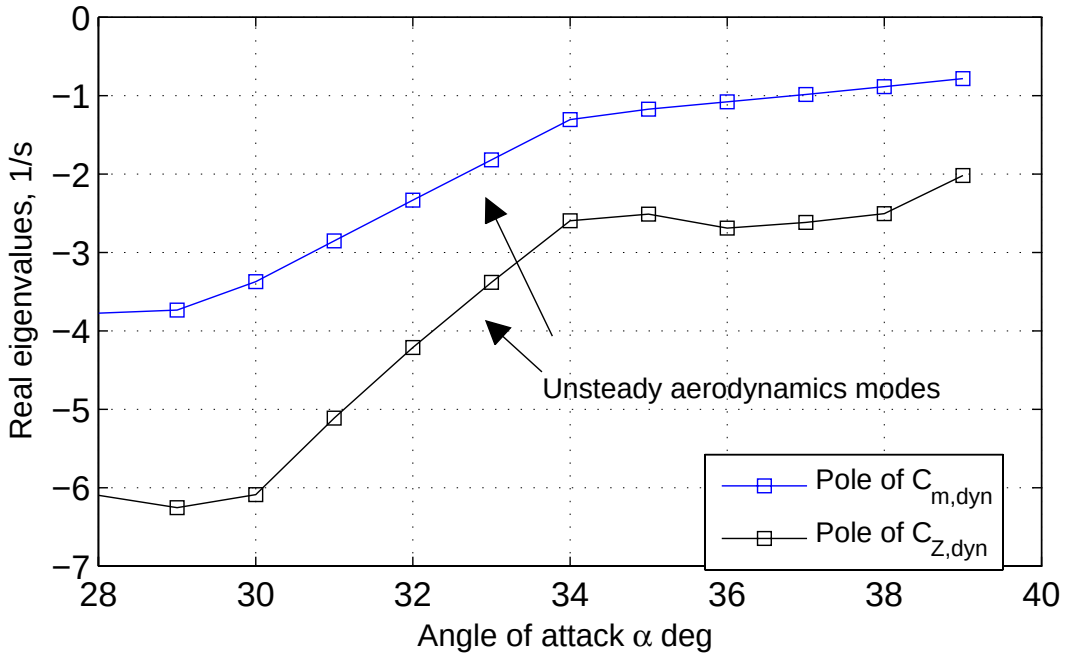

(a) Real-part of the eigenvalues of unsteady components of C_Z and C_m

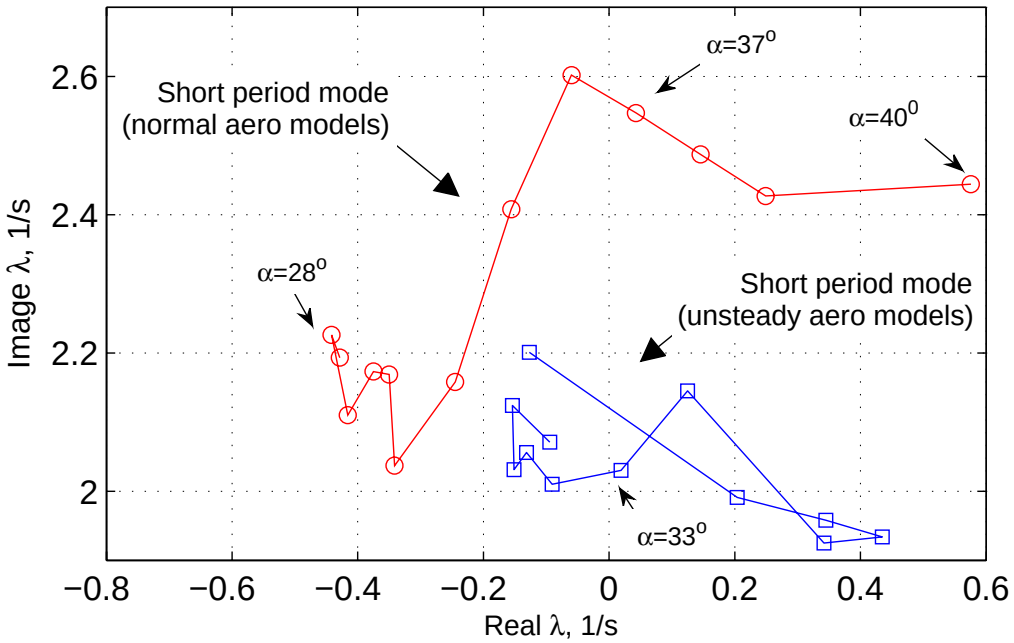

(b) Root-locus of positive eigenvalue of Short-Period mode

Fig. 5.1. Eigenvalue analysis to characterize the effect of longitudinal unsteady aerodynamics on longitudinal modes, at altitude $6000m$ and Mach 0.4

Sr. No.	Aero Phenomena	Mathematical Model
1	Relaxation time-constant	State-space, PoDE
2	Aerodynamic Load Partitioning	PoDE, Simplified Indicial
3	Input history (memory)	Volterra series
4	Nonlinear Unsteady variation	PoDE, ONERA
5	Oscillatory variation at high pitch-rate	ONERA
6	Static Hysteresis or Critical state crossing	BMSH, Nonlinear Indicial

Table 5.1. Aerodynamic features of Models

aerodynamic model for use in flight dynamic analysis and control-law design. The classical methods are not just inaccurate but can produce completely wrong predictions.

The role of nonlinearity in unsteady variation of aerodynamic loads is not evident from linear stability analysis. The nonlinear stability of the trim points in the stall angle-of-attack regimes is characterized by the Region-of-attraction of a trim solution. It is usually bounded and defines the level of critical disturbances. GTA was found to have unstable equilibrium states for lateral-directional modes in the stall angle-of-attack regimes. Close to the boundary of this unstable region, the stable equilibriums have limited stability region. An accurate model of nonlinear unsteady aerodynamics is important for correct prediction of critical external disturbances for stability of a flight mode.

5.4 Comparative Analysis of VVM with Other Unsteady Modeling Approaches

Each of the unsteady modeling approaches presented in literature is hinged on a certain aspect of aerodynamics in the stall angle-of-attack region, as summarized in Table.(5.1). Interpretations of VVM for some of these features of aerodynamics are presented in Section 3.6. This is important as it provides some qualitative validation of the model structure. These model structures pose some limitations which are discussed in Section 1.3. A comparative analysis is performed between VVM and these model structures to identify the capabilities and limitations of VVM, as well as to propose suitable adaptations to VVM to incorporate the features of these models.

5.4.1 Bifurcational Model of Static Hysteresis

There is static hysteresis in variation of coefficients for certain wing-types and airfoils. In these cases, the steady state value of the longitudinal aerodynamic coefficients can have two values in a small range of angle-of-attack in the stall regime. The actual value attained

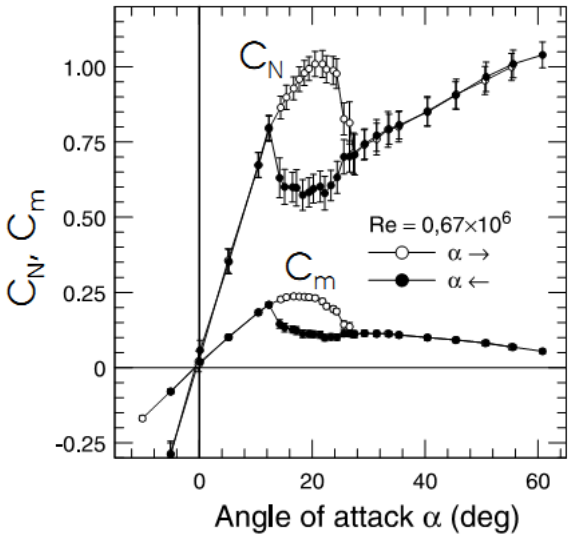

Fig. 5.2. Static hysteresis in variation of longitudinal coefficients of a wing with Aspect-ratio 5.0 and NACA-0018 airfoil, at different Reynold numbers[20].

depends on whether the aircraft was in a quasi-steady pitch-up or pitch-down motion before entering the stall region. For airfoils like NACA-0018 there is static hysteresis in the normal force and pitching moment coefficients at stall, as shown in Fig.(5.2).

As discussed in chapter 2, VVM cannot be used for modeling unsteady aerodynamic loads in presence of static hysteresis in variation of longitudinal coefficients. Hence, a different modeling approach called the Bifurcational model of static hysteresis presented in [20] can be considered to be complementary to VVM. However, there is usually no static hysteresis at stall for a Delta-wing shape and low aspect-ratio configurations of aircrafts; and some airfoils like the Boeing Vertol VR-7 [36]. These methods can together model a broad range of unsteady aerodynamic coefficients in various applications.

Abramov presented a novel approach called "Bifurcational Model of Static Hysteresis" (BMSH) in [20], which is applied for modeling unsteady variation of the normal force coefficient in presence of static hysteresis phenomena in the stall regime. Even other unsteady aerodynamic modeling techniques available in literature cannot include static hysteresis in variation of longitudinal coefficients. The indicial model with critical state crossing in [33] requires special experimental data, and is ad-hoc to some extent. Therefore, the BMSH model is the most promising solution in such cases.

The model structure is similar to the phenomenological model presented in [22] and is equivalent to the PoDE model. The difference is in the method of parameter estimation. In this approach, time-scale parameters on both the branches of the static hysteresis loop are estimated separately from SAFO data by linear regression of in-phase and out-of-phase derivatives. Other parameter functions, namely $a_1(\alpha), a_2(\alpha), a_3(\alpha)$ of the PoDE model, are determined by the value of the coefficient on the two branches of the static hysteresis

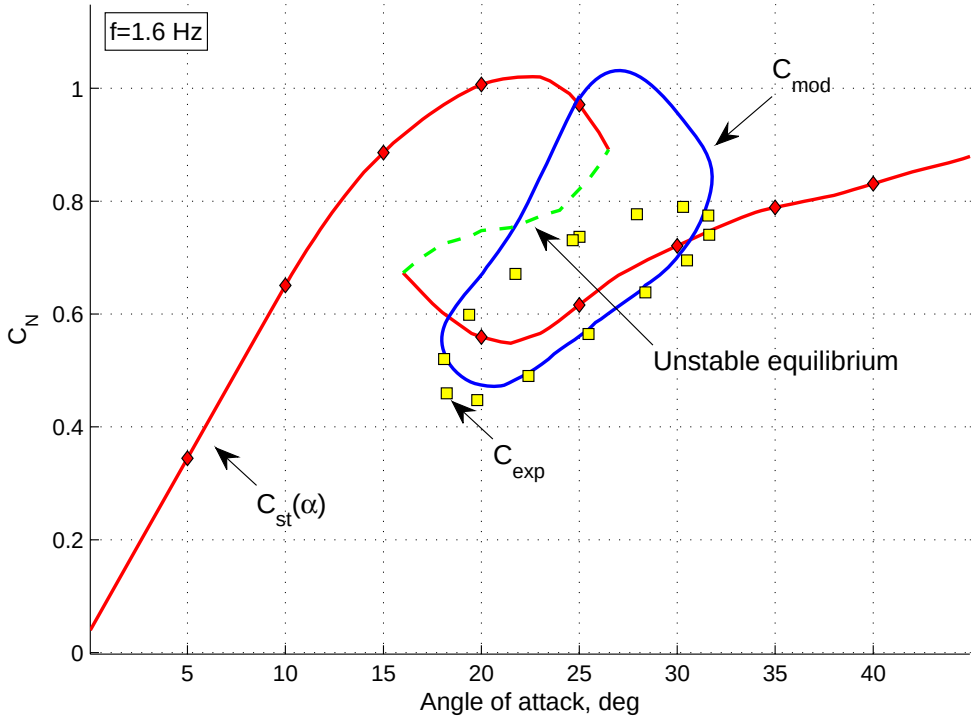

(a) case 1

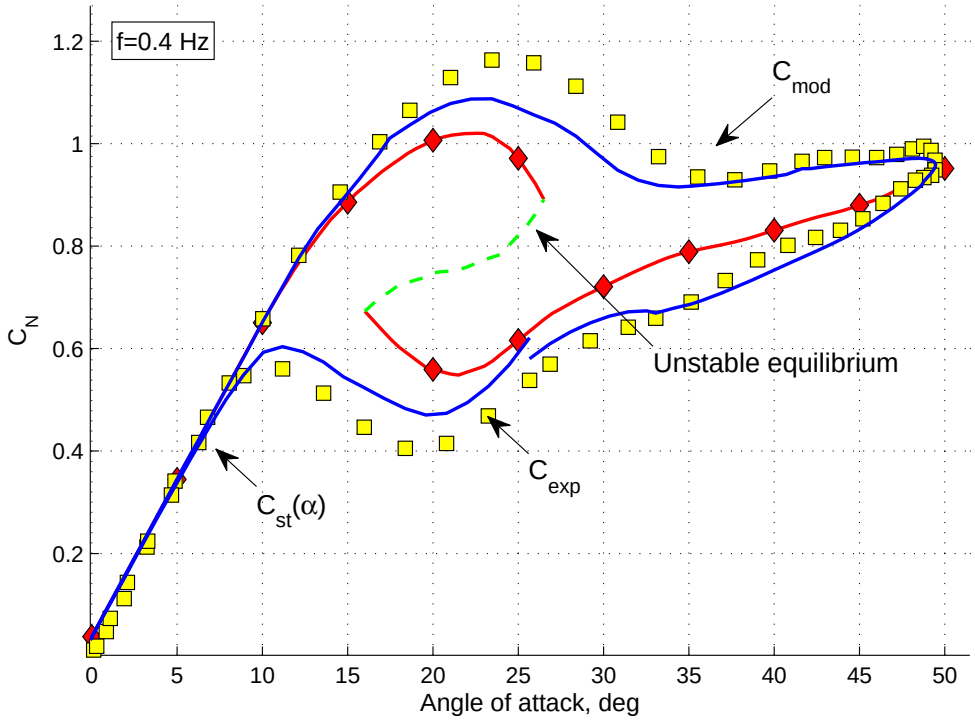

(b) case 2

Fig. 5.3. Simulation using PoDE model for Delta-65^o wing; good accuracy in simulation (case1), bad accuracy in simulation (case2) [20]

loop and outside it. In the estimation equations, a constraint equation on these parameters is set to have two real stable and one real unstable root for the cubic polynomial of dynamic component of load. It is expected that very large value of time-scales at the critical points of the static hysteresis, and nonlinear nature of time-scale function can model the non-linearity in unsteady variation.

The accuracy of simulation is found to be significantly poor in some cases. Consider the model output for two harmonic input cases given in Fig.(5.3) from [20]. In the first case in Fig.(5.3,a), the oscillation crosses both the critical states of the static hysteresis in $C_{N_{st}} \, vs \, \alpha$, and the model accuracy is satisfactory. However, in the second case in Fig.(5.3,b), there is only one critical state crossing involved, and the model accuracy is poor. This happens because the second stable root of the model in the stall region attracts the unsteady variation component $C_{N_{dyn}}(t)$ strongly. Hence, the match of model output to experimental data is inaccurate.

The model is based on an implicit assumption that use of time-scale parameter estimated from SAFO data is sufficient to capture unsteady variation of aerodynamic coefficients. This assumption is usually good for the normal force coefficient only. In LAFO test data, second and third harmonics are significant for pitching moment coefficients. In BMSH approach, parameter $a_2(\alpha), a_3(\alpha)$ of polynomial terms are not determined from LAFO data. These are determined by the value of coefficient on the two branches of static hysteresis and the constraint equation. Therefore, nonlinearity in the unsteady variation of coefficients is not modeled by the second and third degree polynomial terms as it does in the case of Abramov-Goman modeling approach. This can lead to inaccuracies in the results for the cases where unsteady variation of coefficients is significantly nonlinear.

In conclusion, BMSH is the only model in literature that can capture the static hysteresis as well as unsteady variation in the normal force coefficient. The accuracy of the model output becomes unsatisfactory for large amplitude inputs, and the motions involving single critical state crossing.

5.4.2 Volterra Series based formulations

In the literature, there have been two approaches for modeling nonlinear unsteady aerodynamics based on the Volterra series. Both the approaches for modeling unsteady aerodynamics using the Volterra series concentrated on mathematical simplification of the model structure so that the kernels can be identified using commonly available harmonic input response data for coefficients. In the current work, we formulated the model structure in a parametric from and made use of its harmonic input response properties to provide a simple algorithm for its estimation using variety of wind tunnel test data.

A formulation proposed by W. Silva is based on approximation of the Volterra series in discrete-time domain [56, 55]. This method is similar to the Nonlinear Auto-regressive modeling approach in [61]. The experimental data for parameter estimation is generated from CFD methods using unit impulse inputs. This approach met with a limited success at best. It failed to capture even the second kernel due to nonlinearity in the normal force coefficient accurately. It was also an erroneous application as the unsteady aerodynamics in transonic regime is bifurcational in nature. There is a jump in the values of force and moment coefficients due to shock induced unsteady flow separation. Such a strong nonlinearity which exhibits bifurcation or jump between the stable states cannot be modeled by the Volterra series or its modifications. The use of unit impulse input in pitch-rate is also impractical for use on a dynamic wind tunnel test rig.

In the second approach proposed by Reisenthel, he used a parametric combination of orthogonal functions for approximation of the Volterra kernel shapes [40]. These parameters were then estimated using forced oscillation wind tunnel data. While this method produced a model of fairly good consistency across the data set, it requires estimation of very large number of parameters even for the second kernel. For first kernel nine basis functions are used, while for the second two-dimensional kernel it is a 10×10 matrix. Estimation of third kernel is infeasible [40]. Contrary to this, only three parameter functions are to be estimated for a two-state model in VVM. Another significant disadvantage is that it is a black-box model like the neural-network based approaches in [37, 39], and offers little mathematical or physical interpretations.

Thus, VVM offers several advantages over other Volterra series based modeling approaches presented in literature.

5.4.3 Indicial Theory based formulations

Linear indicial model, as discussed in Chapter 1, has been used widely for modeling unsteady variation of aerodynamic coefficients. This theory actually belongs to the class of the models based on functional expansion of nonlinear system response, originally proposed by Vito Volterra. Tobak and Lamnabhi presented a generic functional expansion formulation of the Nonlinear indicial framework in the form of an infinite series [28, 99] as,

$$\begin{aligned} C_L(t) &= C_{L_{dir}} + C_{L_{int2}} + C_{L_{int3}} + \dots \\ C_{L_{dir}} &= \sum_n \int_0^t a_n(t-\xi_1)[\alpha(\xi_1)]^n d\xi_1 \\ C_{L_{int2}} &= \sum_{m,n} \int_0^t [\alpha(\xi_2)]^m d\xi_2 \int_0^t b_{mn}(t-\xi_1)(t-\xi_2)[\alpha(\xi_1)]^n d\xi_1 \end{aligned} \tag{5.3}$$

This series is shown to be a super-set of all the functional expansion formulations, and that both the Volterra series and Linear indicial models are obtained from its leading terms. In this sense, the fundamental equations of indicial theory and Volterra Series have a common origin.

The Nonlinear Indicial theory further employs three basic assumptions to obtain a simplified model; (i) a limited history of inputs affects the current output (i.e. nonlinear systems with fading memory); (ii) variation of the aerodynamic coefficient is continuous and analytic (i.e. Frechet differentiability and Taylor series expansion at each α_0), and (iii) the deficiency functional is an exponential decay function. The first two of these assumptions were also made for the nonlinear system in Eq.(2.2) (PoDE) to derive Volterra variational equations from it in chapter 2. Also, the system is assumed to have a single stable steady-state ($a_1 < 0$), which automatically implies an exponential decay of the linear component or the first kernel-state $x_1(t)$. Therefore, the basic mathematical assumptions made in linear indicial model and VVM are also the same.

A significant point of difference between these two unsteady model structures is that the VVM structure has multiple parameter functions to model nonlinearity in unsteady variations, while the linear indicial model still has only two parameter functions ($a(\alpha)$ and $b_1(\alpha)$). In this form, the linear indicial model is simply equivalent to the single state VVM. So, when the accuracy of an estimated model is insufficient, there is no method proposed in the literature to improve it. Hence, it is an ineffective approach in the cases like the pitching moment coefficient of GTA. A three-state VVM is shown produce accurate results for $C_m(t)$ of GTA

However, it is possible to use an alternative form of the deficiency functional $F_{a_\alpha}(\cdot)$ in the Linear indicial model to accommodate more parameter functional dependencies, and this may improve the modeling results using it.

The accuracy of Linear indicial model and VVM for modeling $C_m(t)$ of F16XL were compared using the results in [30]. Results for Linear indicial model are available for only three test cases in [30], the worst of which is given in Fig.(5.4). It shows that the response output of indicial model is qualitatively satisfactory, in which higher frequency variations are completely filtered out. As discussed in Section 4.5, VVM produces similar result with a single-state model, while the two-state model is fairly accurate as seen in Fig.(5.4,b). Therefore, although the VVM follows from a similar mathematical approach as linear indicial model, it is better suited to model the nonlinear variations in unsteady aerodynamic loads with higher accuracy.

It is important to note that parameter estimation approach used in the two studies is different. In parameter estimation of VVM, the functional $a(\alpha), K_1(\alpha)$ are defined by a number of node-points in the relevant angle-of-attack range. In case of Indicial model in

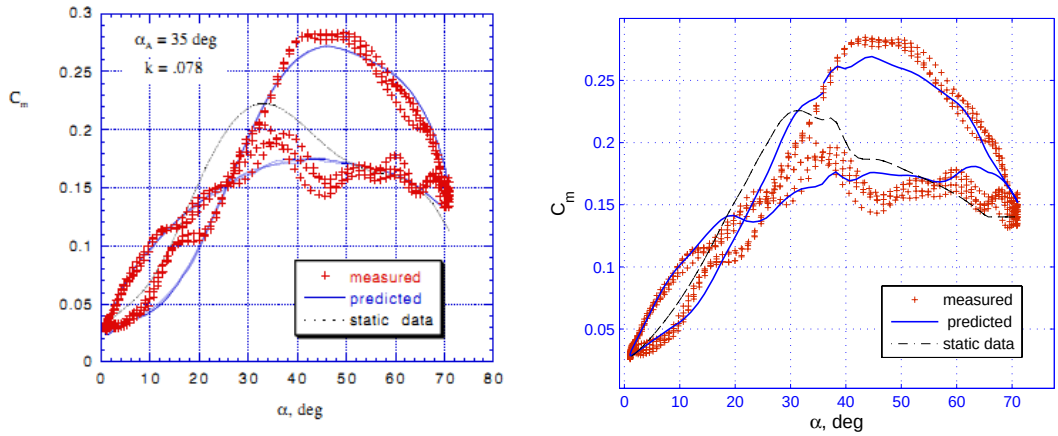

(a) Indicial model response (b) VVM response

Fig. 5.4. Comparison of pitching moment responses of VVM and linear indicial model in [30] for F16XL aircraft, due to harmonic input with $\alpha_0 = 35^o, \Delta\alpha = 35^o, k = 0.078$.

[30], the analogous parameters are defined by quadratic polynomial functions as discussed in the next subsection. This restricts the parameters functions to attain a certain shape, and hence the poor accuracy.

An alternative parameter estimation approach for Indicial model of C_m of F16XL was used in [45]. The results of simulation are quite accurate. In this approach, $C_{m_{\alpha,st}}(\alpha)$ is used as an estimation parameter. It is then compared with the values obtained from $C_{m_{st}}(\alpha)$ from wind tunnel tests, to find that the match between them is poor. However, the question is whether such an approach makes a physical sense? When the model is held static at a particular angle-of-attack, $C_m(t)$ must always converges to $C_{m_{st}}(\alpha)$ as it is obtained in wind tunnel experiments. However, using this parameter estimation approach it converges to a different estimated $C_m \, vs. \, \alpha$. Thus, the accuracy of the results obtained is inconsequential. In case of VVM, $C_{Z_{\alpha,st}}(\alpha)$ is used as a constraint equation so that the estimated parameters always meet this condition.

For modeling the aerodynamic coefficients which exhibit critical states, a Nonlinear Indicial model has been proposed. In this model, a transient functional is introduced at the points of critical state crossing, while the responses on both the sides of the critical state are modeled by disparate Indicial models with different time-scales [33]. Therefore, the Nonlinear Indicial model uses an additional functional to capture the transients. Similar approach can also be considered for VVM, and it will model the bifurcational effect of critical state crossing.

5.4.3.1 Defining parameter variations by polynomial functions

Nonlinearity in unsteady variations is accounted for, to some extent, by defining the parameters as nonlinear functions of angle-of-attack, also evident from the case studies in Chapter 4. However, to place the angle-of-attack node-points of the parameter functions at an appropriate position and in optimum number, many a trials are required. This problem is significantly simplified by predefining the shape of parameter functions using polynomials, as proposed in [30].

$$a(\alpha) = a_0 + a_1\alpha + a_2\alpha^2 + A_1(\alpha - \alpha_1)^2 + A_2(\alpha - \alpha_2)^2 \tag{5.4}$$

Klein and Murphy presented an estimation approach in which the parameter functions of time-scale and dynamic gain $a(\alpha), K_1(\alpha)$ are approximated by a cubic polynomial in α, as given in Eq.(5.4) [30]. In this definition, a_0, a_1, a_2, A_1, A_2 are the parameters to be estimated. The parameters α_1, α_2 are called knot points and are fixed at the regions of significant nonlinearity. This method was shown to produced satisfactory results for modeling the F16XL longitudinal coefficients in [30]. The other advantage of this method is that the sensitivity of the estimated model parameters can be computed as Cramer-Rao bounds. This also indicates the accuracy of the estimated model [43].

This approach can also be easily implemented for VVM. However, as seen in the case of C_m of GTA, the parameter functions are so nonlinear that these cannot be approximated by cubic-polynomials. Hence, this method is good for modeling only the mildly nonlinear coefficients, like that for F16XL. Thus, it can be concluded that the VVM is a more powerful approach for system identification of nonlinear unsteady variation of aerodynamic coefficients; and it has direct connection to the indicial model in its fundamental form.

5.4.4 ONERA Dynamic Stall model

There is some commonality between the mathematical formulations of VVM and ONERA models. The ONERA model is based on partitioning of the aerodynamic loads. This model makes use of a second order differential of the unsteady aerodynamic load at stall, to reproduce higher frequency oscillations in response to sinusoidal input. This concept is especially pertinent to the case of rotor craft blades which experience unsteady loads due to leading edge flow-separation at high frequency pitching motion. This basic similarity between the two model structures is presented in this section. ONERA dynamic

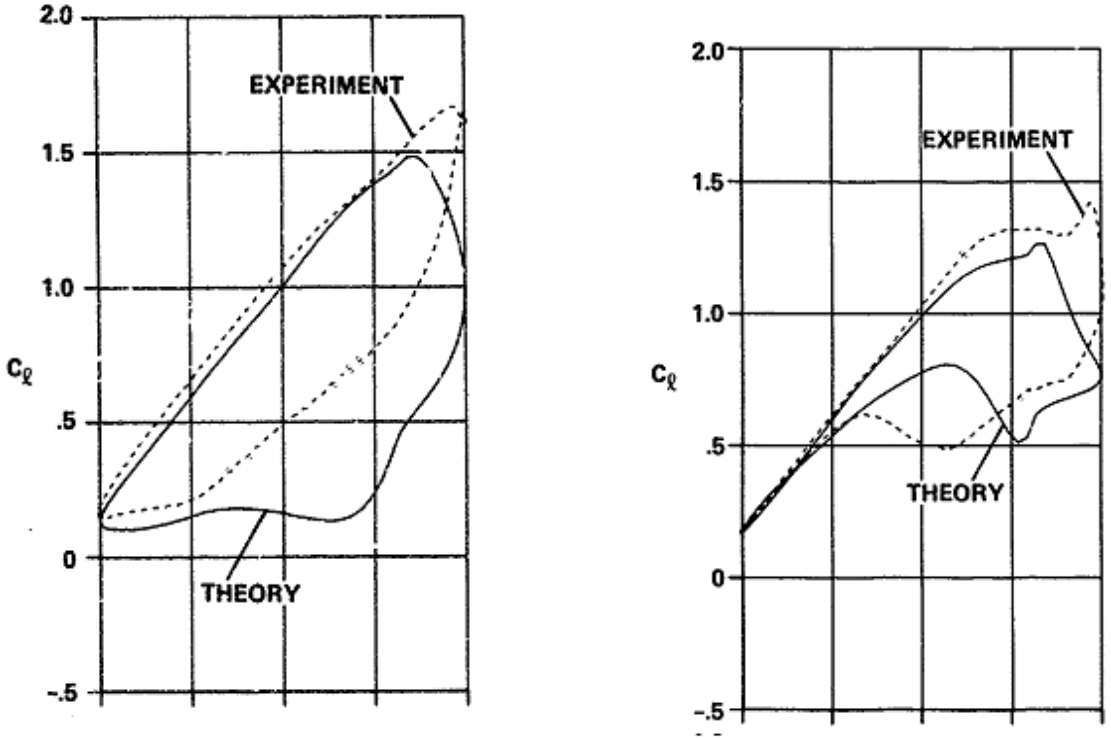

(a) For k=0.15 (b) For k=0.05

Fig. 5.5. Simulation of the response of ONERA Dynamic Stall model of C_N of Boeing Vertol VR7 airfoil to large amplitude forced sinusoidal input $\alpha_m = 10^o$, $\Delta\alpha = 10^o$ [35].

stall model is introduced in chapter 1, and it is restated here to aid the discussions.

$$\begin{aligned} C_L(t) &= F_1 + F_2 \\ \dot{F}_1 + \lambda F_1 &= \lambda F_l + (\lambda s + \sigma)\dot{\alpha} + s\ddot{\alpha} \\ \ddot{F}_2 + a\dot{F}_2 + rF_2 &= -(r\Delta + e\dot{\Delta}) \end{aligned} \tag{5.5}$$

At low angle-of-attack, $\Delta = 0$ and hence $C_L(t) = F_1(t)$. It is shown that the parameters σ and s are actually in-phase and out-of-phase derivatives considering small amplitude oscillation input in angle-of-attack. The component of load F_1 corresponds to the terms $C_{L_{st}}[\alpha(t)]$ and $C_{L_q}[\alpha(t)]q(t)$ in VVM. Both the structures simply capture the elliptical response to sinusoidal input at low angle-of-attack. Therefore, both these forms are equivalent at low angle-of-attack or small amplitude oscillation input.

The component F_2 in ONERA model captures the unsteady variations in the stall region. This is similar to the C_{dyn} component of VVM. The ONERA model includes second order differential equation of F_2 (the unsteady component of load). This higher order differential operator is useful to account for higher frequency vibrations seen in the variation of pitching moment coefficient measured in harmonic input tests. This

is a special feature of the ONERA dynamic stall model. In case of VVM, the higher order harmonics in the aerodynamic load response are reproduced by the second and third kernel-states in the model. Thus, the order of differential operator is the primary difference between VVM and ONERA model.

Application of this modeling approach to the forced oscillation test data of the Boeing Vertol-VR7 airfoil was presented in [35]. The model parameters are estimated using the entire data set consisting of input non-dimensional frequencies in the range $[0.01\ 0.25]$. An example of simulation results for low and high frequency inputs is given in Fig.(5.5). The qualitative fit and accuracy are not good in either of the cases presented in the figure. This due to the anomaly at very high frequency pitching motion, which is discussed in Section 4.8. The problem is that the same model is used to capture the unsteady variations at lower and higher pitching frequencies although the associated physical phenomena are totally different.

$$
\begin{aligned}
&C_{dyn}(t) = x_1(t) + x_2(t) + x_3(t) \\
&p_2\frac{d^2x_1}{dt^2} + p_1\frac{dx_1}{dt} + a_1x_1 = b_1u(t) \\
&p_2\frac{d^2x_2}{dt^2} + p_1\frac{dx_2}{dt} + a_1x_2 + a_2x_1^2 = b_2x_1(t)u(t) \\
&p_2\frac{d^2x_3}{dt^2} + p_1\frac{dx_3}{dt} + a_1x_3 + 2a_2x_1x_2 + a_3x_1^3 = b_2x_2u(t) + b_3x_1^2u(t)
\end{aligned}
\tag{5.6}
$$

Inspired by ONERA dynamic stall model, a second order differential form of VVM can be defined as given in Eq.(5.6). This is obtained from Volterra variational equations by considering the differential operator to be second order, i.e. $F(d/dt) = p_2\frac{d^2}{dt^2} + p_1\frac{d}{dt} + a_1$. This formulation of VVM has a richer topology. The second order differential structure has two poles to model the nonlinear unsteady effect of each aerodynamic load. If both the poles are real and negative, then this model can capture the effect of two time-scales. This is particularly useful for modeling the aerodynamic loads of helicopter blade airfoils as its pitching frequency cover both leading edge and trailing edge flow separation which have different time-scales. The coupling of unsteady poles and rigid body modes can model stronger aeroelastic phenomena, similar to that observed in a number of studies using ONERA model [14].

If the second order differential VVM has a pair of complex conjugate poles, the unsteady variation of coefficients can be like a limit cycle oscillation. In this case, like a spring-mass oscillator system, the model structure will have a certain natural frequency where the nonlinear unsteady effects are stronger irrespective of input amplitude. So, this model can exhibit the amplitude dependence of nonlinearity as well as a resonance frequency or other properties typical of second order differential systems. Hence, it can

be used to model much stronger influence of unsteady aerodynamics on flight mechanics. Thus, VVM can be extended to exhibit the properties of ONERA dynamic stall model.

5.4.5 Identification using novel input types

5.4.5.1 Schroeder Sweep input

The use of Schroder-sweep input response data for unsteady aerodynamic modeling was demonstrated in [31] for the first time. In this work, Murphy.et.al. used Schroder-sweep input response data from water tunnel tests to estimate the parameters of a simplified linear indicial model of normal force coefficient. In this section, the approach and advantages of using a VVM for identification of unsteady aerodynamic loads using the test data with Schroder-sweep inputs are presented.

$$u_N(t) = \sum_{1}^{N} A \sin(k\omega t + \phi_k) \tag{5.7}$$

$$\phi_{k+1} - \phi_k = \frac{\pi k^2}{N} \tag{5.8}$$

Schroeder sweep is a wide-band input that consist of combination of multiple sine waves [100]. A typical Schroeder sweep input is given by Eq.(5.7). The frequency of each sine is an integral multiple of the base frequency ω, and it has N sine wave components. These sine waves have phase ϕ_k as given in Eq.(5.8). This makes the peak-to-peak amplitude of the input to be minimum and Root-Mean-Square to be maximum simultaneously, as first proved by Schroeder in [100]. This ensures that the input power is maximum to obtain best signal-to-noise ratio, while variation of amplitudes remains practical. Its unique advantage is that a single test can provide systems response data for multiple harmonic inputs. However, the use of data for the purpose of estimation depends on the linear or nonlinear nature of systems response for the input conditions.

For a chosen Schroeder-sweep input, if the response of $C_Z(t)$ or $C_m(t)$ is found to be linear, it can be used for estimation of the first-kernel state parameters of VVM. This can be done by adopting an approach similar to the two-step regression method used with small amplitude forced oscillation test data. Using the Schroder-sweep input response of the force or moment coefficient, we can estimate in-phase and out-of-phase derivatives at multiple frequencies. This is done by taking a Fourier transform of the response at the component frequencies of the Schroeder-sweep input. Thus, it is possible to estimate $a(\alpha_0), K_1(\alpha_0)$ from a single Schroeder input test with three-five component frequencies. This is more efficient than performing SAFO tests with one frequency at a time.

In the cases when super-harmonics are also excited due to nonlinear nature of unsteady

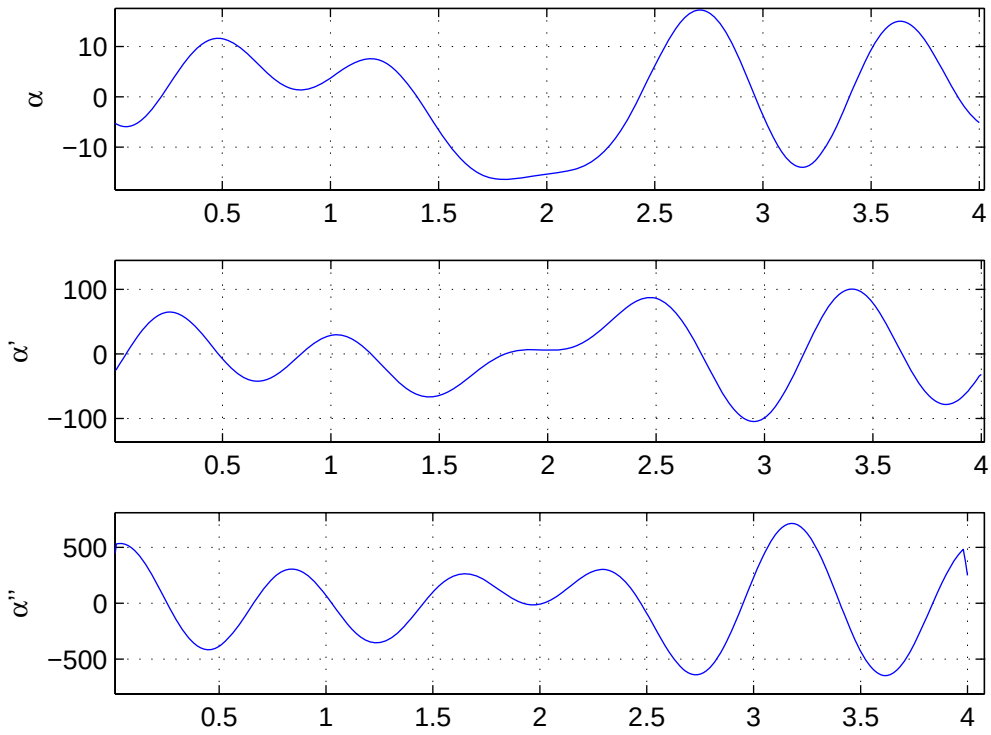

Fig. 5.6. A Schroder-sweep input with maximum amplitude $A = 20^o$, component frequencies $f = 0.25,\ 0.5,\ 0.75,\ 1,\ 1.25Hz$, proposed for dynamic wind tunnel tests.

aerodynamics, we can consider a two or three state VVM. The parameter estimation is done by output-error method. As demonstrated in the case of C_m of F16XL, using VVM approach we can get satisfactory results by appropriate choice of number of states. It is not necessary to classify the wind tunnel test data as small amplitude and large amplitude because VVM gets inherently tuned to match linear and nonlinear unsteady aerodynamics, valid for the maximum input used in experiments. This implies that one can choose a Schroeder sweep input of appropriate amplitude and bandwidth, and use output-error method for estimation of model parameters of an aerodynamic coefficient.

Here is an example of Schroeder-sweep input which is suitable for advanced pre-programmable dynamic test rig which can implement a desired anlge of attack trajectory shape. For a Schroder-sweep, assume that the maximum amplitude is $A = 20\,\mathrm{deg}$, component frequencies are $f = 0.25,\ 0.5,\ 0.75,\ 1,\ 1.25Hz$, and sampling rate is $100Hz$. Then the input to the WT model is defined in Fig.(5.6). In this input, note that the maximum pitch-rate is $100\,\mathrm{deg}/s$, and pitching acceleration is $520\,\mathrm{deg}/s^2$. Currently available forced oscillation test rigs are capable of implementing fast model maneuvers. For example, the NASA-LaRC forced oscillation test rig has capability to implement maximum pitch rate of $260\,\mathrm{deg}/s$, and pitch acceleration of $2290\,\mathrm{deg}/s^2$. However, these

are usually mechanically geared for harmonic inputs and cannot implement other dynamic maneuvers.

Note that, this single input covers a range of amplitudes and a bandwidth, which is likely to be sufficient for modeling. Thus, using Schroeder-sweep tests and VVM approach is a good combination for modeling, and a promising idea for the future.

5.4.5.2 Other dynamic input

Step and ramp motions inputs are other wide-band inputs which can be useful in identification. Their spectrum is usually defined by a two or three term Fourier Series. Even though, the trajectory of angle of attack used in experiments may not be exactly like a step or ramp, it is still possible to correlate the spectrum of input to the output using the advanced spectrum correlation methods available in literature [49]. In this case the arguments presented for Schroeder sweep input still hold good and a similar approach applies. Thus, use of step and ramp inputs is also a promising proposition for novel dynamic wind tunnel tests.

W.Silva presented use of phased impulse inputs for estimation of unsteady aerodynamic impulse responses using CFD outputs and wind tunnel test data [56]. The parameter functions of VVM can be estimated more easily than the Volterra kernel shapes. The method given in [56] is useful for estimation of only first and second kernels. However, a VVM structure with three states can also be estimated by this method and this significantly enhances the models capability.

With the advent of CFD methods for nonlinear unsteady aerodynamics of delta-wing configurations, it is envisaged that such inputs which are not possible in a wind tunnel test, can now be used for identification using VVM much more efficiently.

5.5 Summary

VVM of longitudinal coefficients of GTA was integrated with 6DOF equations of motion for simulation and analysis. It was shown that the longitudinal unsteady aerodynamic loads significantly effect the frequency and stability of the Short-period mode, using the tools from linear systems analysis. VVM was compared to Volterra series based modeling approaches, Indicial theory based approaches and the ONERA dynamic stall model, to present its similarities and adaptations to these successful approaches. Further, VVM is amenable to identification using variety of input types due to its harmonic input response properties.

Chapter 6

Analysis and Modeling of Abrupt Wing Stall

6.1 Introduction

The flight envelope boundary at high angle-of-attack and high sub-sonic Mach number is restricted by nonlinear and unsteady aerodynamics which drastically affect the aircraft's stability and handling qualities. The aerodynamic phenomenon is usually reflected by onset of unintended rolling motion about body axis and is termed as Abrupt Wing Stall (AWS) [5]. This flight envelope boundary is of specific importance for a high-performance aircraft as it is used in a high-speed turn maneuver. However, due to lack of understanding of aerodynamics and safety concerns, this part of the envelope is conservatively curtailed for all the high-performance aircraft [101].

At high angle-of-attack and high subsonic Mach number shock pockets are formed on the upper surface of a delta-wing. These have two or three equilibrium flow-conditions, and can abruptly switch between them. This causes the flow on wings to be asymmetric and unsteady. In terms of aerodynamic loads, it causes static hysteresis in rolling moment versus side-slip, and loss of roll damping in the sense of traditional aero-derivative formulation. The asymmetric flow on the wings and its unsteady nature are visualized in the condensation pattern on the F-18E aircraft in flight as presented in Fig.(6.1). The resulting flight dynamics can exhibit different types of lateral instability, like slow roll-off (heavy wing), rapid rolling to a non-zero bank angle (wing-drop) and periodic body-axis rolling motion (wing-rock).

The unsteady aerodynamics at high angle-of-attack and high sub-sonic Mach number is different from that at low Mach number due to presence of a strong nonlinearity in $C_l \, vs. \, \beta$. As discussed in previous chapters, VVM is not suitable for modeling such bifurcations in dynamics. Hence, a different approach for modeling the unsteady variation of $C_l(t)$ as witnessed in AWS conditions is presented in this chapter.

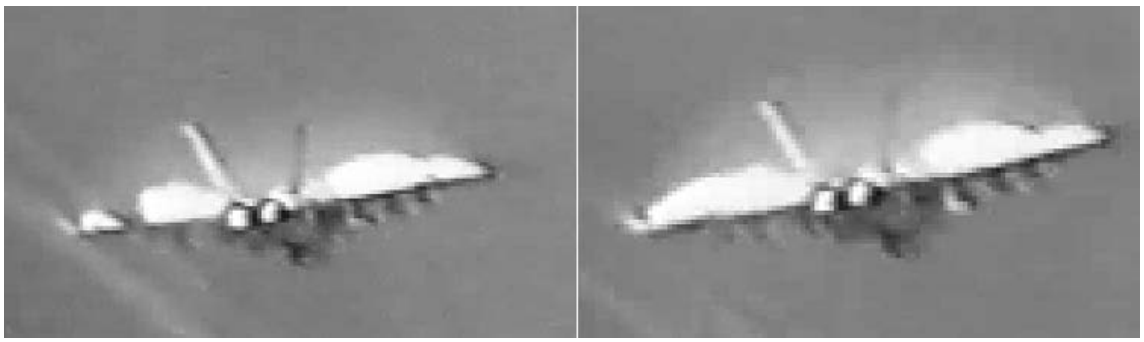

Fig. 6.1. Asymmetric flow and its disappearance in a moment, as seen in the natural condensation pattern that appears on F-18E aircraft wing during flight at AWS conditions [5].

The topic is not widely stated in literature. A recent research program on this subject was pioneered by NASA-Langley Research Center with industry collaborators, as summarized in [5]. The papers from this program provide a good overview of AWS modeling and analysis technology. The phenomena is investigated using wind tunnel tests, flight tests, mathematical modeling and piloted simulation studies. The final approach that evolved is based on use of static and FTR test data for development of an aerodynamic model. They also presented a semi-empirical model based on piloted flight simulation evaluation studies. Both the models are qualitatively sufficient for flight simulation studies. Some of these concepts developed in the NASA AWS program are summarized in the next section.

The aerodynamic modeling approaches developed in the NASA AWS program are not generic for application to modeling AWS of other delta-wing aircraft. Other modeling approaches proposed in literature for modeling similar aerodynamic phenomena cannot be used either. Hence, a comprehensive approach to model unsteady rolling moment coefficient using static and FTR wind tunnel test data is presented in this chapter. The proposed model is called Bifurcational Model of Aerodynamic Asymmetry (BMAA). This model is in the form of differential equations and can be integrated with a 6DOF simulation framework easily. It has number of parameters which can be tuned to match the rolling moment coefficient from experimental data.

In Section 6.2, the literature on experimental studies in wind tunnel tests and modeling methods are summarized, to indicate the principles of modeling AWS phenomena. In Section 6.3, a semi-empirical criteria is presented for determining the angle-of-attack and Mach number conditions for occurrence of AWS using Free-to-roll wind tunnel test data. In Section 6.4, BMAA structure and its estimation process using static and Free-to-roll wind tunnel test data are presented. This model is used to perform closed-loop simulation studies of GTA, in order to examine its effect on flight dynamics, in Section 6.5.

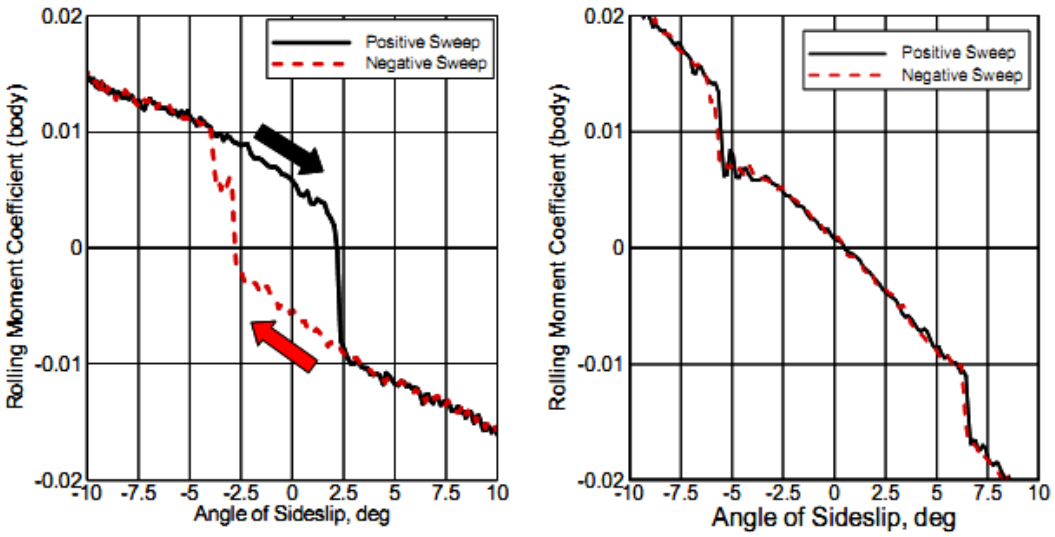

Fig. 6.2. Variation in C_l versus β obtained from β-sweep tests on F35 aircraft, left figure in AWS Angle-of-attack region, right figure just before entering in AWS Angle-of-attack [103].

6.2 Literature Review of Abrupt Wing Stall Phenomena

6.2.1 Experimental Studies for Characterizing AWS

Wind tunnel test data from static and FTR tests is used to predict the flight envelope region of occurrence of AWS, and model the variation of aerodynamic loads in these conditions. Flight simulation studies and flight test data serve the purpose of validation of the model and study its effect on flight dynamics. In this section, we present the important aspects of AWS from all such studies. Some of these principles are used in aerodynamic modeling and flight simulation studies presented in this thesis.

Experiments in wind tunnel tests involving pressure measurements at several points on the upper surface of the wing, have revealed many important features of the aerodynamics of AWS. The tests were performed on a scaled model of F18E/F at NASA-Langley Transonic wind tunnel, and the observations are available in [102]. The model was found to experience significant regions of separated flow and unsteady motion of shock waves. The shock waves have a bi-stable or in some cases tri-stable states on the upper surface of the wing. It abruptly changes its location in response to even a small change in angle-of-attack of the order of 1^o. The change in location was of the order of magnitude of 25% of the wing root-chord and time-scale of its unsteady motion was of the order $2Hz$ considering the aircraft-scale. Therefore, the aerodynamic loads acting on the aircraft are significantly unsteady and abrupt to affect the flight mechanics of the aircraft.

There are no established methods from wind tunnel experiments or computational modeling available for prediction of occurrence of AWS, until recently. In the NASA AWS-program, wind tunnel experiments on FTR rig were shown to be effective to predict

the occurrence of AWS for the F18E and F35 aircraft fairly accurately [5, 104]. FTR rig provides a single degree-of-freedom in body-axis rolling motion, while the pitch-angle θ of the scaled aircraft model is held fixed. The FTR rigs were actually developed to characterize an aircraft's wing-rock motion at low-speed and high angle-of-attack. They also provide information on the roll-damping characteristics of the aircraft [105]. Although the aircraft model used in the wind tunnel is not dynamically scaled, the characteristics of AWS from FTR rig and the resulting flight simulation were found to correlate well with the flight test data [102, 106]. The Figure-of-merit used to predict the conditions of occurrence of AWS as devised in the NASA-AWS program is discussed in details in Section 6.3.

Indications for occurrence of AWS can also be obtained from static wind tunnel test data [107]. The rolling moment coefficients versus sideslip becomes nonlinear at the critical angle-of-attack α_c of occurrence of AWS. At approximately the same α_c there is distinct sharp break in the normal force coefficient versus angle-of-attack. The root-mean-square value of rolling moment recorded by the sensor over a certain time interval when the model angle-of-attack is fixed at α_c, is significantly larger than the averaged value of the same data. At least two of these indicators have been observed to occur at α_c [105, 107].

These indicators were defined as Figure-of-merit based on static test data. These were found to be necessary but not sufficient conditions for occurrence of AWS [107]. Figures (6.2) are an example of the variation in rolling moment coefficient versus side-slip from the quasi-steady beta-sweep wind tunnel tests on the F35-JSF aircraft [103, 108]. The static hysteresis is significant and it can be extremely unsteady at certain angle-of-attack. Therefore, static wind tunnel data is important for modeling C_l at specific (α, M) conditions for occurrence of AWS, and its further validation from FTR data is essential [106].

6.2.2 Mathematical Modeling Techniques

Since AWS mainly causes body-axis rolling motion, the rolling moment coefficient is modeled to reproduce its effects in flight dynamics. The two approaches which were developed in the NASA-AWS program, and the general principles for modeling AWS are presented in this section. Three other mathematical structures used for modeling similar phenomena are also discussed in brief.

$$C_l(\phi) = C_{l,st}(\phi) + C_{l_{dyn}}(\phi, \frac{pb}{2V}) \tag{6.1}$$

In the first approach given in [105], the rolling moment coefficient is split into static

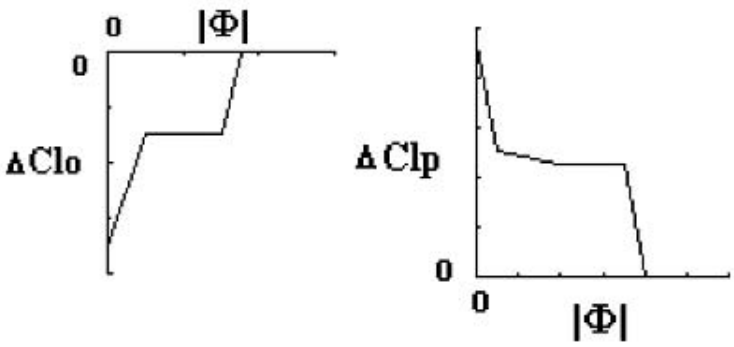

Fig. 6.3. Variation of ΔC_{l_p} and ΔC_{l_0} in the AWS model qualitatively estimated using Free-to-roll Wind tunnel data [105].

component $C_{l,st}(\phi)$ and an unsteady or dynamic component $C_{l_{dyn}}(\phi, \frac{pb}{2V})$ as given in Eq.(6.1) . The former component is obtained from static wind tunnel tests performed to get the variation of rolling moment coefficient versus roll angle. The FTR tests provide time-history of quasi-steady state variations in $C_l(t)$ and $\phi(t)$ in AWS conditions. This is compared with the model output assuming $C_{l_{dyn}}(\alpha_0) = C_{l_0}(\alpha_0) + C_{l_p}(\alpha_0)\frac{pb}{2V}$ at a particular α_0 in the AWS region. The estimated values of C_{l_0} and C_{l_p} can reproduce the sustained oscillations as seen in FTR tests. To trigger the abrupt fast rolling motion and to adjust the maximum bank angle, these parameters are shaped as functions of ϕ. The resulting $\Delta C_{l_0}(\phi)$ and $\Delta C_{l_p}(\phi)$ that define $C_{l,dyn}(\phi)$ obtained from various flight simulation studies are found to have a trend as given in Fig.(6.3).

The simulation results of this model considering only the roll degree-of-freedom produce a reasonably good match with the FTR data. However, this model is still an incremental approach and devoid of the topology of $C_l(t)$ as a function of $\beta(t)$ or $\phi(t)$ due to static hysteresis and unsteady variations. The shape of static hysteresis in $C_{l_{st}}(\alpha_0)\, vs.\, \beta$ is completely ignored. Also, this model can produce roll-off in only one direction at a time, while that in case of actual flight is arbitrary.

$$\begin{aligned} C_l &= C_{l0} + C_{l_p}(\frac{pb}{2V}) + C_{l_\beta}\beta + K_{ail}C_{l,\delta_{ail}}\delta_{ail} + C_{l,AWS} \qquad (6.2) \\ C_{l,AWS} &= \Delta C_{l0}(\alpha) + \Delta C_{l_p}(\alpha)\frac{pb}{2V} \end{aligned}$$

In the second approach, the rolling moment coefficient is modeled using the flight test data. The model structure incorporates an incremental ΔC_{l0} and ΔC_{l_p} components, and a reduction factor for aileron effectiveness, as given in Eq.(6.2). Hence, the model structure is still an incremental model, with $C_{l,AWS}$ being non-zero only in the AWS region. These components are estimated by System-identification techniques using flight test data, as

well as pilot ratings [71]. The α range of $C_{l,AWS}$ is carefully modeled to capture the different nature of rolling motion depending on pitch-rate. The piloted evaluation of this model in flight simulation studies is compared to the pilot ratings from flights tests in AWS conditions to further tune the model [105].

Such a model is useful primarily for pilot training to fly into AWS, as the pilot ratings of this model were very good [109, 110]. These methods for AWS modeling and analysis were applied in the initial design phases of F-35. It was reported to be useful to avoid AWS on the aircraft before undertaking the flight tests [103]. However this model is also a simplistic incremental model which does not consider the static hysteresis and characteristic time-scale of unsteady variation. Thus, both the models for simulating AWS are useful only for the purpose of flight simulation studies, and their use in flight dynamic analysis is unreliable.

An aerodynamic phenomena due to static hysteresis and unsteady variation of loads gives rise to a periodic rolling motion of the aircraft called wing-rock. It happens due to asymmetric vortex breakdown at high angle-of-attack and low Mach number flight in the near-stall conditions. It is experienced by many delta-wing aircraft. Goman.et.al presented an approach for modeling the rolling moment coefficient due to this phenomena [111]. The model structure is similar to the PoDE model, and the model parameters are estimated using the rolling-moment time-histories from FTR wind tunnel tests. Although this model reproduces the dynamic hysteresis, it cannot model the static hysteresis in $C_l \, vs. \, \beta$. Similarly, static hysteresis and the associated bifurcational nature was modeled using differential equations in [112, 113]. This model reliably captures the static hysteresis in galloping amplitude versus wind speed, observed for an under-slung load in the shape of a square prism. However, these models were found to be unsuitable for application to AWS modeling.

Rolling moment variation in AWS was obtained by Computational Fluid Dynamics (CFD) techniques in [114]. In this work, the so-called Radial Basis Functions are used to successfully model the static and dynamic hysteresis in rolling moment coefficient versus sideslip. The model structure is similar to Neural-network type models, and a wide-band input called Chirp was used for model training. A similar technique was presented for modeling the C_l of X31 aircraft using training data from CFD computations in [115]. However, these are "Black-box" models or just data-true models which are not of much interest for modeling AWS.

A generic nonlinear differential equation structure for modeling hysteresis, called the Bouc-Wen model was introduced in 1971 [116]. It has been widely applied for modeling structural and other mechanical systems. The phenomena of hysteretic restoring force in response to a displacement input, and depending on the direction of velocity, is common

to many systems. The model structure consists of an internal state and its differential equation which give rise to static hysteresis in steady state. Hence, the hysteresis in $C_l \, vs. \, \beta$ can be modeled by this structure.

However, this method has three disadvantages (i) the output of the model for certain parameter combinations may diverge to infinity, that is the structure is not always bounded-input-bounded-output stable, (ii) there is no definite approach for estimation of parameters and these are identified by trial and error, (iii) it is a black-box model and offers no physical interpretations [116]. Due to these basic disadvantages, this method is not used for modeling the variation of C_l in AWS regimes.

6.3 Predicting Occurrence of AWS

6.3.1 Wind Tunnel Data

The Generic Tailless Aircraft was tested in an industrial-grade wind tunnel on both static and FTR rigs, and a part of this data was available for research activities. The static wind tunnel tests were performed to obtain aerodynamic loads in quasi-steady alpha-sweep and beta-sweep. The beta-sweeps are performed in only one direction, either as increasing beta or decreasing beta, at angle-of-attack of $[20, 22, 24, 26]deg$ and Mach numbers of $[0.7,\ 0.8,\ 0.9]$. The tests were performed only at lower angle-of-attack for higher Mach numbers, so the test matrix is not square.

The same wind tunnel model was also used in FTR wind tunnel tests. These tests were performed in a quasi-steady alpha-sweep from 0 to $26\,\mathrm{deg}$ angle-of-attack range, and Mach numbers of $[0.7, 0.8, 0.9, 0.95]$. All forces and moments acting on the aircraft were recorded. The data was filtered using a $20Hz$ low-pass digital filter. The pitch-pause tests, explained later in this section, were not performed for GTA.

6.3.2 FTR Figure-of-Merit for AWS

In order to interpret the entire data set available from FTR tests to arrive at predictions of lateral activity due to AWS, some Figure-of-Merit (FOM) have been proposed in literature [106, 107]. The uncommanded lateral activity is considered to be significant if the roll-off happens at a sufficiently fast rate. Otherwise, it is expected that the slower motion will be easily damped out due to roll-rate feedback in the control law of the aircraft. Based on this concept an averaged Roll-rate FOM was proposed in [106] using the data from FTR pitch-pause tests, and it is considered to be the most reliable indicator of AWS. In the pitch-pause test using a FTR rig, the scaled aircraft model is disturbed to a non-zero initial condition in roll-angle. The model sets into sustained roll oscillations when it enters

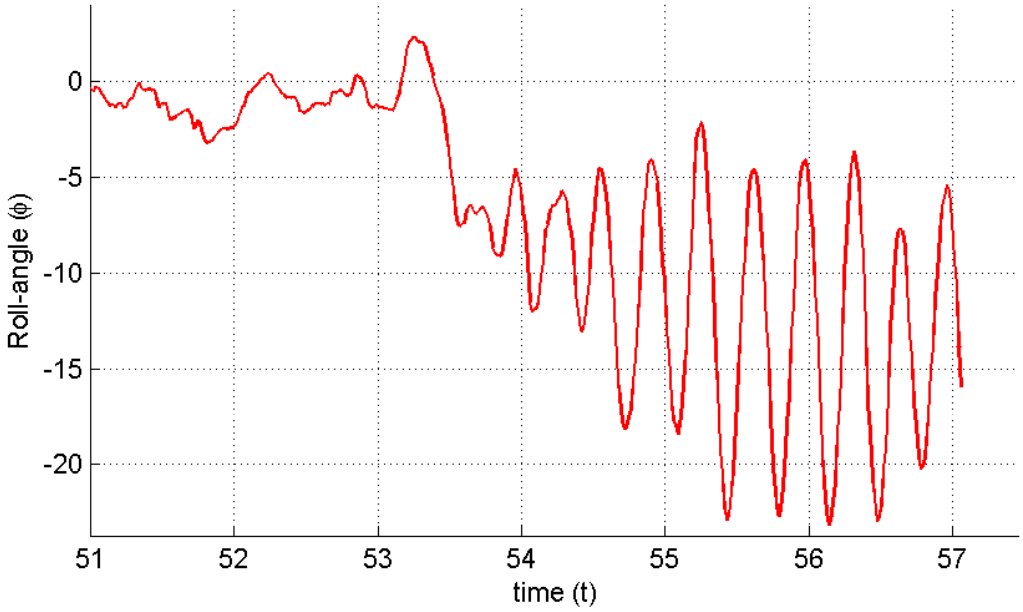

Fig. 6.4. Roll-angle versus time recorded in a Pitch-sweep Free-to-roll test on GTA at $M = 0.8$

AWS region. This test is repeated over a relevant range of pitch angles. These data from FTR pitch and pause tests are used to compute Roll-rate FOM.

The Roll-rate FOM is determined by the amplitude and speed of uncommanded lateral motion or oscillations. First the average roll rate between consecutive local maxima and minima points in the time-history of C_l are computed, and then the maximum value from this set is used as the Roll-rate FTR FOM at that pitch angle. It is non-dimensionalised to account for the effect of change in wind speed (hence, Mach number).

Roll-rate FOM, as defined above, cannot be applied to the data from pitch-sweep tests on the FTR rig. In a pitch-sweep test, the pitch angle is increased in a quasi-steady manner at a rate of $1 \deg /s$ over the relevant range of pitch angle. In a pitch-pause test the pitch-angle is held fixed when the model sets into sustained roll oscillations. Therefore, we cannot compute an averaged maximum roll-rate response at each pitch angle using pitch-sweep test data.

A sample of roll-angle time history from a pitch-sweep test is presented in Fig.(6.4). In this figure, note that the model sustains roll oscillations about a non-zero roll-angle and over a range of pitch angle. However, at the points of significant lateral instability, the rate of roll-off motion is at least one order of magnitude higher than the pitch-up rate. Hence, the roll-off rate computed from pitch-sweep test may still be an indicator of the occurrence of AWS.

Roll-rate FOM was computed for GTA using pitch-sweep test data at different Mach

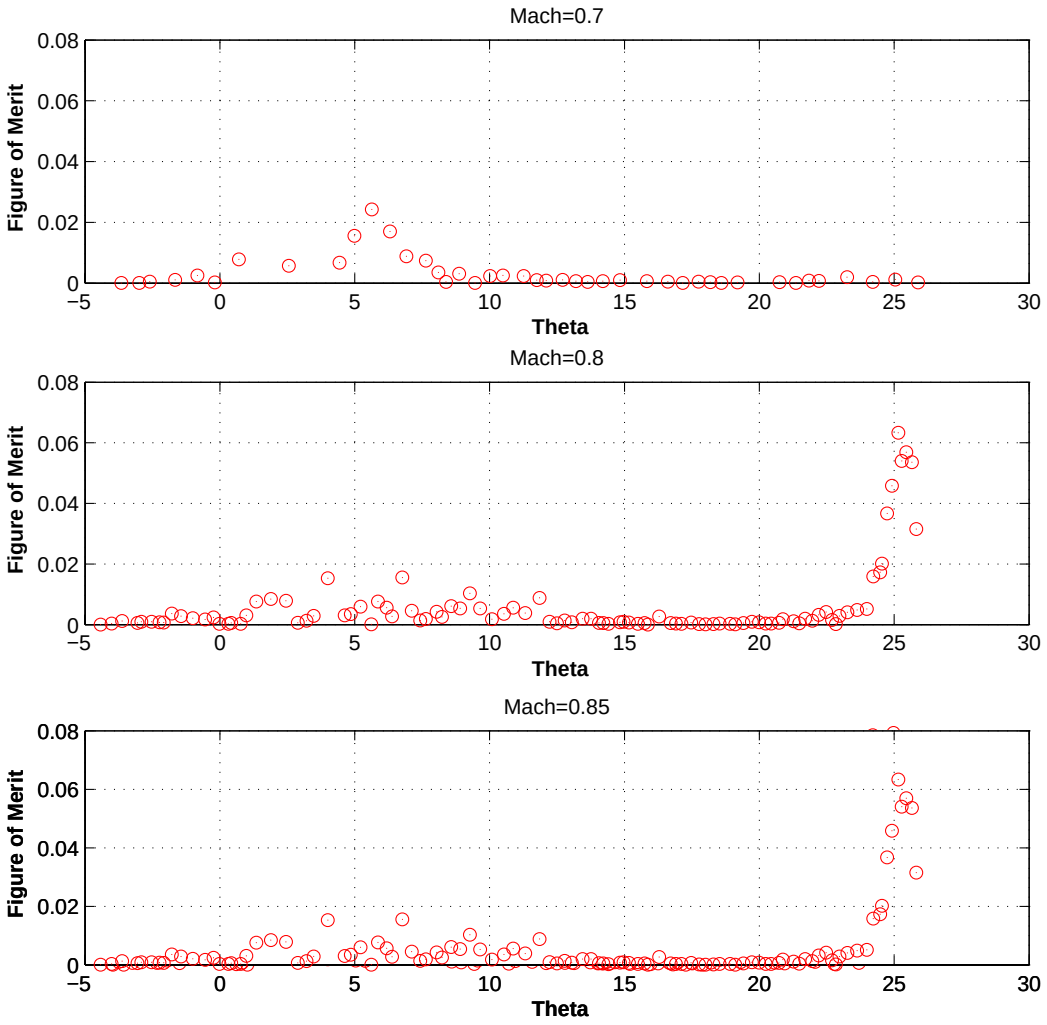

Fig. 6.5. Averaged maximum roll-rate Figure-of-merit estimated at different Mach numbers from Free-to-roll test data for GTA.

numbers, and it is presented in Fig.(6.5). The value of threshold FOM for the cases of of F-18 [108] and F-35 [103] aircraft by correlation of lateral activity observed in FTR tests with the flight test data is obtained as 0.0186 (roll-rate measured in deg/s). The same threshold value was used for analysis of Roll-rate FOM of GTA. In Fig.(6.5), the points of high FOM at pitch angle of 24^o are clearly separated from other points. However, there are several points at much lower pitch angle which are close to this threshold level. This is because the aircraft model rolls significantly at low angle-of-attack even for small asymmetric flow disturbances in the wind tunnel to counter-act the effect of side-slip. So, these points are false indicators. Raising the threshold any further leads to an optimistic prediction. Therefore, to avoid this confusion a slightly different definition of FOM is

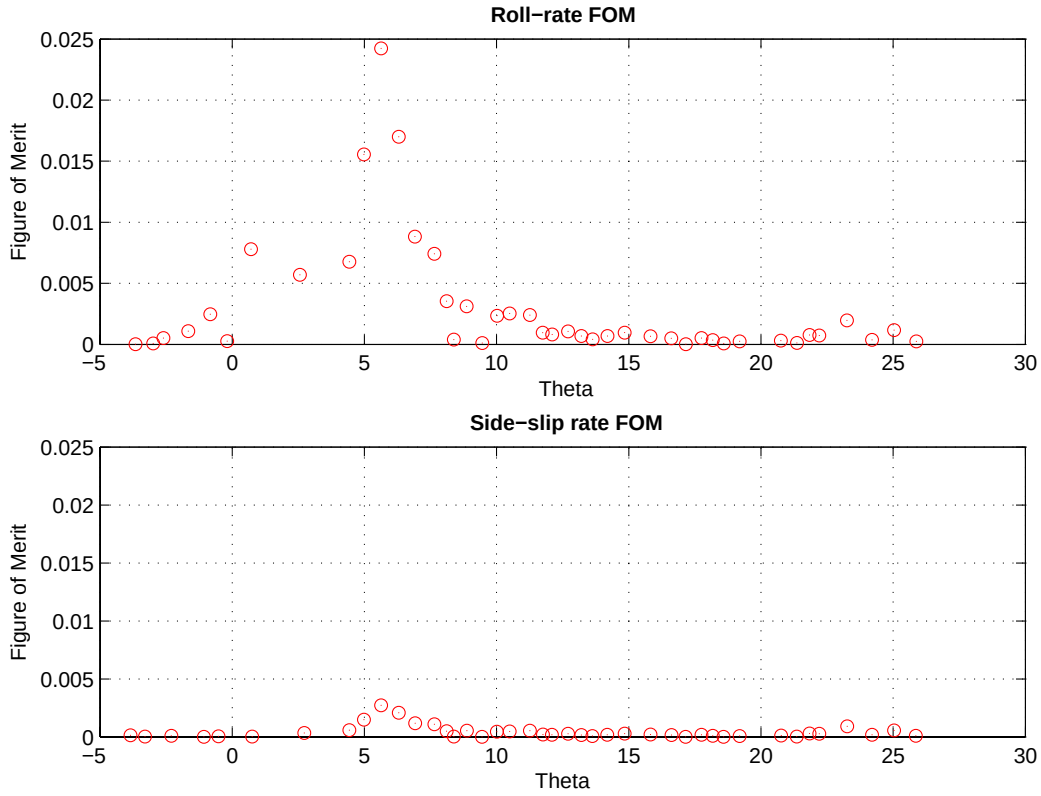

Fig. 6.6. Comparison between the Figures-of-merit based on averaged maximum rates of ϕ and β in the Free-to-roll test data for Mach number 0.7.

proposed.

The new FOM proposed is based on averaged side-slip rate. The body-axis rolling motion of an aircraft in Free-to-roll condition is governed by the kinematics equation $\beta = sin(\theta)\phi$. Therefore, a body-axis roll produces sideslip that is proportional to the roll-angle, with the pitch-angle as constant of proportionality. Thus, side-slip produced by rolling motion is significant at higher pitch angle only. At low pitch angle (or angle-of-attack), any roll-off due to minor flow asymmetries gets automatically neglected. Hence, a new FOM is computed using side-slip angle time-history instead of roll-angle time-history, following the same procedure.

A comparison of Roll-rate and Side-slip rate based FOM is presented in Fig.(6.6). While Roll-rate FOM shows significant lateral activity for $\theta = 6^o$, the Side-slip rate FOM does not show any significant difference with respect to other points. Thus, the false indication of AWS or lateral instability can be avoided using side-slip rate FOM.

While a boundary for occurrence of AWS is established, the prediction can be off the mark by about $1^o - 2^o$. This happens due to non-ideal nature of external flow conditions and miscellaneous vibrations in the wind tunnel. The aerodynamic load acting on the

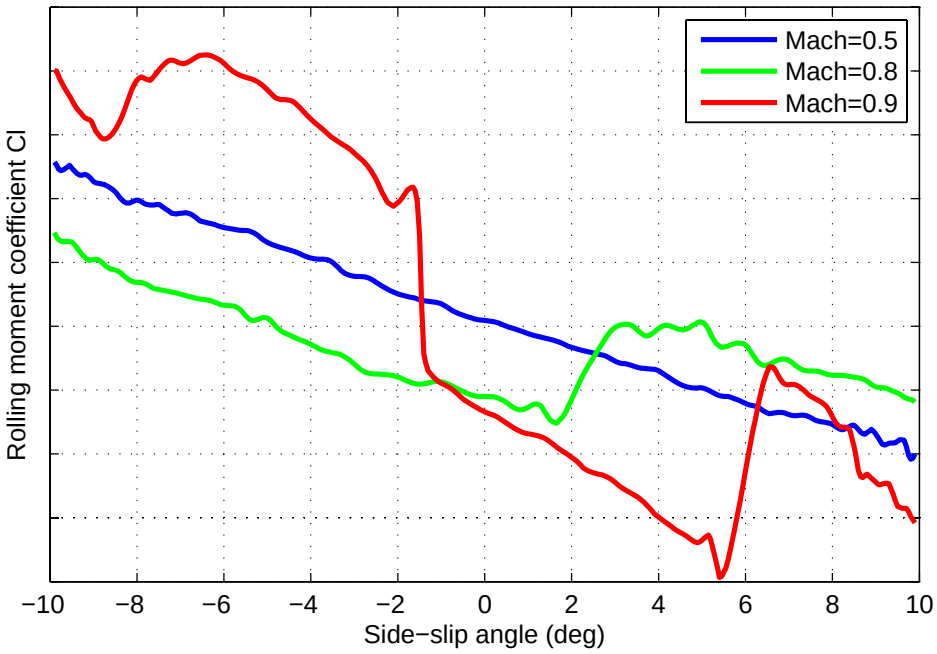

Fig. 6.7. C_l versus β at a pitch angle in AWS region for different Mach numbers, obtained from β-sweep tests on GTA.

model is very high due to high dynamic pressure. Hence, the entire sting is found to vibrate, especially on entry into AWS conditions. This interferes with the flow on the model. Also, the geometry and inertia of the wind tunnel model are not dynamically scaled, and this affects the initial triggering of the rolling motion. Hence, these results should be interpreted with some tolerances. To account for this, the aero-model is developed to simulate AWS at lower angles-of-attack. Some indications are also observed in the static wind tunnel data. For example, in Fig.(6.7) there is a jump in values of rolling moment coefficient at $\beta = 2^o$ for $M = 0.8$, and at $\beta = 6^o$ for $M = 0.9$. There is no such jump at $M = 0.7$. This shows the static hysteresis in C_l versus β. However, the data is available for beta-sweep in only one direction, and hence the exact nature of static hysteresis cannot be determined. These indicators further validate the prediction of (α, M) combinations for occurrence of AWS.

6.4 Mathematical Modeling of AWS

6.4.1 Bifurcational Model of Aerodynamic Asymmetry

The model of AWS is required to reproduce the features of lateral instability as known from wind tunnel test, as well the variation of aerodynamic coefficients due to asymmetric

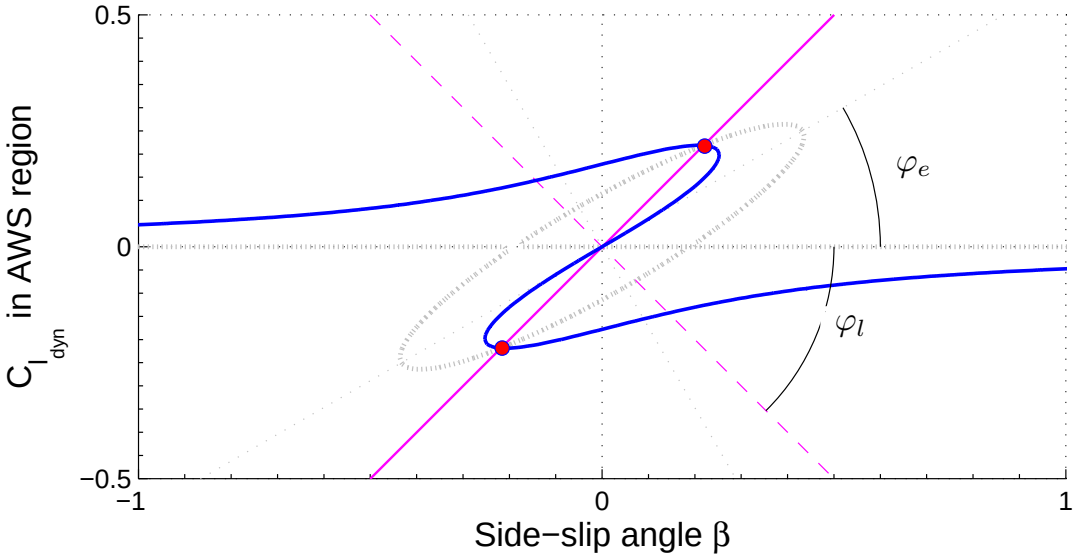

Fig. 6.8. Approximate shape of static hysteresis in $C_l\, vs.\, \beta)$ produced by the parameter values of $k_h = 2, \varphi_e = 30^o, \varphi_l = -45^o$ of BMAA model.

shock-induced flow separation. Such a model is useful in flight simulation studies as well as analysis. The methods for modeling such a phenomena presented in literature are inadequate. So a novel model structure for AWS modeling referred to as Bifurcational model of aerodynamic asymmetry (BMAA) is proposed in this section. The structure is shown to reproduce the variation in rolling moment coefficient as a function of (α, β, M).

$$C_l(\alpha, \beta, \delta C) = C_{l_{st}}(\alpha, \delta C) + C_{l_p}(\alpha) \cdot \frac{pb}{2V} + C_{l_\beta}(\alpha) \cdot \beta + C_{l_{dyn}}(\alpha, \beta) \tag{6.3}$$

The static hysteresis and unsteady effects are modeled using an incremental component of the rolling moment coefficient. Consider the components of C_l given in Eq.(6.3). Of these, the first three components are as in the low angle-of-attack aero-database of the aircraft. The component $C_{l_{dyn}}(t)$ is included as an add-on component and it represents the unsteady incremental effect of AWS due to asymmetric load. The component $C_{l_{st}}(\alpha, \delta C)$ is known from static wind tunnel tests and it is retained as it is in the AWS region. The derivative $C_{l_\beta}(\alpha)$ is well-defined up to the start of AWS region. The angle-of-attack of occurrence of AWS α_{cr} at a particular Mach number is known from the analysis presented in the previous section. It is clear from experimental data in Fig.(6.7), that $C_l\, vs.\, \beta$ has a hysteresis at $\alpha > \alpha_{cr}$. This implies that the derivative C_{l_β} is not a constant over the relevant range of β. So in BMAA, the value of C_{l_β} at $\alpha > \alpha_{cr}$, is fixed

to be equal to its value at α_{cr}. The remaining components $C_{l_p}(\alpha)$ and $C_{l_{dyn}}(t)$ are required to reproduce both the static hysteresis and unsteady variations in $C_l(t)$.

The mathematical structure of BMAA for a bistable hysteresis in $C_{l_{dyn}}(t)$ is given by Eq.(6.4). The structure represents an intersection of an inclined ellipse and a straight line which results in two stable equilibrium branches and a unstable branch. The linear differential equation with characteristic time-scale τ captures the unsteady nature of variations due to change in side-slip angle. The various parameters of the model affect the shape of the static hysteresis curve in a certain way as discussed in the following paragraphs.

$$\begin{aligned} x &= k_\beta \beta; \;\; y = k_l C_{l_{dyn}} \\ x_1 &= x\cos(\varphi_e) + y\sin(\varphi_e) \\ y_1 &= -x\sin(\varphi_e) + y\cos(\varphi_e) \\ x_2 &= x\cos(\varphi_l) + y\sin(\varphi_l) \\ \tau\frac{dy}{dt} &= \left(1 - \frac{x_1^2}{a^2} - \frac{y_1^2}{b^2}\right) y + k_h \times x_2 \end{aligned} \tag{6.4}$$

In this equation, k_β and k_l represent the scaling parameters for the states β and $C_{l_{dyn}}$ respectively. These are used to match the values associated with static hysteresis produced by the model to that known from experimental data. In effect, these are merely sizing parameters, after an appropriate shape of the curve is obtained.

The static hysteresis curve can be described by the hysteresis function $F(x_1, x_2, y_1, y) = \left(1 - \frac{x_1^2}{a^2} - \frac{y_1^2}{b^2}\right) y + k_h \times x_2$. This function consists of intersection of the line x_2 of slope $\tan(\varphi_l)$ with the ellipse $(1 - \frac{x_1^2}{a^2} - \frac{y_1^2}{b^2})$. Parameters (a, b) are the semi-major and semi-minor axes of the ellipse respectively. These determine the maximum incremental C_l due to AWS at $\beta = 0$, and range of β over which hysteresis loop is seen in the static WT test data, respectively.

The solution of the hysteresis function is as shown in Fig.(6.8). It can be shaped using parameters $(k, \varphi_e, \varphi_l)$. Definition of these parameters is indicated in Fig.(6.8), along with their effect on the geometry of $F(x, y)$. Parameter φ_e is the inclination of the semi-major axis of the ellipse. The effect of variation in φ_e angle on $F(x_1, x_2, y_1, y)$ is shown in Fig.(6.9). $90^o - \varphi_l$ is the slope of line. The intersection of the ellipse with the line produces two saddle points. Parameter k_h defines how far the bistable dependence shaping static hysteresis is moved away from two saddle points on the ellipse. The resulting two-dimensional bifurcational structure in the static hysteresis region is required to be similar to the the shape of $C_{l_{st}} \, vs. \, \beta$ as known from experimental data.

The hysteresis function obtained has two stable equilibriums and one unstable

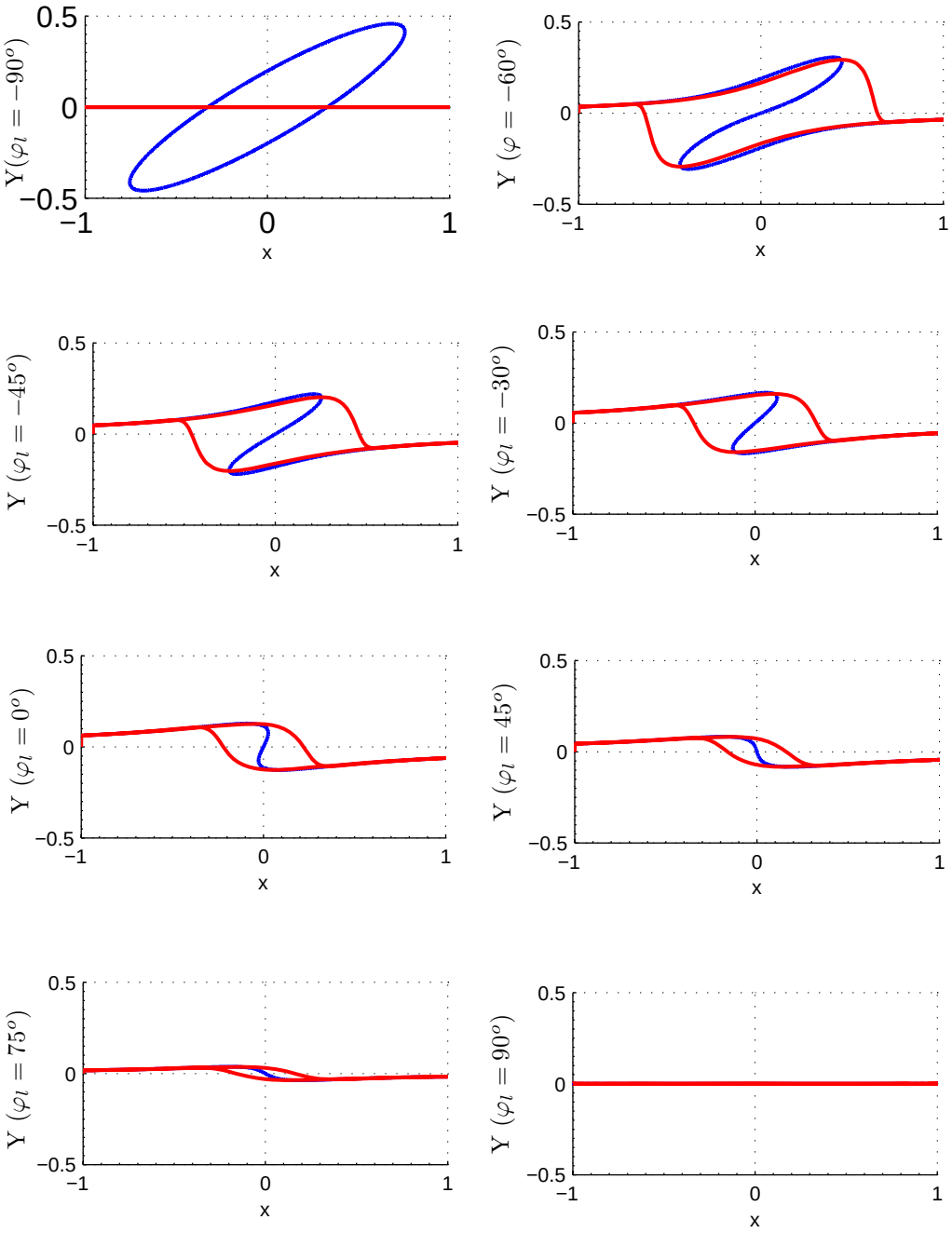

Fig. 6.9. Effect of parameter φ_l on the shape of hysteresis curve (blue line) and unsteady variations of $C_l(\beta)$(red-line) for $k_h = 2, \varphi_e = 30^o$.

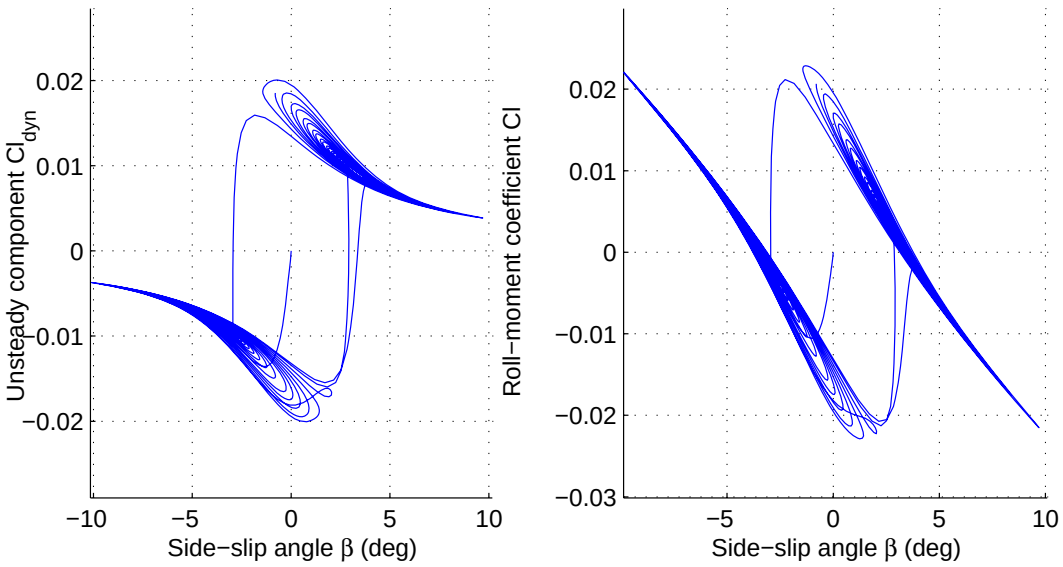

Fig. 6.10. Variation of $C_l(\beta)$ in Free-to-roll simulation of BMAA model using wind tunnel model moment of inertia.

equilibrium that acts as a separatix point. The hysteresis function can be very effectively shaped by a proper selection of the parameters $(a, b, k_h, \varphi_e, \varphi_l)$. In a steady-state or on entry into the AWS region, $C_{l_{dyn}}(t)$ converges to one of the two non-zero values of the rolling moment coefficient at $\beta = 0$. This triggers rolling motion of the aircraft to the left or right depending on sign of triggered disturbances. The amplitude and frequency of dynamic oscillations in $\phi(t)$ is determined by the time-scale parameter τ, and linear roll damping parameter C_{l_p}. Smooth variation of the rolling moment during crossing of bifurcation points in a dynamic maneuver is due to the first order differential equation.

The parameter estimation process is presented using GTA data in the next section.

6.4.2 Parameter Estimation and Simulation

The parameters of the model are estimated in two steps to match $C_l \, vs. \, \beta$ from static wind tunnel test data and unsteady variations seen in the time-histories from FTR data. As stated earlier, the beta-sweep test data is available for increasing β only, as given in Fig.(6.7). So the shape of static hysteresis is not clearly known. FTR data from pitch-pause test are not available to estimate the damping and time-constant for the model. Hence, the features of oscillations from pitch-sweep test data are used for modeling and parameter tuning. Firstly, the model parameters are estimated to obtain a reasonable fit for $C_l \, vs. \, \beta$, at a particular (α_0, M_0) corresponding to the maximum magnitude of ΔC_l due to AWS. Then, the parameters τ, C_{l_p} are estimated to tune it to oscillations observed

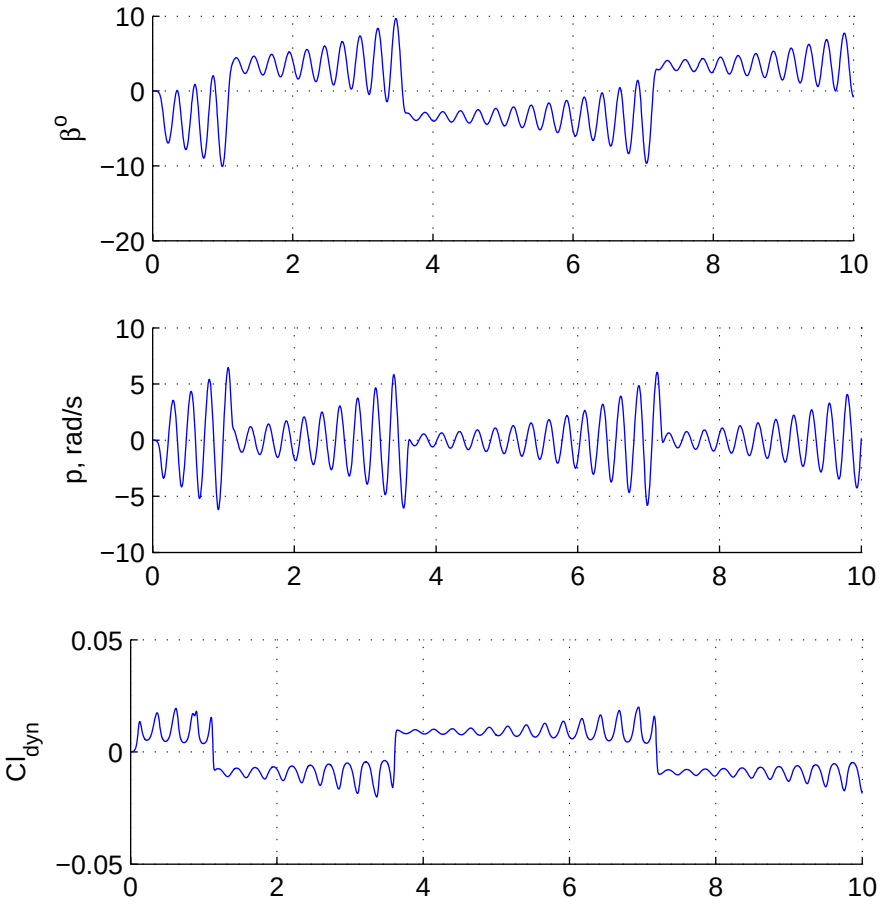

Fig. 6.11. FTR simulation of the estimated BMAA model using GTA model moment of inertia.

in FTR.

The parameters $(a, b, k_h, \varphi_e, \varphi_l)$ are fixed to reproduce a shape similar to that seen in static wind tunnel test data. $C_{l_{dyn}} \, vs. \, \beta$ shape, as shown in Fig.(6.8), is found to reproduce the shape of $C_l \, vs. \, \beta$ similar to that in Fig.(6.7). Therefore, the parameter values of $(k_h, \theta_e, \varphi_l) = (2.0, 30^o, -45^o)$ were selected for the model. The parameter values $(a, b) = (0.5, 0.1)$ were used in Fig.(6.8). These are now scaled to make the range of static asymmetry to be $\Delta\beta = 2^o$ and the magnitude of maximum asymmetric rolling moment at AWS to be $\Delta C_{l,max} = 0.017$.

In the next step, the parameters τ, C_{l_p} are tuned to match the frequency of bank angle oscillations to that from FTR tests. From FTR pitch-sweep test data, the frequency of oscillation is required to be $3.5Hz$ and $\dot{\phi}_{max} = 3.5rad/s$. The wind tunnel model moment of inertia is used in the tuning process, as these dynamics properties are used to match the wind tunnel model characteristics of motion. The mathematical model response after

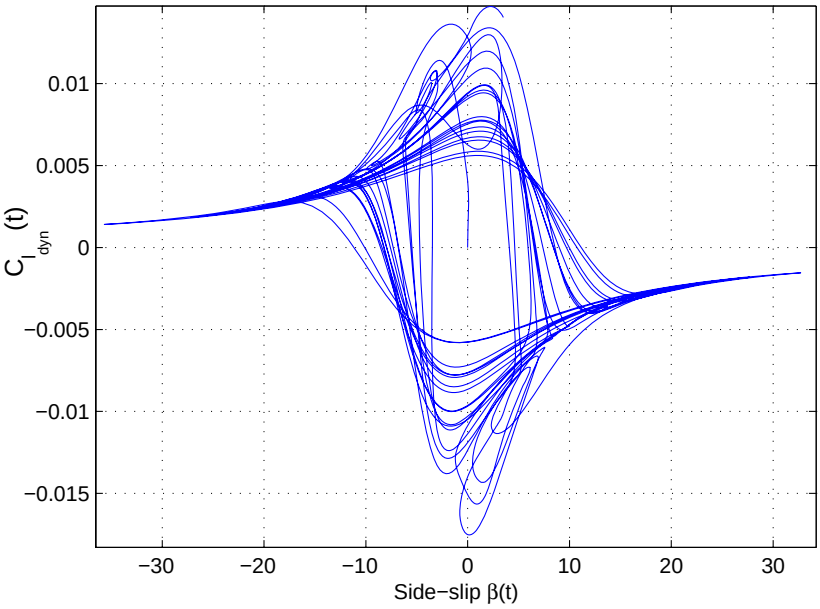

Fig. 6.12. Variation of $C_l(\beta)$ in FTR simulation of BMAA using GTA aircraft moment of inertia.

the best possible parameter tuning is presented in Fig.(6.10). For values of $(\tau, C_{l_p}) = (60, 0.02)$, the features of static and dynamic hysteresis are satisfactorily matching the FTR wind tunnel processes.

$$\begin{aligned} \dot{p} &= \frac{\rho V^2 S b}{2 I_{xx}} C_l \\ C_l &= f(\theta, p, \beta) \\ \dot{\beta} &= p sin(\theta) \end{aligned} \tag{6.5}$$

The dynamics of wind tunnel model in Free-to-roll conditions is governed by Eq.(6.5), for which the the rolling moment is defined as in equations (6.4) and (6.3). Time-histories of the relevant states in this 1DOF simulation, using the wind tunnel model inertia are presented in Fig.(6.11). One can see that there are oscillations about $\beta = \pm 5^o$, and the oscillations intermittently switch from the left-roll to the right-roll angles. It is also evident that the frequency of oscillation is $4Hz$ and $p_{max} = 4rad/s$. Thus, the estimated parameters provide a rather good qualitative model of the rolling moment coefficient in AWS conditions.

This model obtained for a particular (α_0, M_0), while AWS effects are observed over a range of angles-of-attack and Mach numbers. To model this effect continuously over the critical range of flight parameters, an interpolation of the $C_{l_{dyn}}(t, \alpha_0, M_0)$ between $(0, \alpha_{min}, M_{min})$ and $(0, \alpha_{max}, M_{max})$ is used to obtain $C_{l_{dyn}}(t)$ at any intermediate con-

dition (α, M). The resulting model is found to reproduce the function $C_l(\alpha, \beta, M, \dot{\alpha}, \dot{\beta})$ satisfactorily.

The same model parameters but with the geometric and inertia properties of the full-scale aircraft was used in 1DOF or roll-only simulations, and the resulting $C_l \, vs. \, \beta$ process is presented in Fig.(6.12). Although, the shape is retained, dynamic hysteresis stretches over the interval $\Delta\beta = 10^o$. This is due to the different values of the relative moment-of-inertia in case of the wind-tunnel-model and the aircraft, as well as due to difference in geometric parameters.

Dr.Nikolay Abramov contributed to writing a MATLAB class file for the mathematical model and Roll degree-of-freedom dynamics. He helped in obtaining the first estimate of parameters which produced the desired shape of static hysteresis curve. All the other work including Literature survey; modeling and parameter estimation for improving accuracy of the results; Free-to-roll data analysis; One-DOF and Six-DOF flight simulations studies were done by me.

6.5 Flight Simulation Studies

The AWS model presented in the previous section was used in flight simulation studies to examine the effect of AWS on flight dynamics and demonstrate its consistency with features of flight test results reported in literature. AWS is known to occur typically in wind-up turn and pull-up maneuvers. Hence, these two maneuvers were performed on the aircraft real-time simulation platform available at CSIR-NAL.

The GTA being a delta-wing configuration is inherently unstable and is stabilised using a feedback control mechanism. A functional block diagram of the longitudinal control system used in this study is presented in Fig.(6.13). The lateral controller used provided a roll-rate feedback, and hence an appropriate damping to the closed-loop system. Two case-studies are presented in this section for the closed-loop system which has the AWS model incorporated in it.

6.5.1 Pull-up Maneuver in 6DOF

GTA simulation was first trimmed to a certain lower angle-of-attack at an altitude $H = 12000m$ and Mach $M = 0.8$. A pull-up maneuver was initiated using a full aft pitch stick input for two seconds pulse, after which it is returned back to zero. The AWS region is defined by the Mach number range $[0.75\, 0.9]$ and the angle-of-attack range $[24^o\, 28^o]$. Engine throttle is held constant in this simulation.

The resulting attitude dynamics of the aircraft on entering the AWS region is presented in Fig.(6.14). The primary response of GTA is a roll-off motion, and it attains a

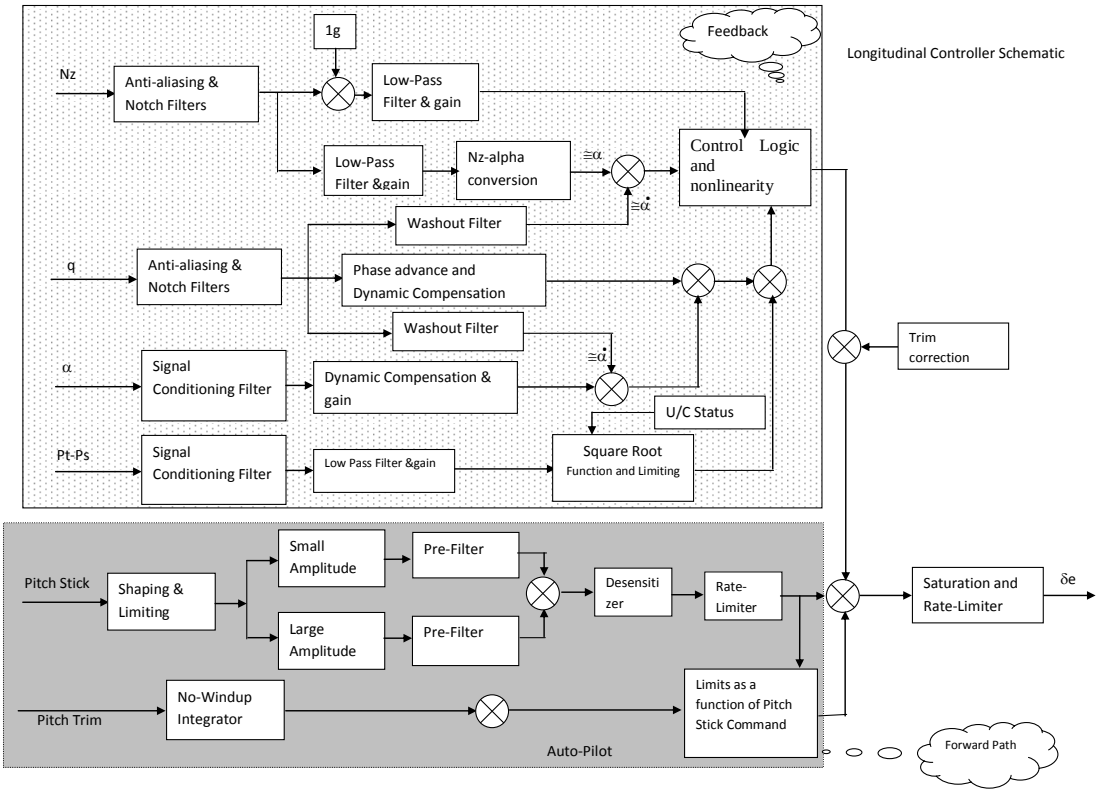

Fig. 6.13. Functional block-diagram of a longitudinal control mechanism implemented for GTA 6DOF flight simulation studies.

steady state with a different non-zero roll-angle. Angle-of-attack remains approximately constant in the AWS regime, and side-slip remains very small. Note that, as expected, the roll rate increases for lower damping gain in the control law and decreases for higher damping gain.

6.5.2 Steady-turn Maneuver in 5DOF

Similar results are obtained for simulation of a wind-up turn in 5DOF system of motion equations. In a wind-up turn, the aircraft is expected to turn at constant speed and decreasing altitude. This is equivalent to a steady-turn maneuver in 5DOF system of motion equations, where trim in $\dot{V}$ is left out for balancing thrust and altitude effects. Aircraft is first trimmed in a steady-turn maneuver at lower angle-of-attack at an altitude $H = 12000m$ and Mach $M = 0.8$. Then a step input in longitudinal pitch-stick is applied for two seconds impulse and returned back to zero. The resulting attitude dynamics is presented in Fig.(6.15). On entering the AWS region, the aircraft experiences an intensive roll-off motion of more than 360^o, and then performs a slow rolling motion. The roll-off motion is mild and can be easily controlled by a pilot. Therefore, the prototype control

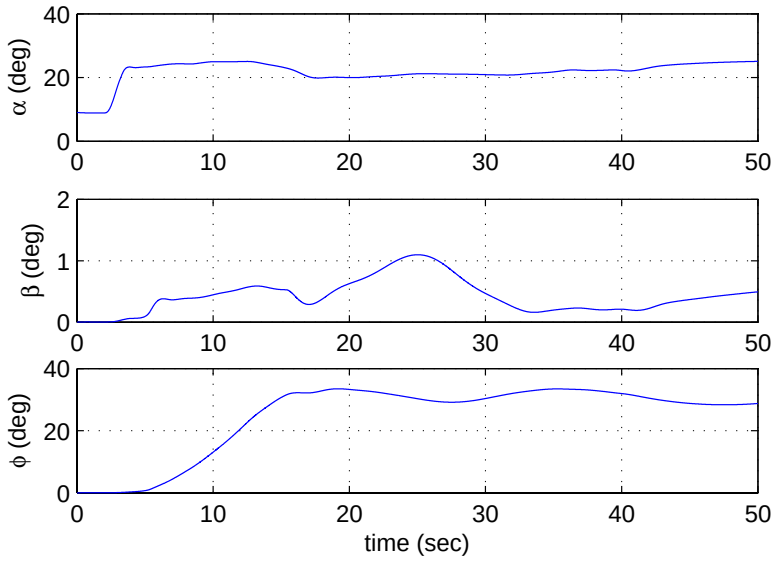

Fig. 6.14. Closed-loop 6DOF simulation of Pull-up maneuver of GTA with AWS model.

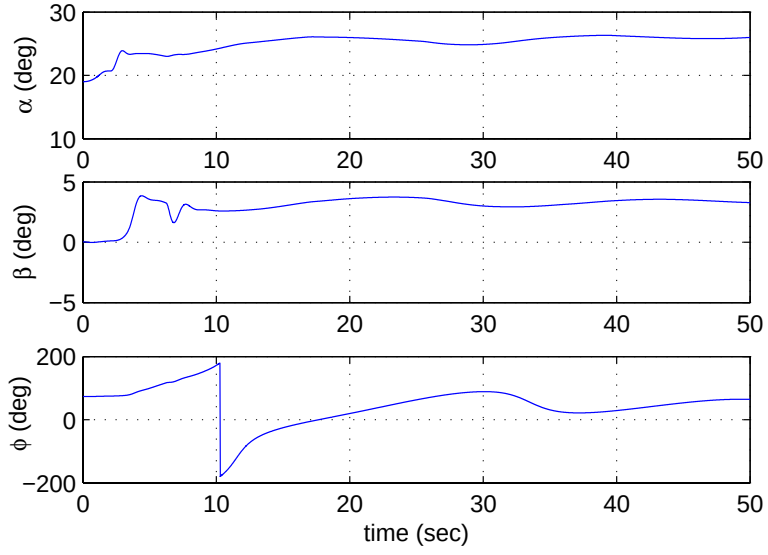

Fig. 6.15. Closed loop 5DOF simulation of steady turn maneuver of GTA with AWS model.

law is found to effectively mitigate the rolling motion due to AWS effectively. It is also important to note that the sideslip angle is restricted to a small value, indicating that the rolling motion is actually a velocity vector roll as intended in the control law design.

This type of analysis is of great value in control law design and pre-flight simulation training of a new aircraft design.

6.6 Summary

A brief review of the methods of modeling AWS phenomena and other phenomena of similar type available in literature was given, to indicate the principles of modeling AWS phenomena. A Figure-of-merit based on averaged maximum side-slip rate was shown to be an effective criteria for predicting AWS using FTR data. A novel model with rich topology called the Bifurcational model of aerodynamic asymmetry was proposed along with its estimation methodology. An approximate model of rolling moment coefficient of desired features was developed for AWS phenomena of GTA aircraft, and then it shown to be satisfactory for flight simulation studies.

Chapter 7

Conclusions and Future Directions

7.1 Conclusions

Following is the list of important conclusions made from this thesis:

1. VVM is formulated based on Volterra Series and features of nonlinear unsteady variation of aerodynamic loads. The kernel-states of VVM have special harmonic input response properties. It is shown that the model structure can be determined from harmonic input response data based on these properties. A step-wise parameter estimation procedure is formulated for use with forced oscillation wind tunnel data.

2. VVM is able to reproduce nonlinear unsteady variations, typically observed for the pitching moment coefficients of delta-wing aircraft configurations. This includes damping and anti-damping loops in the oscillation cycle, and shift of the mean of steady oscillation cycle from static test measurements. The cases studies presented show its ability to fit across a large data-set consistently.

3. VVM structure inherently includes the fundamental features of nonlinear unsteady aerodynamic loads, independent of the experimental data, like (i) linear variations for small amplitude inputs and nonlinear variations for large amplitude inputs; (ii) different effective time-constant of longitudinal unsteady loads for pitch-up and pitch-down motions (iii) dependence of unsteady load on history of input or initial conditions, (iv) super-harmonics of input frequency in the response aerodynamic load, due to large amplitude or high-bandwidth inputs. This implies that the model is more than just ”a data-true only” model.

4. VVM is more rigorous than all the approaches presented in literature for modeling the unsteady aerodynamic loads which are significantly nonlinear. VVM is consistent with all the models presented in literature in their linearized form. It

bears mathematical connections to, and in some cases can be adapted to, the State-space Polynomial Differential model, Linear indicial model, Volterra series based models, and the ONERA Dynamic Stall model.

5. The mathematical features and parameter estimation methodology of VVM which makes it a powerful approach for modeling the unsteady loads are: (i) Rigorous model structure (ii) Correlation of the features of unsteady aerodynamics to its physical interpretations (iii) Being a parametric model in the State-space differential form, it facilitates simulation and linear analysis of the flight modes (iv) Simple and flexible identification process using comprehensive forced oscillation wind tunnel test data (v) Open to innovations in model structure and estimation methodology.

6. VVM can be easily integrated with any 6DOF flight simulation framework. It is amenable to flight dynamic analysis using classical tools from linear systems theory. It is shown the Short-period mode frequency and stability are significantly effected by unsteady aerodynamic loads.

7. VVM can be effectively used for estimation using data from the experiments performed using Schroeder-sweep, Step, Ramp and Impulse inputs in angle-of-attack.

8. The Bifurcational Model of Aerodynamic Asymmetry is a topologically rich structure which can model the static hysteresis and unsteady variations in rolling moment coefficient versus the side-slip. This model is shown to produce satisfactory results for modeling the AWS phenomena of GTA aircraft using free-to-roll wind tunnel test data.

7.2 Future Directions

This thesis has opened up many new research possibilities, some of which we intend to take up in the near future are listed here:

1. Application of VVM to unsteady aerodynamics of helicopter blade airfoils, to capture the unsteady effects across the range of relevant pitching frequencies.VVM may capture the longitudinal unsteady effects due to different aerodynamic phenomenon over this range of inputs. Second order differential VVM can be used for the purpose.

2. Using the Khrabrov-Greenwell model of steady pitch-rate derivative to compute it for the airfoils whose forced oscillation test data is given in literature. Since pitch-

rate derivative is a function of flow-separation point, a unsteady model of flow-separation point can be formulated in the form of VVM. Such a coupled model will present an approach to simultaneously model the effect of pitch-rate as well as unsteady aerodynamic loads due to change in flow-incidence angles, for airfoils and can be considered for high aspect-ratio wings.

3. Exploiting the flexibility of the model structure and parameter estimation process to other unsteady aerodynamics applications like flapping-wing aerodynamics, aeroelastic modeling, wind-turbine unsteady aerodynamics, vortex breakdown location or the flow separation point on the wings etc.

4. Control Law design for the Stall angle-of-attack region, using a flight dynamic model which incorporates the VVM, for the flight envelope extension of the delta-wing aircraft configurations.

5. Methodology for parameter estimation of VVM using Schroeder Sweep input test data is of great interest. Similarly, parameter estimation using inputs like Step, Ramp and Impulses can given more insights in to the identification of unsteady aerodynamic loads. This will be done if and when the WT data is available to the authors.

6. Application of VVM methodology to modeling of nonlinear mechanical systems which exhibit input amplitude and frequency dependent nonlinear variations.

7. Formulation and identification of VVM for lateral-directional moment coefficients, using the appropriate forced oscillation wind tunnel test data.

8. Investigation of a formulation which can bridge the gap between VVM and PoDE structures such that it can exhibit bifurcational dynamics of PoDE and harmonic input response properties of VVM

Bibliography

[1] Multiple, "Technologies for Highly Manoevarable Aircraft," Conference Proceedings CP-548, NATO-AGARD, October 1993.

[2] Hamilton, W., Andrews, H., and et. al., J. C., "Manuever Limitations of a Combat Aircraft," AGARD-Advisory Report 155A, NATO, France, August 1979.

[3] Tristrant, D., "Analysis of Nonlinear and Unsteady Data for Mathematical Modeling," *Cooperative Program on Dynamic Wind Tunnel Experiments of Manoeuvring Aircraft*, AGARD AR-305, France, 1996, pp. 1–6.

[4] Pelletier, A. and Nelson, R., "The Unsteady Aerodynamics of Slender Wings and Aircrafts undergoing Large Amplitude Manuevers," *Progress in Aerospace Sciences*, Vol. 39, 2003, pp. 189–248.

[5] Hall, R. M. and Woodson, S. H., "Introduction to the Abrupt Wing Stall program," *Journal of Aircraft*, Vol. 41, No. 3, May-June 2004, pp. 425–435.

[6] Greenwell, D., "A Review of Flight Dynamic Modeling for Flight Dynamics of Manoeuvrable Aircraft," *AIAA Atmosperic Flight Mechanics Conference and Exhibit*, AIAA 2004-5276, Providence, Rhode Island, 2004.

[7] Theodorsen, T., "General Theory of Aerodynamic Instability and The Mechanism of Flutter," Report 496, NACA Langley Memorial Aeronautical Laboratory, March 1935.

[8] Wagner, H., "Uber die Entstehung des Dynamischen Auftreibues von Tragflugeln," *ZAMM*, Vol. 5, No. 1, February 1925, pp. 17–35.

[9] Kussner, H. G., "Zussamenfassender Bericht uder den Instationer Auftrieb von Flugeln," *Luftfahrtforshchung*, Vol. 13, No. 12, December 1936, pp. 410–424.

[10] Iliff, K. and Wang, K. S. C., "Extraction of Lateral-Directional Control and Stability Derivatives for the Basic F18 Aircraft at High-Angles-of-Attack," NASA-TM 4786, NASA Dryden Flight Research Centre, February 1997.

[11] Goman, M. G. and Khrabrov, A. N., "State-space representation of Aerodynamic Characteristics of an Aircraft at High-angle-of-attack," *AIAA Journal of Aircraft*, Vol. 31, No. 5, 1994, pp. 1109–1115.

[12] Tobak, M. and Schiff, L., "On The Formulation of The Aerodynamic Characteristics in Aircraft Dynamics," NASA-TM 1976-208969, NASA Ames Research Centre, January 1976.

[13] Leishman, J. G., "Challenges in Modeling the unsteady Aerodynamic of Wind Turbines," *Wind Energy*, Vol. 5, 2002, pp. 85–132.

[14] Majhi, J. R. and Ganguli, R., "Helicopter Blade Flapping with and without Small Angle Assumption in Presence of Dynamic Stall," *Applied Mathematical Modeling*, Vol. 34, 2010, pp. 3726–3740.

[15] Ho, S., Nassef, H., Ponsinssirirak, N., Tai, Y.-C., and Ho, C.-M., "Unsteady Aerodynamics and Flow Control of Flapping Wing Flyers," *Progress in Aerospace Sciences, Elsevier*, Vol. 39, 2003, pp. 635–681.

[16] Greenwell, D., "Difficulties in the Application of Stability Derivatives to the Manoevering Aerodynamics of Combat Aircraft," *21st ICAS Congress*, No. A98-31466, ICAS, Melbourne, Australia, 1998, pp. 1–12.

[17] der Schaft, A. J. V., "On Realisation of Nonilnear Systems Described by Higher Order Nonlinear Differential Equations," *Mathematical Systems Theory*, Vol. 19, 1987, pp. 239–275.

[18] Volterra, V., *Theory of Functionals and of Integral and Integro-differential Equations*, Dover Publications Inc., New York, 1930, 2005.

[19] Singh, J. and Jategaonkar, R. V., "Identification of Lateral-Directional Behaviour in Stall from Flight Data," *AIAA Journal of Aircraft*, Vol. 33, No. 3, 1995, pp. 627–630.

[20] Abramov, N., *Modelling of Unsteady Aerodynamic Characteristics for Aircraft Dynamics Applications at High Angles of Attack*, Phd thesis, De Montfort University, June 2005.

[21] Abramov, N. B., Goman, M. G., Khrabrov, A. N., and Kolinko, K. A., "Simple Wings Unsteady Aerodynamics at High Angle of Attack : Experimental and Modeling Results," *AIAA Atmosperic Flight Mechanics Conference and Exhibit*, AIAA 1999-4013, Chicago, Illinois, 1999.

[22] Abramov, N., Goman, M., Greenwell, D., and Khrabrov, A., "Two Step Regression Method for Identification of High-Incidence Unsteady Aerodynamic Model," *AIAA Atmosperic Flight Mechanics Conference and Exhibit*, AIAA 2001-4080, Providence, Rhode Island, 2001.

[23] Abramov, N., Goman, M., and Khrabrov, A., "Aircraft Dynamics at High Incidence Flight with Account of Unsteady Aerodynamic Effects," *AIAA Atmosperic Flight Mechanics Conference and Exhibit*, AIAA 2004-5274, Providence, Rhode Island, 2004.

[24] de. Oliveira Neto, P. and Lutze, F., "First order Unsteady Aerodynamic Model that Includes Static Hysteresis Phenomena," *AIAA Atmosperic Flight Mechanics Conference and Exhibit*, AIAA 2002-4803, Monterey, California, 2002.

[25] Fan, Y., *Identification of an Unsteady Aerodynamic Model up to High Angle of Attack Regimes*, PhD Thesis, Virginia Polytechnic Institute and State University, 1997.

[26] Singh, J. and Jategaonkar, R. V., "Flight Determination of Configruational Effects on Aircraft Stall Behaviour," *AIAA Atmosperic Flight Mechanics Conference and Exhibit*, AIAA 1996-3441, San Diego, CA, 1996.

[27] Pashilkar, A. A. and Pradeep, S., "Aerodynamic Modeling using Multivariate orthogonal Polynomials," *AIAA Atmosperic Flight Mechanics Conference and Exhibit*, AIAA 1999-4014, Monterey, California, 1999.

[28] Tobak, M. and Chapman, G., "Nonlinear problems in Flight Dynamics involving Aerodynamic Bifurcations," NASA-TM 86706, NASA Ames Research Centre, January 1985.

[29] Tobak, M., Chapman, G., and Schiff, L., "Mathematical Modeling of the Aerodynamic Characteristics in Flight Dynamics," NASA-TM 85880, NASA Ames Research Centre, January 1984.

[30] Klein, V. and Murphy, P. C., "Estimation of Aircraft Nonlinear Unsteady Parameters From Wind Tunnel Data," NASA-TM 1998-208969, NASA Langley Research Centre, December 1998.

[31] Klein, V., Murphy, P. C., Curry, T. M., and Brandon, J., "Analysis of Longitudinal Static and Oscillatory Data of the F16-XL Aircraft," NASA-TM 1997-206276, NASA Langley Research Centre, December 1997.

[32] Murphy, P. C., Klein, V., and Frink, N., "Unsteady Aerodynamic Modeling in Roll for the NASA Generic Transport Model," *AIAA Atmosperic Flight Mechanics Conference and Exhibit*, AIAA 2012-4652, Minneapolis, Minnesota, 2012.

[33] Myatt, J., *Unsteady Aerodynamic Modeling by load partitioning*, PhD Thesis, Stanford University, 1997.

[34] Allwine, D., Strauler, J., Lawrence, D., Jenkins, J., and Myatt, J., "Nonlinear Modeling of Unsteady Aerodynamics at High Angle-of-attack," *AIAA Atmosperic Flight Mechanics Conference and Exhibit*, AIAA 2004-5275, Providence, Rhode Island, 2004.

[35] McAlister, K. W., Lambert, O., and Petot, "Application of ONERA Model of Dynamic Stall," NASA-TP 2399, NASA Ames Research Centre, November 1984.

[36] McCroskey, W. J., McAlister, K. W., Carr, L. W., and Pucci, S. L., "An Experimental Study of Dynamic Stall on Advanced Airfoils, Volume 1. Summary of Experiments," NASA-TM 84245, NASA Ames Research Centre, July 1982.

[37] Faller, W. E. and Schreck, S. J., "Unsteady Fluid Mechanics Applications of Neural Networks," *Journal of Aircraft*, Vol. 34, No. 1, January 1997, pp. 48–55.

[38] Ignatyev, D. I. and Khrabrov, A. N., "Model of Unsteady Aerodynamic Characteristics at High Angle-of-attack with Nonlinear Dependency in Angular Rate," *29th ICAS Congress*, No. 2014-0449, ICAS, St. Petersburg, Russia, September 2014.

[39] Schroeder, M. R., "Neural network modeling of unsteady aerodynamic characteristics at high angles of attack," *Aerospace Science and Technology*, Vol. 2015, No. 41, December 2014, pp. 106–115.

[40] Resisenthel, P., "Prediction of Unsteady Aerodynamic Forces via Nonlinear Kernel Identification," *AIAA/NASA Langley International Forum on Aeroelasticity and Structural Dynamics*, AIAA, Williamsburg, VA, 1999.

[41] Pashilkar, A. A., "Flow Incidence Rate Model of Unsteady Aerodynamics at High Angles of Attack," *19th Applied Aerodynamics Conference*, AIAA 2001-2469, Anaheim, California, 1999.

[42] Kyle, H., Lowenberg, M., and Greenwell, D., "Comparative Evaluation of Unsteady Aeordynamic Modeling Approaches," *AIAA Atmosperic Flight Mechanics Conference and Exhibit*, AIAA 2004-5272, Providence, Rhode Island, 2004.

[43] Klein, V. and Morelli, E. A., *Aircraft System Identification: Theory and Practice*, American Institute of Aeronautics and Astronautics, 2006.

[44] Murphy, P. C. and Klein, V., "Validation of Methodology for Estimating Aircraft Unsteady Aerodynamic Parameters from Dynamic Wind Tunnel Tests," *AIAA Atmosperic Flight Mechanics Conference and Exhibit*, AIAA 2003-5397, Austin, Texas, 2003.

[45] Pamadi, B., Murphy, P. C., Klein, V., and Brandon, J., "Prediction of Unsteady Aerodynamic Coefficients At High Angle-of-attack," *AIAA Atmosperic Flight Mechanics Conference and Exhibit*, AIAA 2001-4077, Austin, Texas, 2001.

[46] Kim, S., Murphy, P. C., and Klein, V., "Evaluation and Analysis of F16XL Wind Tunnel Data Dynamic Tests," *AIAA Atmosperic Flight Mechanics Conference and Exhibit*, AIAA 2003-5396, Austin, Texas, 2003.

[47] Billings, S. A., "Identification of Nonlinear Systems - A Survey," *IEE Proceedings D Control Theory and Applications*, Vol. 127, Nov 1980, pp. 272–285.

[48] Marmerelis, V. Z., *Nonlinear Dynamic Modeling of Physiological Systems*, Wiley-IEEE, 2004.

[49] Stephen Boyd, Y. S. T. and Chua, L. O., "Measuring Volterra Kernels," *IEEE Transactions On Circuits and System*, , No. 8, 1983, pp. 571–577.

[50] Evans, C., Rees, D., Jones, L., and Weiss, M., "Periodic Signals for Measuting Nonlinear Volterra Kernels," *IEEE Transactions On Measurement and Instrumentation*, Vol. 45, No. 2, 1996, pp. 362–371.

[51] Rugh, W. J., *Nonlinear System Theory: The Volterra/Weiner Approach*, The John Hopkins University Press, 1981.

[52] Marques, F. D. and Belo, E. M., "Identification of Aircraft Nonlinear Dynamics using Volterra Series," *21st ICAS Congress*, No. A98-31484, ICAS, Melbourne, Australia, September 1998.

[53] Omran, A. and Newman, B., "Peicewise Global Nonlinear Modeling and Charactirisation of Aircraft Dynamics," *Journal of Guidance Control and Dynamics*, Vol. 32, No. 3, 2005, pp. 749–759.

[54] Pranzenica, R., Reisenthel, P., Kurdila, A., and Brenner, M., "Volterra Kernel Extrapolation for Modeling Nonlinear Aeroelastic Systems at Novel Flight Conditions," *Journal of Aircraft*, Vol. 44, No. 1, January 2007, pp. 149–162.

[55] Silva, W., "Identification of Nonlinear Aeroelastic Systems Based on the Volterra Theory: Progress and Opportunities," *Nonlinear Dynamics*, Vol. 39, 2005, pp. 25–62.

[56] Silve, W. A., Piatak, D. J., and Scott, R. C., "Identification of Experimental Unsteady Aerodynamic Impulse Responses," *Journal of Aircraft*, Vol. 42, No. 6, 2005, pp. 1548–1552.

[57] Resisenthel, P. H., "Development of Nonlinear Indicial Model for Maneuvering Fighter Aircraft," *AIAA Atmosperic Flight Mechanics Conference and Exhibit*, AIAA 1996-0896, 1996.

[58] Reisenthel, P. H., "Application of Volterra functions to X-31 Aircraft model Motion," *AIAA Applied Aerodynamics Conference*, AIAA 2009-3269, San Antonio, Texas, 2009.

[59] Resisenthel, P. and Battencourt, M., "Extraction of Nonlinear Indicial and Critical State Responses from Experimental data," *37th AIAA Aerospace Sciences Meeting and Exhibit*, AIAA 1999-0764, Reno, NV, January 1999.

[60] Billings, S. A., *Nonlinear System Identification: NARMAX Methods in Time, Frequency and Spatio-Temporal Domains*, Wiley, 2013.

[61] Gersche, G., Wroden, K., Vakakis, A. F., and Golinval, J.-C., "Past, Present and Future of Nonlinear System Identification in Structural Dynamics," *Mechanical Systems and Signal Processing*, Vol. 20, 2006, pp. 509–522.

[62] Bedrosian, E. and Rice, S. O., "Output Properties of Volterra Systems (Dynamic Systems with Memory) Driven by Harmonic and Gaussian Inputs," *Proceedings of IEEE*, Vol. 59, No. 12, 1971, pp. 1688–1707.

[63] Foster, J., Cunningham, K., Fremaux, C., Shah, G., Stewart, E., and et. al., R. R., "Dynamics Modeling and Simulation of Large Transport Airplanes in Upset Conditions," *AIAA Guidance, Navigation, and Control Conference and Exhibit*, AIAA 2005-5933, San Francisco, California, 2005.

[64] Groen, E. e. a., "SUPRA - Enhanced Upset Recovery Simulation," *AIAA Modeling and Simulation Technologies Conference*, AIAA 2012-4630, Minnesota, Minneapolis, USA, August 2012.

[65] Fucke, L., Groen, E., Goman, M., Abramov, N., Wentink, M., Nooij, S., and Zaichik, L., "Final results of the supra project: Improved Simulation of

Upset Recovery." *28th Congress of the International Council of the Aeronautical Sciences*, No. 2012-964, ICAS, Brisbane, Australia, September 2012, pp. 4607–4616.

[66] Helie, T. and Laroche, B., "Computation of Convergence Bound for Volterra Series of Linear-Analytic Single-Input Systems," *IEEE Transactions On Automatic Control*, Vol. 56, No. 9, 2011, pp. 2062–2072.

[67] Gilbert, E. G., "Functional Expansions for the Response Nonlinear Differential Systems," *IEEE Transactions On Automatic Control*, , No. 6, 1977, pp. 909–921.

[68] Boyd, S. and Chua, L. ., "Fading Memory and the Problem of Approximating Nonlinear Operators with Volterra Series," *IEEE Transactions On Circuits and System*, , No. 11, 1985, pp. 1150–1161.

[69] Li, L. M. and Billings, S. A., "Estimation of Generalised Frequency Response Functions for quadratically and cubically nonlinear systems," *Journal of Sound and Vibration*, Vol. 330, 2011, pp. 461–470.

[70] Brenan, M. J., Kovacic, I., Carella, A., and Waters, T. P., "On the jump-up and jump-down frequencies of the Duffings oscillator system," *Journal of Sound and Vibration*, Vol. 318, 2008, pp. 1250–1261.

[71] Jategaonkar, R. V., *Flight vehicle System Identification: A Time Domain Methodology*, American Institute of Aeronautics and Astronautics, 2006.

[72] Cunnigham, A. M. and den Boer, R. G., "Low-speed Unsteady Aerodynamics of Pitching Straked Wing at High Incidence-PartI:Test Program," *Journal of Aircraft*, Vol. 27, No. 1, 1990, pp. 23–30.

[73] Cunnigham, A. M. and den Boer, R. G., "Low-speed Unsteady Aerodynamics of Pitching Straked Wing at High Incidence-PartII:Harmonic Analsysis," *Journal of Aircraft*, Vol. 27, No. 1, 1990, pp. 31–41.

[74] Gursul, I., "Review of Unsteady Vortex Flows over Slender Delta Wing," *Journal of Aircraft*, Vol. 42, No. 2, 2005, pp. 299–319.

[75] Ericson, L. E., "Pitch Rate Effects on Delta Wing Vortex Breakdown," *Journal of Aircraft*, Vol. 33, No. 3, 1996, pp. 639–642.

[76] Ericson, L. E., "Vortex Charactersitics of Pitching Double-Delta Wings," *Journal of Aircraft*, Vol. 36, No. 2, 1999, pp. 349–356.

[77] Ericson, L. E., "The time-History Effects on a Rolling 65-Degree Delta-Wing-Body Configuration," *Journal of Aircraft*, Vol. 36, No. 3, 1999, pp. 489–495.

[78] Smith, M. S., "Analysis of Wind Tunnel Oscillatory data of the X31," NASA-CR 208725, NASA Langley Research Centre, February 1999.

[79] Reisenthel, P., Xie, W., and Gurusul, I., "An analysis of Fin Motion Induced Vortex Breakdown," *37th AIAA Aerospace Sciences Meeting and Exhbit*, No. 99-0316, AIAA, Reno, NV, 1999.

[80] Brunton, S. L., *Unsteady Aerodynamic Models for Agile Flights at Low Reynolds Numbers*, PhD Thesis, Princeton University, 2012.

[81] Boelens, O. J., Badcock, K. J., Elmilgui, A., Abdol-Hamid, K. S., and Massey, S. J., "Comparison of Measured and the Block Structured Simulation results for the F16XL Aircraft," *AIAA Journal of Aircraft*, Vol. 46, No. 2, March-April 2009, pp. 377–384.

[82] Brandon, J. and Foster, J., "Recent Dynamic Measurements and Considerations for Aerodynamic Modeling of Fighter Airplane Configurations," *AIAA Applied Aerodynamics Conference*, 1998-4447, New Orleans, Lousiana, June 1998.

[83] Pattison, J., Lowenberg, M. H., and Goman, M. G., "Multi-Degree-of-Freedom Wind Tunnel Maneuver Rig for Dynamic Simulation and Aerodynamic Model Identification," *AIAA Journal of Aircraft*, Vol. 50, No. 2, March-April 2013, pp. 551–566.

[84] Sen, A., Bhange, P., and Wahi, P., "A 5 Degree-of-Freedom Rig for Wind Tunnel Tests of Aerospace Vehicles," *AIAA Atmosperic Flight Mechanics Conference and Exhibit*, AIAA 2009-5605, Chicago, Illinois, 2009.

[85] Khrabrov, A. and Greenwell, D., "Influence of Steady Pitch-rate on 2-D Airfoil Aerodynamic Characteristics at Incidence," *Journal of Aircraft*, Vol. 43, No. 5, September 2006, pp. 1552–1555.

[86] Omran, A. and Neuman, B., "Nonlinear Cause.Effect Analysis for a Second Order System using Volterra Kernels," *American Control Conference*, AACC, Baltimore, MD, USA, 2010, pp. 2706–2711.

[87] Peng, Z. K. and Lang, Z. Q., "On Convergence of Volterra-series representation of Duffing's Oscillator Subjected to Harmonic Excitation," *Journal of Sound and Vibration*, Vol. 305, 2007, pp. 322–332.

[88] Bommanahal, M. and Goman, M., "Nonliear Unsteady Aerodynamic Modeling by Volterra Variational Approach," *AIAA Atmosperic Flight Mechanics Conference and Exhibit*, AIAA 2012-4654, Minnesota, Minneapolis, USA, August 2012.

[89] Klein, V. and Murphy, P. C., "Aerodynamic Parameters of High Performance Aircraft Estimated From Wind Tunnel and Flight Test Data," *Symposium on Identification for Integrated Aircraft Development and Flight Testing*, NASA TM-97-207993, Madrid, Spain, May 1998, pp. 18.1–18.20.

[90] Murphy, P. C. and Klein, V., "Estimation of Aircraft Unsteady Aerodynamic Parameters from Dynamic Wind Tunnel Testing," *Atmospheric Flight Mechancis Conference*, AIAA 2001-4016, Montreal, Canada, August 2001, pp. 1–9.

[91] Goman, M., Khramtsovsky, A., Usoletsev, S., Vinogodrov, Y., and Tyrtyshnikov, S., *PII Scientific Package: the Textbook*, Central Aerohydrodynamic Institute TsAGI, Moscow, Russia, 1st ed., November 1993.

[92] Usoletsev, S. and Khramtsovsky, A., *Package for Interactive Identification user guide*, Central Aerohydrodynamic Institute TsAGI, Russia, 2nd ed., November 2002.

[93] Goman, M., Khrabrov, A., and Usoltsev, S., "Identification of Unsteady Aerodynamic Model of a Delta-wing at High Angels of Attack," *10th IFAC Symposium on System Identification*, SYSID94, 1994.

[94] Goman, M., Khrabrov, A., and Usoltsev, S., "Unsteady Aerodynamic Model for Large Amplitude Maneuvers and its Parameter Estimation," *11th IFAC Symposium on System Identification*, SYSID97, 1997.

[95] Murphy, P., "Modeling Discussion (between) Goman Bommanahal Murphy," email, June 2013, Discussion on Wind tunnel testing, data-processing, and nonlinear nature of unsteady aerodynamics, in the context of F16XL wind tunnel test data.

[96] McAlister, K. W., Pucci, S. L., McCroskey, W. J., and Carr, L. W., "An Experimental Study of Dynamic Stall on Advanced Airfoils, Volume 2. Pressure and Froce Data," NASA-TM 84245, NASA Ames Research Centre, September 1982.

[97] Goman, M. G., Khramtsovsky, A. V., and Kolesnikov, E. N., "Evaluation of Aircraft Performance and Maneuvearbility by Computation of Attainable

Equilibrium Sets," *AIAA Journal of Guidance Control and Dynamics*, Vol. 31, No. 2, 2008, pp. 329–339.

[98] Abramov, N. B., Goman, M., Kolesnikov, E., and Sidoryuk, M., "Investigation of Attainable Equilibrium Sets for Evaluation of Flight Control Laws," *48th AIAA Aerospace sciences Meeting and Exhibit*, AIAA, Orlando-Florida, 2010, pp. 1–12.

[99] Fliess, M., Lamnabhi, M., and Lamnabhi-Larrigue, F., "An Algebraic Approach to Nonlinear Functional Expansions," *IEEE Transactions on Circuits and Systems*, Vol. 30, No. 8, August 1983, pp. 554–570.

[100] Schroeder, M. R., "Synthesis of low peak-factor signals and binary sequences with low auto-correlations," *IEEE Transactions of Information Theory*, Vol. 1, No. 1, January 1970, pp. 85–89.

[101] Chambers, J. R. and Hall, R. M., "Historical Review of Uncommanded Lateral-Directional motions at Transonic Conditions," *Journal of Aircraft*, Vol. 41, No. 3, May-June 2004, pp. 436–447.

[102] Schuster, D. and Byrd, J., "Transonic Unsteady Aerodynamics of the F/A-18E under Conditions Promoting Abrupt Wing Stall," *Journal of Aircraft*, Vol. 41, No. 3, May-June 2004, pp. 485–492.

[103] McConnell, J., "Use of Transonic Free to Roll Testing in the Design Phase of the Joint Strike Fighter," *Aerodynamic Measurement Technology and Ground Testing Conference*, AIAA 2006-3925, San Francisco, Californica, June 2006.

[104] Capone, F. J., Owens, D. B., and Hall, R. M., "Development of Transonic Free-to-Roll Test Capability," *Journal of Aircraft*, Vol. 41, No. 3, May-June 2004, pp. 456–463.

[105] Cook, S. P., Kokolios, A., Page, A., Chambers, J., Neiwoehner, R., Owens, D. B., and Roesch, M., "Integrated Approach to Assessment of Transonic Abrupt Wing Stall for Advanced Aircraft," *Journal of Aircraft*, Vol. 42, No. 3, May-June 2005, pp. 646–652.

[106] Owens, D. B., Capone, F. J., Hall, R. M., Brandon, J. M., and Chambers, J. R., "Transonic Free-to-Roll analysis of Abrupt wing stall on military aircraft," *Journal of Aircraft*, Vol. 41, No. 3, May-June 2004, pp. 474–484.

[107] Lamar, J. E., Capone, F. J., Hall, R. M., and McMillin, S. N., "Usefulness of Transonic Model Static Data in Predicting Flight Abrupt-Wing-Stall," *Journal of Aircraft*, Vol. 41, No. 3, May-June 2004, pp. 464–473.

[108] Owens, D. B., McConnell, J., Brandon, J. M., and Hall, R. M., "Transonic Free-To-Roll Analysis of the F/A-18E and F-35 Configurations," *AIAA Atmosperic Flight Mechanics Conference and Exhibit*, AIAA 2004-5053, Providence, rhode Island, August 2004.

[109] Kokolios, A., Cook, S. P., and Neiwoehner, R., "Use of Piloted Simulation for Evaluation of Abrupt-Wing-Stall Characteristics," *Journal of Aircraft*, Vol. 42, No. 3, May-June 2005, pp. 641–645.

[110] Capone, F. J., Owens, D. B., Hall, R. M., Lamar, J. E., and McMillin, N. S., "Reveiw and Recommended Experimental Procedures for Evaluation of Abrupt Wing Stall Charcateristics," *Journal of Aircraft*, Vol. 41, No. 3, May-June 2004, pp. 448–455.

[111] Goman, M. G., Khrabrov, A. N., and Khramtsovsky, A. V., "Chaotic Dynamics in Simple Aeromechanical System," *Fractal Geometry, Mathematical Methods, Algorithms and Applications*, edited by Blackledge, Evans, and Turner, chap. 1, Harwood Publishing, 1st ed., September 2002, pp. 1–16.

[112] Greenwell, D. and Garcia, M. T., "Autorotational Dynamics of a Low Aspect Ratio Rectangular Prism," *Journal of Fluids and Structures*, Vol. 49, June 2014, pp. 640–653.

[113] Greenwell, D., "Geometry Effects on Autoroation of Rectangular Prisms," *Journal of Wind Engineering and Industrial Aerodynamics*, Vol. 132, June 2014, pp. 92–100.

[114] Jeans, T. L., Jirasek, A., McDaniel, D. R., Bergeron, K., and Cummings, R., "Modeling the Nonlinear Dynamic Roll of Generic Fighter Using Delayed Detached Eddy Simulation," *Journal of Aircraft*, Vol. 49, No. 4, July-August 2012, pp. 1110–1125.

[115] Ghoreyshi, M., Post, M. L., Cummings, R., Raonch, A. D., and Badcock, K., "Transonic Aerodynamic Loads Modeling of X31 Aicraft," *30th AIAA Applied Aerodynamics Conference*, 2012-3127, New Orleans, Lousiana, June 2004.

[116] Ikouhane, F. and Rodellar, J., *Systems with Hysteresis: Analysis, Identification and Control using Bouc-Wen Model*, Wiley, September 2007.

Appendix A

Parameter Estimation Theory

A.1 Least Squares Regression

In this section, the general formulae used in least-squares regression and analysis of the estimated parameters are presented. The detailed mathematical derivations and assumptions used, are available in the textbook by E. A. Morelli [43].

$$y = X\theta \tag{A.1}$$

$$z = X\theta + \nu \tag{A.2}$$

Consider a system whose dynamics is governed by Eq.(A.1). In this equation, y is the output of the system and X is a vector of linear or nonlinear functions of the independent variables ξ_i. The objective of regression is to estimate the model parameters θ given the systems output measurements and independent variables. The postulated model is not the exact representation of system dynamics. Hence, there is uncertainty in the model parameters θ. The output measurements z are often corrupted by random noise ν. Therefore, the regression equation is given by Eq.(A.2).

$$J = \frac{1}{2}(z - X\theta)V^{-1}(z - X\theta) \tag{A.3}$$

$$V = \nu\nu^T \tag{A.4}$$

Assuming that there are no probability models for θ and ν, this problem can be classified as the so-called "Least Squares Model". The best estimate of the parameters of such a model is given by a minimum of the weighted sum of the square of the difference between model output and measured output. Therefore, the cost function for estimation of parameters is Eq.(A.3). Here, V^{-1} is the weighting matrix. It can be either specified by judgement of relative errors in measurement or it can be simply taken as the noise co-variance matrix as defined in Eq.(A.4).

$$\frac{\partial J}{\partial \theta} = 0; \qquad \frac{\partial^2 J}{\partial \theta^2} > 0 \tag{A.5}$$

$$\hat{\theta} = (X^T V^{-1} X)^{-1} X^T V^{-1} z \tag{A.6}$$

$$Cov(\hat{\theta}) = (X^T V^{-1} X)^{-1} \tag{A.7}$$

The parameter estimate $\hat{\theta}$ is obtained at the minimum of the cost function J, and hence it must satisfy the equations (A.5). The solution of this equations is obtained as in Eq.(A.6), and this defines the estimated value of $\hat{\theta}$. Since, the model error is not known in the first step, we can assume it to be a certain non-singular matrix, and then it is estimated for the successive steps using the prediction error $\nu = z - X\hat{\theta}$. This iterative estimation converges to a certain value of $\hat{\theta}$ in few steps.

$$Cov(\hat{\theta}) = (X^T V^{-1} X)^{-1} \tag{A.8}$$

$$\theta_j = \hat{\theta} \pm 1.96 s(\hat{\theta}_j) \tag{A.9}$$

The co-variance matrix of the estimated parameters is given by Eq.(A.8). The variance of each estimated parameter θ_j is given by the diagonal term d_{jj} of $Cov(\hat{\theta})$, as $var(\theta_j) = s^2(\hat{\theta}_j) = d_{jj}$. This gives the 95% confidence bounds for the estimated parameters as in Eq.(A.9).

$$R^2 = \frac{\hat{\theta}^T X^T z - N\bar{z}^2}{z^T z - N\bar{z}^2} \tag{A.10}$$

The Coefficient of determination R^2 represents the extent of variation in output measurements that is captured by the model, and it is computed as in Eq.(A.10). Here N is the total number of measured points in z, and $\bar{z}$ is the average of all the values.

A.2 Two-Step Regression

$$C_{\alpha,\omega_0}(\alpha_0) = aC_{\dot{\alpha},\omega_0}(\alpha_0) + [C_{\alpha,st}(\alpha_0) + K_1 - C_{\dot{\alpha}}(\alpha_0)] \tag{A.11}$$

Two-step Regression method is used to compute time-scale $a(\alpha_0)$ and dynamic-gain $K_1(\alpha_0)$ parameters. Recall the Eq.(A.11) obtained by linearisation of the single-state VVM at angle-of-attack α_0. This gives the linear relation between $C_{\alpha,\omega_0}(\alpha_0)\, vs.\, C_{\dot{\alpha},\omega_0}(\alpha_0)$. The in-phase C_α and out-of-phase $C_{\dot{\alpha}}$ derivatives at n angle-of-attack points are given in the Small amplitude forced oscillation test data. At each α_0,

derivatives are available for m input frequencies ω_0.

In the first-step of regression, $a(\alpha_0)$ is estimated using Eq.(A.11) . For this consider, $z = C_\alpha(\omega, \alpha) \in R^{n \times m}$ and $X = C_{\dot{\alpha}}(\omega, \alpha) \in R^{n \times m}$ in Eq.(A.2), to get the estimates $\theta = a(\alpha) \in R^n$. Then the parameter bounds and R^2 are computed using the prediction error $\nu = z - X\hat{\theta}$, as given in section $A.1$.

$$\begin{aligned} Cz_{\alpha,\omega_0}(\alpha_0) &= Cz_{\alpha,st}(\alpha_0) + \frac{K_1\omega^2}{a^2+\omega^2} \\ Cz_{\dot{\alpha},\omega_0}(\alpha_0) &= Cz_q(\alpha_0) - \frac{K_1 a}{a^2+\omega^2} \end{aligned} \tag{A.12}$$

In the second step of regression, the equations (A.12) derived in chapter 3 are used for estimation of $K_1(\alpha_0)$ and $C_q(\alpha_0)$. Using the results of step 1, compute $X1(i,j) = -a_i^2/(a_i^2 + (\omega_j)^2)$, $X2(i,j) = X1(i,j)/a_i$ at each angle-of-attack $\alpha_i \in R^n$ and input frequency $\omega_j \in R^m$. Now, the variables are computed as in Eq.(A.13), and used to perform least-squares regression and the get the results $\hat{\theta} = [K_m\, K_1\, Cq]^T$. Parameter bounds and R^2 are computed to check the quality of regression fit.

$$z = [C_\alpha(\omega,\alpha) C_{\dot{\alpha}}(\omega,\alpha) C_{\alpha,st}(\alpha)]^T \tag{A.13}$$

$$X = \begin{pmatrix} ones(m,1) & X1 & zeros(m,1) \\ zeros(m,1) & X2 & ones(m,1) \\ 1 & -1 & 0 \end{pmatrix} \tag{A.14}$$

A.3 Output-Error Method

$$\hat{R} = \frac{1}{N}\sum_{i=1}^{n} \nu_i \nu_i^T \tag{A.15}$$

$$J(\theta) = \frac{1}{2}\sum_{i=1}^{n} [z(i) - y(i)] \hat{W}^{-1} [z(i) - y(i)]^T \tag{A.16}$$

Consider a deterministic system $y = h(x)\theta$, which is linear in parameters. The measurements of outputs of this system $z(i) = y(i) + \nu(i)$ and the states $x(i)$ are available. The objective of parameter estimation is to estimate the parameters of the postulated model $y(i) = h_M(x(i))\theta$. The output errors or the residuals of the model are given by $\nu(i) = z(i) - y(i)$. The weighting matrix W is defined as in Eq.(A.15). Then the cost function J for optimization is given by Eq.(A.16). Since the available data set is very large, the minimum of this cost function is estimated using optimization algorithms like steepest-descent, gradient, genetic algorithm etc. The value of parameters at the minimum value of J is the best estimate of parameters $\hat{\theta}$ consistent with the given data set.

This method is used to estimate the VVM parameters using Large amplitude forced oscillation test data.

Appendix B

Identification Results for Longitudinal Coefficients of F16XL

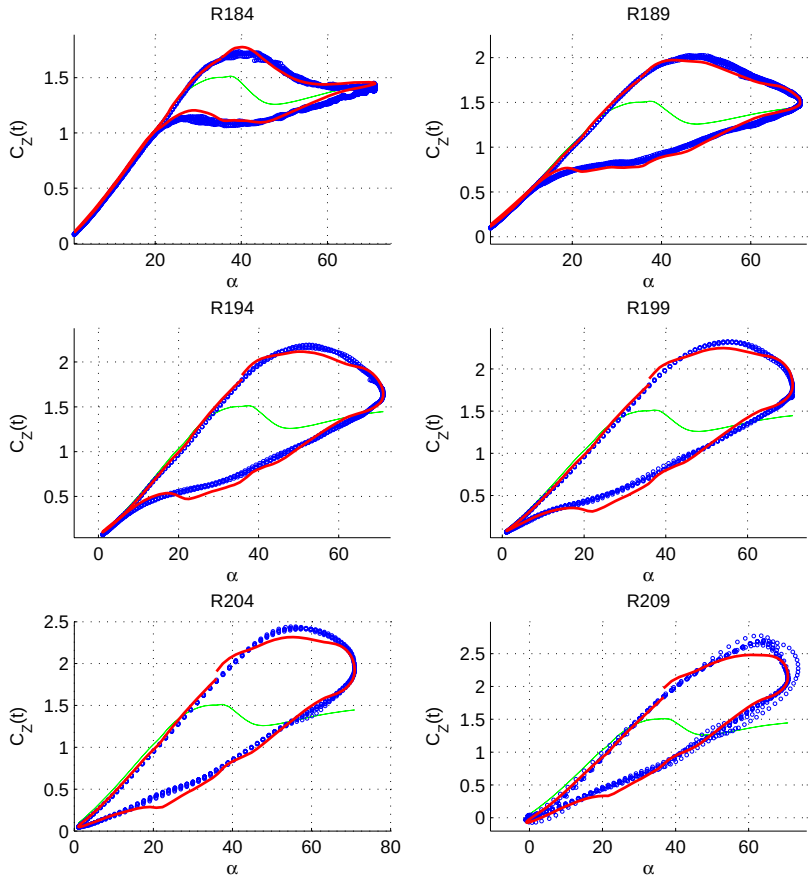

Fig. B.1. Simulation results for C_Z of F16XL, part 1

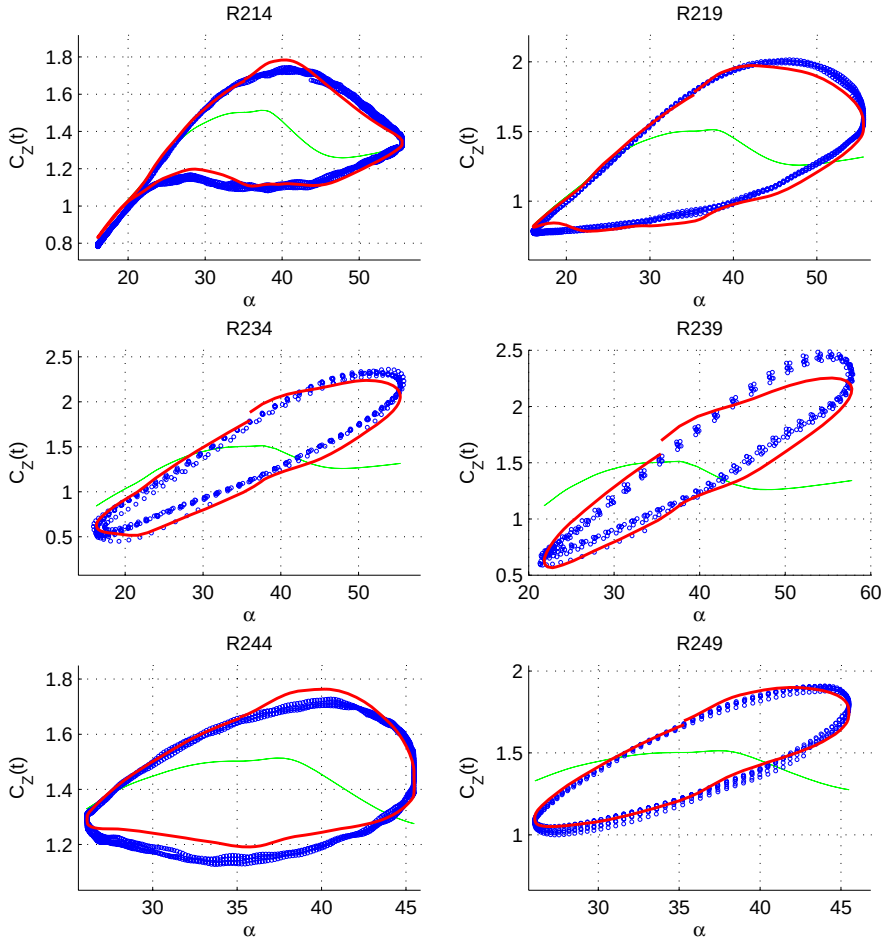

Fig. B.2. Simulation results for C_Z of F16XL, part 2

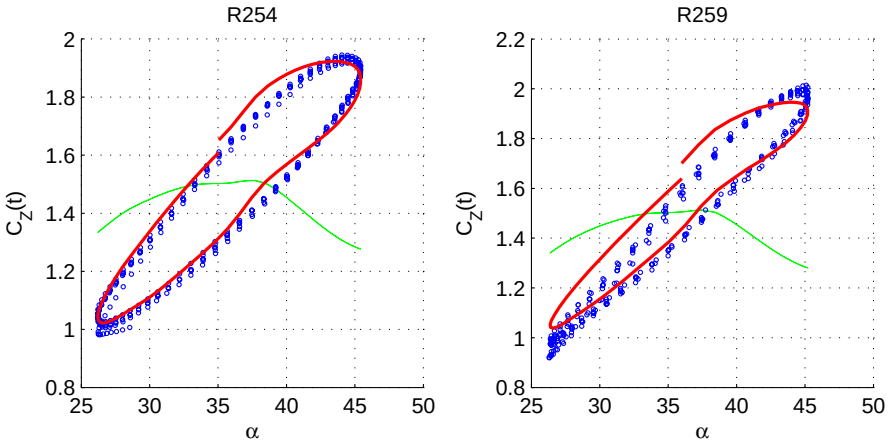

Fig. B.3. Simulation results for C_Z of F16XL, part 3

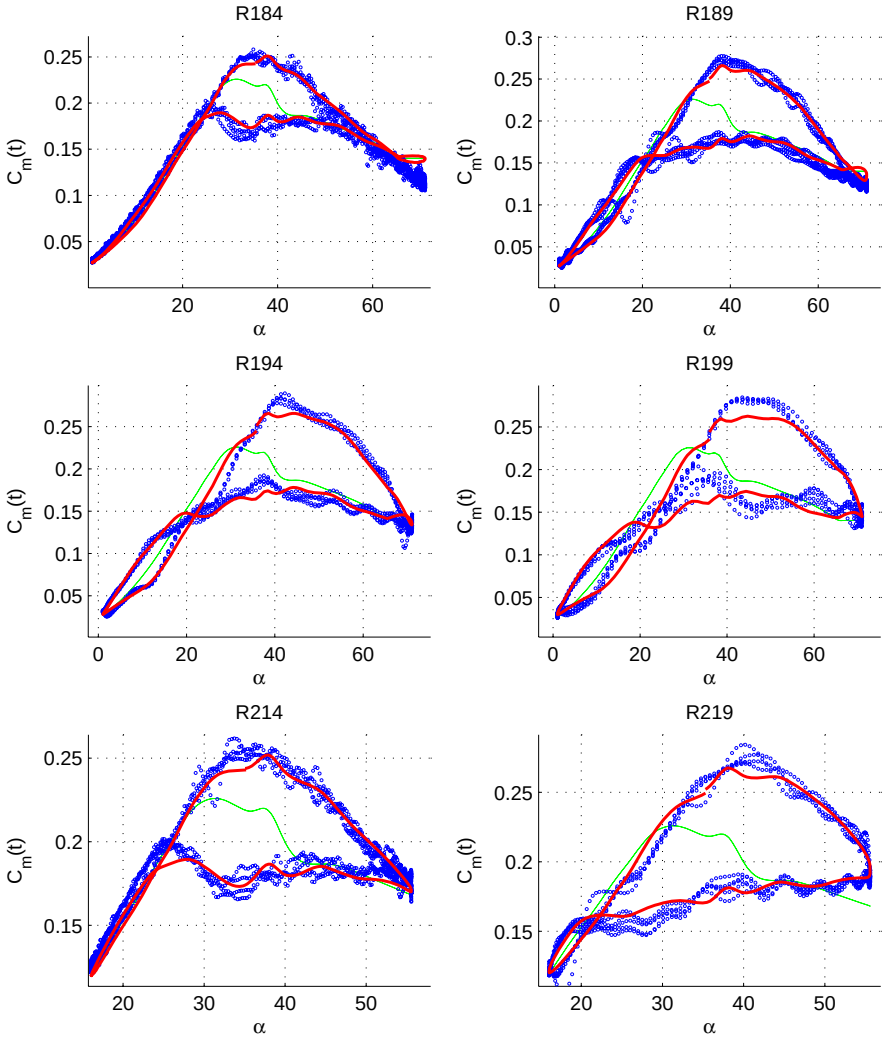

Fig. B.4. Simulation results for C_m of F16XL, part 1

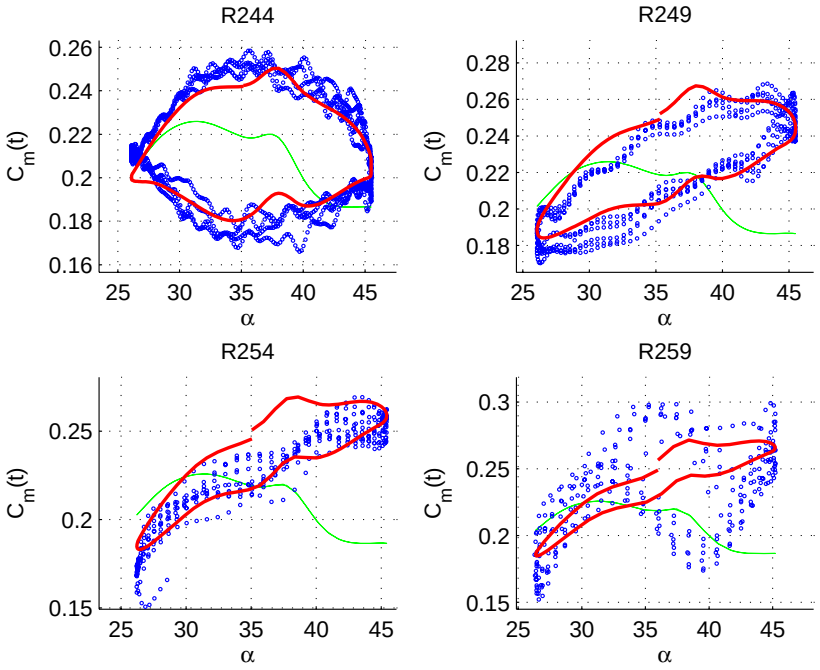

Fig. B.5. Simulation results for C_m of F16XL, part 2

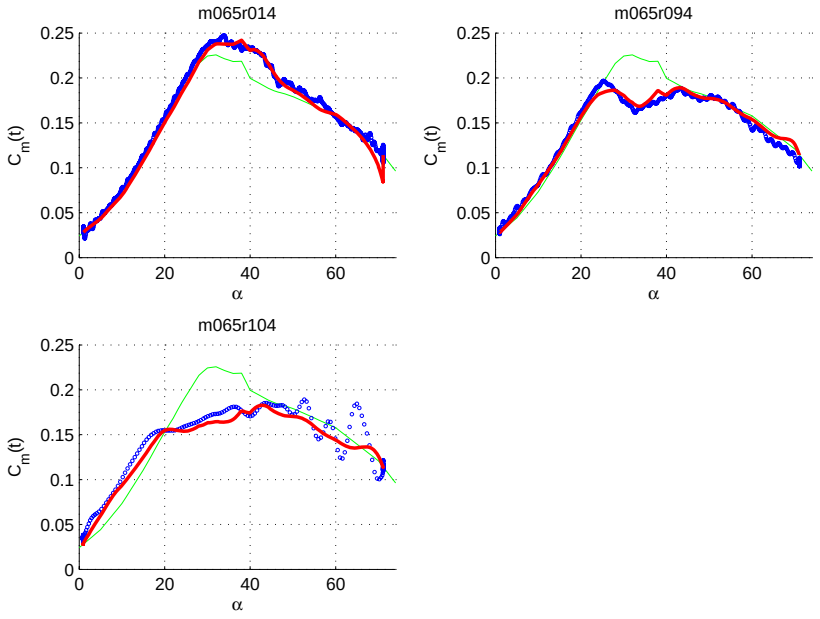

Fig. B.6. Ramp-pitching input simulation results for C_m of F16XL, part 1

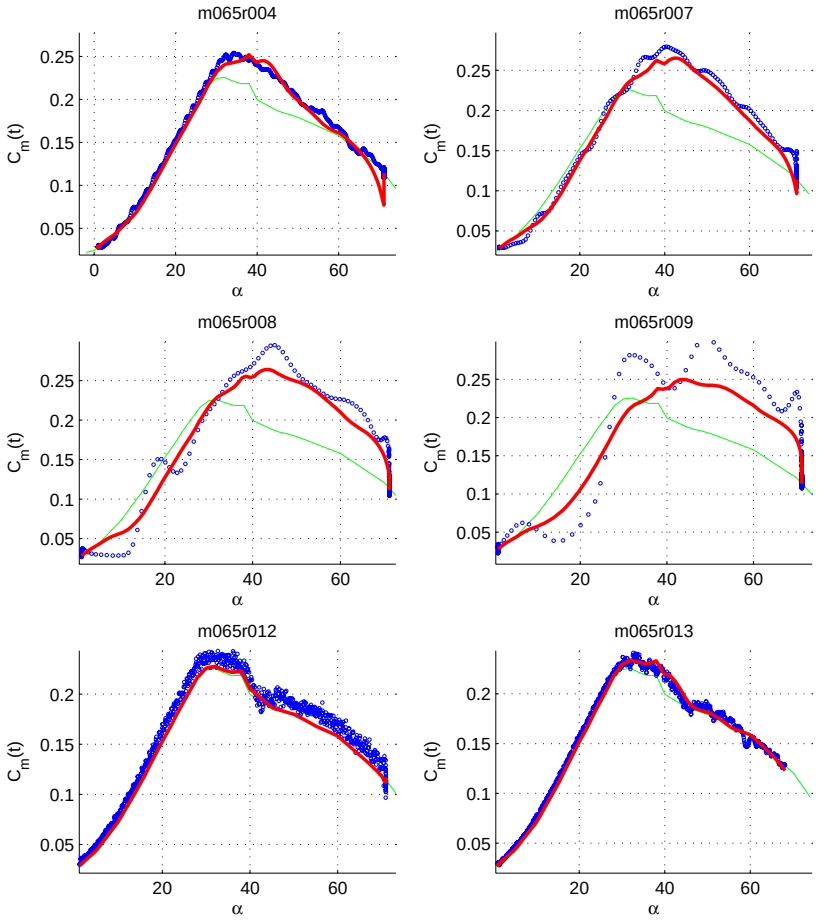

Fig. B.7. Ramp-pitching input simulation results for C_m of F16XL, part 2

Appendix C

Identification Results for Longitudinal Coefficients of GTA

Sr. No.	**Polar**	α_0 deg	$\Delta\alpha$ deg	fHz
1	RO3	15	15	0.5
2	RO8	15	15	1
3	R13	15	15	1.5
4	R18	25	15	0.5
5	R23	25	15	1
6	R28	25	15	1.5
7	R33	35	15	0.5
8	R38	35	15	1
9	R43	35	15	1.5
10	R58	30	20	0.5
11	R63	30	20	1
12	R68	20	25	0.5
13	R73	20	25	1
14	R78	30	25	0.5

Table C.1. Large amplitude forced oscillation wind tunnel test Polars for GTA

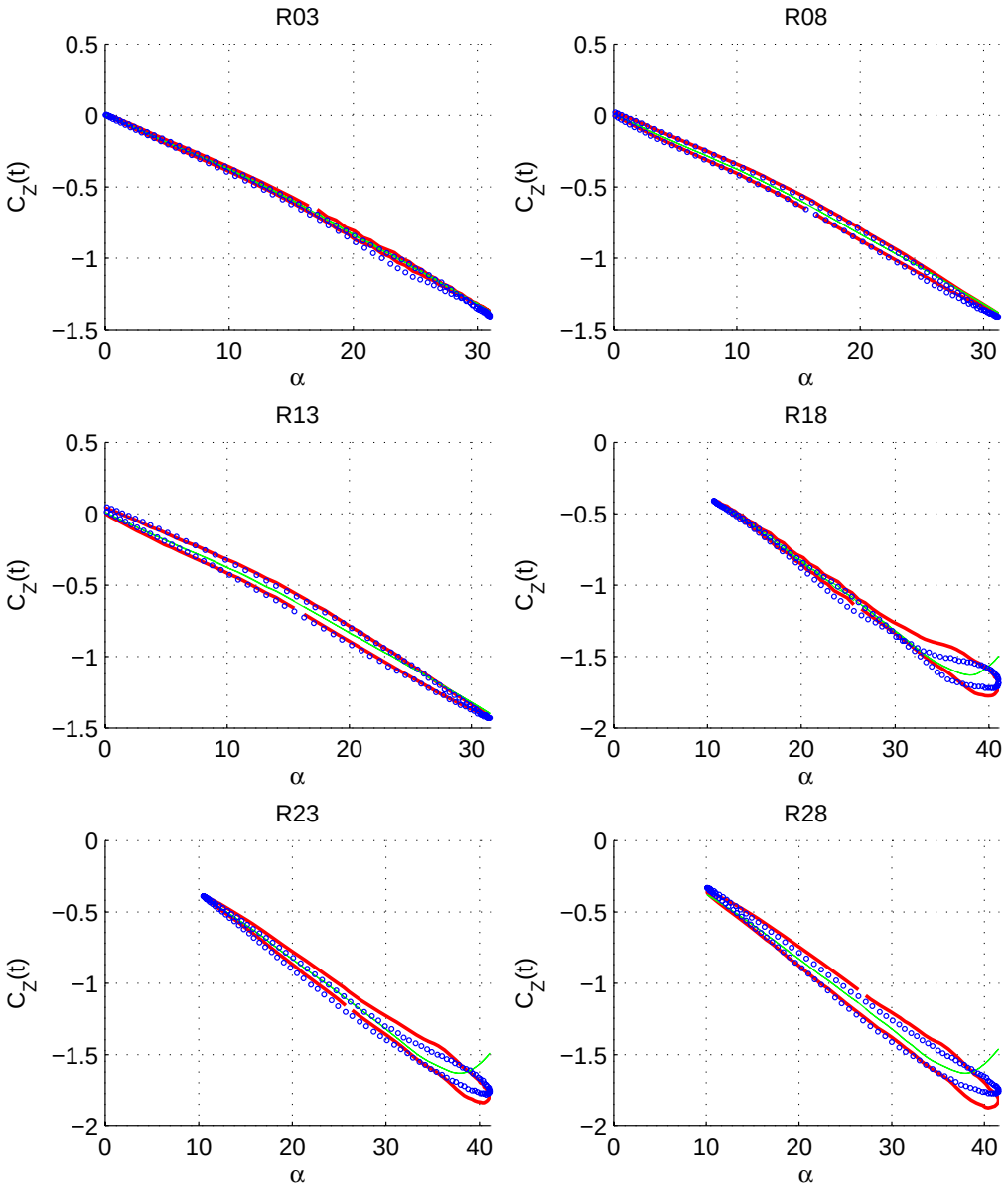

Fig. C.1. Simulation results for C_Z of GTA, part 1

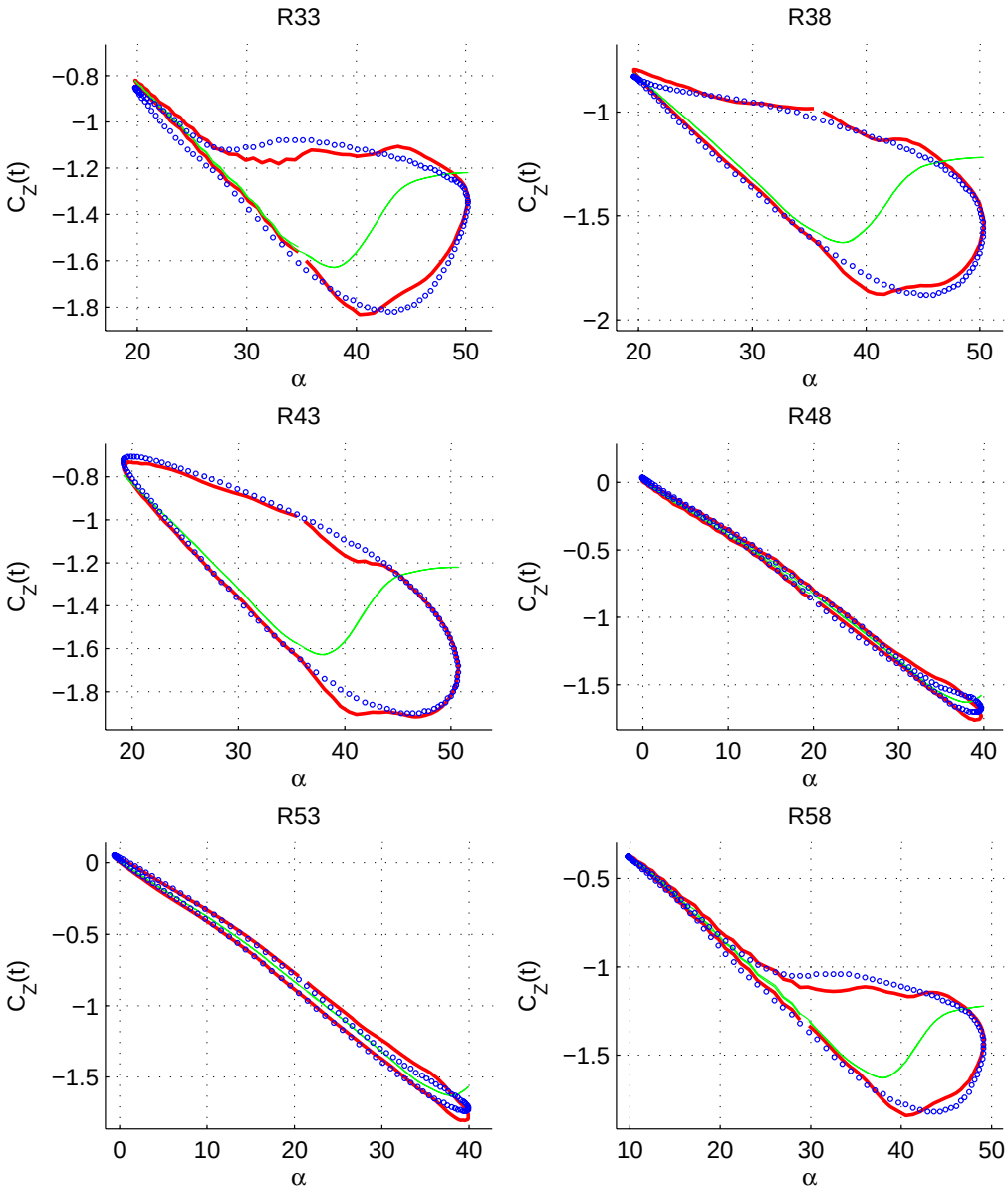

Fig. C.2. Simulation results for C_Z of GTA, part 2

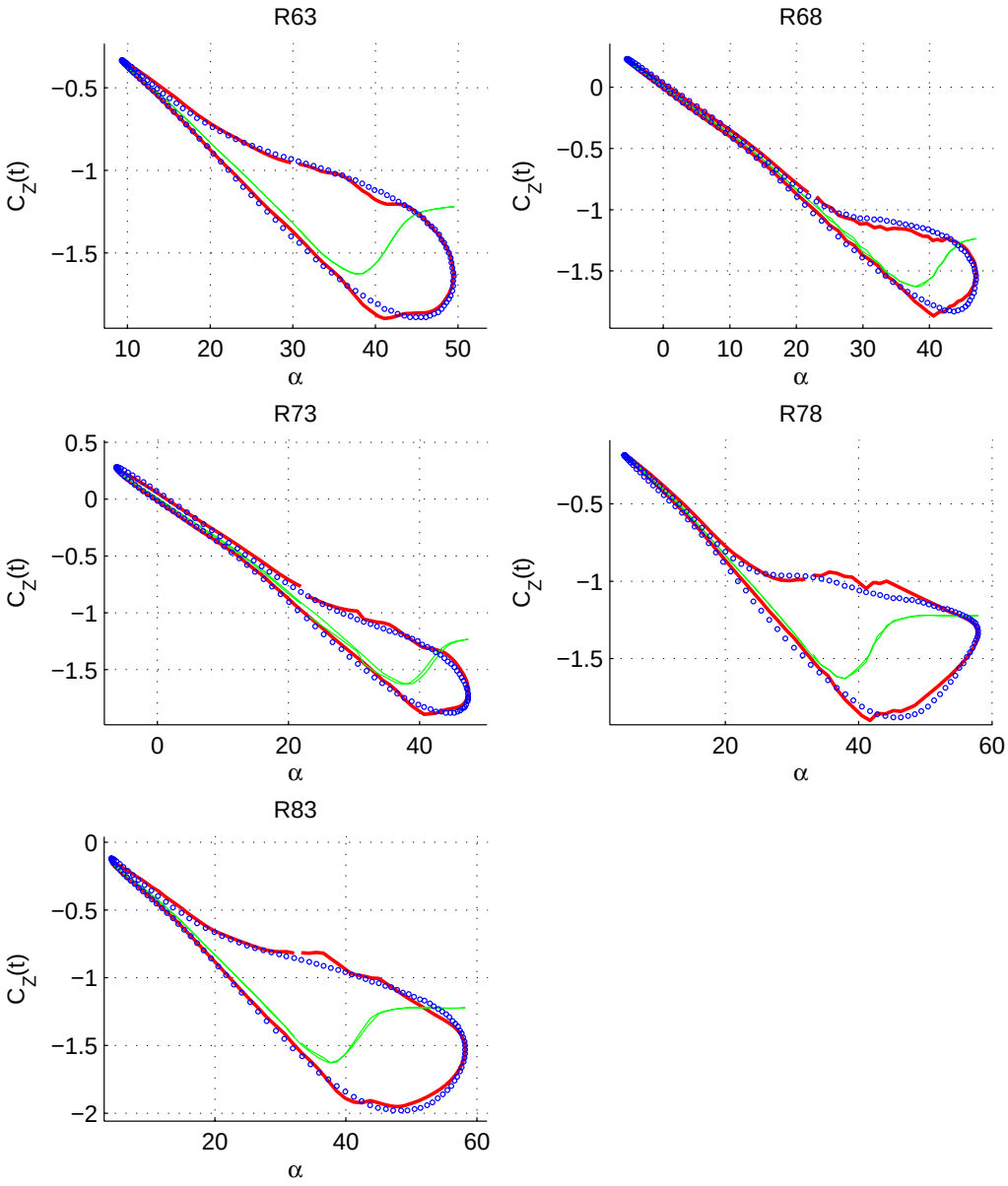

Fig. C.3. Simulation results for C_Z of GTA, part 3

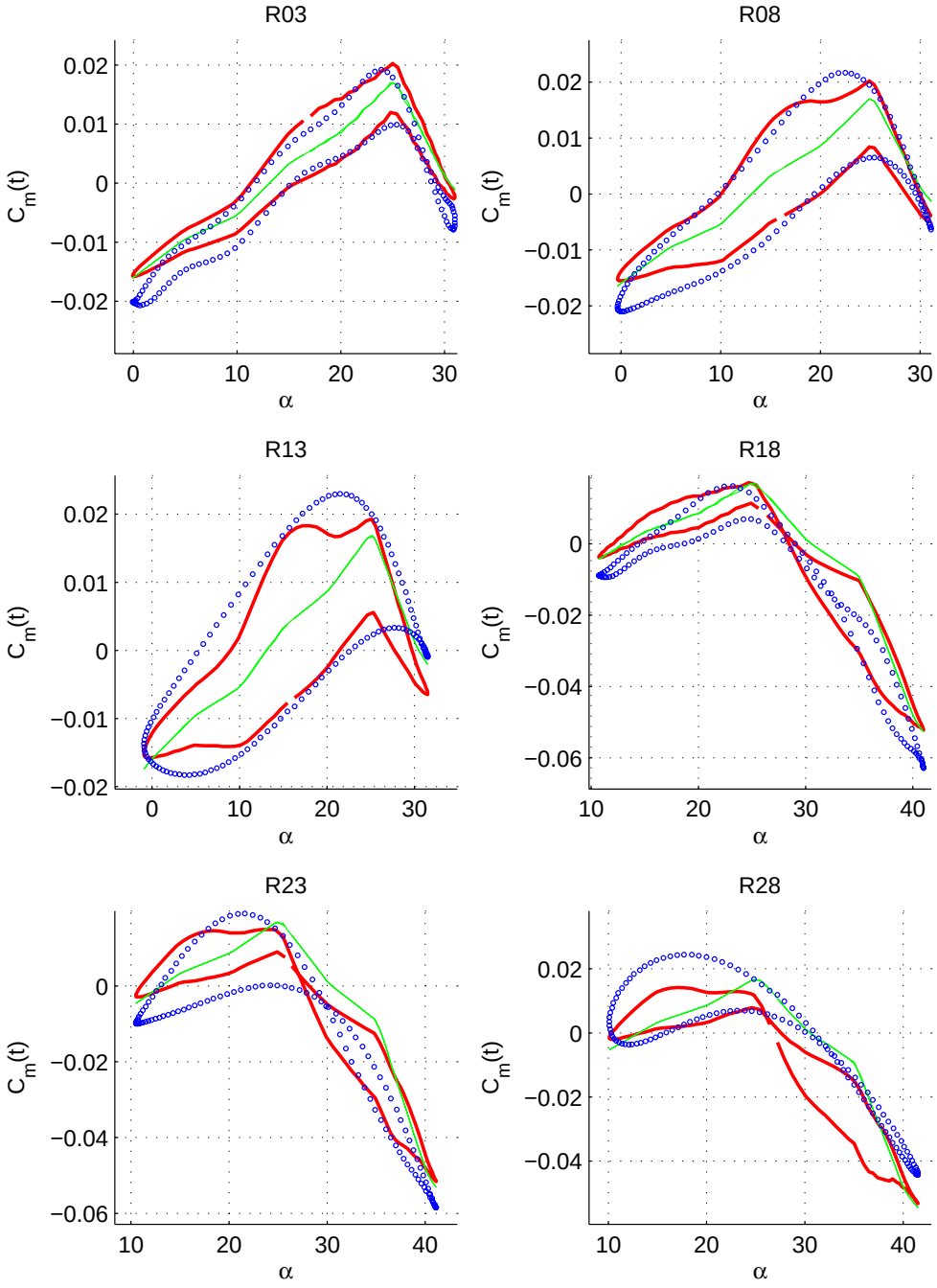

Fig. C.4. Simulation results for C_m of GTA, part 1

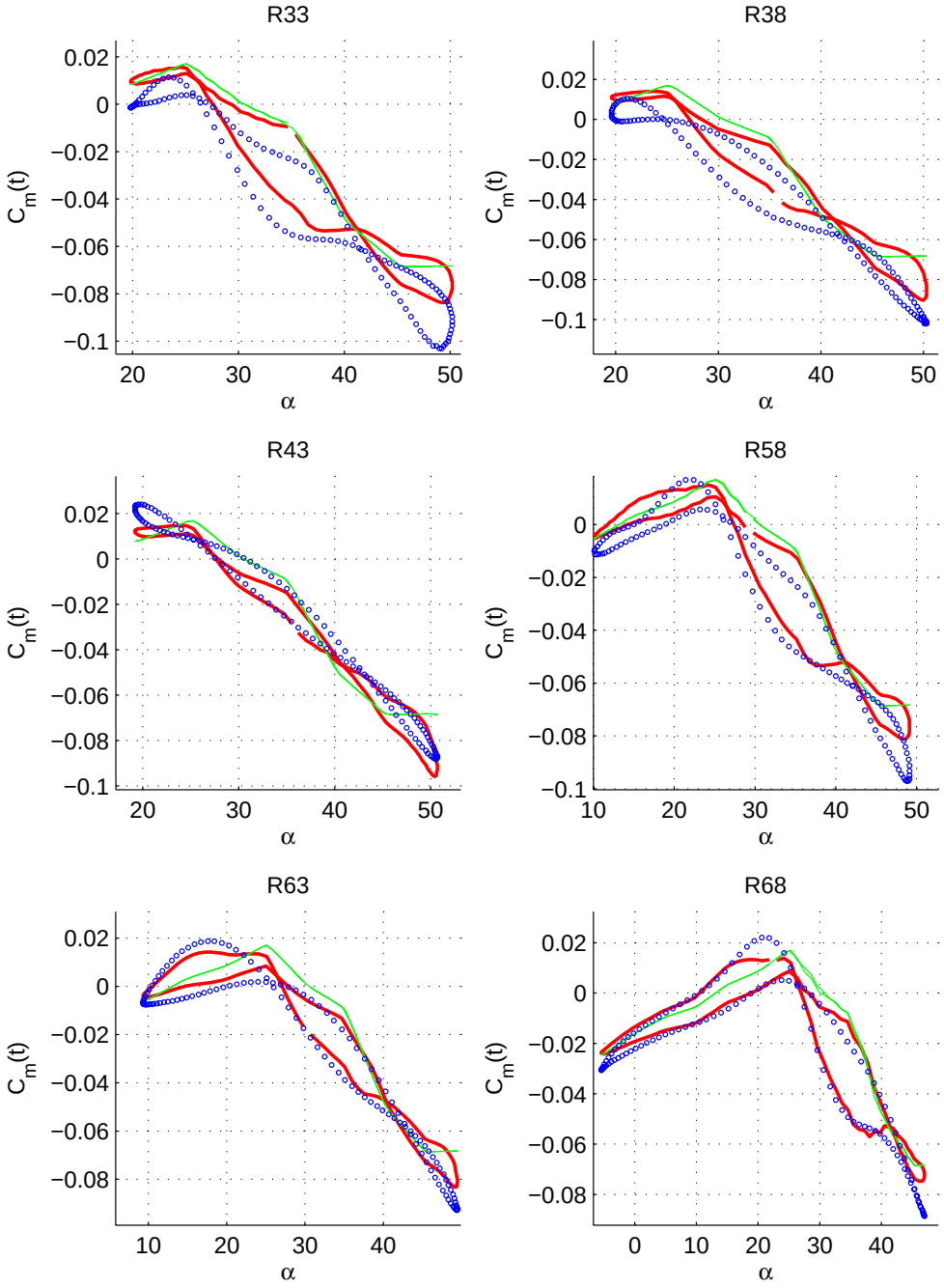

Fig. C.5. Simulation results for C_m of GTA, part 2

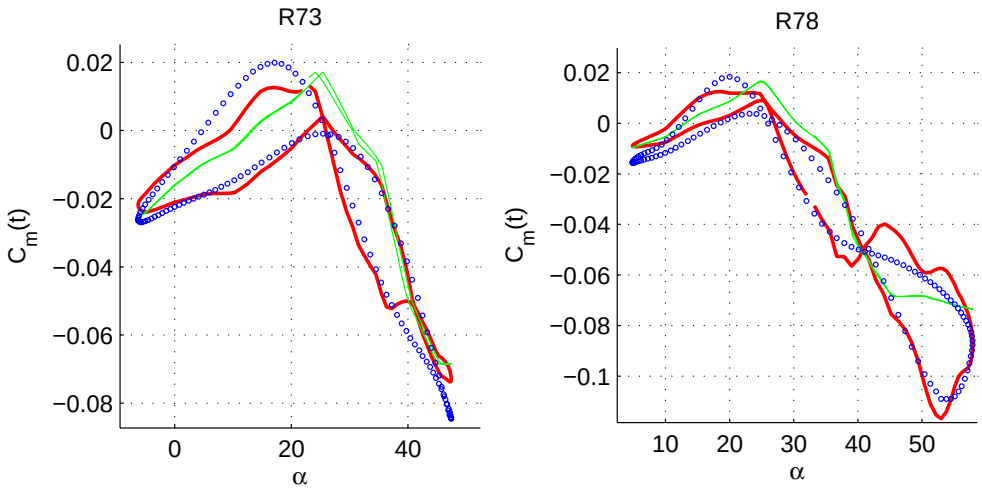

Fig. C.6. Simulation results for C_m of GTA, part 3

AIAA Atmospheric Flight Mechanics Conference
13 - 16 August 2012, Minneapolis, Minnesota

AIAA 2012-4654

Nonlinear Unsteady Aerodynamic Modeling by Volterra Variational Approach

Mallesh Bommanahal*
National Aerospace Laboratories - CSIR, Bangalore 560 017, India
Mikhail Goman†
De Montfort University, Leicester LE1 9BH, United Kingdom

The aerodynamics at high-angle-of-attack is an unsteady and nonlinear phenomena in time. In this paper, we present a phenomenological and mathematically rigorous approach to nonlinear modeling of the unsteady aerodynamics based on Volterra variational equations. The model consists of differential equations of internal states corresponding to different kernels of the Volterra series. The model structure is generic as the number of states can be chosen contingent on available wind tunnel test data and fidelity of the model desired. Model parameters are estimated using forced oscillation wind tunnel test data. We present modeling of the normal force coefficient of a delta-wing aircraft. We find that two-states are sufficient for accurate modeling of the normal force coefficient in small and large amplitude oscillations in pitch at different frequencies. We show that the model is consistent with various experimental observations reported in literature. In the end we compare it with other models proposed in literature.

Nomenclature

Cz = normal force coefficient
Cm = pitching moment coefficient
h_i = i-th Volterra kernel
τ_i = time-variable of i-th kernel
q = pitch rate
ω = frequency of oscillation
x_i = i-th state of Volterra variational equations
α = angle of attack

Subscript
i = variable number

I. Introduction

Flight dynamics modeling and analysis at high-angle-of-attack is important in the design process of both high performance aircraft and civil transportation aircraft. For a high performance aircraft, it is required for verification of flight envelope protection features and recovery from unstable modes like spin. It is also necessary for parameter estimation of high-angle-of-attack aerodynamic coefficients using flight test data[1] In recent times, pilot training for recovery of the aircraft from attitude upset situation has received wide attention from the aviation safety point of view.[2] All these tasks require a fairly accurate high-angle-of-attack aerodynamic model. In the near-stall and post-stall angle-of-attack regimes, aerodynamic loads depend on the aircraft motion history. This is reflected in the form of dynamic hysteresis in variation of aerodynamic

*Scientist, Flight Mechanics and Control Division, AIAA Member.
†Professor, Faculty of Technology, Senior AIAA Member.

forces and moments with angle-of-attack.[3] The classical method of using acceleration and stability derivatives (in-phase/out-phase derivatives) in the form of lookup tables grossly fails in this situation.[4] Therefore, special methods for mathematical modeling of high-angle-of-attack unsteady aerodynamics are necessary.

Different modeling techniques have been proposed in literature, but currently there is no generally agreed method used in the industry due to various reasons. A high-angle-of-attack aerodynamic model should meet following requirements in order to be acceptable to the industry:

- The model shall be compatible with the classical look-up table type aerodynamic model and computationally efficient for use in a real-time flight simulator.
- The model accuracy should be satisfactory for simulation as well as computational analysis. If required, it shall be possible to improve fidelity of the model using more wind tunnel test data.
- Robust methods for identification using wind tunnel test data and reliable methods for validation using flight test data are necessary.
- State-space form of the model is suited for analysis using classical tools.
- For preliminary design phase considerations, it should be possible to obtain a qualitative aerodynamics model using the limited data available.

These requirements are met to a large extent by the Volterra variational equations based approach proposed in this paper.

The model structures proposed in literature are built around two major ideologies, (i) State-space approach and (ii) Nonlinear indicial response approach. Goman and Khrabrov proposed the State-space approach with an internal state representing vortex breakdown location or flow separation point.[5] Later, Abramov and Goman presented a phenomenological model using differential equation of the pitching induced lift force component.[6] Indicial response approach starts with a rigorous mathematical structure, but after simplifications reduces to a linear differential equation.[7] Linearized form of these and other models are generally equivalent, while their nonlinear extensions are mostly empirical.[8,9] However, presence of higher order harmonics in the normal force or pitching moment response to sinusoidal pitching oscillations proves that the unsteady aerodynamics of delta, double-delta and strake-delta wings is a nonlinear phenomena in time.[10–12] Therefore, a rigorous approach to nonlinear modeling is essential for high-fidelity flight simulation. The Volterra variational equations based approach provides a systematic approach to nonlinear modeling.

Volterra variational equations consist of an infinite set differential equations of internal states which correspond to a convolution integral terms in the Volterra series for a single input. For unsteady modeling only one to three states maybe required depending on (i) the nonlinearity of coefficient (ii) fidelity of the model desired and (iii) forced oscillation wind tunnel test data available. The first state represents linear response of the system and its time-constant is equal to the time-scale of unsteady variations due to small amplitude or low-frequency input. Higher order states introduce corrections due to effects of nonlinearity. Recently this theory was used to obtain a piecewise-global-nonlinear model for longitudinal flight dynamics.[13] The Volterra series theory is widely used for nonlinear modeling of physiological systems and has lead to many theoretical and methodological developments.[14]

We present a novel parameter estimation technique using the classical sinusoidal forced oscillation wind tunnel test data. For small amplitude pitching motions the unsteady variation of loads is linear.[11,12] Hence, we linearize the proposed unsteady model at a certain mean angle-of-attack. This gives a linear relation between in-phase and out-of-phase derivatives of normal force coefficient. This linear relation is also true for some other models.[9] This equation is used to obtain time-scale of unsteady variations using small amplitude (3 degrees) forced oscillation (SAFO) data by weighted least squares method. In wind tunnel tests, some large amplitude pitching oscillation inputs excite higher order harmonics or nonlinear variation of unsteady normal force. Therefore, we classify the large amplitude wind tunnel test data into linear and nonlinear response sets for the purpose of parameter estimation. Then, the linear and nonlinear response parameters of the Volterra variational model are estimated separately. We find that this approach produces different results as compared to the commonly used approach of using the entire data-set for estimation of all the parameters simultaneously.

In second section we present an introduction to Volterra series and Volterra variational equations. In the same section, we present the generic unsteady aerodynamic model structure based on this theory. In the third section, we present parameter estimation of the Volterra variational model of unsteady aerodynamics

using dynamic wind tunnel test data. Some of the issues in parameter estimation using forced oscillation data are also highlighted. In the last section we present phenomenological interpretations of the parameters of the model and comparison with some other models proposed in literature.

II. Model structure based on Volterra variational equations

Use of Volterra series as a functional expansion of the response of dynamical system was first brought to light by N. Weiner in 1942. Subsequently, the so called 'Volterra-Weiner' theory was advanced further for identification of variety of nonlinear dynamical systems.[15] The theory is very rich for the purpose of modeling dynamic system using experimental data and for analytical predictions using the nonlinear model. In case of unsteady aerodynamics, data from dynamic and static wind tunnel tests are available and the model structure itself is unknown. We propose to obtain a generic model structure based on the so called Volterra variational equations, which is amenable to variety of dynamic wind tunnel test data for parameter estimation.

The Volterra series theory is widely used in biomedical and electrical engineering for modeling weakly nonlinear systems with memory.[14] In aerospace engineering the Volterra series based approaches have been used for modeling aero-elastic response;[16] reduced-order-modeling in CFD computations[17] and modeling aircraft nonlinear dynamics.[13,18] Direct identification of Volterra kernels is a complex task, especially for mechanical systems since it may be impractical to design experimental setup for special inputs like the Gaussian-white-noise. Therefore, we use an adaptation of the Volterra series called the Volterra variational equations which is useful for parametric modeling.[15]

We first present some fundamentals about Volterra series theory to orient the reader to mathematical basis of this approach. However, one can skip this to directly look at the model structure. Then, we present Volterra variational equations and the model structure.

A. Volterra series theory

The main advantage in use of Volterra series for modeling and analysis of nonlinear dynamical systems is its strong underlying analytical framework. The Volterra series offers a nonparametric approach to modeling nonlinear dynamical system and requires no specification of model structure.

Volterra series can be considered to be an extension of the linear systems theory concept of using convolution integral of impulse response and any continuous input to represent the system response. While for static nonlinear systems polynomial expansion would suffice, for nonlinear dynamical systems with memory, the input-output relation is in the form of an infinite series of multidimensional convolution integrals, as presented in Eq.(1).

$$y(t) = h_0(t) + \int h_1(\tau_1)u(t-\tau_1)d\tau_1 + \sum_{2}^{n}\int_0^\infty ... \int_0^\infty h_n(\tau_1,\tau_2,..\tau_n)\prod_{1}^{n} u(t-\tau_n)d\tau_n \tag{1}$$

where $y(t)$ is the system response to any arbitrary input $u(t)$. Term $h_n(\tau_1,...,\tau_n)$ is called the n-th order kernel of the Volterra series and represents the memory effect of the system. $h_0(t)$ is zero-input response of the system, and is usually a constant. $h_1(\tau_1)$ is the linear response kernel. In case of a linear systems it is the single input impulse response of the system. Higher-order kernels are important when there is significant influence of the past inputs on response.

The basic premise of Volterra series is that the response to any continuous, causal and time-invariant system to any arbitrary input can be exactly represented by the Volterra series. However, for the purpose of modeling physical systems the series is truncated to a finite number of terms. This truncated series is convergent for modeling a physical system with fading memory and bounded inputs, as shown by Boyd and Chua.[19] The bounds on inputs depend on physical properties of the system. Volterra series truncated to second or third degree kernels is useful to model weakly nonlinear dynamical systems. In any case, interpretation and identification of the kernels beyond third degree is a complex and foreboding task. Thus, application of Volterra series to model a nonlinear dynamical system boils down to identification of Volterra kernels.

Direct identification of the second or higher order Volterra kernels using experimental data requires some special inputs. Three major approaches are summarized here: (i) Kernel estimation of truncated Volterra series by using multiple impulse inputs and repeated experiments, (ii) parametric approximation of kernels

by expansion on orthogonal functions, and parameter estimation, (iii) determination of discrete Volterra kernels using high-order correlation functions and colored Gaussian inputs.[20] The experiments required for methods (i) and (iii) are difficult to implement for mechanical systems, while method (ii) requires estimation of very large number of parameters.

An equivalent representation of Volterra series in the form of differential equations is called the Volterra variational equations. Volterra variational equations is a more attractive option for modeling, as traditionally dynamical systems are modeled in state-space form and variety of analysis techniques are available. Moreover, this is a parametric representation of system dynamics and therefore yields to simple parameter estimation techniques using variety of dynamical experimental data.

B. Volterra variational equations

In this section we present derivation of the Volterra variational equations for a class of nonlinear dynamic system represented by Eq.(2), as available in Ref.([15]).

$$\begin{aligned} \dot{x}(t) &= a(x(t),t) + b(x(t),t)u(t),\ t \geq 0 \\ y(t) &= c(t)x(t) + y_0(t),\ x(0) = 0 \end{aligned} \tag{2}$$

where, $y_0(t)$ is the zero-input response. We present the derivations for single-input-single-output system, although it can be generalized to higher dimensional vectors. We assume that the system is linear-analytic so that its state derivative $\dot{x}$ can be expanded into power series of state-vector $x(t) \in \Re^1$ and scalar input $u(t) \in \Re^1$ as,

$$\begin{aligned} \dot{x}(t) &= A_1(t)x^1(t) + A_2(t)x^2(t) + A_3(t)x^3(t) + ... \\ &\quad + B_0(t)u(t) + B_1(t)x^1(t)u(t) + B_2(t)x^2(t)u(t) + ... \\ y(t) &= c(t)x(t) + y_0(t),\ x(0) = 0 \end{aligned} \tag{3}$$

Assume a general input $\gamma u(t)$, where γ is an arbitrary constant. Then, considering Volterra series representation, since it is a linear sum of the response due to each kernel $h_i(\tau_1, .., \tau_i)$ of the expansion, the response of the system is given by,

$$x(t) = \sum_{i=1}^{\infty} \gamma^i x_i(t) \tag{4}$$

where $x_i(t)$ is the internal-state corresponding to the kernel $h_i(\tau_1, .., \tau_i)$. Substituting Eq.(3) and Eq.(4) in the system dynamics Eq.(2), and comparing the coefficients of γ^n, we get Eq.(5). Here only first three terms of the infinite set of internal states are presented. These are called the Volterra variational equations.

$$\begin{aligned} \dot{x}_1(t) &= A_1(t)x_1(t) + B_0(t)u(t),\ x_1(0) = 0 \\ \dot{x}_2(t) &= A_1(t)x_2(t) + A_2(t)x_1^2(t) + B_1(t)x_1(t)u(t),\ x_2(0) = 0 \\ \dot{x}_3(t) &= A_1(t)x_3(t) + A_2(t)[x_1(t)x_2(t) + x_2(t)x1(t)] + A_3(t)x_1(t)^3 + \\ &\quad B_1(t)x_2(t)u(t) + B_2(t)x_1(t)^2u(t),\ x_3(0) = 0 \end{aligned} \tag{5}$$

This structure has some special features. Just like $h_1(\tau_1)$, the first state $x_1(t)$ represents linear response to any arbitrary input. The second and higher order states are significant only when the system dynamics is expected to be nonlinear. Differential equations of each state is a function of input and all lower order states only. This facilitates truncation of the set to a finite number of states. All the states have the same time-constant A_1, but the effective time-scale of the nonlinear system dynamics is modified by second and higher order internal states.

The nonlinear terms in the differential equations of higher order states can be selected to reduce the number of parameters to be identified. These nonlinear terms change the effective time-scale of variation of response when there is large-amplitude or high-frequency change in input. The Carleman linearisation approach[15] and Volterra-Gilbert equations[21] are other attractive options for nonlinear modeling of dynamic systems in the form of differential equations.

C. Model Structure Specification

Model structure specification is the first step in system identification process, but not independent of other steps. The model structure is based on experimental observations reported in the literature. The model structure is generic and therefore applicable to a variety of airframe configurations like Double-delta, Straked-delta etc. exhibiting complex flow phenomena. The specific model structure for a given aerodynamic coefficient can be determined during the process of parameter estimation using the forced oscillation wind tunnel test data as presented in the next section.

At high-angle-of-attack wing vortices dominate the aerodynamic forces and moments acting on the aircraft. At certain angle-of-attack these vortices breakdown on the wing surface and change the pressure distribution drastically. In static conditions, the vortex breakdown happens at an approximately fixed location on the wing. The normal force variation with angle-of-attack in static conditions are captured from the static wind tunnel test, called $Cz_{st}(\alpha)$. However, when the aircraft is pitching up ($\dot{\alpha} > 0$) or pitching down($\dot{\alpha} < 0$) in stall or post-stall angle-of-attack regimes, the vortex flow above the wing changes with a certain finite time-delay. This causes dynamic hysteresis in vortex breakdown location and therefore in variation of normal force and pitching moment coefficient.[22] Assume that this dynamic component of normal force over $Cz_{st}(\alpha)$, be denoted by $C_d(t)$. Therefore, the normal force variation for a maneuvering aircraft at a particular subsonic Mach number and zero side-slip is given by,

$$Cz(\alpha(t), \dot{\alpha}(t)) = Cz_{st}(\alpha(t)) + C_d(\dot{\alpha}(t), \alpha(t)) \tag{6}$$

In this structure, $C_d(\dot{\alpha}(t), \alpha(t))$ represents the unsteady aerodynamic effects or dynamic hysteresis. It is modeled using forced oscillation wind tunnel test data.

We model $C_d(t)$ in the form of truncated set of Volterra variational equations. For this system, $C_d(t)$ is the output and $\dot{\alpha}(t)$ is the input. The vortex-flow readjustment happens with time-delay and this delay is reflected in $Cz(t)$ in pitching motion. It is known that $Cz(t)$ depends on both $\dot{\alpha}$ and the initial α_0 when ramp pitch-up is applied. Thus, $C_d(t)$ depends on pitching motion history and is a system with memory. $Cz(t)$ converges to Cz_{st} in a finite time when ($\dot{\alpha} = 0$). This system has a stable equilibrium point $[(C_d(t), \dot{\alpha}(t)) = (0, 0)]$ for the entire $\alpha \in [-90^o, 90^o)$ range. Also, the input $\dot{\alpha}$ has bounds based on possible aircraft open-loop flight conditions. These bounds should be considered while deciding the frequencies of the dynamic wind tunnel tests. Therefore, $C_d(t)$ satisfies the conditions of convergence of a truncated form of Volterra variational model as proved by Boyd and Chua.[19]

The exact number of internal-states to be used in modeling can be identified using forced oscillation data and is an iterative process. We propose the model structure for $C_d(t)$ as,

$$\begin{aligned}
C_d(t) &= x_1(t) + x_2(t) + x_3(t) \\
\dot{x}_1(t) &= a(t)x_1(t) + K_1(t)u(t),\ x_1(0) = 0 \\
\dot{x}_2(t) &= a(t)x_2(t) + K_{21}(t)x_1^2(t) + K_{22}(t)x_1(t)u(t),\ x_2(0) = 0 \\
\dot{x}_3(t) &= a(t)x_3(t) + 2K_{21}(t)x_1(t)x_2(t) + K_{31}(t)x_1^3(t) + \\
&\quad K_{22}(t)x_2(t)u(t) + K_{32}(t)x_1^2(t)u(t),\ x_3(0) = 0
\end{aligned} \tag{7}$$

In the above structure, parameters are function of time. It is known from various wind tunnel and water tunnel experiments that the time-constant of delay in vortex flow readjustment is a function of (α, β). Hence, in model Eq.(7) we map the parameters to be function of (α, β). This is valid because in any maneuver (α, β) can be mapped as a function of time. $Cz_{st}(t)$ is mapped similarly. We can also include the Mach dependence of the normal force by mapping the model parameters as a function of Mach number. Therefore the generic model structure for unsteady aerodynamic modeling is given by Eq.(8).

$$\begin{aligned}
Cz(\alpha(t), t) &= Cz_{st}(\alpha(t)) + C_d(t) \\
C_d(t) &= x_1(t) + x_2(t) + x_3(t) \\
\dot{x}_1(t) &= a(\alpha(t))x_1(t) + K_1(\alpha(t))\dot{\alpha}(t),\ x_1(0) = 0 \\
\dot{x}_2(t) &= a(\alpha(t))x_2(t) + K_{21}(\alpha(t))x_1^2(t) + K_{22}(\alpha(t))x_1(t)\dot{\alpha}(t),\ x_2(0) = 0 \\
\dot{x}_3(t) &= a(\alpha(t))x_3(t) + 2K_{21}(\alpha(t))x_1(t)x_2(t) + K_{31}(\alpha(t))x_1^3(t) + \\
&\quad K_{22}(\alpha(t))x_2(t)\dot{\alpha}(t) + K_{32}(\alpha(t))x_1^2(t)\dot{\alpha}(t),\ x_3(0) = 0
\end{aligned} \tag{8}$$

where we have not indicated (β, M) dependence for the sake of brevity. In this structure, x_1 indicates the linear response of unsteady aerodynamics to $\dot{\alpha}(t)$ input, and $K_1(t)$ is the dynamic gain parameter. The magnitude of x_2 is depends on x_1 and $\dot{\alpha}(t)$. It is likely to be significant when there is large amplitude change in α or $\dot{\alpha}$.

This model structure is suitable to build a full-alpha range aerodynamic model by integrating it with the classical look-up table type low-alpha aerodynamic model. In the lookup table aerodynamic model damping derivative or out-of-phase derivative is used in the form of look-up table. In high-alpha regime, the damping derivative is a function of frequency and amplitude of oscillations in pitching motion. Hence, the look-up tables type aerodynamic model is invalid in high angle-of-attack flight envelope.[4] In the proposed model structure, the dynamic component is incremental to the load in quasi-steady flow-state. Therefore, due to Eq.(6), it is possible to integrate the proposed model with the look-up table type quasi-steady aerodynamic model using the assumption in Eq.(9). In low-alpha region $K_1(\alpha) \simeq 0$ and $Cz_q(\alpha)$ is used to model the quasi-steady effect; while in high-alpha region, $Cz_q(\alpha) \simeq 0$ and unsteady aerodynamics is characterized by $C_d(t)$.

$$Cz(\alpha(t), t) = Cz_{st}(\alpha(t)) + Cz_q(\alpha(t)) \cdot q\bar{c}/2V + C_d(t) \tag{9}$$

For the purpose of real-time flight simulation, tables of the model parameters as a function of (α, β, M) can be incorporated with other tables; while the differential equations of the $C_d(t)$ model can be augmented to the aircraft 6DOF dynamics equations for numerical integration. The model also requires very low computational power.

If digression from the rigorous analytical proof of convergence of the model to Volterra series is permitted, one can also choose nonlinear terms in the second and third state equations. This will be necessary, if one wishes to reduce the number of parameters to be estimated. Selection of terms may not be empirical or ad hoc, but the interpretation of the standard kernel can be utilized. For example, some mathematical interpretation of the nonlinear terms in the second state equation was provided by Omran and Neuman.[23] Note that, there exists rigorous proof for convergence of the model with only bilinear nonlinearity term $K_{21}x_1(t)u(t)$ in the second state differential equation.[15] It is not necessary to have only linear form of the input signal in the differential equations. However, the kernel for quadratic and higher degree input contains a singularity, which may be invalid for physical systems. Moreover, for such cases convergence of the truncated Volterra series representation cannot be assured.

III. Parameter Estimation Techniques

Classically small amplitude and large amplitude sinusoidal forced oscillation test data are used for parameter estimation of the unsteady model by Output error method, and all the parameters are estimated simultaneously. In this paper, we introduce a new approach to parameter estimation in which we classify the wind tunnel test data based on nonlinear characteristics of unsteady variation.

High Performance Research Aircraft (HPRA) is a delta-wing tail-less aircraft. The data were obtained from static and forced oscillation wind tunnel tests in an industrial grade wind tunnel. Small amplitude forced oscillation tests were conducted at mean angle-of-attack from -5 to 70 degrees at an interval of 5 degrees, for three frequencies of sinusoidal input $(0.5, 1, 1.5)Hz$. Then, the in-phase and out-of-phase derivatives are obtained by harmonic analysis of the raw data. Large amplitude forced oscillation (LAFO) test data at two amplitudes $(15^o, 25^o)$ and three frequencies $(0.5, 1, 1.5)Hz$ was also obtained. We obtain an accurate model of $C_Z(t)$ for HPRA using this data.

A. General Approach to Parameter Estimation

We link parameter estimation of the Volterra variational model with its mathematical structure, available wind tunnel test data and physical characteristics of unsteady aerodynamics. For this, one may have to perform iterations of the cycle: (i) model structure determination, (ii) parameter estimation and (iii) validation. In this section we present a general approach that can be adopted for parameter estimation of the Volterra variational model of any aircraft using small and large amplitude forced oscillation test data.

The unsteady aerodynamics at high angle-of-attack is both amplitude and frequency dependent phenomenon.[12] It is dominant in the stall and post-stall angle-of-attack regimes. Generally, unsteady variation in normal force coefficient is linear for pitch oscillations of small amplitude $(\Delta\alpha < 5^o)$ and low frequency.[11,12]

Therefore small amplitude forced oscillation test data should be used to estimate the model parameters representing linear response characteristics. $x_1(t)$ corresponds to linear response of the system, while $x_2(t)$ is significant only for nonlinear response. Hence, we consider the model structure in equations (8),(9) with only $x_1(t)$, to estimate $a(\alpha)$ and $K_1(\alpha)$. The small amplitude forced oscillation test data is available as in-phase and out-of-phase derivatives for three frequencies at certain mean angle-of-attack α_0. Hence, we shall linearize the linear response model of $C_Z(t)$ at α_0 and co-relate it with the SAFO data.

In a small amplitude forced oscillation test, the wind tunnel model is oscillated in pitch in a sinusoidal motion given by, $\alpha(t) = \alpha_0 + \Delta\alpha sin(\omega t)$. The measured normal force coefficient $Cz(t)$ is converted to in-phase derivative $Cz_\alpha(\alpha_0)$ and out-of-phase derivative $Cz_{\dot\alpha}(\alpha_0)$ by harmonic analysis of the time-series data. Hence, the steady-state response of the normal force coefficient can be stated as,

$$Cz(t) = Cz_0(\alpha_0) + Cz_{\alpha,\omega_0}(\alpha_0)\Delta\alpha sin(\omega t) + Cz_{\dot\alpha,\omega_0}(\alpha_0)\frac{\omega\bar c}{2V}\Delta\alpha cos(\omega t) \tag{10}$$

where, $\bar c$ is mean aerodynamic chord and V is the constant air speed.

Now we consider the response of the Volterra-variational model given by equations (8),(9). In small amplitude pitching motion, the model response is approximately linear representing the system characteristics at α_0. Hence, we consider only first state of the model to be significant. The output $C_d(t)$ to the input $\dot\alpha = \Delta\alpha\omega cos(\omega t)$ is given by,

$$\begin{aligned}\dot C_d(t) &= \dot x_1(t)\\ &= a(\alpha_0)x_1(t) + K_1(\alpha_0)\dot\alpha(t)\\ &= a(\alpha_0)C_d(t) + K_1(\alpha_0)\frac{\omega\bar c}{2V}\Delta\alpha cos(\omega t)\end{aligned} \tag{11}$$

Solving this differential equation, we get the steady-state solution as

$$C_d(t)_{ss} = \frac{K_1\Delta\alpha\omega^2}{a^2+\omega^2}sin(\omega t) - \frac{K_1\Delta\alpha\omega a}{a^2+\omega^2}cos(\omega t) \tag{12}$$

We linearize Eq.(9) at α_0 and then substitute the above equation to get the overall normal force coefficient response of the model as,

$$\begin{aligned}Cz(t)_{ss} &= Cz_0(\alpha_0) + Cz_{\alpha,st}(\alpha_0)\Delta\alpha sin(\omega t) + Cz_q(\alpha_0)\frac{\omega\bar c}{2V}\Delta\alpha cos(\omega t)\\ &+ \frac{K_1\omega^2}{a^2+\omega^2}\Delta\alpha sin(\omega t) - \frac{K_1 a}{a^2+\omega^2}\frac{\omega\bar c}{2V}\Delta\alpha cos(\omega t)\end{aligned} \tag{13}$$

Note that, in a forced oscillation test $\dot\alpha(t) = q(t)$. Finally, comparing the steady state response from the experimental data Eq.(10) and model output Eq.(13), we get the relation between model parameters and experimental derivatives as,

$$\begin{aligned}Cz_{\alpha,\omega_0}(\alpha_0) &= Cz_{\alpha,st}(\alpha_0) + \frac{K_1\omega^2}{a^2+\omega^2}\\ Cz_{\dot\alpha,\omega_0}(\alpha_0) &= Cz_q(\alpha_0) - \frac{K_1 a}{a^2+\omega^2}\end{aligned} \tag{14}$$

Rearranging the terms in Eq.(14), we get a linear relation between $Cz_{\alpha,\omega_0}(\alpha_0)$ and $Cz_{q,\omega_0}(\alpha_0)$ as,

$$Cz_{\alpha,\omega_0}(\alpha_0) = aCz_{\dot\alpha,\omega_0}(\alpha_0) + [Cz_{\alpha,st}(\alpha_0) + K_1 - Cz_q(\alpha_0)] \tag{15}$$

Using Eq.15, we can estimate $a(\alpha_0)$ by Least squares error technique. The estimated values of $a(\alpha_0)$ for HPRA is presented in next section. Equations 14,15 are similar to the ones obtained for linearized form of some other models.[6,7,24]

It is difficult to estimate the dynamic gain parameter $K_1(\alpha)$ accurately using SAFO data only. It can be estimated using the modified 2-step regression approach presented in the next section. The results obtained match the SAFO data very well. However, the 2σ bound on it is very large at certain angles-of-attack. Hence, this estimate is not sufficiently accurate for the purpose of high-fidelity simulation and analysis. It can at best be used for qualitative studies in the preliminary design phase if only small amplitude forced

oscillation test data is available. Also, we cannot estimate it using time-series data from SAFO tests because of low signal-to-noise ratio. Therefore, we need to use the time-series data from LAFO tests for which linear response is the dominant characteristic.

We propose a *split identification* approach to estimate the model parameters using LAFO data. The variation of an aerodynamic coefficient due to sinusoidal inputs can be linear or nonlinear depending on amplitude and frequency of the input. So, we should first classify the LAFO data into linear response set and nonlinear response set, and use the former for estimation of $K_1(\alpha)$. The estimated values of $(a(\alpha), K_1(\alpha))$ are then fixed, and $K_{21}(\alpha), K_{22}(\alpha)$ are estimated from the nonlinear response data set by output error method. If the two-state model is not able to produce a good fit to the given data or better accuracy is desired, the third internal state should be considered in the model structure.

The estimated values of $K_1(\alpha)$ from SAFO and LAFO linear response set are compared. A consistency between the estimates provides validation, as same results are obtained using two different data sets. A simplistic approach could be to utilize the entire data-set to estimate all the model parameters simultaneously by Output-error method. $K_1(\alpha)$ obtained from this approach will be different from that obtained by split-identification approach proposed earlier. $K_1(\alpha)$ estimated using this approach can produce erroneous results in small amplitude simulations as it is tuned to produce the nonlinear response characteristics accurately.

There is very little research done on data gathering and parameter estimation side of system identification of unsteady aerodynamics. A novel rig to implement multiple degree-of-freedom maneuver in a wind tunnel has been proposed.[25] Such a rig can be used to obtain data from dynamic experiments for the purpose of modeling. Another novel method is to use a broadband input for both, model parameter estimation and validation.[26] The Volterra variational model presented in this paper offers rich mathematical and physical interpretations useful for this purpose.

B. Linear Model Parameter Estimation

The linear response model parameters, $a(\alpha_0)$ and $K_1(\alpha_0)$ are estimated in two steps, following the method called 2-step regression method.[6] The first step is to estimate $a(\alpha_0)$ using linear relation between in-phase and out-of-phase derivatives. This linear relation was proved in section A. Estimated values of $a(\alpha_0)$ for HPRA are fairly accurate as presented in Table 1.

Table 1. Time-constants identified from SAFO by regression

α_0	25	30	35	40	45	50	55	60
a(α_0)	-7.408	-6.9751	-5.6491	-3.7683	-4.8504	-9.4858	-18.8751	-7.5178
$2s(\hat{a})$	13.4377	12.8882	4.247	0.1841	0.4322	1.5467	35.8374	4.0051

The second step is to estimate $K_1(\alpha)$ using Eq.(14) and SAFO data. The value of $Cz_{\alpha,st}(\alpha_0)$ is obtained from the static wind tunnel test by curve-fitting, and used as the constraint equation. $Cz_{\alpha,\omega_0}(\alpha_0)$ and $Cz_{\dot{\alpha},\omega_0}(\alpha_0)$ are available from SAFO test data for $\alpha_0 \in [-5^o - 75^o]$. $Cz_q(\alpha_0)$ and $K_1(\alpha_0)$ are the unknown parameters in the Eq.(14), and are estimated by Least Squares error (LS) method. We find that the estimates obtained do not produce a good fit to data, as seen in in Fig.(1b). This fallacy in estimation of $K_1(\alpha)$ by 2-step regression approach can be explained. The amplitude of 3 degrees in forced oscillation test implies that the dynamic tests cover angle-of-attack range of 6 degrees. In the near-stall and pot-stall regimes, there is drastic change in value of $Cz_{\alpha,st}(\alpha)$ over 6 degrees range. Hence, $Cz_{\alpha,st}(\alpha_0)$ represents an average value of $Cz_{\alpha,st}(\alpha)$ over the test angle-of-attack range, with some deviation. Therefore, using a constant value $Cz_{\alpha,st}(\alpha_0)$ in estimation of $K_1(\alpha_0)$ is incorrect. The static nonlinearity in $Cz(\alpha)$ cannot be ignored. This causes error in parameter estimation if we consider $Cz_\alpha(\alpha_0)$ as a constraint. We introduce an innovation here allowing more robust identification procedure.

We use Weighted Least Squares (WLS) technique with the weighting function given by inverse of the covariance matrix of residuals. We use $Cz_{\alpha,st}$ value as a measurement, with an appropriate value of covariance to represent variations in its value over the range of oscillation in angle-of-attack. Now, we estimate $K_1(\alpha)$ by applying weighted least squares algorithm, and iterate it by updating the covariance matrix of residuals after each iteration. We find that this recursion converges, and the estimates obtained produce very good match with wind tunnel test data, as seen in Fig.(1a). Thus, the modified 2-step regression presented in this paper produces robust estimate using 3 degree amplitude forced oscillation test data.

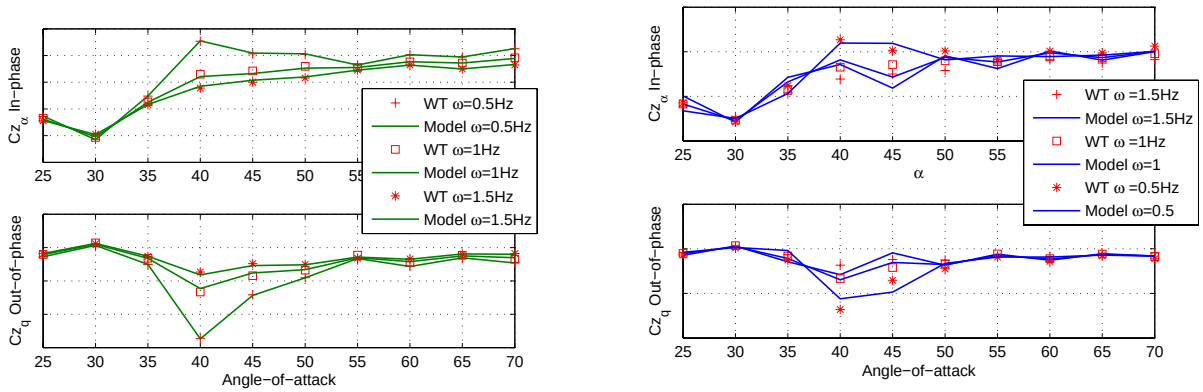

(a) Weighted Least Squares estimate

(b) 2-Step regression estimate

Figure 1. Results of linear response parameter estimates obtained by WLS and LS methods

When we use the single state Volterra variational model to simulate large amplitude oscillations in pitch, variation in $Cz(t)$ obtained do not match the wind tunnel test data. Therefore, as explained earlier, we estimate $K_1(\alpha)$ using the linear response set of the large amplitude forced oscillation test data. As expected, this linear response Volterra variational model fails to produce a good match with nonlinear response set pitching oscillation of amplitude 25^o, as seen in Fig.(2). The match is qualitatively good, but inaccurate in the angle-of-attack ranges $[25^o\ 35^o]$ in pitch-down and $[45^o\ 55^o]$ in pitch up. Therefore, a higher order model or a nonlinear response model is required to produce accurate results.

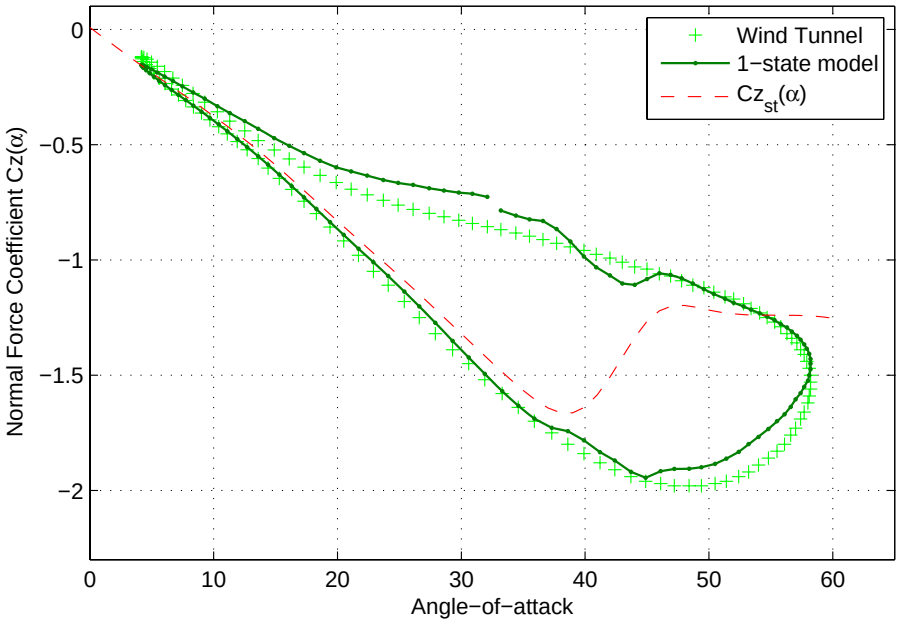

Figure 2. Simulation of large amplitude motion using single-state Volterra variational model

C. Nonlinear Model Parameter Estimation

The parameters for nonlinear response characteristics can be obtained using the large amplitude forced oscillation test data by two approaches : (i) *Direct approach* : use all the available LAFO data with the 2-

state model to simultaneously estimate (K_1, K_{21}, K_{22}) (ii) *Split identification approach* : Estimate K_1 using the linear-response-data-set and then estimate $K_{21}(\alpha)$ and $K_{22}(\alpha)$ using the nonlinear-response-data-set.

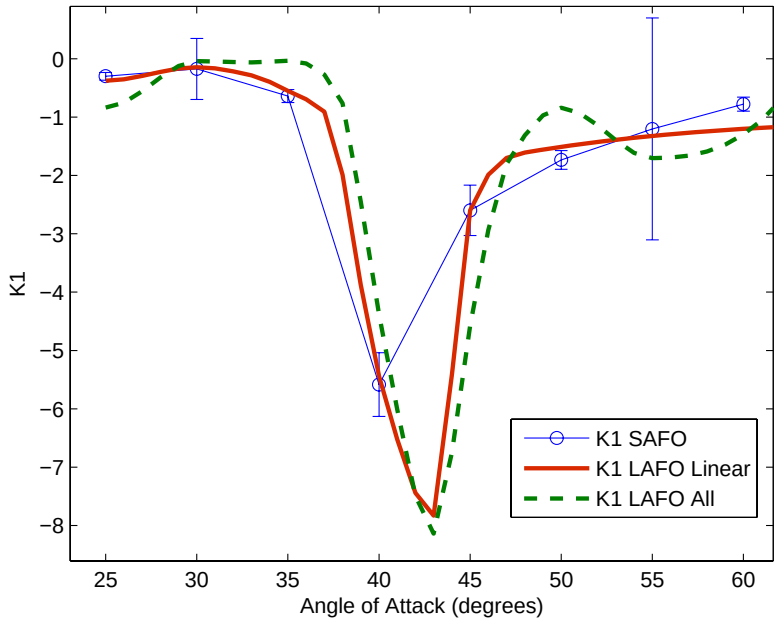

Figure 3. Comparison of dynamic gain parameter (K1) estimated by three methods

To identify the parameters (K_1, K_{21}, K_{22}) by the Direct approach is a straightforward task. It seems to produce a good match with the experimental data. However, the question arises whether this is realistic? In simultaneous estimation of (K_1, K_{21}, K_{22}), contribution of linear and nonlinear terms to the response can compensate for each other. Due to this, the linear response characteristics during low-amplitude or low-frequency pitching motion are likely to be erroneous. One way to check this is by comparing the estimated $K_1(\alpha)$ from direct identification approach and modified 2-step regression. As seen in Fig.(3) the estimates for these two cases do not compare well.

$K_1(\alpha)$ estimated from the LAFO linear response data set is consistent with the estimates from modified 2-step regression, as seen in Fig.3. $K_1(\alpha)$ curve passes through the 2σ bounds of the $K_1(\alpha)$ estimated by modified 2-step regression approach. Also, note that the trends in $K_1(\alpha)$ obtained from both direct and split identification approaches are similar. This model estimated by Split identification approach produces good match with the variety of wind tunnel data of different amplitude and frequency of oscillation in pitching motion, as seen in Fig.(4). This shows the robustness of the model to simulate unsteady effects of normal force coefficient for wide range of amplitude and frequency of pitching motion.

IV. Discussion of Results

A. Phenomenological Interpretations

The Volterra variational model offers rich mathematical and phenomenological interpretations. It is consistent with physical phenomena associated with vortex flows affecting aerodynamic loads as reported in literature. This further increases the confidence of engineers using the mathematical model. The physical interpretation of model parameters is useful for comparing the features of different configurations in preliminary design phase.

The response of flow-separation point or the vortex breakdown location to small amplitude step change in angle-of-attack is linear, with a finite time-lag that has been estimated by many researchers.[3] As shown in section III A, the Volterra variational model with one-internal state produces linear response to small amplitude motion, and the time-constant of variation in $C_Z(t)$ can be estimated. However the relation between the two time-constants is yet to be discovered.

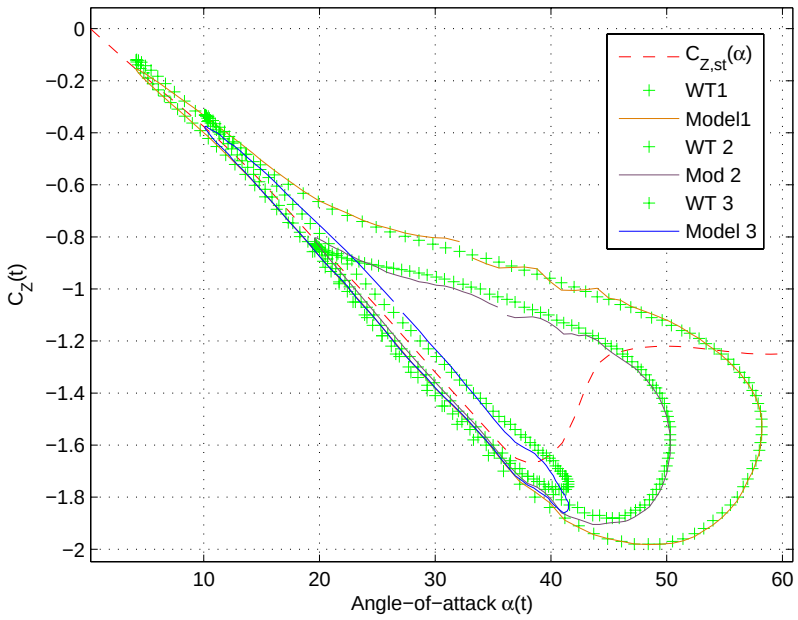

Figure 4. Simulation using 2-states Volterra variational model ($WT1$: $\alpha_0 = 25^0, \Delta\alpha = 15^0, f(Hz) = 1.5$), ($WT2$: $\alpha_0 = 35^0, \Delta\alpha = 15^0, f(Hz) = 1.0$),($WT3$: $\alpha_0 = 30^0, \Delta\alpha = 25^0, f(Hz) = 1.0$)

For large amplitude oscillations of angle-of-attack the unsteady variation of aerodynamic loads is nonlinear.[11] This is because the time-constant depends on the direction of pitching motion of the aircraft and it is also a function of both amplitude and frequency of oscillation.[12] These physical features of unsteady load variation can be explained using the two-state Volterra variational model in Eq.(8). For this model, we can approximate the differential equation for $C_d(t)$ as,

$$\begin{aligned} \dot{C}_d(t) &= \dot{x_1}(t) + \dot{x_2}(t) \\ &= a(\alpha)x_1(t) + K_1(\alpha)\dot{\alpha}(t) + a(\alpha)x_2(t) + K_{22}(\alpha)x_1(t)\dot{\alpha}(t) + K_{21}(\alpha)x_1(t)^2 \\ &\simeq [a(\alpha) + K_{22}(\alpha)\dot{\alpha}(t) + K_{21}(\alpha)C_d(t)]C_d(t) + K_1(\alpha)\dot{\alpha}(t) \end{aligned} \tag{16}$$

where $\alpha(t)$ is replaced by α. As explained earlier, $x_2(t)$ is significant when either $\dot{\alpha}(t)$ or $x_1(t)$ is significantly large. Therefore, contribution of $x_1(t)$ to $C_d(t)$ is dominant, as also seen in simulations. So, we approximate $C_d = x_1$, and then Eq.(16) is approximately linear in $C_d(t)$. Then the effective time-constant for variation in $C_d(t)$ is : $[a(\alpha) + K_{22}(\alpha)\dot{\alpha} + K_{21}(\alpha)C_d(t)]$. From this expression, we observe that the effective time-constant depends on frequency of pitching motion and magnitude of the dynamic component of normal force $C_d(t)$. In the stall and post-stall regimes, the magnitude of $C_d(t)$ is very large and this makes the effective time-constant function of amplitude of oscillation. It is also evident that the time-constant of the model depends on direction of pitching motion. Thus, time-constant of the Volterra variational model is consistent with its features observed in experiments.

Reisenthel, Xei and Gurusul observed in their experiment on effect of oscillating fin on vortex breakdown location that the time-constant for upstream motion of vortex breakdown location is larger than that for downstream motion.[27] Upstream motion of vortex breakdown location corresponds to pitch-up and downstream motion to pitch-down. Therefore, time-constant for pitch-up is larger than that in pitch-down motion. This phenomena is demonstrated by the proposed model Eq.(16), if parameter estimation gives $K_{21}(\alpha) < 0$.

The linearized equations of the Volterra variational model in Eq.(15) are similar to that obtained by Abramov, Goman, and Khrabrov.[6] From this similarity, we also find that $K_1(\alpha) = \Delta Cz(\alpha) = Cz_{att}(\alpha) - Cz_{st}(\alpha)$. Here, $Cz_{att}(\alpha)$ is the normal force with no flow separation or vortex breakdown on the wings, and it can be obtained from the Polhamus suction-analogy method. Therefore, $K_1(\alpha)$ actually represents the loss in normal force due to vortex breakdown on the wings.

The model structure and the parameter estimation procedure proposed in this paper are also phenomeno-

logical. $C_d(t)$ converges to zero when the aircraft moves out of the stall regime. For small amplitude motion, the variation is linear and $x_2 = 0$, while for large amplitude motion in the near-stall and post-stall angle-of-attack regimes x_2 is significant. It excites second harmonic of the input frequency in $C_Z(t)$ response. Thus, the model is consistent with the observations from wind tunnel tests.[10,11]

There exists literature on systematic analysis of the nonlinear terms in the second state. For a sinusoidal input of frequency ω, the steady-state response of the two term model brings 2nd harmonic into the picture. Bilinear and quadratic nonlinearity terms in $\dot{x}_2$ equation modify the steady state and initial response characteristics differently, as elaborated in a recent work by Omran and Neuman.[23] The bilinear term does not modify the time-scale and therefore initial response, but changes the steady state. The quadratic term changes the settling time of the response. Therefore, a combination of both these terms produces amplitude and rate dependence of the effective time-constant of unsteady variation. This concept needs to be developed further.

B. Comparison with Other Approaches

As demonstrated earlier, the linearized form of Volterra variational model in Eq.(14) is equivalent to the linearised form of the state-space model[5] and the general nonlinear differential equation approach.[9] Thus, the linearised form of Volterra variational model is consistent to linear response characteristics of other models. However, high-angle-of-attack unsteady aerodynamics is nonlinear in nature with respect to time variations in $C_Z(t)$ as evident from the Power-spectrum-density maps of aerodynamic load and pressure variations data obtained in wind tunnel tests.[10–12] Therefore, nonlinear modeling is more important and the Volterra variational model is a mathematically rigorous and phenomenologically rich approach.

The major nonlinear unsteady aerodynamic modeling approaches presented in literature are : (1) state-space approach by Goman and Khrabrov[5] (2) Nonlinear indicial approach,[7,28] and (3) Nonlinear differential equation approach by Abramov, Goman and Khrabrov.[6] The nonlinear indicial approach, after several simplifications, reduces to the form of Eq.(16) as presented in Ref.([7]). This model structure is exactly equivalent to the single-state Volterra variational model. Klein and Murphy's concept of assuming the model parameters as a polynomial function of alpha can also be used in Volterra variational modeling. However, this assumption restricts the variation of parameters to be smooth while in reality they may vary in a nonlinear manner. The state-space model performs very well in simulation of wind tunnel and flight test maneuvers,[5] but it cannot explain the excitation of higher-order harmonics in aerodynamic load response to sinusoidal input. Abramov and Goman's method of using cubic polynomial of the dynamic component of aerodynamic load, in effect, gives rise to second and third harmonics in the response. This is not easily evident in their model. Many other nonlinear models introduce nonlinearity in an ad-hoc manner with no firm mathematical grounding. The nonlinear response characteristics appear in the form of corrections, in the Volterra variational model. This is intuitive and useful for analysis.

V. Conclusions

The modeling approach presented in this paper is generic and hence useful to model aerodynamic characteristics specific to any given aircraft. The capability of the model structure needs to be tested by application of this approach to data from similar delta-wing aircrafts as well as transport aircrafts. A number of approximation techniques that simplify the kernel identification process are also available. There are papers that deal with the physical interpretation of Volterra kernels, especially for physiological systems, which should be utilized for analytical predictions. Any system identified is unreliable unless it is validated. The response of this model to generic non-sinusoidal input should be validated from wind tunnel and water tunnel tests. This method offers new physical and mathematical insights which can be further probed using some of the novel wind tunnel techniques.

Acknowledgments

Authors wish to thank Mr.Shyam Chetty for his encouragement to undertake this research. The first author also thanks Dr.Abhay Pashilkar, Dr. Nikolay Abramov and Dr. Amitabh Saraf for their support and guidance.

References

[1]Heller, M., Holmberg, J., and David, R. P., "Significance of Unsteady Aerodynamic Effects in F/A-18C/D Pitching Moment," *AIAA Atmosperic Flight Mechanics Conference and Exhibit*, AIAA 2006-6485, Keystone, Colorado, 2006.

[2]Foster, J., Cunningham, K., Fremaux, C., Shah, G., Stewart, E., and et. al., R. R., "Dynamics Modeling and Simulation of Large Transport Airplanes in Upset Conditions," *AIAA Guidance, Navigation, and Control Conference and Exhibit*, AIAA 2005-5933, San Francisco, California, 2005.

[3]Gursul, I., "Review of Unsteady Vortex Flows over Slender Delta Wing," *Journal of Aircraft*, Vol. 42, No. 2, 2005, pp. 299–319.

[4]Greenwell, D., "Difficulties in the Application of Stability Derivatives to the Manoevering Aerodynamics of Combat Aircraft," *International Conuncil of Aeronautical Sciences*, AIAA-ICAS, Melbourne, Australia, 1998, pp. 1–12.

[5]Goman, M. G. and Khrabrov, A. N., "State-space representation of Aerodynamic Characteristics of an Aircraft at High-angle-of-attack," *AIAA Journal of Aircraft*, Vol. 31, No. 5, 1994, pp. 1109–1115.

[6]Abramov, N., Goman, M., and Khrabrov, A., "Aircraft Dynamics at High Incidence Flight with Account of Unsteady Aerodynamic Effects," *AIAA Atmosperic Flight Mechanics Conference and Exhibit*, AIAA 2004-5274, Providence, Rhode Island, 2004.

[7]Klein, V. and Murphy, P. C., "Estimation of Aircraft Nonlinear Unsteady Parameters From Wind Tunnel Data," NASA-TM 1998-208969, NASA Langley Research Centre, Hampton, VA, December 1998.

[8]Kyle, H., Lowenberg, M., and Greenwell, D., "Comparative Evaluation of Unsteady Aeordynamic Modeling Approaches," *AIAA Atmosperic Flight Mechanics Conference and Exhibit*, AIAA 2004-5272, Providence, Rhode Island, 2004.

[9]Greenwell, D., "A review of Flight Dynamic Modeling for Flight Dynamics of Manoeuvrable Aircraft," *AIAA Atmosperic Flight Mechanics Conference and Exhibit*, AIAA 2004-5276, Providence, Rhode Island, 2004.

[10]Cunnigham, A. M. and den Boer, R. G., "Low-speed Unsteady Aerodynamics of Pitching Straked Wing at High Incidence-PartI:Test Program," *Journal of Aircraft*, Vol. 27, No. 1, 1990, pp. 23–30.

[11]Cunnigham, A. M. and den Boer, R. G., "Low-speed Unsteady Aerodynamics of Pitching Straked Wing at High Incidence-PartII:Harmonic Analsysis," *Journal of Aircraft*, Vol. 27, No. 1, 1990, pp. 31–41.

[12]Tristrant, D., "Analysis of Nonlinear and Unsteady Data for Mathematical Modeling," *Cooperative Program on Dynamic Wind Tunnel Experiments of Manoeuvring Aircraft*, AGARD AR-305, 1996.

[13]Omran, A. and Newman, B., "Peicewise Global Nonlinear Modeling and Charactirisation of Aircraft Dynamics," *Journal of Guidance Control and Dynamics*, Vol. 32, No. 3, 2005, pp. 749–759.

[14]Marmerelis, V. Z., *Nonlinear Dynamic Modeling of Physiological Systems*, Wilay-IEEE, 2004.

[15]Rugh, W. J., *Nonlinear System Theory: The Volterra/Weiner Approach*, The John Hopkins University Press, 1981.

[16]W.Silva, "Identification of Nonlinear Aeroelastic Systems Based on the Volterra Theory: Progress and Opportunitie," *Nonlinear Dynamics*, Vol. 39, 2005, pp. 25–62.

[17]Reisenthel, P. H., "Application of Volterra functions to X-31 Aircraft model Motion," *AIAA Applied Aerodynamics Conference*, AIAA 2009-3269, San Antonio, Texas, 2009.

[18]Marques, "Application of Volterra functions to X-31 Aircraft model Motion," *American Control Conference*, IEEE, Minnepolis, MN, 1987.

[19]Boyd, S. and Chua, L. ., "Fading Memory and the Problem of Approximating Nonlinear Operators with Volterra Series," *IEEE Transactions On Circuits and System*, , No. 11, 1985, pp. 1150–1161.

[20]Billings, S. A., "Identification of Nonlinear Systems - A Survey," *IEE Proceedings D Control Theory and Applications*, Vol. 127, Nov 1980, pp. 272–285.

[21]Gilbert, E. G., "Functional Expansions for the Response Nonlinear Differential Systems," *IEEE Transactions On Automatic Control*, , No. 6, 1977, pp. 909–921.

[22]Pelletier, A. and Nelson, R., "The Unsteady Aerodynamics of Slender Wings and Aircrafts undergoing Large Amplitude Manuevers," *Progress in Aerospace Sciences*, Vol. 39, 2003, pp. 189–248.

[23]Omran, A. and Neuman, B., "Nonlinear Cause.Effect Analysis for a Second Order System using Volterra Kernels," *American Control Conference*, AACC, Baltimore, MD, USA, 2010, pp. 2706–2711.

[24]Abramov, N., Goman, M., Greenwell, D., and Khrabrov, A., "Two Step Regression Method for Identification of High-Incidence Unsteady Aerodynamic Model," *AIAA Atmosperic Flight Mechanics Conference and Exhibit*, AIAA 2001-4080, Providence, Rhode Island, 2001.

[25]Pattison, J., Lowenberg, M., and Goman, M., "A Multiple Degree-of-Freedom Rig for Wind Tunnel determination of Dynamic data," *AIAA Atmosperic Flight Mechanics Conference and Exhibit*, AIAA 2009-5727, Chicago, Illinois, 2009.

[26]Murphy, P. C. and Klein, V., "Validation of Methodology for Estimating Aircraft Unsteady Aerodynamic Parameters from Dynamic Wind Tunnel Tests," *AIAA Atmosperic Flight Mechanics Conference and Exhibit*, AIAA 2003-5397, Austin, Texas, 2003.

[27]Reisenthel, P., Xie, W., and Gurusul, I., "An analysis of Fin Motion Induced Vortex Breakdown," *37th AIAA Aerospace Sciences Meeting and Exhbit*, No. 99-0316, AIAA, Reno, NV, 1999.

[28]Resisenthel, P. H., "Development of Nonlinear Indicial Model for Menuvering Fighter Aircraft," *AIAA Atmosperic Flight Mechanics Conference and Exhibit*, AIAA 1996-0896, 1996.

Symposium on Applied Aerodynamics and Design of Aerospace Vehicle (SAROD 2013)
November 21-23, 2013, Hyderabad, India

Mathematical Modeling of Abrupt Wing Stall of a Generic Tailless delta wing Aircraft for Flight simulation

M. Deva Prakash*, Mallesh Bommanahal+, Amitabh Saraf*

* – Scientists, Integrated Flight Control Systems Directorate, Aeronautical Development Agency, Bangalore-560017
+ – Scientist, Flight Mechanics & Control Division, National Aerospace Laboratories, Bangalore – 560017
(email: malleshb@nal.res.in , devaprakash@nal.res.in)

ABSTRACT

Abrupt Wing Stall occurs on delta wing aircrafts at high angle-of-attack and high subsonic Mach number flight conditions. Fighter aircrafts enter this region of the flight envelope in high-energy combat and hence it is important to evaluate and mitigate this phenomenon. It occurs due to unsteady motion of shock pockets on the wing, resulting in abrupt lateral-directional motions. This phenomenon is difficult to predict reliably using wind tunnel experiments, and hence extensive simulation studies are essential to evaluate aircraft performance and safety in this flight condition. We developed a comprehensive model of this phenomena using Free-to-roll and static wind tunnel test data. It can simulate wing-drop in right or left orientation, and reproduce static hysteresis in lateral-directional moment coefficients versus sideslip. This model is useful for piloted evaluations in real-time flight simulator.

Key Words: Abrupt Wing stall, transonic lateral instability, static hysteresis

NOMENCLATURE

AWS - Abrupt Wing Stall

FTR - Free-to-roll

GTA – Generic Tailless delta wing aircraft

FOM – Figure of Merit

α_c - Critical angle of attack

β_c - Sideslip angle beyond which hysteresis in rolling moment coefficient ceases to exist

1. INTRODUCTION

Abrupt Wing Stall (AWS) has been known to occur on several high performance aircraft with swept back wings at high angle-of-attack and high subsonic Mach number [1, 2]. This phenomenon occurs due to complex flow mechanisms like shock/boundary layer interactions and unsteady movement of transonic shocks on the surface of the wing causing sudden change in pressure distribution. This results in an uncommanded lateral-directional motion in the form of wing drop or wing rock. This is a sudden event and causes significant degradation of handling qualities. In some cases, it can lead to departure outside the normal flight envelope. As many as 20 fighter aircrafts have experienced this problem since advent of high performance delta wing configurations. Since it occurs in a critical part of the combat flight envelope, it may prohibit the best utilization of the aircraft's manoeuvring capabilities. So it is important to model this phenomenon in simulations to evaluate its impact on mission performance and safety.

Modeling AWS is a complex task because it is a dynamic phenomenon and it is sensitive to external flow conditions. Specialized dynamic wind tunnel testing is required to capture this phenomenon in realistic conditions. Recently, AWS occurring on F18-C/D Super-hornet and F35 JSF were extensively studied and characterised using Free-to-roll wind tunnel tests by NASA and Lockheed Martin [4, 5]. In this paper, we present analysis of Free-to-roll Wind tunnel data for a Generic Tailless delta wing Aircraft (GTA) to identify characteristics of AWS in section 2. We then present a comprehensive approach for aerodynamic modeling of AWS for use in a Real-time-simulator and flight dynamic analysis in sections 3 and 4.

2. PREDICTING OCCURRENCE OF ABRUPT WING STALL

2.1 Prediction using Free-to-roll tests:

Free-to-roll testing is a dynamic wind tunnel test technique used to identify the potential for uncommanded lateral motions. It is reported that these tests show excellent agreement with flight test results in terms of angle of attack for onset of uncommanded lateral motions. To assess the proneness of GTA to uncommanded lateral motions, FTR tests were conducted in an Industrial-grade Free-to-roll test rig (FTR) using a 1:15 scale GTA model. In this rig, aircraft is free to roll about its body axis and all other degrees of freedom are restrained. The model can be set at a particular angle-of-attack and side-slip to the flow-angle. However, in the current tests the aircraft model was subjected to a slow sweep in angle-of-attack. All forces and moments acting on the aircraft model were recorded.

Detailed analysis of Free-to-roll test data indicated existence of AWS for GTA. From Fig (1), we observe that the wind tunnel model experiences a sudden roll-off at a certain angle-of-attack θ and the model remains locked in this banked position up to θ+3 deg.

2.1.1 Figure of merit computation:

In order to interpret the entire data set available from FTR tests to arrive at the predictions of the presence of lateral activity due to Abrupt wing stall some figures-of-merit have been proposed in literature [3, 4]. It is to be noted that the uncommanded lateral activity can be considered to be significant if the roll-off happens at a fast rate. Otherwise, it is expected that such a roll off motion will be easily damped out due to roll-rate feedback in the control law of the aircraft. A figure of merit based on rate of change of roll angle computed from time series data obtained from FTR pitch-pause tests has been proposed in [5]. The average roll rate between consecutive local maxima and local minima in the data is computed, and their maxima is considered as the FTR figure of merit at that pitch angle.

$$\text{FTR FOM} = \left|\frac{d\phi}{dt}\right|_{\max} \qquad \ldots. (1)$$

This FOM takes into account both the amplitude and rate of the uncommanded lateral motion. This FOM is then non-dimensionalised by multiplying it by (b/2V), to account for the effect of change in speed (hence, Mach number). This FOM cannot be used on time series data generated from pitch-sweep tests done on GTA since AOA is continuously changing. Therefore, we adopted a different approach to compute the FOM using pitch sweep test data.

Instead of roll angle time series data, we used angle of sideslip computed from θ and φ for computation of FOM. Body-axis roll off motion leads to a significant angle-of-side-slip at high angle-of-attack only. This naturally puts out the false alarm raised by the low angle-of-attack roll-off which may be due to flow disturbances in the wind tunnel. Therefore a modified figure of merit based on angle of sideslip computed from θ and φ is proposed.

$$\text{Modified FTR FOM} = \left|\frac{d\beta}{dt}\right| * \left(\frac{b}{2V}\right) \qquad \ldots (2)$$

Significant lateral activity is identified by a threshold FTR FOM value of 0.01. Since the AOA decreases due to roll-off, the FOM computed here is not applicable after the initial roll-off has occurred. Thus, the FOM computed from the pitch-sweep test data can only be used at the instance of roll-off and not at angles of attack beyond that.

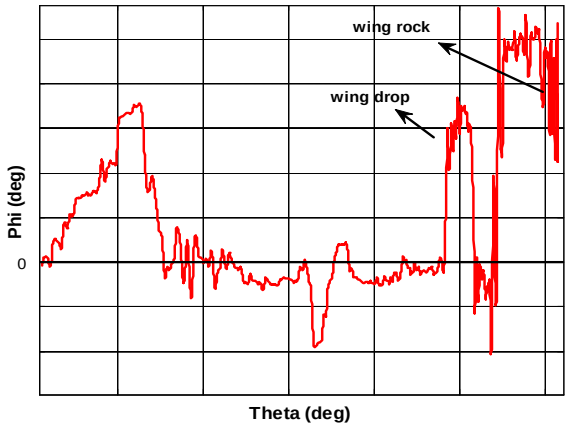

Figure 1. Regions of uncommanded lateral activity from FTR tests

2.2 Prediction using static force & moment data:

At high angles-of-attack and high-Mach number conditions the aircraft model in FTR rig experiences very high loads resulting in vibration of the sting and model. Triggering of the AWS phenomena is sensitive to such vibrations as well as wind tunnel disturbances if any. The angle-of-attack θ obtained from FTR tests is not accurate and the expected variance is 2 degrees [3]. Therefore, data from multiple sources in addition to FTR tests need to be interpreted simultaneously to obtain a reliable prediction of θ.

AWS can also be observed from static wind tunnel test data based on multiple qualitative criteria. Force and moment measurements from Static Wind tunnel tests can also provide indications of potential uncommanded lateral motions. Some qualitative criteria using static wind tunnel data are proposed in [6]. In this paper, we propose some new criteria using static test data to identify AWS tendencies. These qualitative figures of merit can be useful in the conceptual design stage itself to identify AWS tendencies in a particular configuration, as conducting FTR tests is expensive. For example, as seen in Fig (2) the rolling moment coefficient versus roll angle shows strong local nonlinearity at angle-of-attack θ_0. This indicates a drastic change in local flow conditions which is anticipated to be due to AWS. It is to be noted that since AWS is a body-axis roll phenomenon, it is more appropriate to look at C_l Vs φ rather than C_l Vs β.

We propose following qualitative criteria in addition to the ones already existing in literature to identify AWS from static wind tunnel data:

Rolling moment vs. phi plot:

- Presence of large asymmetry and nonlinearity near φ=0 [6]
- Loss of dihedral stability around φ=0 even for a small increase in AOA
- Presence of large jumps and multiple equilibria due to flow instability signify hysteresis which can result in wing drop

C_{Lift} vs. alpha plot:

Change in lift curve slope due to asymmetric wing stall resulting in loss of lift [Ref 6]

Fig 2 shows that static wind tunnel data of GTA satisfy many of these qualitative criteria. Within one degree increase in pitch angle from θ_0-1 to θ_0, large asymmetry in rolling moment builds up along with a local loss in dihedral stability near φ=0. Subplots 3 & 4 of Fig 2 also indicate possibility of multiple equilibria. Therefore static wind tunnel data of GTA also indicate a possibility of uncommanded lateral motions due to AWS at θ_0 which matches very well with FTR predictions. We thereby confirm the presence of uncommanded lateral motions from both FTR tests and static force and moment tests. Consistency across multiple criteria increases the confidence of prediction. Based on these two approaches for identifying uncommanded lateral motions, the AOA at which AWS is triggered for different Mach numbers is identified. In order to study the impact of these uncommanded lateral motions on the flying qualities of the aircraft, it is essential to model the phenomenon and perform open and closed loop simulation analysis.

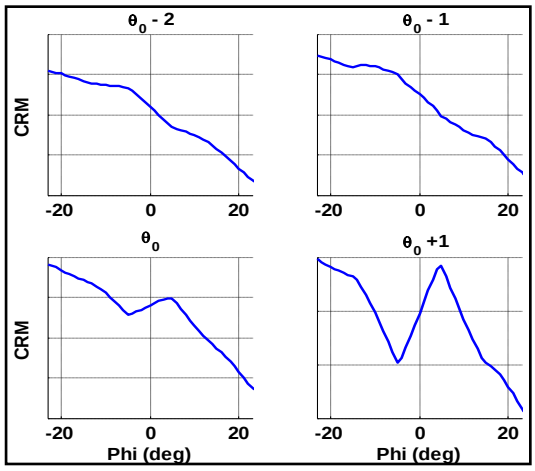

Figure 2. Local nonlinearities observed in rolling moment coefficient from wind tunnel data

3. MODELLING OF ABRUPT WING STALL

AWS occurs due to complex flow mechanisms on the upper surface of the wing. Pressure distribution measurements on a delta wing showed the existence of a bistable or tristable state for shocks, and shock location can rapidly change between them with small change in flow conditions [1]. The shock locations on either wing could be asymmetric, resulting in wing-drop motion.

The kinematic coupling resulting from the aircraft roll-off motion about body-axis results in variation of roll-damping, which in turn could give rise to wing-rock motion. A classical aerodynamic model contains tables for symmetric and asymmetric components of rolling moment and yawing moment coefficients. The asymmetric coefficients produce rolling/yawing motion even from symmetric aircraft orientation. Such a simplistic model can produce only continuous rolling motion. This is not a correct representation of the flight mechanics due to AWS as it is known to cause wing-rock or wing-drop type of motion. Also, a classical aero database model may not include local nonlinearities (like in Fig 2) and static hysteresis that is found to occur at high-alpha high Mach number conditions. Such a classical aero database of GTA was available and from simulations we found that it could not simulate the flight mechanics of AWS. Therefore we developed a mathematical model of this phenomenon to simulate it in 6DOF flight simulations.

An incremental model is proposed as it can be easily retrofitted with the available aero-database. AWS can be triggered to cause right or left wing-drop depending on small disturbances in the flow field. This rolling motion is about the body-axis. From static wind tunnel tests it was found that the aircraft exhibits hysteresis in lateral-directional moment coefficients against sideslip depending on the direction of yawing motion. Static hysteresis in rolling and yawing moment coefficients implies that there exist two stable equilibrium flow conditions for same aircraft states. Depending on small external flow disturbances or aircraft micro-asymmetry, the aerodynamic force/moment can alternate to either of these two equilibrium conditions.

The mathematical model for Abrupt wing stall consists of the following components

i) Static hysteresis in rolling moment coefficient
ii) Static hysteresis in yawing moment coefficient
iii) Roll damping derivative as a function of sideslip angle

3.1 Static hysteresis modelling

The static hysteresis in C_l and C_n is modelled as an aerodynamic bifurcation with respect to angle of attack. The AWS model for static hysteresis has one stable real solution (C_l=0) outside the static hysteresis region whereas within the static hysteresis region, it has two stable non-zero real solutions and one unstable real solution (C_l=0). The two stable real solutions within the static hysteresis region depend on non-zero values of rolling moment coefficient at zero side-slip. All the features incorporated into the proposed mathematical model of AWS are shown in the Flowchart-1 and Flowchart-2. The structure of the hysteresis model is kept simple so that it can easily be integrated with the existing GTA aerodynamic model.

The static hysteresis loop for C_l is modelled symmetrical with respect to sideslip and the size of the hysteresis loop is determined from static wind tunnel data. The aerodynamic bifurcation model with respect to angle of attack is as shown in Fig 3. If AOA is less than α_c, then C_l=0 is the only stable solution. α_c is the angle of attack beyond which AWS is triggered. This α_c was determined from FTR data as discussed in section 2. If AOA is greater than α_c, then Cl can attain two possible values, C_{l1} and C_{l2}, due to static hysteresis. When $\alpha > \alpha_c$ and angle of sideslip is within the static hysteresis region, then $C_l=C_{l1}$ for $\dot{\beta}>0$ (the rolling moment variation follows the upper red curve in Fig 4), otherwise $C_l=C_{l2}$. β_c is the sideslip angle where the hysteresis loop in C_l ceases to exist and is determined from static wind tunnel data. Outside the static hysteresis region, $C_l=C_{l1}$ for $\beta \geq 0$ and $C_l=C_{l2}$ for $\beta<0$. This model for static hysteresis in rolling moment coefficient is presented in Flowchart-1. Fig 4 shows the comparison of static hysteresis model of the rolling moment coefficient at M = 0.8 with the wind tunnel data.

Flowchart – 2 explains the static hysteresis model of the yawing moment coefficient. Wind tunnel data showed that the hysteresis loop for C_n is not symmetrical with respect to sideslip. Let β_{c1} and β_{c2} ($\beta_{c1}<0$, $\beta_{c2}>0$) be the sideslip angles within which static hysteresis exists. If AOA is less than α_c, then the yawing moment coefficient varies linearly as a function of sideslip angle with C_n=0 at zero sideslip angle. For AOA greater than α_c, C_n is modeled as,

$$C_n = C_{n\beta}\beta + \delta C_{n\beta}(\beta+\beta_{c1})k_1 + \delta C_{n\beta}(\beta+\beta_{c2})(1-k_1) \quad (3)$$

The parameter k_1 in the above equation is either 0 or 1 depending upon the value of $\dot{\beta}$. $\delta C_{n\beta}$ used in the equation is the slope of C_n within the hysteresis region and is estimated from wind tunnel data along with β_{c1} and β_{c2} for each Mach number and AOA. Outside the static hysteresis region, yawing moment coefficient is given by,

$$C_n = C_{n0} + C_{n\beta}\beta \quad (4)$$

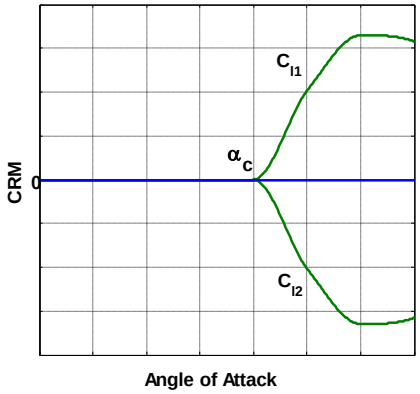

Figure 3. Aerodynamic bifurcation in C_l vs AOA

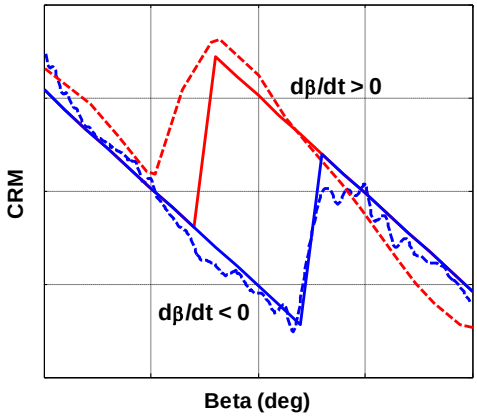

Figure 4. Static hysteresis model for rolling moment coefficient at M = 0.8 (Dotted lines – Wind tunnel; data, Solid lines – AWS model)

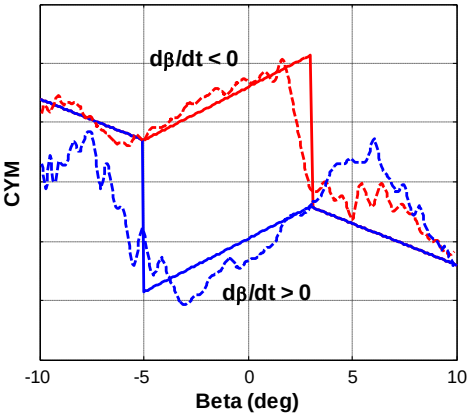

Figure 5. Static hysteresis model for yawing moment coefficient at M = 0.8 (Dotted lines – Wind tunnel; data, Solid lines – AWS model)

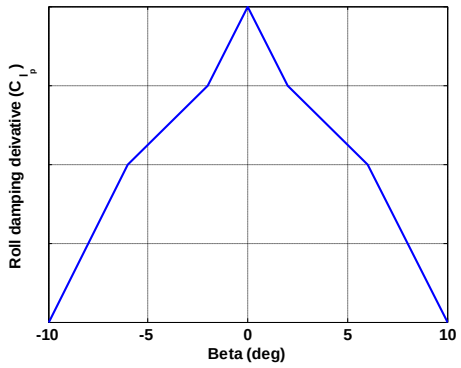

Figure 6. Model of roll damping derivative as a function of sideslip angle

Fig 5 presents comparison of the static hysteresis model for the yawing moment coefficient at M = 0.8 with the experimental data used to create the model. With the above described models for the rolling and yawing moment coefficients, it is now possible to account for the asymmetry, local nonlinearities and static hysteresis.

3.2 Model for roll damping derivative:

It has been reported in literature that as a delta wing rolls at high AOA, the roll damping increases with sideslip angle opposing the rolling motion induced by the asymmetry [7]. In addition to modelling the static hysteresis in lateral-directional moment coefficients, the roll damping derivative is also modelled as a function of sideslip angle in the regions where uncommanded lateral motions occur (see Fig 6). At lower sideslip angles the roll damping is small; and as the aircraft rolls about body-axis, the roll damping increases with increase in sideslip angle. Therefore, the aircraft does not roll continuously due to asymmetry but settles on to a non-zero sideslip angle where the moments are balanced. The roll damping derivative in the GTA aero-database which is a function of AOA and Mach number is multiplied by a parameter *k* which is a function of sideslip angle. The parameter *k* is tuned to match the wing-drop amplitude from the FTR test data.

The AWS model described above is integrated with the GTA aerodynamic model and used in offline closed and open loop simulations.

4. RESULTS & DISCUSSION

Offline simulations were performed using the GTA aerodynamic model integrated with AWS model described in the previous section. Maneuvers normally used for flight testing at high AOA such as wind-up turns and banked pull-ups were simulated.

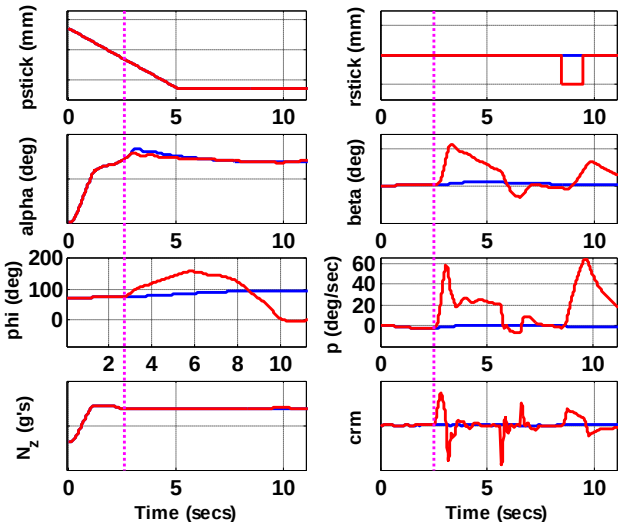

Figure 7. Simulation time history of wind-up turn with (Red) & without (Blue) AWS model

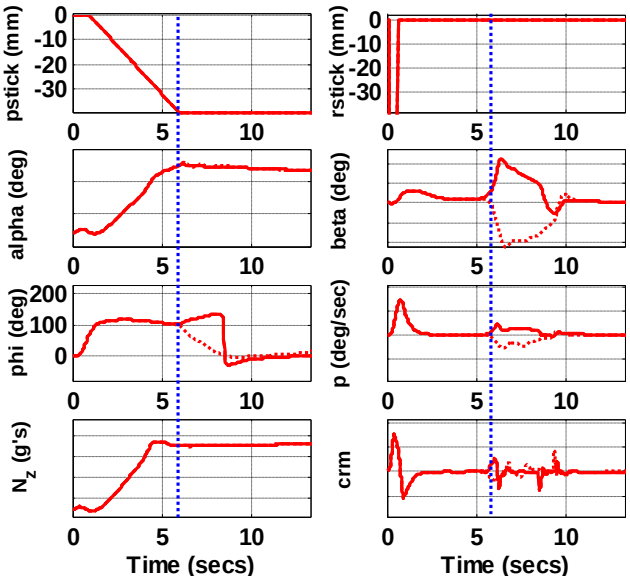

Figure 8. Effect of disturbances in triggering uncommanded lateral motions (Solid line – Positive $\dot{\beta}$ disturbance, Dotted line – Negative $\dot{\beta}$ disturbance)

Fig 7 shows the simulation time history of a wind-up turn performed at 0.8 Mach with and without the AWS model in the AOA range where uncommanded lateral motions were found to occur. It is observed that there is no roll-off during the maneuver when the AWS model is not present (blue curve). It is observed from the figure that with the AWS model (red curve), as the AOA exceeds the critical angle of attack, a sudden uncommanded roll motion is encountered at t=2.5 secs as predicted and seen from Free-to-roll tests. The magenta coloured dotted line in the figure indicates the initiation of roll-

off; it can be clearly seen that the roll-off motion is not due to control inputs as the roll stick input is zero at that instant. As the aircraft starts to roll, the roll damping also increases which results in arresting the roll-off motion at t=6 secs where the roll rate becomes zero. Since the sideslip angle is non-zero and because of the stable dihedral effect, the aircraft starts to recover from the roll-off and tends to come back to a wings level attitude around t=7 secs. Because of the static hysteresis loop in rolling moment versus sideslip, the rolling moment during the recovery follows a different variation (lower curve in Fig 4) which results in a negative rolling moment (see last subplot of Fig 7) being generated which eventually recovers back the aircraft from the roll-off condition.

Fig 8 shows the simulation time history of a banked pull-up with the AWS model. Here again the aircraft experiences an uncommanded roll motion as it exceeds the critical angle of attack marked by blue dotted line in Fig 8. The aircraft recovers from the roll-off motion around t=8 secs and comes back to wings level flight. The recovery mechanism is same as explained in the previous paragraph. The direction of roll-motion is dependent on the flow disturbances. The effect of the flow disturbances in triggering uncommanded lateral motions is also seen from Fig 8. Here artificial disturbances were introduced which resulted in different roll-off scenarios depending on whether $\dot{\beta}$ is greater than zero or less than zero.

The uncommanded lateral motions seen in simulation, although not severe results in degraded flying qualities. The roll rate during these motions is of the order of 50-60 deg/sec. The proposed AWS model captured the aircraft flight physics resulting from AWS quite well and can be used to perform real time piloted simulations before actually conducting flight tests in these regions of the envelope.

5. CONCLUSION & FUTURE WORK:

A simple mathematical model for AWS is proposed accounting for asymmetries, local nonlinearities and static hysteresis which is capable of simulating uncommanded lateral-directional motions resulting from Abrupt wing stall. This aerodynamic model was used to study the effect of AWS on aircrafts' flying qualities. Future work includes developing control strategies to minimize the effect of this phenomenon so that it doesn't hamper the handling qualities when performing rapid maneuvers in this critical part of the flight envelope.

Acknowledgment

The authors would like to express their sincere thanks to Director, ADA and Technology Director (IFCS), ADA for granting permission to publish this work. The authors also thank the members of the National control law team for providing valuable inputs for this work.

REFERENCES

[1] RM Hall, SH Woodson, "Introduction to the Abrupt Wing Stall program", *Journal of Aircraft*, Vol 41 No.3, 2004

[2] JR Chambers, RM Hall, "Historical Review of Uncommanded Lateral-Directional motions at Transonic Conditions", *Journal of Aircraft*, Vol 41 No.3, 2004

[3] DB Owens et al, "Transonic Free-to-Roll analysis of Abrupt wing stall on military aircraft", *AIAA Journal of Aircraft*, Vol 41 No.3, 2004

[4] JK McConnell, "Use of Transonic Free to roll testing in the design phase of the Joint Strike Fighter", *AIAA Aerodynamic measurement technology and ground testing conference*, 2006

[5] DB Owens et al, "Transonic Free-To-Roll Analysis of the F/A-18E and F-35 Configurations", *AIAA Atmospheric Flight Mechanics conference & Exhibit*, August 2004

[6] JE Lamar et al, "Usefulness of Transonic Model Static Data in Predicting Flight Abrupt-Wing-Stall", *AIAA Journal of Aircraft*, Vol 41 No.3, 2004

[7] DM Schuster, JE Byrd, "Transonic Unsteady Aerodynamics of the F/A-18E under Conditions Promoting Abrupt Wing Stall", *AIAA Journal of Aircraft*, Vol 41 No.3, 2004

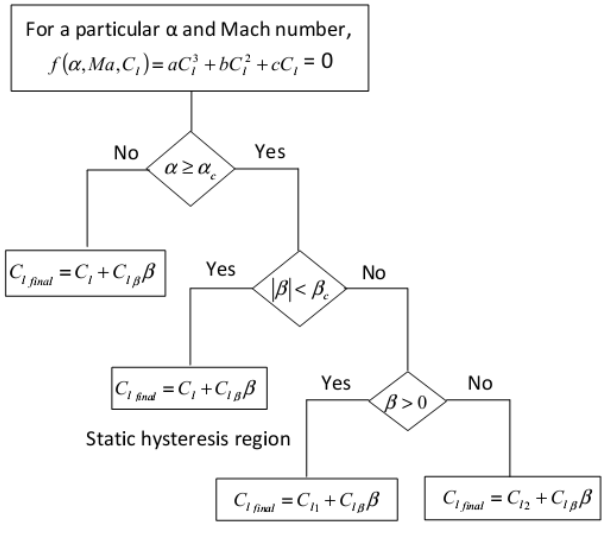

Flowchart-1. Algorithm for Static hysteresis modeling in rolling moment coefficient

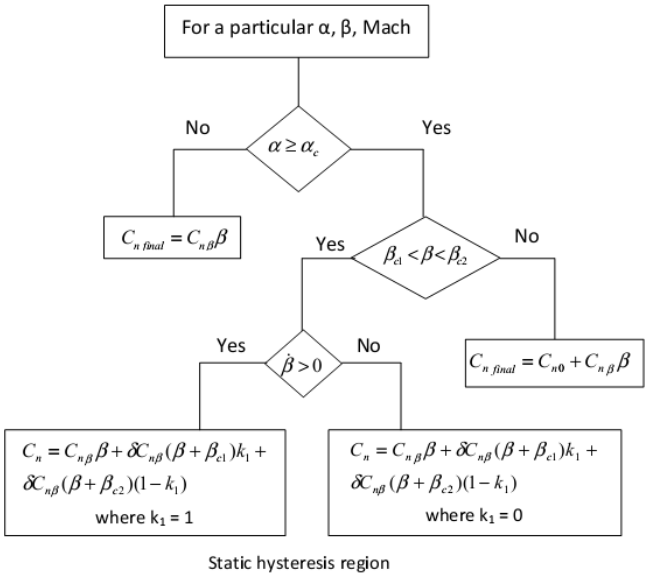

Flowchart-2. Algorithm for Static hysteresis modeling in yawing moment coefficient

Author Profiles:

M Deva Prakash graduated in Aeronautical engineering from Madras Institute of Technology, Chennai in 2010 and has been working in ADA since then in the area of flight dynamics & control. His interests include aerodynamic modeling, flight dynamics & control.

Mallesh Bommanahal graduated with a Dual degree (B.Tech and M.Tech) in Aerospace Engineering with specialization in Dynamics and Control, from IIT Bombay in 2009 and has been working as Scientist at the NAL ever since. His research interests include unsteady aerodynamics, High-alpha Flight mechanics, Mathematical modeling and Nonlinear dynamics.

Dr. Amitabh Saraf is Group Director (Flight Control Laws) and Sc/Engr 'G' at Aeronautical Development Agency. He is a member of National Control Law Team for Light Combat Aircraft since 1992. He completed his B.Tech (Mech) from IIT Bombay in 1990, M Tech by Research (Systems and Control Engg) from IIT Bombay in 1992, Ph D (Aerospace) from IISc Bangalore in 2001 and was Post Doctoral Researcher at University of California, Irvine, USA during 2002-2003. His areas of interest are systems modeling and simulation, aircraft flight control systems design, air-data systems design and parameter estimation of flight vehicles.

29th Congress of the International Council of the Aeronautical Sciences
St. Petersburg, Russia; September 7-12, 2014

FLIGHT ENVELOPE EXPANSION VIA ACTIVE CONTROL SOLUTIONS FOR A GENERIC TAILLESS AIRCRAFT

N.Abramov*, M.Bommanahal, S. Chetty**, M.Goman*, E.Kolesnikov*, PVS. Murthy****
***De Montfort University, UK, ****CSIR-National Aerospace Laboratories, Bangalore, India**

Keywords: *flight envelope expansion, HAoA modeling, attainable equilibrium sets, command stability augmentation system, regions of attraction, wing-rock, spin, numerical simulation*

Abstract

Aircraft dynamics at high angles of attack due to loss of stability and control essentially limits its manoeuvrability. Modern control systems implement flight envelope protection at the cost of maneuverability to improve safety in these conditions. Flight envelope boundaries, which are set taking into account deterioration of stability and controllability due to separated flow, can be expanded by appropriate design of control laws. However, such a design requires extensive analysis of the maneuver envelope of the airframe and its utilization by the flight envelope protection laws. The reliability of this analysis depends on the adequate aerodynamic modeling which captures nonlinear unsteady variation of aerodynamic loads in these flight regimes. Two novel models for unsteady aerodynamics at low and high subsonic Mach numbers are described. These models and prototyping control laws are used for closed loop computational analysis. The computational methodology of clearing flight control laws for flight envelope expansion of a Generic Tailless Aircraft (GTA) is addressed.

1 Introduction

Flight safety of military and commercial transport aircraft is directly connected with their behaviour at high angles of attack and reliability of its flight envelope protection. Expansion of flight envelope leads to increase in manoeuvrability of military aircraft, while effective flight envelope protection helps to avoid loss-of-control in flight (LOC-I) for civil transport aircraft [1]. The results obtained during the collaborative research project between CSIR-NAL, India and De Montfort University (DMU) highlight the main problems and limitations in expansion of GTA flight envelope. We performed evaluation of prototype control laws with objective of their redesign for extension of flight envelope. This paper presents the employed methodology and computational framework developed earlier at DMU with some preliminary results and analysis.

A number of methodological challenges were addressed and effectively implemented for finding feasible solutions to the formulated objective. Firstly, the methods for adequate modeling of GTA aerodynamics in the extended flight envelope to capture unsteady variation of coefficients due to separated flow, vortex breakdown, onset of aerodynamic asymmetry, etc. were developed [1, 5, 6, 7, 8, 9]. These models were augmented to the classical aerodynamic database. Secondly, a systematic investigation of GTA nonlinear dynamics to characterize its critical flight regimes in the extended envelope for the airframe was conducted. This provided a clear understanding of GTA's susceptibility to lateral-directional loss of control, behaviour in wing rock and spin modes, etc. [11, 12, 13]. Thirdly, the clearance of flight control laws in the extended flight envelope based on computation of attainable equilibrium sets and regions of attraction for GTA with command and stability augmentation system has been effectively implemented [14].

Based on deep insights into the problems gained at this stage, it is anticipated that the de-

sign of efficient control laws for extended flight envelope will be a success. The developed computational framework will be used and adjusted for this purpose.

2 Aerodynamic Modeling in the Extended Flight Envelope

The flight envelope Of Mach versus α is restricted at two boundaries due to deterioration in aerodynamics. At one boundary there is vortex-breakdown on wings and at the other boundary there is asymmetric shock induced flow separation on the wings. These phenomena result in unsteady and nonlinear variation of aerodynamic loads [3, 5, 7]. Traditional methods of wind tunnel tests and aerodynamic models are insufficient for formulating flight control and testing strategies. Therefore, aerodynamic modeling for these flight conditions has been pursued for the past two decades. In this section, we present novel models for these phenomena in the form of nonlinear differential equations.

Both these models were developed for GTA using experimental data from industrial grade wind tunnels. These were easily integrated to classical data-table aero-models for the purpose of real-time simulation and off-line flight dynamic analysis.

2.1 Modeling High-angle-of-attack unsteady aerodynamics

At low-speed, high angle-of-attack flight conditions the delta wing aerodynamics is dominated by vortex flow on the wing. This vortex flow readjusts to change in external flow conditions, that is α and β, with a certain time-lag. This has been observed in flow visualization studies and dynamic wind tunnel test data. This causes the variation in aerodynamic forces and moments in a dynamic maneuver to be significantly different from that obtained from aero-database. This does not alter the possible aircraft trims, but affects dynamics and local stability characteristics.

Modeling the unsteady variation in aerodynamic forces and moments requires special experimental data and mathematical system identification techniques, like that in [5, 7]. Classically wind tunnel test response of aerodynamic coefficients obtained by forced oscillations in pitch, roll and yaw for various amplitude and frequency inputs are used for modeling this phenomena. We present a Volterra variational equations based model that can be estimated using forced oscillation test data [4, 8]. It can also be used for estimation using flight test data or other dynamic tests like the ones done on a 5DOF rig [10].

Forced oscillation wind tunnel test data showed that the variation in coefficients is nonlinear for large amplitude and linear for small amplitude sinusoidal alpha input. Also, the damping derivatives estimated from small amplitude forced oscillation wind tunnel test data are strong functions of frequency. All these effects are captured by a single model structure presented here.

The normal force dependence on angle-of-attack in static conditions be given by $Cz_{st}(\alpha)$, and the increment over it due to unsteady aerodynamics be $C_d(t)$, then variation of normal force $Cz(t)$ in a maneuver is,

$$Cz(\alpha(t),t) = Cz_{st}(t) + Cz_q(t)\cdot q\bar{c}/2V + C_d(t) \quad (1)$$

We model $C_d(\dot{\alpha}(t))$ in the from of Volterra variational equations. This system has a stable equilibrium point $[C_d(t),\dot{\alpha}(t)) = (0,0)]$ for the entire $\alpha \in [-90^o, 90^o)$ range. For model structure of Eq.(1), $Cz(t)$ converges to Cz_{st} in a finite time when $(\dot{\alpha} = 0)$. The nonlinear model for $C_d(t)$ in the form of Volterra-variational equations is given by Eq.(2).

$$\begin{aligned} C_d(t) &= x_1(t) + x_2(t) + x_3(t) \\ \dot{x}_1(t) &= a(\alpha(t))x_1(t) + K_1(\alpha(t))\dot{\alpha}(t),\ x_1(0) = 0 \\ \dot{x}_2(t) &= a(\alpha(t))x_2(t) + K_{20}(\alpha(t))x_1^2(t) + \\ &\quad K_{21}(\alpha(t))x_1(t)\dot{\alpha}(t),\ x_2(0) = 0 \end{aligned} \quad (2)$$

In this structure, first kernel state x_1 indicates the linear response of unsteady aerodynamics to $\dot{\alpha}(t)$, with a as time-scale parameter. The magnitude of x_2 is likely to be significant when there is large amplitude change in α or $\dot{\alpha}$, and it produces second harmonic component in response to sinusoidal input.

In a small amplitude forced oscillation test, wind tunnel model is oscillated in pitch in

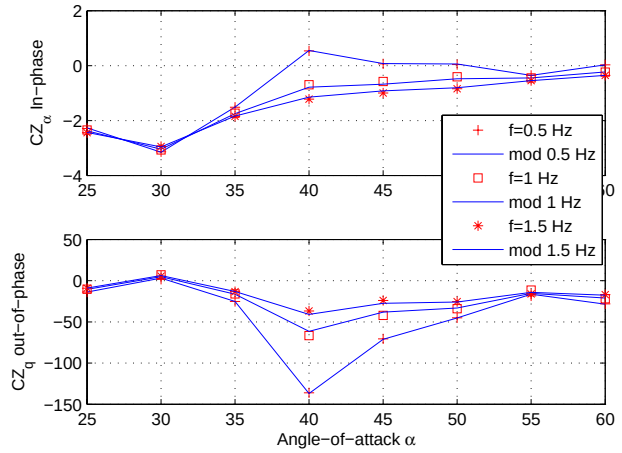

Fig. 1 Comparison of the in-phase and out-of-phase aerodynamic derivatives predicted by aerodynamic model and extracted from experimental data for Cz of GTA.

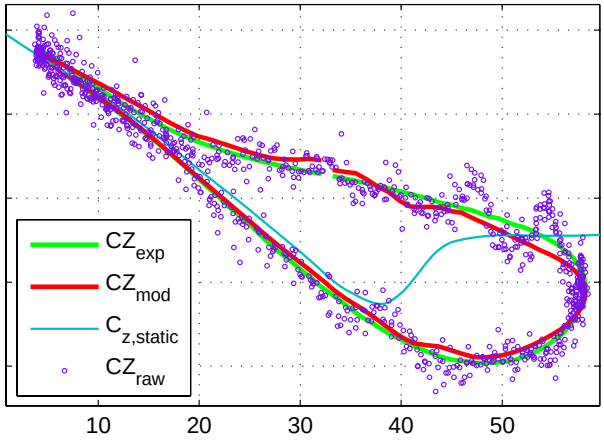

Fig. 2 Comparison of predicted and experimental aerodynamic responses for Cz of GTA.

a sinusoidal motion given by, $\alpha_{exp}(t) = \alpha_0 + \Delta\alpha sin(\omega t)$. The measured normal force coefficient $Cz(t)$ is converted to in-phase derivative $Cz_\alpha(\alpha_0)$ and out-of-phase derivative $Cz_{\dot\alpha}(\alpha_0)$ by harmonic analysis of the time-series data. Therefore, the steady-state response of the normal force coefficient is given by,

$$Cz(t) = Cz_0(\alpha_0) + Cz_{\alpha,\omega_0}(\alpha_0)\Delta\alpha sin(\omega t) + Cz_{\dot\alpha,\omega_0}(\alpha_0)\frac{\omega\bar c}{2V}\Delta\alpha\cos(\omega t) \quad (3)$$

Since small amplitude data shows linear variation of $Cz(t)$, we consider only first kernel state in $C_d(t)$. For parameter estimation using this data we linearize the model in Eq.(2), and get its steady state response to $\alpha_{exp}(t)$ as,

$$Cz(t)_{ss} = \left[Cz_{\alpha,st}(\alpha_0) + \frac{K_1\omega^2}{a^2+\omega^2}\right]\Delta\alpha sin(\omega t) \quad (4)$$
$$\left[-\frac{K_1 a}{a^2+\omega^2}\frac{\bar c\omega}{2V} + Cz_q(\alpha_0)\frac{\omega\bar c}{2V}\right]\Delta\alpha\cos(\omega t)$$

Comparing Eq.(4) and Eq.(3), we get the following relation between experimental derivatives and model parameters,

$$\begin{aligned} Cz_{\alpha,\omega_0}(\alpha_0) &= Cz_{\alpha,st}(\alpha_0) + \frac{K_1\omega^2}{a^2+\omega^2} \\ Cz_{\dot\alpha,\omega_0}(\alpha_0) &= Cz_q(\alpha_0) - \frac{K_1 a}{a^2+\omega^2} \end{aligned} \quad (5)$$

Rearranging the terms in Eq.(5), we get a linear relation between $Cz_{\alpha,\omega_0}(\alpha_0)$ and $Cz_{q,\omega_0}(\alpha_0)$. This relation is used in a two-step regression as proposed in [9], to obtain estimate of parameters $(a, K1)$ at each α_0 for which data is available. The model matches the experimental data consistently as shown in Fig. 1.

The nonlinear variation can be captured by considering the second kernel state in the model. Estimated parameter functions $(a(\alpha), K1(\alpha))$ are fixed, and parameters $(K_{20}(\alpha), K_{21}(\alpha))$ are estimated from large amplitude forced oscillation data by output-error minimization. For GTA, this data is available at three mean $\alpha = (15, 25, 35)$ and three frequencies $f = (0.5, 1, 1.5)Hz$. The response of the estimated model in one case with $\alpha_m = 30\,\text{deg}, \delta\alpha = 25\,\text{deg}$ is shown in Fig. 2. The match is excellent. For pitching moment coefficient three state Volterra variational model gave sufficiently accurate match to the experimental data. Linear part of this model is equivalent to linearized form of other model structures proposed in literature, but this is the first model that provides a systematic approach to model nonlinear variations in coefficients. In nonlinear form, it is also equivalent to the polynomial differential model proposed in [1, 9].

2.2 Modeling Abrupt Wing Stall at High Subsonic Mach number

At high-subsonic Mach number and moderate angle-of-attack flight conditions, some aircrafts experience an abrupt asymmetrical wing stall leading to wing-drop or roll-off [2, 3]. This part of the flight envelope is critical for aircraft maneuvering capabilities. The sudden event of roll-off causes degradation of handling qualities and can lead to departure outside the normal flight envelope. If the resulting instability is mild it can be removed by roll-rate feedback in the control law, else it requires an aerodynamic fix on the aircraft.

Free-to-roll (FTR) test is now accepted experimental wind tunnel method for investigation of abrupt wing stall (AWS) along with classical static and unsteady tests. In FTR, the aircraft model has single degree-of-freedom about its roll-axis and can be set at different attitudes specified by pitch angle θ. For GTA, FTR data showed an onset of wing-rock at $\alpha = 26$ deg about a non-zero side-slip at transonic Mach number. There is also an indication of static hysteresis in the rolling moment coefficient versus β at transonic Mach numbers seen from quasi-steady wind tunnel tests. The objective for modeling is to complement model (2), which is capturing only mild nonsingular nonlinearities, with bifurcational properties. A novel bifurcational model of aerodynamic asymmetry (BMAA) splits the rolling moment coefficient into four components, the first three components are from the aero-database, and $Cl_d(t)$ is the incremental effect of aerodynamic asymmetry due to AWS. BMAA for $Cl_d(t)$ is given by the following equations:

$$C_l(\alpha(t),\beta(t)) = C_{l_{st}}(\alpha) + C_{l_p}(\alpha)\cdot p(t)\bar{b}/2V + C_{l_\beta}(\alpha)\cdot\beta(t) + C_{l_d}(\alpha(t),\beta(t)) \quad (6)$$

$$\begin{aligned} x &= f(\beta); y = g(C_{l_d}) \\ x_1 &= x\cos(\phi) + y\sin(\phi) \\ y_1 &= -x\sin(\phi) + y\cos(\phi) \\ x_2 &= x\cos(\psi) + y\sin(\psi) \\ \tau\frac{dy}{dt} &= \left(1 - \frac{x_1^2}{a^2} - \frac{y_1^2}{b^2}\right) y + k * x_2 \end{aligned} \quad (7)$$

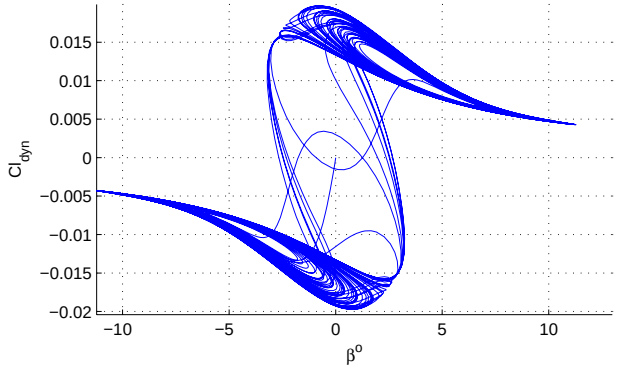

Fig. 3 Variation of the rolling moment coefficient vs β variation simulated using bifurcational AWS model.

where five parameters (a,b,k,ϕ_m,ψ_m) affect the shape of static hysteresis and dynamic properties in steady states. In the hysteresis region there are two stable and one unattainable unstable equilibrium in the center. $C_{l_d}(t)$ triggers rolling motion of the aircraft for $\beta = 0$ to depart to the left or right depending on sign of disturbances. Smooth variation of the rolling moment during the crossing of critical bifurcation points in a dynamic maneuver is due to the first order differential equation with the time-constant τ.

The parameters of the model are estimated in two steps to match FTR data and the rolling moment vs. sideslip from static wind tunnel test data. Parameters (a,b,k,ϕ_m,ψ_m) are used to match the shape of steady variation in rolling moment vs. beta static. Time-scale τ is used to match the frequency of oscillation in $\phi(t)$ to that from FTR tests. The model response for GTA with parameters estimated from FTR data is presented in Fig. 3. The model successfully captures the hysteresis in CRM vs. sideslip and dynamic tests on FTR rig. This model is integrated with the aero-database of GTA for simulation. The open-loop simulation model exhibited a mild wing-drop phenomena ultimately leading to wing-rock while performing a steady turn maneuver.

3 Nonlinear Flight Dynamics Methodology

Flight simulation technology is now widely used in aeronautical design process and also as an effective platform for pilot and crew training. It is recognised that an adequate aerodynamic model extended beyond normal flight envelope allows one to address flight safety issues both in design and by training. Piloted flight simulation can be made more effective based on clear understanding of aircraft nonlinear dynamics. Note that the analysis methods and computational algorithms for investigation of nonlinear flight dynamics during recent years have improved to a level that computational mathematical model is practically identical to the model used on flight simulator. For a reliable investigation, it is essential that the nonlinear representation of aircraft's dynamics meets the best fidelity level possible through selection of equations of motion, different types of aerodynamic model and representation of control system, etc.

3.1 Computational framework

In the present study we rely on computational framework that allows us to conduct comprehensive investigation of aircraft nonlinear dynamics in extended flight envelope using full flight simulation mathematical model without any substantial simplifications. Some elements of this computational framework were presented in [11, 12, 14].

3.2 Motion models for various time scales

Aircraft flight dynamics in 6-dof with rigid body approximation can be considered on different time scales. There are three types of fast modes of longitudinal and lateral-directional motion: the Short-period pitching, Dutch roll oscillations and aperiodic roll subsidence. They have a scale of several seconds and can be analysed using assumption that speed of flight is constant and gravity effect is insignificant. Equations called "Spat5" for angle of attack, sideslip and rotation rates in body axes frame $(p,q,r,\alpha,\beta)^T$ were used for evaluation of all attainable trim conditions and their local stability characteristics for velocity vector roll manoeuvre. Two additional modes of motion associated with variation of flight speed and influence of gravity, phugoid and spiral modes, are much slower, and have roughly ten times higher characteristic time scales. They can be analysed using extended system of equations of motion called "Spat8" with state vector $(p,q,r,\alpha,\beta,V,\theta,\phi)^T$, where V is speed of flight and θ,ϕ are pitch and bank angles respectively. Equilibrium points or trimmed states in this system of equations correspond to a class of helical trajectories with vertical axis of rotation, for example, level flight, horizontal turns, ascending and descending helix trajectories. The full 6-dof simulation is based on "Spat12" system incorporating all twelve states $(p,q,r,\alpha,\beta,V,\theta,\phi,\psi,X,Y,Z)^T$, where ψ is the Euler yaw angle, X,Y,Z are centre of gravity coordinates in the Earth-fixed inertial axes frame.

3.3 Open and closed-loop airframes

Flight control system plays significant role in aircraft dynamics. Command and stability augmentation system (CSAS) improves aircraft responses to pilot control inputs and modifies its reaction to external disturbances via change in the short-period, Dutch roll and roll subsidence motion modes. Block-diagram structure of a typical CSAS for longitudinal channels is shown in Fig. 4. It includes dynamic blocks with additional internal states and nonlinear elements that set constraints on the input and output signals, gain scheduling, etc. Similar block-diagram structures are also used for the lateral and directional channels.

The trim and linearization problem for a closed-loop system bears serious difficulties due to much higher dimension and non-smooth nonlinearities. In this work, we use a two tier procedure for this problem as proposed in [14] by the authors. First, the aircraft model is trimmed at a specified manoeuvre. Then open-loop system is linearized at the estimated values of control effectors and model states. In the second step, the control laws are trimmed at these values of model states and deflection of control surfaces. Then the required pilot stick inputs are identified and the

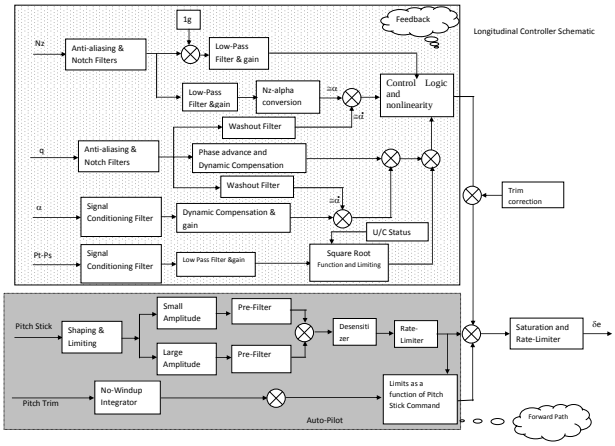

Fig. 4 Block-diagram of the longitudinal command and stability augmentation control system (CSAS).

control laws are linearized. The open-loop equilibrium state is rejected if the required pilot stick inputs exceed their limits. For attainable trims of the closed-loop system, the linearized matrices of aircrafts states and control laws are augmented to obtain eigenvalues for the closed-loop system. Thus, all the attainable equilibrium states are identified for the open airframe, and then the attainable trims, linearization and system closure are executed using the control law equations.

3.4 Flight performance evaluation

Equilibrium states in "Spat8" related to level flight, horizontal turn, etc. characterise aircraft performance characteristics. The eigenvalues of the linearized system describe dynamic properties of the aircraft fast and slow modes of motion. Note that CSAS stabilizes only the fast modes, while phugoid and spiral modes may be left weakly unstable allowing pilot to easily compensate for them. Fig. 5 shows computation of the flight envelope region for a horizontal turn manoeuvre with turn rate $\Omega = 5$ deg/s. The top plot corresponds to the open-airframe having aperiodic instability at low Mach numbers (red points), while the closed-loop system (Fig. 5, middle plot) is stable for all three fast modes of motion in the whole attainable envelope. The bottom plot is visualisation of the level turn. Regions for attainable ascending and descending helical trajectories can be computed in a similar manner with provision of all states and deflections for all control effectors.

Only descending helical trajectories are possible when thrust falls below required level. This trajectory becomes spin when trajectory radius shrinks to the order of several meters. Figure 6 shows examples of one-parametric continuation (Bifurcation diagrams) for equilibrium solutions of "Spat8" system extracted from the computational framework [11]. The top plot presents dependence on elevon at zero aileron setting, and the middle plot shows dependence on aileron at zero elevon setting. Stable equilibrium states are marked in green. Unstable equilibrium states are classified accordingly to distribution of unstable eigenvalues. For example, aperiodically unstable equilibrium with one positive real eigenvalue is marked in red and named as "a1", oscillatory unstable equilibrium with one unstable complex-conjugate pair of eigenvalues is marked in yellow ("o2"), higher order instability is marked by various colors and named accordingly to unstable eigenvalues as "a2", "a1,o2", etc. Graphs in the left column correspond to the open airframe, and those in the right column to the closed-loop system. One can see that CSAS has stabilizing effect only at normal flight conditions with low angles of attack. There are some stabilizing changes for steep spin modes and no qualitative changes for flat spin modes. Time histories in the bottom plot illustrate departure from unstable equilibrium point at high angles of attack to a wing rock attractor. This wing-rock has a quite high periodic time of 30 seconds which allows pilot to apply stabilizing control action.

3.5 Flight maneuverability evaluation and control laws clearance using attainable equilibrium sets

The maneuverability metric depends on achievable magnitudes of angle of attack and rate of rotation. These are defined via computation of attainable equilibrium states in the system "Spat5". For execution of a particular maneuver, its equilibrium state in "Spat5" should be stable while its region of attraction be sufficiently large to com-

pensate for probable external disturbances. The CSAS modifies the local stability characteristics and also changes the shape of attainable equilibrium region. Thus maneuverability metric may be confined or extended by a proper choice of control laws. Fig.7 presents attainable equilibrium states for the open airframe and closed-loop system. The open airframe is aperiodically unstable at law angles of attack in the longitudinal mode and oscillatory unstable at high angle of attack in the lateral-directional mode (top plot). Excluding the defined constraints on pilot inputs, the control law stabilizes most of unstable equilibria, leaving unstable sub-regions with reduced level of instability at high rotation rates and high angles of attack (the middle plot). The attainable envelope can be shaped to preserve only stable attainable equilibria via a proper shaping of input signal constraints [14]. Example of such modification is shown in Fig.7 (bottom plot).

Fig.8 (top plot) shows a two-dimensional cross-section of region of attraction computed for a stable equilibrium point of the closed-loop system at high angles of attack (green points). Perturbed motion with initial conditions from all green points in the plane of sideslip and roll rate in Fig.8 (middle plot) converges back to the equilibrium point. Outside of the region of attraction (red points) perturbed motion departs to the auto rotative steep spin regime (Fig.8, bottom plot).

Although the loss-of-control in flight at high angles of attack is possible, the probability of such event depends on the type of flight maneuver, external disturbances and criticality of pilot's control inputs. Fig.9 (top plot) shows spatial maneuver in a form of ascending trajectory with significant reduction in speed and increase in angle of attack (well beyond normal flight envelope) with subsequent successful transition to a normal flight without being attracted by wing rock and spin modes (bottom plot time histories).

4 Concluding remarks

The methodological principles and computational framework implemented in this study have provided a deep insight into GTA nonlinear dynamic behaviour in extended flight envelope and allowed to perform effective computational clearance of the flight control laws. A further work is planned with objective of redesign of the flight control laws in extended flight envelope.

References

[1] Abramov NB, Goman MG, Khrabrov AN et al. Aerodynamic model of transport airplane in extended envelope for simulation of upset recovery. ICAS-2012-3.1.2, *28th International congress of the Aeronautical Sciences*, 23-28 September 2012, Brisbane, Australia, 2012.

[2] Owens SD B, Capone FJ, Hall RM, et. al. Transonic Free-To-Roll Analysis of the F/A-18E and F-35 Configurations *AIAA Atmospheric Flight Mechanics conference*, Providence, Rhode Island, USA, 2004-4053, Aug 2004.

[3] Schuster DM and Byrd JE. Transonic Unsteady Aerodynamics of the F/A-18E under Conditions Promoting Abrupt Wing Stall. *AIAA Journal of Aircraft*, Vol. 41, No. 3, 2004.

[4] Rugh WJ. *Nonlinear System Theory: The Volterra/Weiner Approach*. The John Hopkins University Press, 1981.

[5] Goman MG and Khrabrov AN. State-space representation of Aerodynamic Characteristics of an Aircraft at High-angle-of-attack. *AIAA Journal of Aircraft*, Vol. 31, No. 5, pp 1109-1115, 1994.

[6] Abramov NB, Goman MG and Khrabrov AN. Aircraft Dynamics at High Incidence Flight with Account of Unsteady Aerodynamic Effects, *AIAA Atmosperic Flight Mechanics Conference and Exhibit*, Providence, Rhode Island, USA, AIAA 2004-5274, Aug 2004.

[7] Klein V and Murphy PC. Estimation of Aircraft Nonlinear Unsteady Parameters From Wind Tunnel Data, *NASA-TM 1998-208969*, NASA Langley Research Centre, Hampton, VA, December 1998.

[8] Bommanahal M and Goman M. Nonlinear unsteady aerodynmiac modeling by Volterra variational approach, *AIAA Atmospheric Flight Mechanics Conf*, Paper AIAA 2012-4654, 13-16 Aug, Minneapolis, MN, 2012.

[9] Abramov NB, Goman MG, Greenwell DI and Khrabrov AN. Two-step linear regression method for identification of high incidence unsteady aerodynamic model. Paper AIAA-2001-

4080, *AIAA Atmospheric Flight Mechanics Conference and Exhibit*, 2001.

[10] Pattinson J, Lowenberg MH and Goman MG. Multi-degree-of-freedom wind-tunnel maneuver rig for dynamic simulation and aerodynamic model identification. *Journal of Aircraft*, Vol. 50, No. 2, pp 551-566, 2012.

[11] Goman MG, Zagainov GI and Khramtsovsky AV. Application of bifurcation methods to nonlinear flight dynamics problems *Progress in Aerospace Sciences* Vol. 33, Issue 9, pp 539-586, 1997.

[12] Goman MG, Khramtsovsky AV and Kolesnikov EN. Evaluation of aircraft performance and maneuverability by computation of attainable equilibrium sets. *Journal of guidance control and dynamics*, Vol. 31, No. 2, pp 329-339, 2008.

[13] Kolesnikov EN and Goman MG. Analysis of Aircraft Nonlinear Dynamics Using Non-Gradient Based Numerical Methods and Attainable Equilibrium Sets, *AIAA Atmospheric Flight Mechanics Conf*, Paper AIAA 2012-4406,13-16 Aug, Minneapolis,2012.

[14] Abramov N, Goman M, Kolesnikov EN and Sidoryuk ME. Investigation of Attainable Equilibrium Sets for Clearance of Flight Control Laws. Paper AIAA 2010-491, *48th AIAA Aerospace Sciences Meeting*, 4-7 January 2010, Orlando, Florida, 2010.

5 Contact Author Email Address

Mail to: mgoman@dmu.ac.uk

Copyright Statement

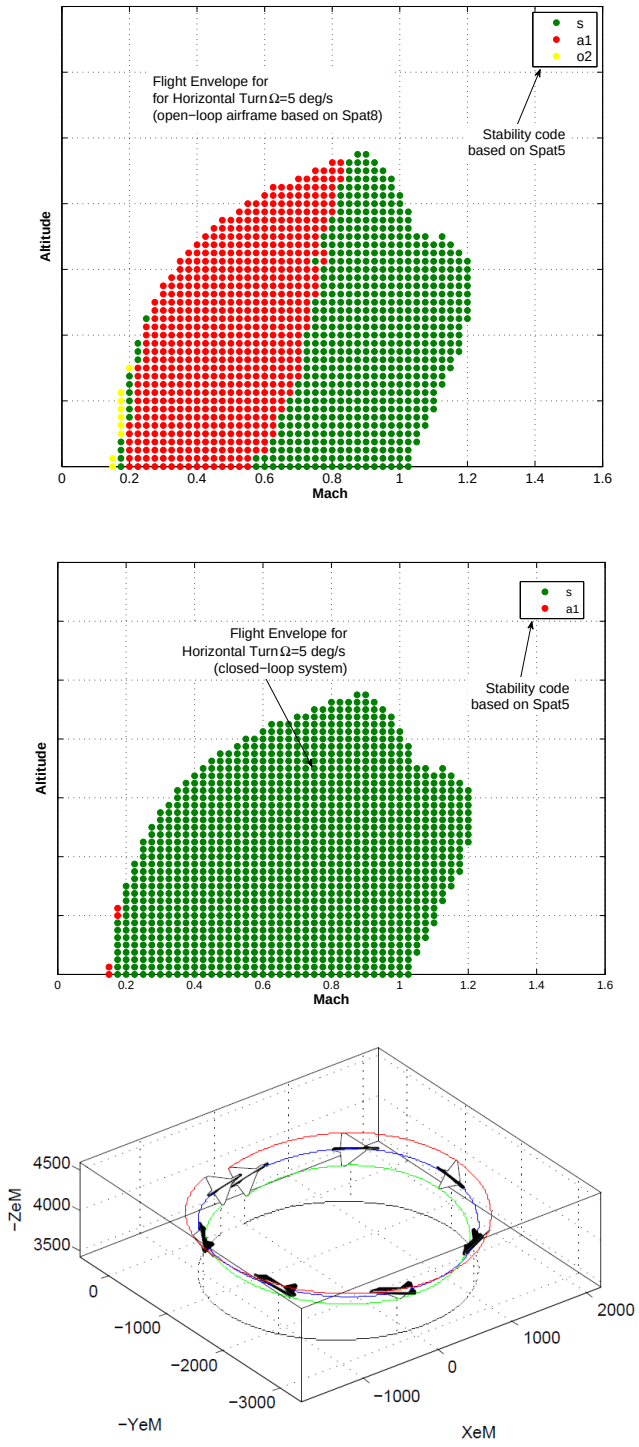

Fig. 5 Flight envelope for horizontal turn with yaw rate 5 deg/s computed "Spat8" system: Top plot: open airframe, stability code based on "Spat5" system; Middle plot: - GTA with CSAS, stability code based on "Spat5" system; Bottom plot: visualization of horizontal turn executed at altitude 4000m and Mach number 0.4.

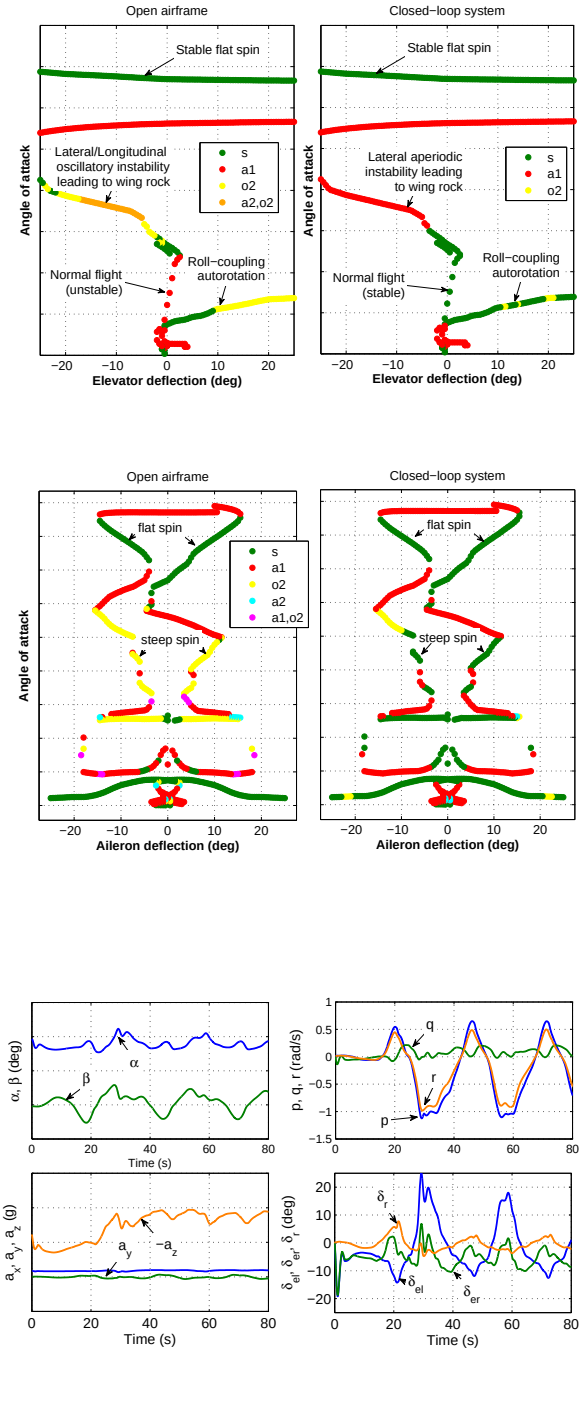

Fig. 6 Top plot: Dependence of equilibrium angle of attack on elevator at zero aileron and rudder for open airframe and with CSAS computed using "Spat8" system; Middle plot: dependence of equilibrium angle of attack on aileron at zero elevon and rudder for open airframe and with CSAS computed using "Spat8"; Bottom plot: Time histories demonstrating transition of the closed-loop system to wing rock motion from trim angle of attack 39 degrees.

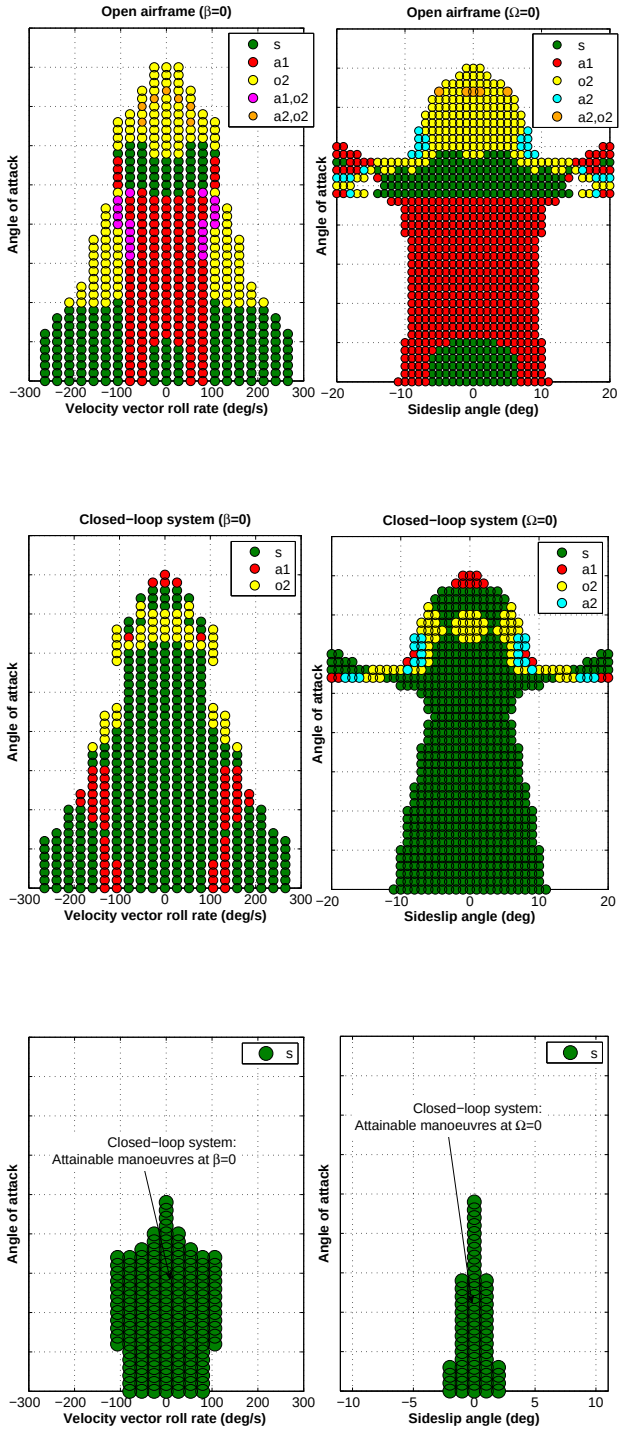

Fig. 7 Attainable equilibrium sets (AES), cross-sections for zero sideslip and zero roll rate, computed using "Spat5" system for subsonic flight regime Mach 0.4 and altitude 6000m: Top plot: AES for open airframe; Middle plot: AES for airframe with CSAS and no constraints on pilot stick inputs; Bottom plot: AES for airframe with CSAS and imposed constraints on pilot stick inputs.

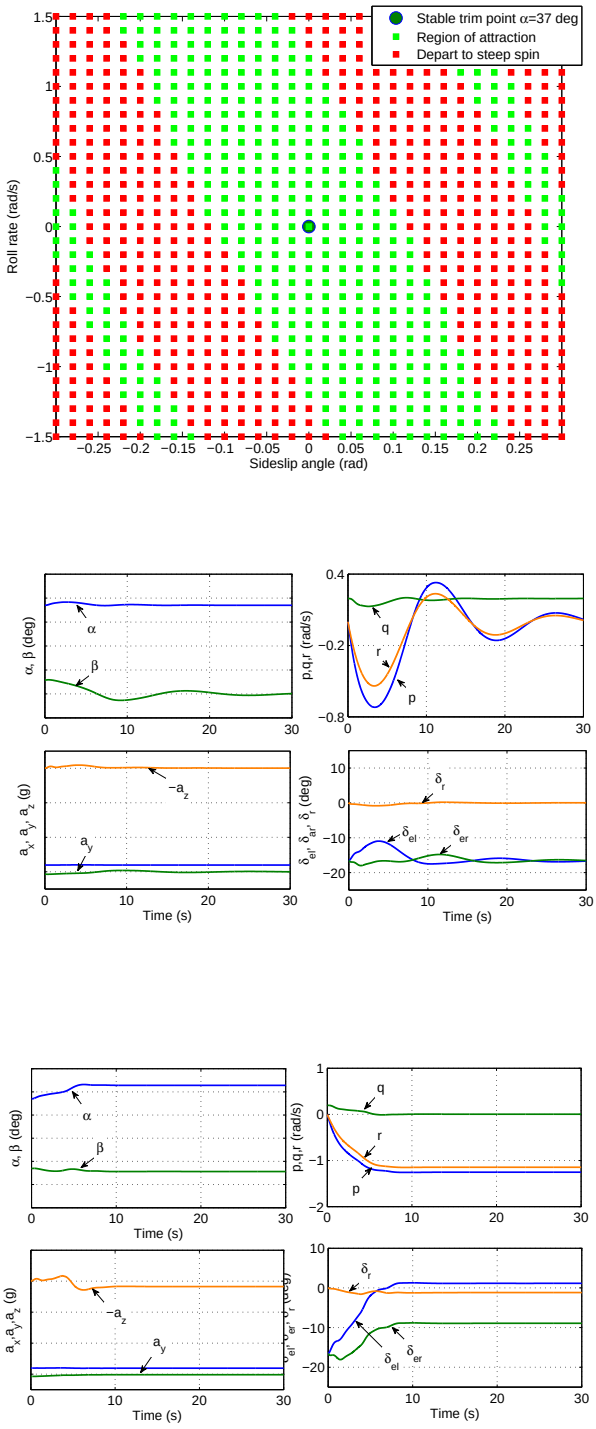

Fig. 8 Top plot: Region of attraction cross-section (p, β) for equilibrium point $\alpha = 37^0$; Middle plot: Process of convergence to the equilibrium point from green points; Bottom plot: Process of departure to the steep spin attractor from red points.

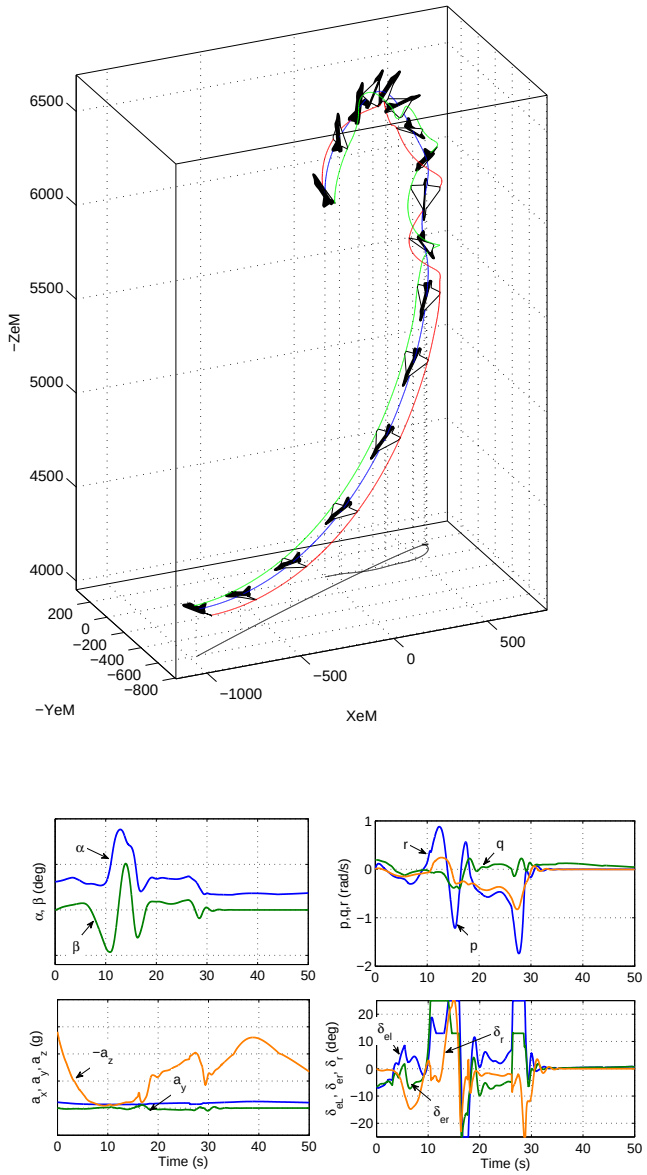

Fig. 9 Transition through regions of aircrat+CSAS system instability during ascending descending flight trajectory. Top plot: trajectory visualization; Bottom plot: time histories for major state variables and control deflections.

Recent Initiatives in Computational Flight Dynamics and Control at CSIR-NAL

Shyam Chetty[*], Mallesh Bommanahal[$], P.V.S Murthy[$], M.G. Goman[#]

Abstract

Aircraft dynamics at high angles of attack can experience loss of stability and control thereby limiting its manoeuvrability. Operating flight envelope boundaries, manoeuvre envelopes in terms of angle of attack and angular rate, are determined taking into account the deterioration in aircraft stability due to changes in aerodynamics produced by flow separation. For this, high fidelity aerodynamic models using static and dynamic wind tunnel test data are developed as a combination of look-up tables and differential equations. The model thus obtained is used for simulation and analysis of stall, spin characteristics using the modern methods of Bifurcation Analysis and Attainable Equilibrium Sets. These methods are computational approaches to flight dynamic analysis, and the results obtained are more reliable than the traditional approximation methods. This end-to-end capability in aerodynamic modelling and flight dynamic analysis, along with sophisticated software tools has been developed in collaboration with De Montfort University, and has been applied to industrial projects of a combat and trainer aircraft configurations.

1. Introduction

An aircraft's capability to fly into high angle-of-attack flight regime has been termed to be one of the determining factors of its combat capability [1]. A high-performance combat aircraft is required to perform a nose-pointing manoeuvre from a tactically advantageous position and a fast turn-around when in a disadvantageous position. This implies that the aircraft must venture into high angle-of-attack at both low speeds and high speeds. However, both these flight envelope boundaries are restricted by complex aerodynamic phenomena which cannot be modelled by classical method of using stability/damping derivatives. Hence, extensive research has been performed on unsteady aerodynamic modelling and flight dynamic analysis at high angle-of-attack flight conditions in the past two decades. At CSIR-NAL, we have successfully implemented these technologies for a delta-wing configuration called the Generic Tailless Aircraft (GTA), and an industrial grade trainer aircraft.

At low-speed and high angle-of-attack near stall, the aircraft wing vortices breakdown on the wings or a flow-separation happens on the airfoil. This flow readjusts to change in flow angles (angle-of-attack or side-slip) with a finite time-lag. Hence, the aerodynamic force or moment acting on the aircraft becomes a function of the aircraft or airfoil's motion history. This phenomenon called unsteady aerodynamics requires special wind tunnel data for mathematical modelling. Many methods have been proposed in literature, the most successful

*** - *Director, NAL, **$** - Scientists, FMCD, NAL, # - Professor, De Montfort Univ., UK*

one being the method described in [2].

The aerodynamic model is developed using a variety of wind tunnel test data like that from static tests, rotary balance test, forced oscillation test etc. The data from the Free-spintests or the Frisbee tests is used for validation of the model thus obtained. We follow the modelling approach presented in [3]. This model has also been validated from flight tests. A model based on these techniques was found to be particularly advantageous in the initial design phases of the Pilatus PC-21 aircraft [4]. At NAL, we have developed an advanced method of nonlinear unsteady aerodynamic modelling based on Volterra Series [5].

Recently, there has been a tremendous interest in the industry on mathematical modelling of transport aircraft dynamics at stall and post-stall dynamics like wing-rock, deep-stall, steep and flat spin etc. Two major research programs have been undertaken by NASA-Langley and EU-FP7 to develop standard methods for modelling, by industry-wide collaborations [11, 12]. The methods primarily developed for high-performance delta wing configuration aircrafts have been extended to transport aircrafts. Thus, the technology is of tremendous significance for the industry.

Aircraft flight dynamics at high angle-of-attack cannot be analysed by linear methods. A bifurcation and continuation technique has sufficiently advanced for use by the industry. In this method, aircraft nonlinear trim modes are computed using full 8-th order equations and there is no need for approximation methods like that proposed by Birhle [13]. A software tool called KRIT developed by Goman and co-workers, is particularly advantageous as it can be used with an industrial grade aerodynamic model in the form of non-smooth data-tables, as well as advanced unsteady aerodynamic models. We performed analysis of a trainer aircraft, and the results obtained were a significant input in the aircraft's design and development activities.

Goman.et.al have developed a novel method for nonlinear flight dynamics analysis called the Attainable Equilibrium Sets (AES) [6]. This method can reproduce the bifurcation diagrams as well as manoeuvre envelope. Software for implementation of this method is under development at De Montfort University (DMU), UK with support from NAL [7].

In this paper, we present the aerodynamic model development using wind tunnel data in section 2. In section 3, we present the Volterra variational approach for nonlinear unsteady aerodynamic modeling. In section 4, we present AES analysis of GTA.An example of bifurcation analysis of a trainer aircraft is presented in section 5.

2. Aerodynamic Modelling using Wind tunnel test data

Aerodynamic modelling of high angle-of-attack aerodynamics involves computation and integration of several components from different types of wind tunnel test data as shown in Fig.1. The static wind tunnel test data from wind tunnel tests is first analysed to check the consistency of data from different sources and stings across the angle-of-attack range of -90 deg to +90 deg. This data is then used to compute the incremental effect of angle-of-attack,

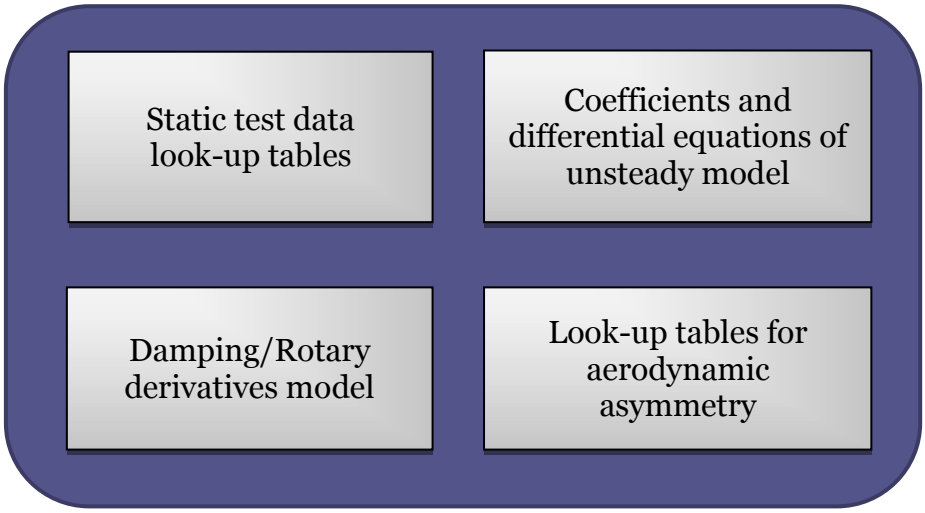

Fig.(1) Components of a High Angle-of-attack Aerodynamic Model

side-slip and control surface deflections, in the form of data tables. These lookup tables and a linear interpolation provide static force and moment coefficients at any aircraft flight condition.

The unsteady aerodynamics at low angle-of-attack is incorporated in the form of stability or damping derivatives obtained from small amplitude forced oscillation test data. These derivatives can also be determined from flight test data or some other empirical methods. These derivatives are also included in the form of a look up table up to stall angles-of-attack. For flight in the normal envelope a model consisting of static and damping derivatives is sufficient for simulation and analysis of aircraft flight dynamics [8].

In the near-stall and stall angle-of-attack regimes the time-scales of unsteady aerodynamics become quite large, and hence need to be modelled using special methods based on dynamic wind tunnel test data. Forced oscillation wind tunnel tests involve aircraft model motion with its angle-of-attack varying in a sinusoidal form. The tests are performed for various amplitude and frequencies in order to match the non-dimensional pitching rate comparable to that expected in flight. This data shows that the normal force and pitching moment coefficient in the stall angle-of-attack regimes is a strong function of angle-of-attack, pitching amplitude and frequency. The same holds true for yawing moment coefficient C_n and rolling moment coefficient C_l due to oscillation in sideslip. Therefore, capturing this entire data-set as a single reduced order model with definite physical co-relation to experimental observations is a challenging problem.

A comparative analysis of the modelling methods shown in literature showed that Goman-Abramov model in the form of nonlinear differential equations is the best method, which produces a model of sufficient fidelity [9]. At NAL, we have developed a novel Volterra variational modelling approach based on similar model structure [5,7].This approach offers a number of practical advantages, and is presented in the next section. The aerodynamic model consists of differential equations, which are augmented to the 6DOF equations of motion for simulation and analysis. Its parameters are included along with other look-up data tables.

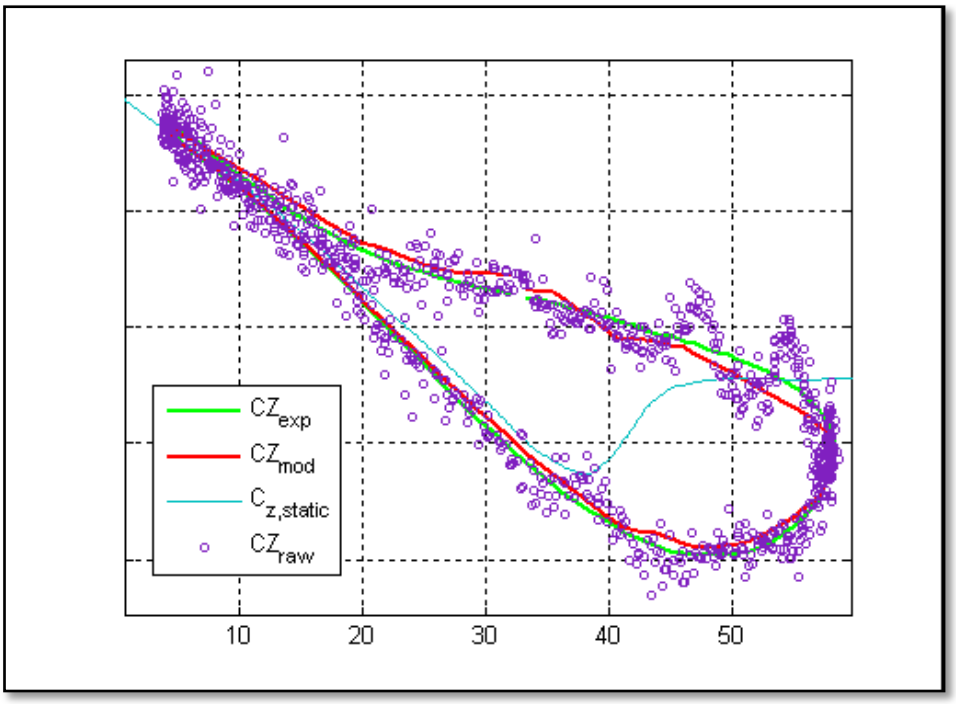

Fig.(2) Volterra variational Model for CZ of GTA.

Rotary balance tests are particularly aimed at capturing the features of steady-spin mode of the aircraft. In this test, the aircraft model is rotated about its wind axis imitating a spinning or coning motion. The test is performed over a sufficiently large range of non-dimensional spin rate. This data is used to compute the incremental effect of coning rate. This is then used to obtain the derivatives of C_{lp} and C_{np} about wind axis in case of simpler variations or it is fitted with a cubic polynomial in case of complex variations [3]. These parameters are also included as data tables and are primarily effective at angles-of-attack well beyond stall.

The aerodynamic model, thus obtained, is used in simulation and flight dynamic analysis. A sample of results from bifurcation analysis of a trainer aircraft and AES analysis of delta-wing configuration are presented in the next sections.

3. Volterravariational Model of Unsteady Aerodynamics

$$\boldsymbol{C_Z(t) = C_{Z,st}(\alpha) + C_{Zq}(\alpha)\frac{\dot{\alpha}c}{2V} + C_d(t)}$$

$$\boldsymbol{C_d(t) = x_1 + x_2 + ..}$$

$$\boldsymbol{\dot{x_1} = \dot{a}(\alpha)x_1 + K_1(\alpha)\dot{\alpha}}$$

$$\boldsymbol{\dot{x_2} = \dot{a}(\alpha)x_2 + K_{21}(\alpha){x_1}^2 + K_{22}(\alpha)x_1\dot{\alpha}} \qquad \textbf{(1)}$$

The Volterra variational model structure developed at NAL is given by Eq.(1). The variables x_1, x_2, x_3 are called kernel states, and these represent the contribution of so-called Volterra kernels to the output. The response of the model to small amplitude inputs is approximately

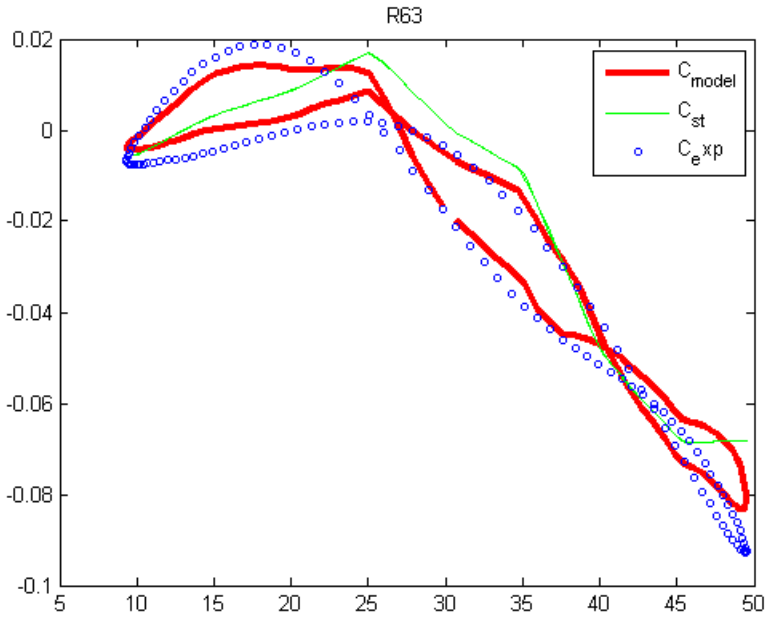

Fig.(3) Volterra variational Model for Cm of GTA.

linear, and requires just one kernel state x_1 to be considered. The response to large amplitudes is nonlinear and requires x_2 and x_3 to be considered as well. This is also a characteristic of unsteady variation of aerodynamic loads, as observed in experimental data.

There are several advantages of using this model. It provides more number of parameters for tuning it to the nonlinearity in variation of coefficients. The number of kernel states to be included in the model can be determined from power-spectrum-density of the sinusoidal input response of the aerodynamic loads. The model parameters can be estimated by simple weighted-least-squares method and output-error methods.

The model was implemented using the forced oscillation wind tunnel data for four amplitudes (3, 10, 15 20) deg and three frequencies (0.5, 1, 1.5) Hz. The results of modelling for C_Z and C_m coefficients are presented in the Figures (2) and (3). The model reliably captured the complex variation in pitching moment coefficient consisting of multiple damping/anti-damping loops of GTA.

4. AES analysis of GTA

A novel method for comprehensive and computationally intensive flight dynamics analysis called Attainable Equilibrium Sets (AES) has been proposed in [6]. In this method, the aircraft trim and stability analysis is performed in a fashion to reflect its Performance, Manoeuvrability and 6DOF flight simulation characteristics by a proper choice of the reduced order sub-system of 6DOF equations of motion of the aircraft. These reduced order sub-systems “Spat5” and “Spat8” arepresented in Fig.(4) as a hierarchical system.

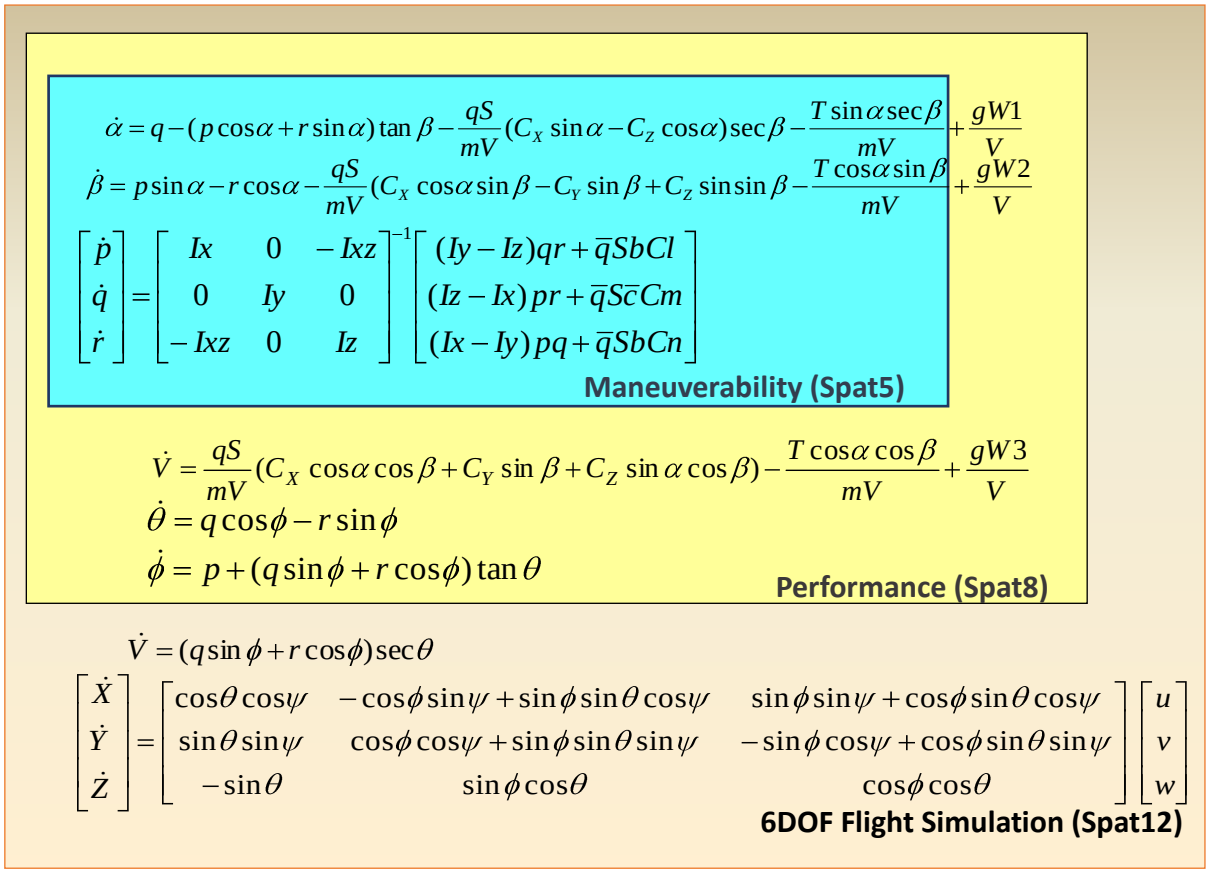

Fig.(4) Computational Methodology of AES for flight dynamic analysis.

From practical considerations, AES can also be implemented for a non-smooth industrial-grade aero-database type of an aerodynamic model. A sophisticated software tool for performing trim and stability analysis using the AES approach is under development at DMU with support of NAL. Sample results shown in Figs.(5a,b) were obtained using these tools.

The AES computations provide the capabilities of an open airframe in the form of manoeuvre envelopes. For example, Figure (5a) presents steady roll-rate capability of the GTA airframe, and stability of different trim modes using a color code. Green indicates a stable trim mode, red one indicates existence of unstable real pole, yellow shows existence of oscillatory unstable mode, etc. Locallystable trim statesnear bifurcation boundary are additionallyevaluated in terms of critical external disturbances and critical combinations of pilot's inputs. The open- and closed-loop AES envelopes characterised with local and non-localstability characteristics are useful tools in the process of control law design and validation of its flight envelope protection features. The AES method is useful in initial stages of design of advanced high-performance aircrafts, as it clearly brings out the effect of aerodynamic parameters, control inputs and actuator constraints on possible airframe capabilities in terms of performance, manoeuvrability and agility. Figure (5b) indicates the attainable roll-rate manoeuvre envelope along with its robustness to side-slip, assuming no constraints in control inputs. Therefore, AES is a sophisticated and practically informative approach to aircraft trim and stability analysis for open airframe and closed-loop system.

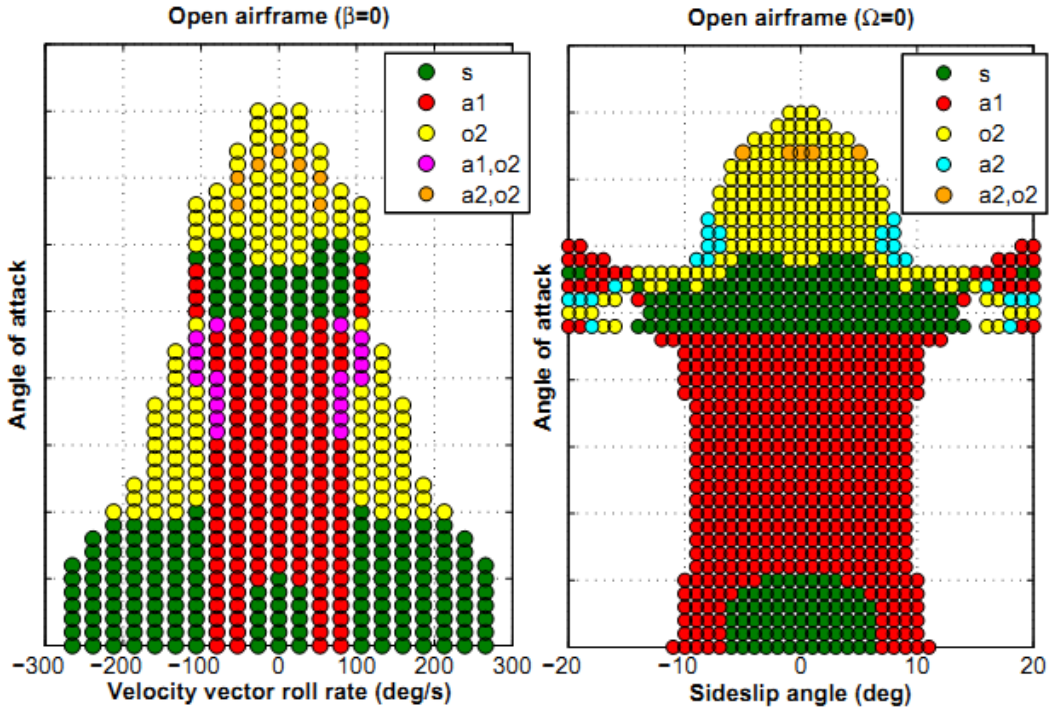

Fig.(5a) Roll-rate and Sideslip Manuever Envelopes computed using AES methods for open Airframe.

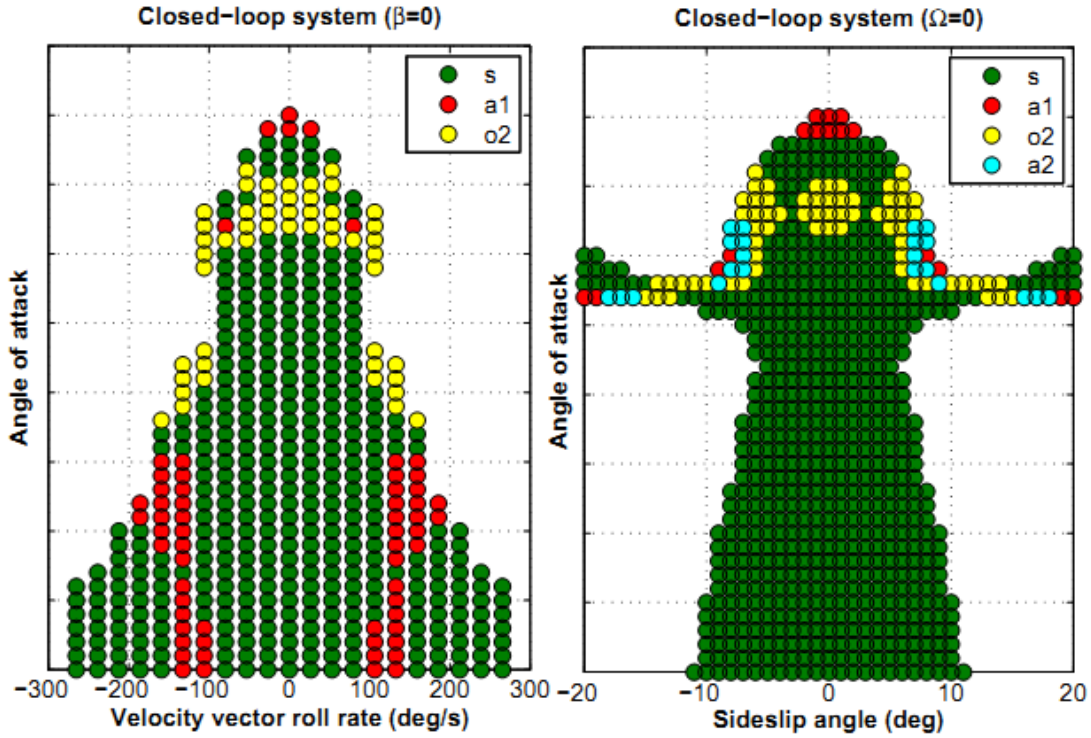

Fig.(5b) Roll-rate and Sideslip Manuever Envelopes computed using AES methods for closed-loop system with no control inputs constraints.

5. Bifurcation analysis of a trainer aircraft

A trainer aircraft is required to fly into spin and recover from it, to orient the trainee pilots to stall, spin, post-stall gyrations etc. The classical methods of predicting spin and rotary balance data are commonly used in the industry. However, these analytical and approximation methods were developed at a time when there were no extended modelling methods and the computational power was severely limited. The modern method of "Bifurcation Analysis" was introduced three decades ago and has matured into effective computational technique for spin prediction.

A sophisticated MATLAB based software called KRIT developed by Goman and Co-workers was used to analyse the characteristics of spin of a trainer aircraft [10]. An example of its bifurcation diagram is presented in Fig.(6). The mode in green indicates stable normal steady flight modes including level flight mode at low angles-of-attack. It is evident that the aircraft can exhibit multiple equilibriums due to nonlinear nature of its dynamics. When the aircraft departs from this normal mode (using large rudder deflection), it enters into a spin mode indicated by the yellow line at 60-65 degrees angle-of-attack.

Further analysis showed that the aircraft can be recovered to normal flight mode using a combination of aileron and elevator control. These predictions were further verified from 6DOF flight simulation studies. It is also important to note that the spin angle-of-attack range and spin-rates were found to be equivalent to that observed in vertical tunnel free-spin test or the Frisbee test.

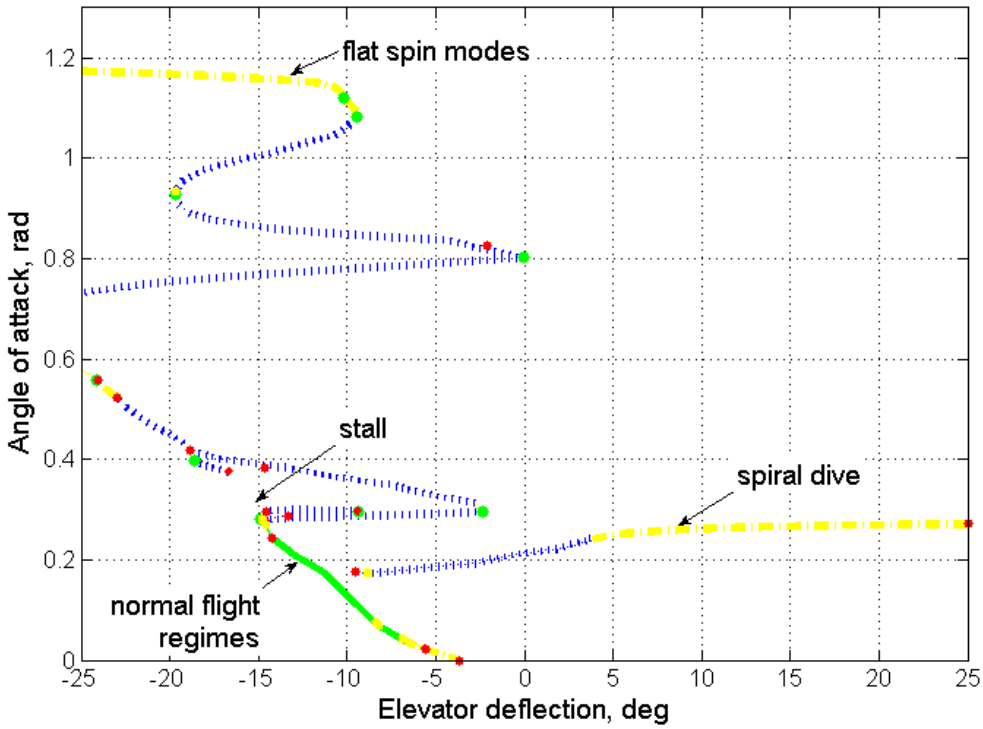

Fig.(6) Bifurcation diagram for trainer aircraft with stable, spin and roll-coupling modes.

6. Conclusions

We have presented an integrated approach to evaluate the computational flight dynamics of modern aircrafts with stringent performance and manoeuvrability requirements stretching into high angle-of-attack flight regime. This is based on high-fidelity aerodynamic modelling covering static and dynamic wind tunnel test data. Accurate analysis of flight modes using AES and bifurcation analysis methods was presented for combat and trainer aircraft configurations. In future, we envisage extending this technology to other categories of aircrafts.

Acknowledgements

All the authors acknowledge the financial support received from ADA, Bangalore, and discussions with the FMCD and CLAW scientists at NAL. Contributions of Nikolay Abramov and Evgeny Kolesnikov in developing software tools are acknowledged.

References

[1] Multiple Authors, "Technologies for Highly Manoevarable Aircraft" NATO-AGARD Conference Proceedings, Oct 1993, AGARD CP-548.

[2] M. G. Goman and A. N. Khrabrov, "State-space representation of Aerodynamic Characteristics of an Aircraft at High-angle-of-attack, AIAA Journal of Aircraft 1994, Vol.31, No. 5, pp.1109-1115.

[3]A. N. Khrabrov, M. Sidoryuk and M. G. Goman, "Aerodynamic Model development and Simulation of Airliner Spin for Upset Recovery", EDP Sciences, Progress in Flight Physics (5)2013 621-636.

[4] Leonardo Manfriani, "Design for Spin", *25th Congress of the International Council of Aeronautical Science,*Hamburg, Germany, 3-8 September 2006,Paper 485.

[5] MalleshBommanahal and Mikhail Goman, "Nonliear Unsteady Aerodynamic Modeling by VolterraVariational Approach", *AIAA Atmospheric Flight Mechanics Conference* 13th -16th August 2012, Minneapolis, Minnesota, USA.

[6] M. G. Goman, A. V. Khramtsovsky and E. N. Kolesnikov, "Evaluation of Aircraft Performance and Maneuvearbility by Computation of Attainable Equilibrium Sets" AIAA Journal of Guidance Control and Dynamics, 2008,Vol.31, No. 2, pp. 329-339.

[7] N.Abramov, M.Bommanahal, S.Chetty, M. Goman, E. Kolesnikov and PVS. Murthy, "Flight Envelope Expansion via Active Control Solution for a Generic Tailless Aircraft", *29th Congress of the International Council of Aeronautical Science,* St.Petersburg, Russia, 7th-12th September 2014, 0591.

[8] J. Singh and R. V. Jategaonkar, "Identification of Lateral-Directional Behaviour in Stall from Flight Data", AIAA Journal of Aircraft, 1995, Vol. 33, No. 3, pp.627-630.

[9] D.Greenwell, "A Review of Flight Dynamic Modeling for Flight Dynamics of Manoeuvrable Aircraf", *AIAA Atmosperic Flight Mechanics Conference and Exhibit 2004,*Providence, Rhode Island, 2004-5276.

[10] M.G.Goman and A.N.Khramtsovsky, "Computational framework for investigation of aircraft nonlinear dynamics". Advances in Engineering Software, Vol. 39, Issue 3, March 2008, pp.167-177.

[11] http://www.supra.aero/home.htm, Project Website

[12] A. Murch and J. Foster, “Recent NASA Research on Aerodynamic Modeling of Post Stall and Spin Dynamics of Large Transport Airplanes” *AIAA Aerospace sciences Meeting and Exhibit*, Reno, Nevada, paper No. 2007-0463, January 2007

[13] W. Bihrle and B. Barnhart, "Spin prediction techniques", Journal of Aircraft, Vol. 20, No. 2 (1983), pp. 97-101.